Graduate Research Program on Climate Change and Water Resources
(CC-WR/INE/UAC-Benin)

ASSESSING THE CLIMATE AND LAND USE CHANGES IMPACT ON FLOOD HAZARD IN OUÉMÉ RIVER BASIN, BENIN (WEST AFRICA)

Dissertation submitted in Partial fulfilment of the requirement for the degree of
Doctor of Philosophy (PhD)

in
Climate Change and Water Resources

at
University of Abomey Calavi (Benin Republic)

by
Jean HOUNKPE

Supervisors:
Prof. Abel A. **AFOUDA**
Prof. Dr. Bernd **DIEKKRÜGER**

Members of the Jury

President: Prof. Dr. Ig. Euloge K. **AGBOSSOU**, University of Abomey Calavi, Benin
Examiner: Prof. Zoubeida **BARGAOUI**, University of Tunis El Manar, Tunisia
Examiner: Prof. Bamory **KAMAGATE**, Nangui Abrogoua University, Ivory Coast
Rapporteur: Prof. Emmanuel A. **LAWIN**, University of Abomey Calavi, Benin
Rapporteur: Prof. Abel A. **AFOUDA**, University of Abomey Calavi, Benin
Rapporteur: Prof. Dr. Bernd **DIEKKRÜGER**, University of Bonn, Germany

Date of defense: 05th September 2016

Dedication

to

God the Father, God the Son and God the Holy Spirit
Josèphine and Hounzonli, my parents
Al-Salama, my darling
Vincent Bosco Smart, my son
Antoine and *Janvier*, my brothers
and all my family.

Acknowledgements

I would like to thank the almighty God, who gave me the commitment, the strength and patience to pass through every thick and thin, to accomplish this thesis. I would like to express my gratitude to the German Ministry of Education and Research (BMBF) and to the West African Science Service Center on Climate Change and Adapted land Use (WASCAL) for providing financial and administrative support to conduct my research, as well as for enabling me to benefit from the collaboration with German and international scientists.

This dissertation could not have been possible without the contributions and supports of many people. First and foremost, I am grateful to my supervisors, Prof. Dr. Bernd Diekkrüger and Prof. Abel Akambi Afouda, who supported me through my doctoral research. Particular thanks to Prof. Dr. Bernd Diekkrüger for his prompt availability whenever needed, to Prof. Abel Akambi Afouda, for his investment in my training since the master program up to the PhD dissertation level. May the Good Lord reward you infinitely.

Special thanks to Prof. Moussa Boukari, director of Laboratory of Applied Hydrology (LHA), to Prof. Daouda Mama, former administrative and financial officer of LHA and actual Vice chancellor of University of Natitingou (Benin), to Dr. Julien Adounkpè, WASCAL GRP CC-WR coordinator, Dr. Fabien Hountondji, Dr. Emmanuel Lawin, Dr. AbdouKarim Alassane, Dr. Eric Alamou.

My special thanks go to all colleagues who provided data and support for this thesis, comments and suggestions during the periodical laboratory presentation, namely Djigbo. F. Badou, Dr. Charlène O. Gaba, Dr. Eliezer I. Biaou, Dr. Ganiyu T. Oyerinde, Dr. Fernand Avahounlin, Dr. Alice Fandohan Bonou, Vincent Azuka, Rita Houguè, Nctha Npo, Firmin Adandédji and many others.

I express my gratitude to everyone belonging to the Hydrology Research Group, especially Dr. Simone Giertz, Dr. Aymar Bossa, Dr. Constanze Leemhuis, Dr. Thomas Cornelissen, Gero Steup, Alexandre-Eudes Danvi, Geofrey Gabiri, Thomas Jütten, Kristian Näschen, Felix Op de Hipt, Claudia Schepp, Yacouba Yira, Inken Rabbel whose contributions in various forms were very valuable. Scientific rigor, commitment, passion and intellectual generosity made the exchanges with them interesting and enjoyable.

Many thanks to Gildas Tossou and everybody working at DGEau (Direction générale de l'eau).

Abstract

Floods have become increasingly frequent raising the question if they were caused by a growing frequency of heavy rainfalls or by an increasing trend in discharges or if they were simply enhanced by changes in land use. To date, little studies concentrated on flood frequency analyses in Benin and no attention was giving to the investigation of potential causes of the growing flood events. There is a lack of information for implementing a flood forecasting and early warning system to reduce flood damage in the country. This gap is bridged by the central theme of this dissertation.

Firstly, we performed trend, break point and non-stationary flood frequency (generalized extreme value distribution) analyses of the annual maximal discharge at the main subbasins of Ouémé basin. We found no statistically significant trend at 5% significance level but some stations exhibited abrupt changes in the data. The non-stationary model more adequately explains a substantial amount of variation in the data. In particular, the GEV-1 model, which incorporates a linear trend in its location parameter, surpasses the other models. **Secondly**, we explored potential changes in heavy rainfall magnitude and frequency through the generalized Pareto distribution by dividing the available data into two parts. For the analysis, rainfall data up to 92 years (1921-2012) were used. For all studied return periods, 82% of the stations show statistically significant change in daily precipitation among which 57% exhibit a positive change and 43% negative change. A positive change is associated with an increase in heavy rainfall over the area of concern. **Thirdly**, we investigated through multi-modelling approach (WaSiM and SWAT models) how changes in land use (different land use scenario) would impact on the flood characteristics (frequency and severity). WaSiM and SWAT models were calibrated and validated. Results show that both models predicted satisfactorily streamflow on the Zou basin at Atchérigbé gauge with the Kling and Gupta efficiency (KGE) between 0.6 and 0.85 and the Nash Sutcliffe efficiency (NSE) between 0.5 and 0.76 for calibration and validation periods. Projected land use maps for the time horizon 2015–2019; 2020-2024 and 2025–2029 combined with two socio-economic scenarios have been used as forcing inputs for the hydrological models. A methodology to assess change in flood frequency and magnitude relatively to the baseline was then applied. According to the median of all scenarios, the magnitude of flood event is shown to increase for most return periods, changes being greatest for low return periods. The overall combined results from WaSiM and SWAT show that a 5-year event may become a 3.4-year or 4.7-year event depending on the scenario. **Finally**, we proposed a framework for implementing the flood forecast and early warning system for the Ouémé catchment. These findings highlight the growing challenges for water resources managers and planners and emphases the need to address potential climate and land use changes impact on water resources while developing water management plans.

Résumé

Les inondations constituent un des phénomènes naturels les plus dévastateurs causant des pertes économiques et des dommages aux populations. De 1900 à 2006, les inondations ont tué en Afrique environ 20.000 personnes et environ 40 millions étaient affectées avec des dommages économiques estimés à 4 milliards de dollars US. Récemment, plusieurs pays de l'Afrique de l'Ouest ont été atteints par des vagues d'inondations : Ouagadougou (Burkina Faso), Dakar (Sénégal), Lomé (Togo) et autres en 2009; Abidjan (Côte d'Ivoire), Niamey (Niger), Cotonou (Bénin) et autres en 2010. Les inondations de 2010 au Benin ont été d'une très grande ampleur avec 680.000 personnes affectées dont 46 morts. Les inondations sont devenues très fréquentes et ceci nous amène à nous poser la question de savoir si ces inondations sont dues à une augmentation de la fréquence des pluies extrêmes (changement climatique) ou à une tendance à l'augmentation des débits au niveau des bassins ou encore simplement à un changement de l'occupation des sols et des états de sol. Jusqu'à présent, peu d'études se sont concentrées sur les inondations au Bénin sans pour autant chercher les causes potentielles de l'augmentation de la fréquence et de la sévérité de ces évènements. Il y a un gap en termes d'information pouvant permettre la mise en place d'un système de prévision et d'alerte précoce aux inondations dans le but de réduire les dommages causés par ces phénomènes. La présente étude a pour objet de combler ce vide à travers le thème: 'Evaluation de l'impact des changements climatiques et des changements d'occupation des terres sur les risques d'inondations dans le bassin de l'Ouémé au Benin (Afrique de l'ouest)'.

Dans un premier temps, nous avons analysé les tendances et les ruptures puis procédé à une analyse fréquentielle non stationnaire des séries de débits maximaux annuels (DMA) des sous bassins de l'Ouémé. Nous n'avons trouvé aucune tendance significative au seuil de 5% dans les séries de DMA mais quelques stations ont montré des ruptures dans leur série de DMA. Nous avons aussi trouvé que les performances des modèles non stationnaires dépassent celles des modèles stationnaires. En particulier, le modèle GEV1 (loi généralisée des valeurs extrêmes) qui incorpore une tendance linéaire dans le paramètre de position (location parameter) explique mieux les variations substantielles dans les données. Nous avons aussi proposé quelques débits de périodes de retour non stationnaires. **Ensuite**, nous avons exploré les changements potentiels dans la fréquence et l'amplitude des pluies extrêmes sur le bassin de l'Ouémé en subdivisant les données disponibles en deux parties dans le temps et en nous servant de la distribution généralisée de Pareto (GPD) pour l'analyse fréquentielle. Pour toutes les périodes de retour utilisées, 82% des stations ont montré un changement significatif dans les séries de pluies journalières avec 57% de changement positif et 43% de changement négatif. Un changement positif étant associé à une augmentation dans l'amplitude des pluies extrêmes. **Par ailleurs**, nous avons, à travers une multi-modélisation, investigué comment les changements d'occupation du sol influencent les caractéristiques des inondations (fréquence et sévérité). Nous avons tout d'abord calibré et validé deux modèles hydrologiques (WaSiM et SWAT). Les résultats montrent que ces deux modèles

ont la capacité de reproduire d'une manière acceptable les débits avec le Nash (NSE) variant entre 0,5 et 0,76 d'une part et KGE variant entre 0,6 et 0,85 d'autre part pour les périodes de calage et de validation. Ensuite, les cartes d'occupation du sol pour les horizons temporels 2015–2019; 2020-2024 et 2025–2029 combinées avec deux scenarios socio-économiques ont été utilisées comme entrées pour les modèles hydrologiques précédemment calibrés et validés. Une méthode pour évaluer les changements dans les caractéristiques des inondations a été appliquée. Considérant la médiane des résultats de tous les scenarios, nous avons trouvé que l'amplitude des inondations augmentera pour la plupart des périodes de retours. Une combinaison des résultats de SWAT et WaSiM montre qu'un évènement de période de retour 5-ans peut devenir un évènement de 3,4-ans ou 4,7-ans dépendamment des scenarios. **Finalement**, nous avons proposé un cadre théorique pour l'implémentation d'un système de prévision et d'alerte précoce aux inondations dans le bassin de l'Ouémé qui peut être étendu à d'autres basins du pays et d'ailleurs.

Ces résultats soulignent les défis grandissants pour les gestionnaires et planificateurs des ressources en eaux et mettent l'accent sur le besoin croissant de prendre en compte les changements climatiques et les changements d'occupation du sol en développant des plans de gestion de ressources en eaux. Des actions structurelles et infrastructurelles doivent être prises pour réduire les risques d'inondation et celles-ci incluent le renforcement du système d'alerte précoce aux innondations, l'amélioration de la sensibilisation et de la préparation des populations aux innondations, le découragement de l'installation des populations dans les bas-fonds et nids d'eau etc.

Content

List of Figures

List of Tables

ARTICLES AND CONFERENCE PAPERS FROM THIS DISSERTATION

Hounkpe, J., Diekkrüger, B. and A. Afouda (2016) : Future change in flood characteristics driven by socio-economic land use change scenarios in a tropical catchment (Zou, Benin). Submitted to Journal of Hydrology.

Hounkpè, J., Diekkrüger, B., Badou, D. & Afouda, A. (2016) Change in Heavy Rainfall Characteristics over the Ouémé River Basin, Benin Republic, West Africa. *Climate 4(1),15, doi: 10.3390/cli4010015.*

Hounkpè, J., Diekkrüger, B., Badou, D. & Afouda, A. (2015) Non-Stationary Flood Frequency Analysis in the Ouémé River Basin, Benin Republic. Hydrology 2(4), 210–229. doi:10.3390/hydrology2040210.

Hounkpè, J., Afouda, A. A. & Diekkrüger, B. (2015) Use of climate indexes as covariates in modelling high discharges under non stationary condition in Ouémé River. E-proceedings 36th IAHR World Congress., 1–5. Available at: http://89.31.100.18/~iahrpapers/85339.pdf.

Hounkpè, J., Afouda, A. A., Diekkrüger, B. & Hountondji, F. (2015) Modelling extreme streamflows under non-stationary conditions in Ouémé river basin, Benin, West Africa. Hydrological Sciences and Water Security: Past, Present and Future, 143–144. Paris, France: IAHS (International Association of Hydrological Sciences). doi:10.5194/piahs-366-143-2015.

1 GENERAL INTRODUCTION

Il est impossible que l'improbable n'arrive jamais.
Gumbel, 1958

1.1 Background

A flood is a hydrometeorological event characterized by high discharges or high water levels or high water velocity. Flooding occurs when water overflows in a space that is normally dry. There are different categories of flooding among which we have: (i) *Riverine Flooding:* a rise in the volume of water in the rivers, streams and storm-water tunnels until these exceed their normal capacities and overflow onto adjacent lands that population used for housing, industry recreation and others and cause severe threat to ecosystem and the services it provides. Flooding from large rivers usually results from large-scale weather systems that generate prolonged rainfall over wide areas. When precipitation is heavy and cannot infiltrate into the soil, most of the volume flows into the drainage system, exceeding its natural discharge capacity. The excess volume that cannot be drained off runs into the flood plain, following the topography to flood the areas near to the rivers. These events occur at random depending on local and regional climatic processes (Tucci, 2007). (ii) *Flash Flooding:* they are characterized by a rapid rise in water level, high velocity, and large amounts of debris. They are capable of tearing out trees, undermining buildings and bridges, and scouring new channels. Major factors causing flash flooding are the intensity and duration of rainfall, the steepness of watershed and stream gradients. The extent and density of watershed vegetation, the natural and artificial flood storage areas and the configuration of the stream bed and floodplain are also important.

The damage related to floods can be direct and/or indirect (Simonovic, 2012). Deaths of people and animals, damage to houses, properties, and standing crops, damage to physical infrastructure, etc. may be the direct consequence of floods. Other effects, such as a change in ecosystem or spread of diseases, may be indirect damage due to floods. A comparison of flooding and all other natural hazards made by Loster (2002) reveals that flooding causes more than half of all the fatalities due to natural catastrophes throughout the world and they are responsible for a third of the overall economic loss. According to the information presented in the Figure 1-1 there is an increasing number of floods throughout the world from 1950 to 2010 and the number of deaths relatively increasing.

Floods are among the most devastating natural hazards in Africa, whereas flash floods are among the greatest hazards arising from tropical cyclones and severe storms. Floods and flash floods cause loss of life, damage to property, and lead to the spread of diseases such as malaria, dengue fever, cholera, and chikungunya. According to Davidson et al. (2007), from 1900 to 2006, floods in Africa killed nearly 20,000 people

and affected nearly 40 million more, and caused damage estimated at about US$4 billion. There is an increasing trend in the resulting damage and deaths due to floods. Therefore, mitigating floods has been recognized internationally as one of the essential component of sustainable development and poverty alleviation as well as one of key measures required for the achievement of the internationally agreed upon UN-Millennium Development Goals (WMO, 2007).

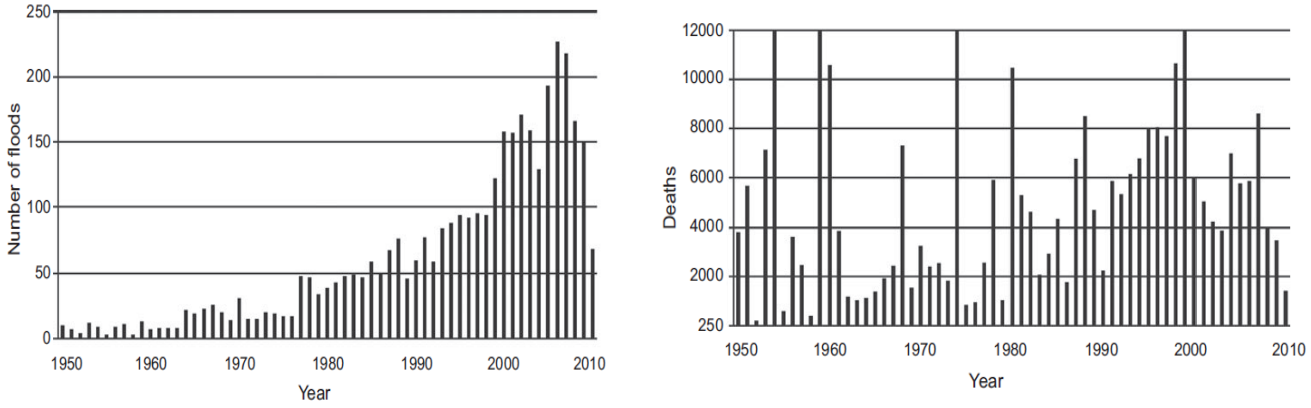

Figure 1-1: The number of flood disasters and deaths caused by flood disasters in the world (source: EM-DAT CRED) after (Simonovic, 2012)

In Benin, a number of extreme floods has occurred over the last 30 years and caused great economic losses. According to the World Health Organization, an estimated of 500 000 people are at risk of flooding (UNOCHA, 2008). Between 1980 and 2009, there have been 14 major floods affecting a total of 2.26 million people (EM-DAT, 2010). The floods in 2008 and 2009 caused widespread damage and displacement, respectively affecting around 158 thousand and 120 thousand people (EM-DAT 2010). The significant populations living in and near recently flooded areas and unwillingness to be relocated exacerbate the risk of flooding (UNOCHA 2008). Recent storms have destroyed mud and straw homes, polluted rivers and washed away roads in Sagon, Tohoue, Dasso, Ouinhi and Za-Kpota. During the 2008 floods, nine out of thirteen districts in the economic capital Cotonou suffered from severe water damage. In 2009, heavy rains led to the government declaring Benin's first state of emergency in recent years (UNOCHA, 2009).

In 2010 alone, Benin has suffered catastrophic floods that affected more than 680,000 people with 46 dead. In total, 55 of the 77 municipalities in the country have been affected to varying degrees, more than 50,000 homes were destroyed, and 150,000 people left homeless. In addition, 278 schools were flooded and 128,000 hectares of farmland or crops destroyed, the destruction of storage resulted in the loss of 12 000 tons of food stocks. The overall magnitude of the loss and damage is estimated to reach the equivalent of 2% of GDP of Benin in 2010 (World Bank, 2011a). Therefore, floods need to be studied in Benin in order to provide scientific information for early warning system and adaptation measures.

1.2 Problem statement

Ouémé River is the most important and largest basin of Benin Republic. It is a tropical catchment of interest where many projects were implemented such as IMPETUS, AMMA CATCH, and others within which many valuable data, comprehensive analyses, and relevant model results related to the fresh water cycle and other associated topics have been compiled. A number of studies have been done in this area in order to better understand its hydrological processes and behaviors (Le Lay, 2006, Lebel *et al.*, 2009, Speth *et al.*, 2010). Many authors have focused on hydrological process analysis and modeling in this basin (Bormann 2005; Bormann & Diekkrüger 2004; Bormann et al. 2005; Diekkrüger et al. 2010) among others. Sintondji (2005) performed the modelling of rainfall-runoff process in the Upper Ouémé catchment (Térou) by extrapolation from the local to the regional scale while Kamagate (2006) explored the hydrological process and runoff origins in the Donga part of Upper Ouémé. The water management aspect was studied as well. The water balance modeling of the Ouémé catchment using the WEAP 'Water Evaluation and Planning' system was done by Höllermann et al. (2010) and the use and constraints on the use of inland valley ecosystems in upper Ouémé catchment by Giertz et al. (2012). Séguis et al. (2011) examined the inter-annual variability of water budget and the origins of streamflow in a crystalline basement catchment (Donga basin). Were also investigated the impact of global change on water resources in the Ouémé catchment (Giertz, Diekkrüger, *et al.*, 2012), on water resources and soil degradation (Giertz *et al.*, 2010), on soil degradation and water quality (Bossa, 2012), on discharge by performing multiple models simulation (Cornelissen *et al.*, 2013). The climatological and statistical analysis of the rainfall regime of the upper Ouémé was done by Lawin (2007). From our knowledge, no study in the Ouémé basin has been done in order to assess the impact of global change on flood risk. This PhD thesis aims to fill this gap by assessing the impact of land use and climate change on flood hazard in Ouémé River.

1.3 Objectives

Flood management strategies pursued over the year in Benin have been largely reactive up to now and made in response to floods threats by relying on international helps. Such a strategy cannot fit the increasing challenges of population pressure on natural resources, the need for economic development, the increasing climate variability and potential climate change which exacerbate the unsustainability of the current practices through which we deal with floods. There is therefore a strong need for a paradigm shift, to move away from the present passive attitude towards a real proactive approach; there is a need to move towards a new culture of prevention, by managing the risk of floods and living with floods. According to WMO (2007), such a need is now the catalyst behind the concept of Integrated Flood Management (IFM), which seeks to integrate land and water resources development in a river basin, there by maximizing

benefits from natural resources and minimizing loss of life. Integrated Flood Management is an approach being promoted by the Associated Program on Flood Management (APFM) which is a joint initiative of WMO (World Meteorological Organization) and GWP (Global Water Partnership). Flood risks are influenced by natural (climate; river basin morphology) and man-made (river channelization; urbanization) factors influencing the frequency of floods and social/economic factors influencing their consequences (Bronstert, 2003).

The general objective of this research work is to provide basic information for planning and decision making on integrated flood management in Benin. Specifically, it will be question:

(1) to analyse the frequency and magnitude of flood in the main subbasins of Ouémé river from the discharge data by using non-stationary distributions;

(2) to investigate how climate change influences the frequency and severity of extreme rainfall in the Ouémé River Basin;

(3) to assess the impact of land use change on flood risk by performing ensemble simulation and to provide scientific insight for flood forecast and early warning system planning.

In this study, various research questions arising from the problems stated above have to be explored such as: (1) what are the factors that contribute to increasing flood risk in the Ouémé River basin? Is there an increasing observed annual maximal discharge accompanying the increasing number and/or severity of floods and what can be the added value of non-stationary modelling approach? (2) How does climate change influence the frequency and severity of extreme rainfall in the Ouémé River Basin or is there any change in the characteristics (intensity and frequency) of extreme precipitation events causing floods? (3) How does land use change affect flood magnitude and flood frequency in this river? Will the magnitude and frequency of extreme weather events increase in the future? What are the limitations of the current flood forecast and early warning system in Ouémé basin and how can we improve it?

1.4 Concept and definitions

- **Climate change**

A change in the state of the climate that can be identified (e.g., by using statistical tests) by changes in the mean and/or the variability of its properties and that persists for an extended period, typically decades or longer. Climate change may be due to natural internal processes or external forcings, or to persistent anthropogenic changes in the composition of the atmosphere or in land use (IPCC, 2012).

- **Disaster risk or risk**

The likelihood over a specified time period of severe alterations in the normal functioning of a community or a society due to hazardous physical events interacting with vulnerable social conditions, leading to widespread adverse human, material, economic, or environmental effects that require immediate emergency response to satisfy critical human needs and that may require external support for recovery (IPCC, 2012). Risk can also be understood as the 'combination of the probability of an event and its consequences'.

- **Extreme event**

An extreme (weather or climate) event is generally defined as the occurrence of a value of a weather or climate variable above (or below) a threshold value near the upper (or lower) ends ('tails') of the range of observed values of the variable. Some climate extremes (e.g., droughts, floods) may be the result of an accumulation of weather or climate events that are, individually, not extreme themselves (though their accumulation is extreme) (Seneviratne *et al.*, 2012)**.** An extreme event in the present climate may become more common, or rarer, under future climate conditions. When the overall distribution of the climate variable changes, what happens to mean climate may be different from what happens to the extremes at either end of the distribution.

- **Flood and inundation**

The overflowing of the normal confines of a stream or other body of water, or the accumulation of water over areas that are not normally submerged. Floods include river (fluvial) floods, flash floods, urban floods, pluvial floods, sewer floods, coastal floods, and glacial lake outburst floods (IPCC, 2012).

- **Hazard**

The potential occurrence of a natural or human-induced physical event that may cause loss of life, injury, or other health impacts, as well as damage and loss to property, infrastructure, livelihoods, service provision, and environmental resources (IPCC, 2012). The aim of a hazard assessment is to characterize hazards according to their most important characteristics such as the probability of occurrence or frequency of hazard events, the intensity and the affected area (ISDR, 2004; cited by (Kloos *et al.*, 2015)).

- **Integrated Flood Management**

It is a process promoting an integrated – rather than fragmented – approach to flood management. It integrates land and water resources development in a river basin, within the context of IWRM, and aims at maximizing the net benefits from the use of floodplains and minimizing loss of life from flooding.

- **Land use, land use and land cover change**

Land use refers to the total of arrangements, activities, and inputs undertaken in a certain land cover type (a set of human actions). The term land use is also used in the sense of

the social and economic purposes for which land is managed (e.g., grazing, timber extraction, and conservation). Land use change refers to a change in the use or management of land by humans, which may lead to a change in land cover. Land cover and land use change may have an impact on the surface albedo, evapotranspiration, sources and sinks of greenhouse gases, or other properties of the climate system and may thus have radiative forcing and/or other impacts on climate, locally or globally (IPCC, 2012). Land use is defined through its purpose and is characterized by management practices such as logging, ranching, and cropping. Land cover is the actual manifestation of land use (i.e., forest, grassland and cropland).

- **Return period**

An estimate of the average time interval between occurrences of an event (e.g., flood or extreme rainfall) of (or below/above) a defined size or intensity.

- **Return value**

The highest (or, alternatively, lowest) value of a given variable, on average occurring once in a given period of time (e.g., in 10 years).

- **Scenario**

A plausible and often simplified description of how the future may develop based on a coherent and internally consistent set of assumptions about driving forces and key relationships. Scenarios may be derived from projections, but are often based on additional information from other sources, sometimes combined with a narrative storyline.

1.5 Flood generation processes and their links to climate and land use changes

Different factors can contribute to increase flood risks. These are climate factors and anthropogenic factors due to changes in the land use patterns. Factors that generate flooding enumerated by Teegavarapu (2012) are precipitation intensity and duration, rainfall-runoff process, surface and subsurface hydrologic conditions, and land-use properties. Also, the antecedent climate, the hydrologic factors and the available reservoir storage affect the possible flooding in a basin. The soil moisture, soil saturation, and groundwater levels (shallow groundwater tables) are determinant factors in flooding events. Saturated soils are not a required precursor to severe flooding.

Due to global warming many subsystems of the global water cycle are likely to intensify, resulting in many regions in an increase of flood magnitude as well as flood frequency. Climate change is making weather less predictable, rains more uncertain and heavy storm rainfalls more likely. Heavy thunderstorm rain appears to have increased in frequency. Urban areas may help to increase thunderstorm activity because their built-up surfaces attain higher temperatures than surrounding areas and create a local air circulation that produces an ’urban heat island’. Dust particles caught up in that circulation act as nuclei

on which moisture in clouds condenses, forming rain droplets that eventually may develop into the large rain drops of a major thunderstorm.

The uniformity of runoff times from different parts of the basin can be critical in creating a flood. The more uniform the response and travel times, the greater the likelihood of the river flow to building up into a high peak flow. Basins that are highly uniform in both process and transmission time may create flood flows out of runoff volumes that in other basins would pass as non-significant events (Simonovic, 2012). Some modifications have intensified the flood hazard while others have reduced it. Some of these modifications are quoted below from Simonovic (2012):

- Deforestation may intensify river flooding by adversely affecting soil structure and volume, reducing infiltration rates, and reducing water storage. These influences are normally more significant during frequent low-magnitude storms. Their effect during increasingly severe flood-producing storms diminishes as prolonged heavy rainfall and/or melting fills available storage and creates widespread conditions of surface saturation and zero infiltration.

- The initial modification of river flood behavior is brought about not by afforestation or deforestation but by associated, temporary, mechanical procedures. For example, ploughing and drainage prior to planting, and skid-road construction and more general compaction during felling may have dramatic, but short-lived effects on runoff volumes and suspended solids loads.

- Forest clearance for agriculture has frequently been blamed for increased flooding downstream. The reduced vegetation cover allows more water to reach the soil more rapidly and returns less to the atmosphere. Surface runoff begins to occur more frequently and rates of erosion begin to rise. Erosion rapidly reduces the depth of the soil and thus its capacity to store water. Flooding is more serious because of the increased volume of water in the environment, because of the increased frequency and volume of surface runoff, and because of the rising levels of affected river beds.

- Agriculture and land drainage are likely to include increases in the total volume of runoff and flood peaks.

- Flood hydrology is influenced directly through the changed timing and volume of quick flow generated from the extensive impermeable surfaces of urban areas, by the import of clean water for domestic and industrial use, and by the generation and export of wastewater through storm water and sewerage systems. The extent to which flood characteristics are modified by urbanization depends very much on the nature of the modified urban surface, on the design of the urban hydrologic system, and on the climate. The main distinguishing characteristic of urban surfaces is that they are less permeable than most of the surfaces they replace.

1.6 Thesis structure

This thesis is organized in eight chapters. The **chapter one** which introduces the work gives a general idea about the research work, the background, the problem statement, the objectives, some concepts classification and definitions and the flood generation processes in relation with climate change and land use change. The **chapter two** is dedicated to the presentation of the research area and it provides information about the geographic location, climate, hydrology, geology, soil and land use etc. In the **chapter three**, Break point and trend analysis were done, and then we did a comparative analysis of stationary and non-stationary generalized extreme value distribution (GEV). We then investigated possible change in extreme discharge which may explain the recent flooding events observed in the basin. The **chapter four** is consecrated to the assessment of climate change impact on heavy rainfall over the study area. This was to identify whether or not the frequency or intensity of extreme rainfall causing floods has changed over the Ouémé basin. The **chapter five** is dedicated to the calibration and validation of two hydrological models (WaSiM and SWAT) and their assessment in simulating high discharge over the Zou catchment at Atchérigbé as case study. The **chapter six** presents how changes in land use /land cover will affect the frequency and the magnitude of flood events in the study area through scenario analysis and multi-modelling approach. Finally, the **chapter seven** summarises the main results of this work and presents the perspectives resulting from this work. Lastly, we presented three appendixes related to respectively the description of the hydrological models, the model parameters used and their initial and final values and the determination of appropriate thresholds (for chapter 4).

2 RESEARCH AREA AND DATA USED

Hydrology is limited as a science by data availability and measurement techniques.
Beven, 2012.

Ultimately, the success of a hydrological model depends critically on the data available to set it up and drive it (Beven, 2012) and hydrology as experimental science need to applied to case study. In this chapter, we presented in one hand the research area through its geographic location, geology and soil, climate, hydrology and land use. In another hand, we presented the hydrometeorological data used in this study and assessed its quality.

2.1 Research area

2.1.1 Location and geography

Republic of Benin is located in West-Africa and geographically between 06°00' to 12°00' northern latitude and 01°00' to 03°40' eastern longitude (Figure 2-1).

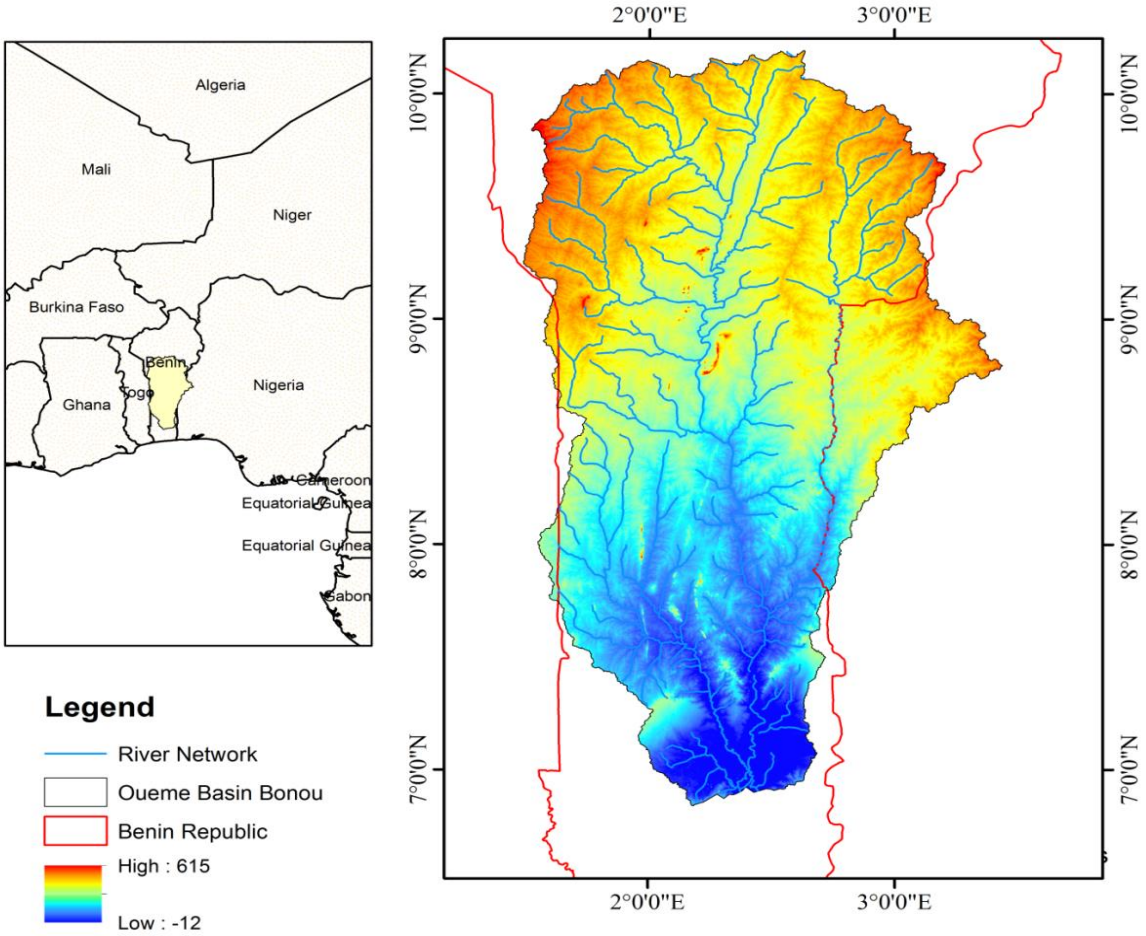

Figure 2-1: Location of the study area

It is bound by Niger to the north, Burkina Faso to the northwest, Nigeria to the east, Togo to the west and the Gulf of Guinea to the south. Benin lies entirely in the tropical sub-Saharan region with a wet and dry climate. A semi-arid environment is met northwards, made up of savannahs and small mountains (about 600 m), while the south of the country consists of a low coastal plain with marshlands, lakes and lagoons.

The study area is the Ouémé River which rises in the Atacora massif in northwestern Benin. It is approximately 49,256 km² in area (Ouémé Bonou) and 500 km in length and flows southward, where it is joined by its main affluent, the Okpara, on the left bank and by the Zou on the right. It then divides into two branches, the western one discharging into Lake Nokoué in the Niger Delta near Cotonou and the eastern into the Porto-Novo Lagoon.

2.1.2 Geology, Geomorphology and Soils of the Ouémé Catchment

Benin has four natural topographical regions: (i) A coastal belt which has four lagoons, the Cotonou, Ouidah, Grand Popo and Porto Novo while further north the land rises slowly to a savannah plateau, (ii) The Lama which is a wide marshy depression, (iii) The Atakora Mountains in the northwest and, (iv) The eastern plains of Borgou and Kandi which slope to the Niger basin.

According to Faure et al. (1998), the geology of Benin consists of two main rock types: metamorphic/crystalline rocks and sedimentary rocks. Benin lies extensively on Precambrian crystalline basement, known as the Dahomeyides or the Benino- Nigerian shield. It consists predominantly of granites, granitoid gneisses, and gneisses. About 20% of Benin are occupied by sedimentary basins (El-Fahem & Kocher, 2008).

The Ouémé catchment is mainly characterized by the Precambrian basement, consists predominantly of complex migmatites granulites and gneisses, including less abundant mica shists, quarzites and amphibolites (Reichert et al., 2010 cited by Bossa (2012)).

The relief in Benin is flat, varying from only a few meters at the coastal plain to the Atacora mountain range in the north-west with its highest elevation at Mt. Sokbaro (658metre). Ferallitic and hydromorphic soils are dominant in the southern part of Benin while it is a crystalline basement in Central part, mainly characterized by Acrisols and Lixisols (sols ferrugineux lessivés). In the Atacora Mountains in north-west Benin, shallow soils (Lithosols sols peu evolués lithiques) are widespread.

Within Ouémé Basin there are four major soil types (Deng, 2007). First in North and center, the crystalline base soils Alfisol, so called “sols ferrigineux”, are dominant. Such soils are expressed by concretion and lateritic crusts, most are sandy. Second in South, a depression with direction western to eastern separates the crystalline base soils. The soils in this depression are mainly comprised of hydromorphic Vertisols, which are sandy loamy to loam soils. Third in South is a sand-stone plain (“Terre de Barre”), here the soils are dominantly deep, fertile and sandy to loamy Acrisol. Fourth after the sand-stone plain follows a coast zone, where the soils are dominated through quartz rich sand and characterized by expanded swamp zone and lagoon water.

2.1.3 Climate

Benin is located in the inter-tropical zone (between 06°10' and 12°25' N). Its climatic condition is therefore typical of the West African climate, which alternates between the monsoon (from the ocean) during the cool and wet season, and the high thermal amplitude Harmattan wind that blows daily during the dry season (from the Sahara) (Aregheore, 2009). Both Monsoon and Harmattan move away alternately towards north and south. Their point of contact forms the Inter-tropical Front (ITF) which is the central point of all precipitation.

The Ouémé Basin, endures a tropical climate subdivided into three climatic zones according to different rainfall regimes (Figure 2-2) by the IMPETUS project classification (Deng, 2007); (i) The north Ouémé with an unimodal rainfall regime which has two seasons: the rainy season from May to October and the dry season which is hot with very low humidity, (ii) The south Ouémé with a bimodal rainfall regime which has two wet seasons, a long one between March and July and a short one between September and mid-November as well as a long dry season between November and March, (iii) The middle Ouémé with a transitional rainfall regime which has a rainy season between March to October, with or without a small dry season during August. Rains mostly originate from the Guinean coast.

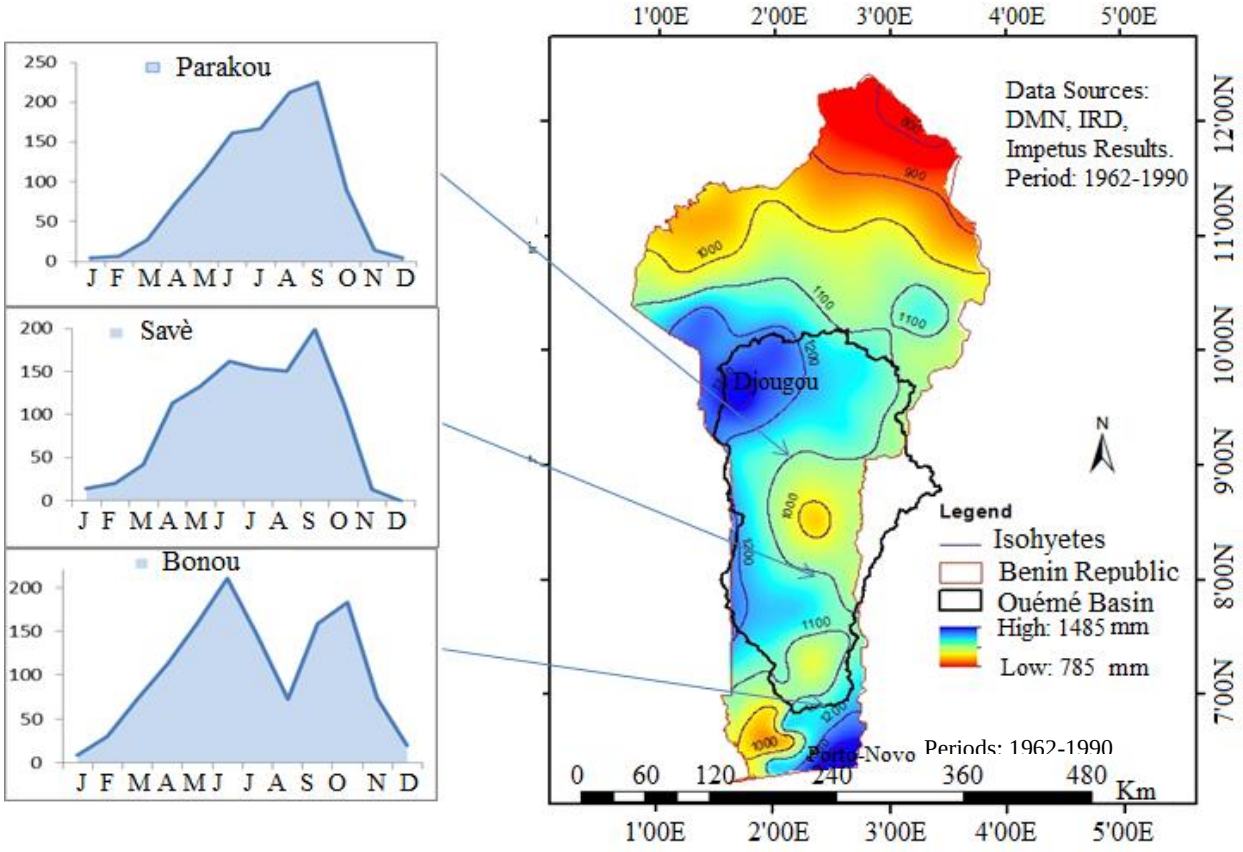

Figure 2-2: Different climatic zones of Ouémé basin

The prevailing dry season wind is the Saharan Harmattan, a hot dry dust laden wind that blows from the northeast and occurs between December and March. Average annual precipitation varies between 960 mm in the north and 1340 mm in the south. Average annual temperature ranges in Cotonou from 23 °C in August to 28 °C in May.

Like in other parts of West Africa, the diurnal peak of rainfall probability varies across Benin depending on the distance of a given station to the ocean and major topographic features (Judex & Thamm, 2008). For example, the inland propagation of the land-sea breeze circulation in the course of the day causes a morning maximum at Cotonou, and a pronounced afternoon maximum at Bohicon.

As far as the rainfall pattern is concerned, Benin's azonality is remarkable both with regard to the total average rainfall level per year, and its level on the rainfall scale (Aregheore, 2009). The highest total average rainfall levels per annum in the northwest (Djougou and surrounding areas) and southeast (Porto-Novo and surrounding areas) is between 1400-1500 mm; and lowest rainfall level in the north and northeast (the Niger valley) and low Mono valley in the southwest 850-1000 mm.

The mean annual temperature of Ouémé basin varies between 26° and 30°. According to Fink et al. (2010), daily WMO (World Meteorological Organization) Class A pan evaporation data for 2006 at six Beninese stations indicate a typical potential evaporation of 10–12 mm/day during the peak of the dry season in northern Benin and this drops to 2–4 mm/day at all stations during the rainy season.

2.1.4 Hydrology

Ouémé River is the most important river of Benin. It rises in the Atacora massif in northwestern Benin. It is approximately 49,256 km² in area (Ouémé Bonou) and about 510 km in length and flows southward, where it is joined by its main affluent, the Okpara (150 km of length), on the left bank and by the Zou (200km of length) on the right. It then divides into two branches, the western one discharging into Lake Nokoué in the Niger Delta near Cotonou and the eastern into the Porto-Novo Lagoon.

Important wetlands (Diekkrüger et al. 2010) are found in the south of Benin (e.g., Lake Nokoué, Lake Ahémé, Lake Toho, and the coastal lagoons), in Pendjari national park and in the floodplains of the Niger River. Inland valleys (in French, bas fonds) that are regularly flooded during the rainy season are widespread. Rainfall and runoff are characterized by below-mean values for the last 30 years. According to the same authors, rainfall-runoff variability is high in the catchment, leading to runoff coefficients varying from 0.10 to 0.26 (of the total annual rainfall), with the lowest values for the savannahs and forest landscapes For all studied sub-catchments, the highest runoff coefficients were obtained in the years with the highest annual rainfall. Irrigation, in fact, plays a minor role in Benin's agriculture.

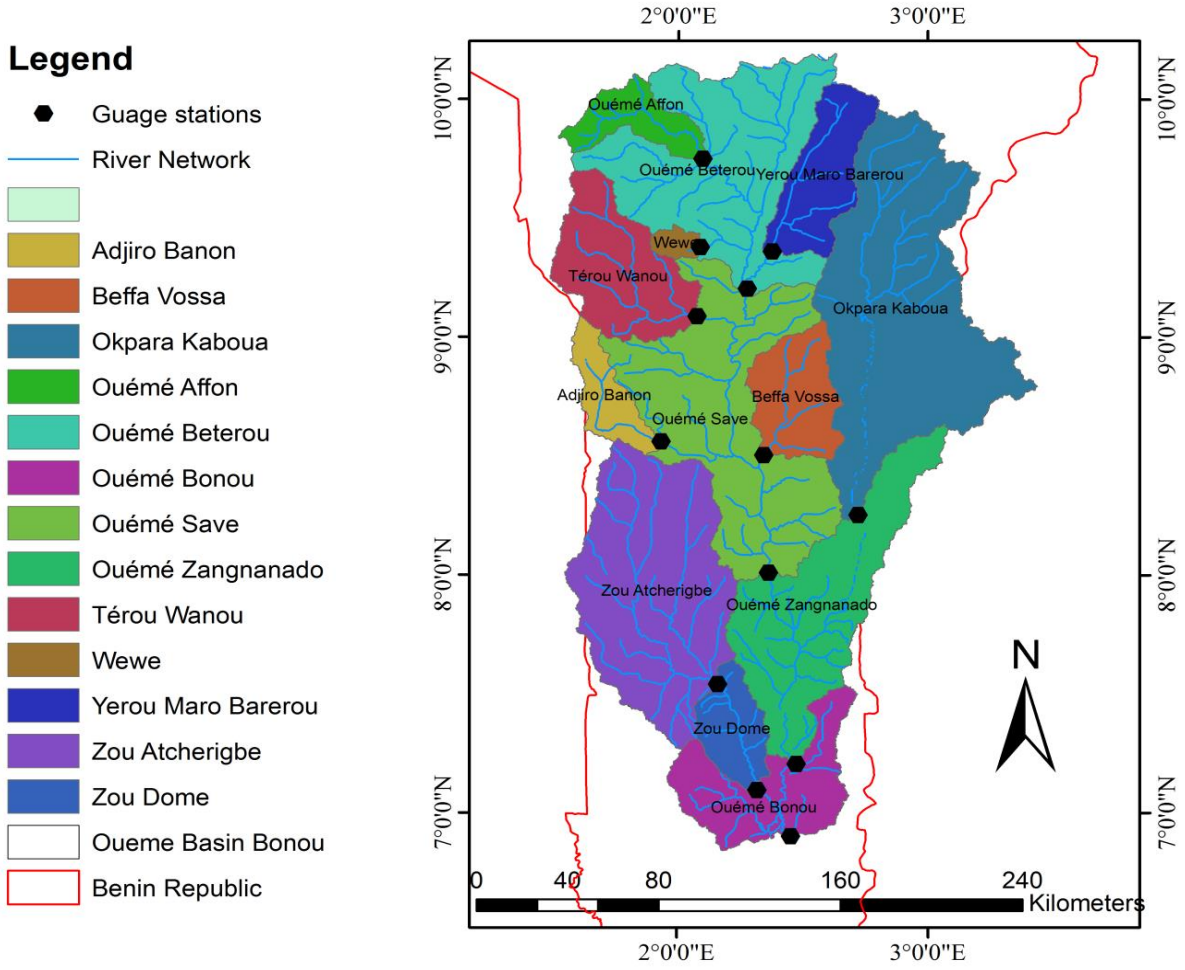

Figure 2-3 Gauged sub-catchments and hydrometric network of Ouémé catchment at Bonou

2.1.5 Vegetation and land use

The study of Wezel et al (1999) cited by Höllermann (2008) distinguishes four different vegetation zones in Benin: Sudanese, Guinea, Guinea-Congolese and Coastal. The Sudanese Zone covers most parts of Central and Northern Benin and is characterized by woodlands and savanna with gallery forest along river courses. According to Peyre De Fabregues (1980), in the Northern Sudanian Zone, vegetation is dominated by Combretaceae and Mimosaceae woodland or single trees with perennial grass layers of Andropogon gayanus (sandy soils), Loudetia spp. (laterite, glacis) and Hyparrhenia spp. (moister sites). South of the Sudanese zone lies the Guinea zone with woodlands, tree and shrub savanna. This zone can be divided into a northern and southern part according to the change from uni- to bimodal rainfall characteristics with more water demanding species in the south. The natural vegetation of the Guinea-Congolese and the Coastal zone is characterized by mosaic forest and savanna (see Figure 2-4).

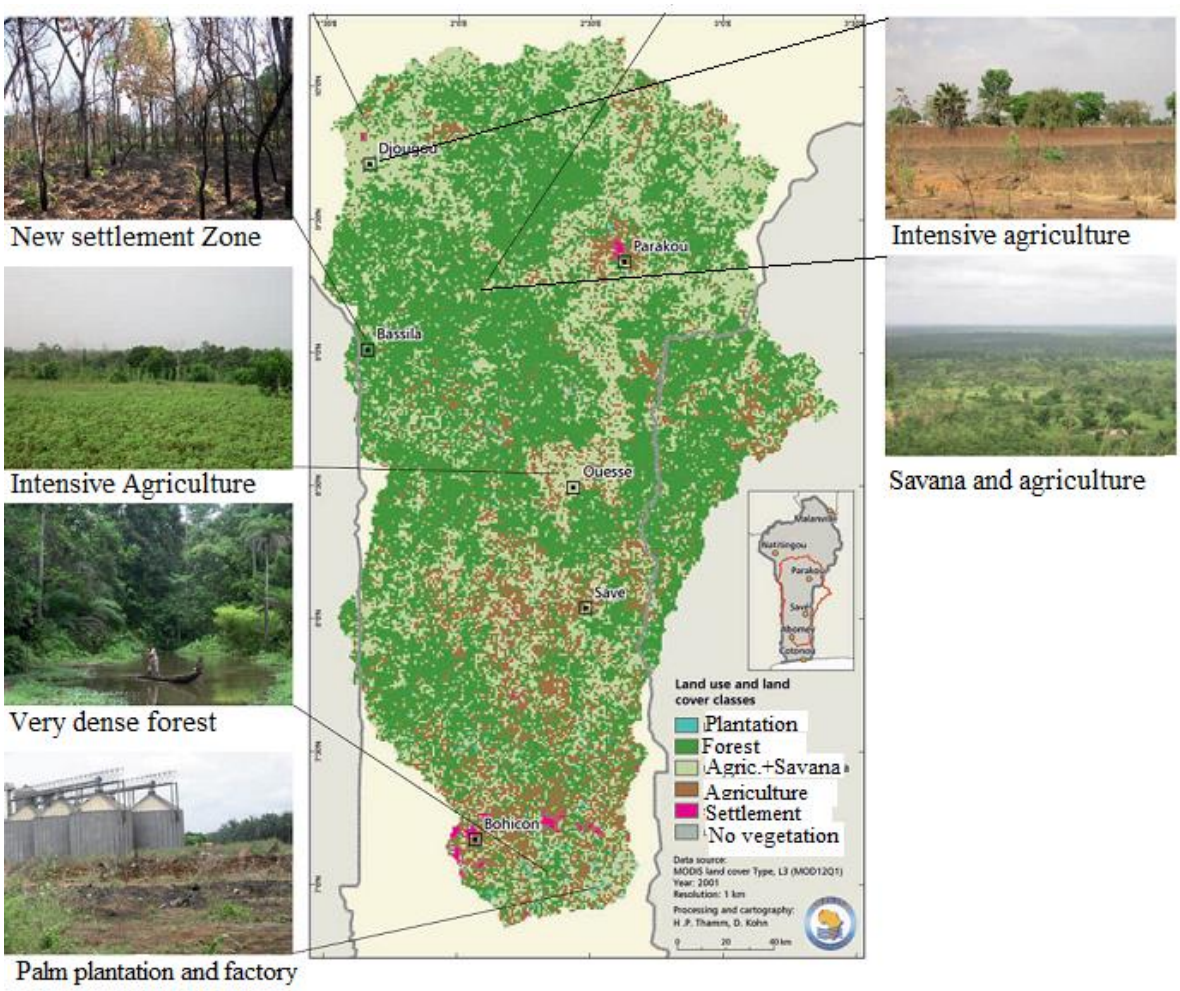

Figure 2-4: Land cover and land use map of the Ouémé catchment with some example pictures (Judex & Thamm, 2008)

In the Ouémé catchment, land use is largely characterized by small-scale agriculture (Judex & Thamm, 2008). In the northern part of the catchment, intensive agriculture can be found around the old settlements. Along the Djougou-Ouberou-Parakou road, agricultural areas are expanding, and, in some areas, even the *forêt classées* are not respected and are converted into farmland. Agricultural activities are mostly subsistence based but also partly oriented towards production for regional markets. A forest belt is located in the middle of the catchment. It has come under increasing pressure by agricultural expansion. Characteristic land use patterns for that zone are a mixture of fields, fallows, and patches of forest. Large teak plantations can be found around Bohicon. The south of the catchment is characterized by large plantations and intensive agricultural land use. At the border with the erosion plain of the Ouémé, dense forests remain that benefit from favorable groundwater availability (e.g., *Forêt de Locoli, Forêt de Lama*). Even tree species of the humid tropics can still be found there.

2.2 Hydrometeorological data

2.2.1 Data availability

The Ouémé basin is the most studied basin in Benin republic in which different projects were implemented for comprehensive analysis of its hydrology, climatology and other fields. These are: the RIVERTWIN project (*Integrated River basin Management in Contrasting Climate Zones: EU Research Project, started in 2004*), IMPETUS project (*Integrative management project for an efficient and sustainable use of freshwater resources in West Africa*), AMMA-CATCH (*Couplage de l'Atmosphère Tropicale et du Cycle Hydrologique /African Monsoon Multidisciplinary Analyses, started in 1997*). During these projects, different instruments were installed to collect valuable data mainly the meteorological data and the hydrological data (quantitative and qualitative). Out of these projects, the DGEau (*Direction Nationale de l'Eau*) runs a network of discharge measurement in collaboration with IRD (*Institut pour la Recherche et le Developpement, France*) whereas the synoptic stations and the rainfall measurement stations are managed by the DMN (*Direction Nationale de la Météorologie*).

Twenty river gauges are available from the national observatory network in the Ouémé catchment (including IRD river gauges); in addition, five gauges have been installed by IMPETUS in the Aguima catchment (Judex & Thamm, 2008). Most of the water level gauges are automatic and others are manually recorded twice a day by an appointed person. In fact, it is the water level that is recorded continuously and using the rating curves, the discharge data is computed. Discharge data are available since 1950 for the DGEau stations and since 1997 for the CATCH gauges. **Table 2-1** shows the river discharge gauges stations used in this study. At Atchérigbé station, discharge measurements have been carried out 64 times among which 10 were done between 2002 and 2007 in order to update the rating curve (DGEau, 2008). It has been notice that the rating curve of this station is stable. The actual rating curve is valid from 1997 up to date (DGEau, 2008). The Zou catchment at this station (Atchérigbé), which water level – discharge curve is shown on **Figure 2-5**, was used for hydrological modelling. The others stations were used for flood frequency analysis and there were chosen due to their lengths that covers the period 1952-2009.

Table 2-1: Discharge stations used in this study. For spatial location, see **Figure 2-3**

Code DGE	Station	River	Data availability	Owner	Long.	Lat.	Size [km²] Catchment
4500105	BETEROU	OUEME	1952–2009	DGEau	2.27	9.20	10083
4500107	BONOU	OUEME	1948–2009	DGEau	2.45	6.90	49285
4500119	SAVE	OUEME	1951–2009	DGEau	2.42	8.00	23491
4501002	ATCHERIGBE	ZOU	1951–2009	DGEau	2.03	7.53	7035
4501005	DOME	ZOU	1952–2009	DGEau	2.33	7.12	4083

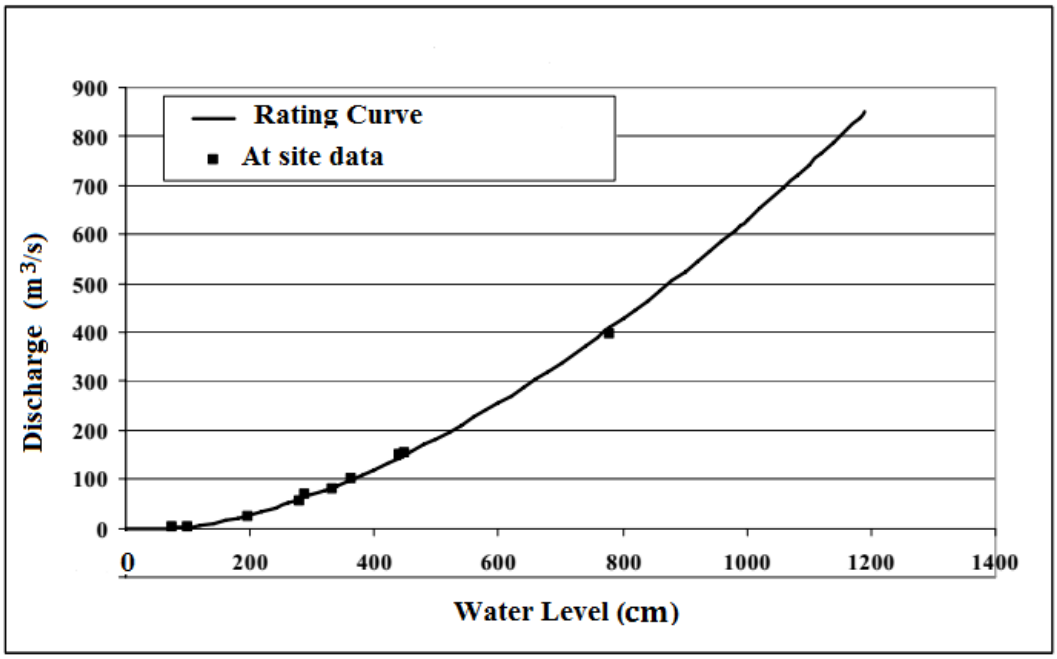

Figure 2-5: Water level discharge relationship for Zou catchment at Atchérigbé gauge (DGEau, 2008), valid from 1997 up to date.

For the climate data, the observations consisted of long-term rainfall measurements by a national network (starting in 1921), synoptic observations (starting in 1960), a dense research network of rainfall and climate observations in the Haute Vallée de l'Ouémé (HVO, since 1997) (Diederich & Simmer, 2010). The whole national rainfall network under DMN counted roughly 100 measurement sites by 2005 (Diederich & Simmer, 2010), against roughly 65 for the upper Ouémé catchment by 2006, which has been equipped by the Germans GLOWA-IMPETUS project (started in 2000) and IRD-CATCH/AMMA (Pohle et al., 2010, cited by Bossa et al. (2012)). Two synoptic stations (Savè and Bohicon) and 34 rainfall stations were used in this study. The choice of the rainfall stations were guided by the data length (that must be as long as possible to allow flood frequency analysis, roughly with data length of 45 years at least). In other hand, for the hydrological modelling, the two synoptic stations in the influence of the Zou catchment at Atchérigbé gauge were considered.

Table 2-2: Long-term annual mean values for the synoptic stations (Judex & Thamm, 2008). T [°C] is the average annual temperature, Tmin [°C] is the minimum annual temperature, Tmax [°C] is the maximum annual temperature, RR [mm] is the mean annual rainfall, NRR [d] is the number of days with more than 1 mm of rainfall and SUN [h] is the total sunshine duration per year. All the data are averaged over the period of 1961-1990.

Station	T [°C]	Tmin [°C]	Tmax [°C]	RR [mm]	NRR [d]	SUN [h]
Savè	27.4	21.9	32.8	1105	75	2203.6
Bohicon	27.6	22.6	32.5	1105	77	2176.8

Table 2-3: Rainfall and climate stations used in this study with their coordinates, data length and percentage of missing year. For spatial distribution of these stations, please refer to Figure 2-6.

No.	ID	Station Name	Longitude (degree)	Latitude (degree)	Elevation (m)	Creation Date	Last Record	Missing year (%)
1	0000D058	Abomey	1.98	7.18	260	1921	2012	2
2	0000D054	Agouna	1.7	7.55	240	1968	2012	16
3	0000D046	Aklamkpa	2.02	8.22	193	1968	2012	29
4	0000D045	Bante	1.88	8.42	264	1942	2012	4
5	0000D037	Bassila	1.67	9.02	384	1950	2010	15
6	0000D024	Bembereke	2.67	10.2	491	1921	2010	0
7	0000D036	Beterou	2.27	9.2	252	1953	2012	12
8	0000D026	Birni	1.52	9.98	430	1953	2012	19
9	0000D059	Bohicon	2.07	7.17	166	1940	2010	1
10	0000D061	Bonou	2.5	6.93	10	1946	2012	14
11	0000D051	Dassa-Zoume	2.17	7.75	155	1941	2010	0
12	0000D030	Djougou	1.67	9.7	439	1921	2010	8
13	0000D047	Gouka	1.95	8.13	242	1968	2012	7
14	0000D027	Ina	2.73	9.97	358	1947	2010	7
15	0000D022	Kalale	3.38	10.3	410	1957	2012	9
16	0000D056	Ketou	2.6	7.35	118	1950	2012	2
17	0000D044	Kokoro	2.62	8.4	231	1969	2012	5
18	0000D019	Kouande	1.68	10.33	442	1931	2010	6
19	0000D060	Lonkly	1.65	7.15	110	1955	2012	5
20	0000D067	Niaouli	2.12	6.7	105	1941	2010	0
21	0000D028	Nikki	3.2	9.93	402	1921	2010	12
22	0000D033	Okpara	2.73	9.47	295	1956	2012	5
23	0000D042	Ouesse	2.38	8.5	233	1964	2012	2
24	0000D034	Parakou	2.6	9.35	392	1921	2010	4
25	0000D032	Partago	1.9	9.53	397	1969	2012	36
26	0000D035	Penessoulou	1.55	9.23	369	1969	2012	31
27	0000D043	Pira	1.72	8.65	315	1968	2012	7
28	0000D050	Savalou	1.98	7.93	174	1921	2010	19
29	0000D049	Save	2.47	8.03	199	1921	2012	0
30	0000D031	Semere	1.37	9.55	386	1969	2012	13
31	0000D038	Tchaourou	2.6	8.87	325	1937	2010	19
32	0000D052	Tchetti	1.67	7.63	353	1964	2012	21
33	0000D041	Toui	2.6	8.67	316	1944	2012	7
34	0000D057	Zagnanado	2.33	7.25	102	1921	2012	1

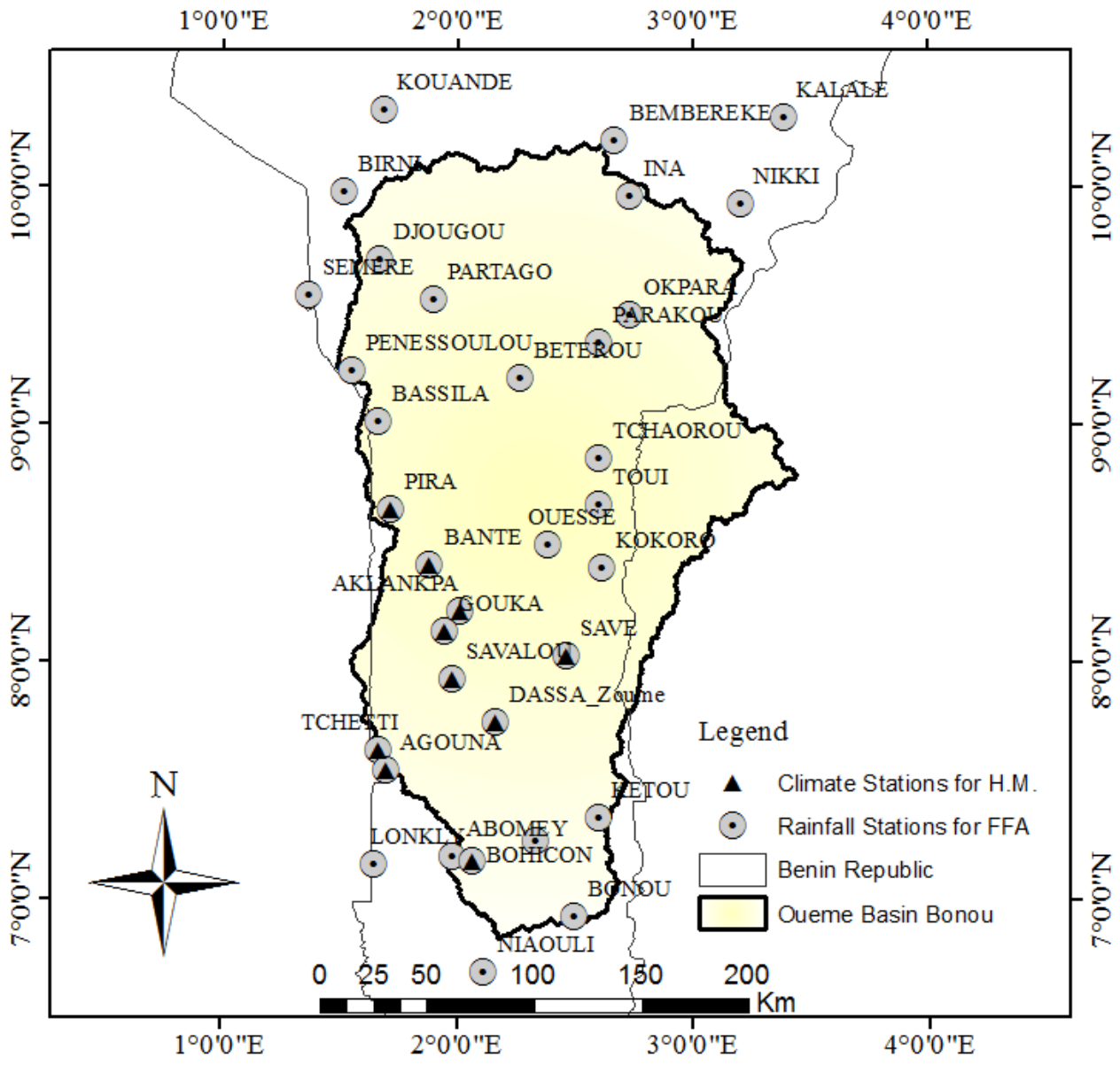

Figure 2-6 Climate stations data used for hydrological modelling (H.M) and flood frequency analysis (FFA).

2.2.2 Data quality assessment

The success of hydrological modelling depends on the quality of data involved in the process. The quality of data affects the quality of the hydrometeorological analysis. Data that have been collected and recorded manually by human hands are bound to have some problems with it quality. These range from the reading errors, the transcription errors

during recording on paper and the digitalization errors when typing the data etc. Other types of error can be due to the malfunctioning or poor maintenance of the equipment.

The reading errors can arise from the inattention of the reader or unclean (dirty) equipment. Even in the case where the variable has been well read, an error can result from the transcription of the variable to a copy note with for instance the decimal point put in a wrong place. Human error in entering the data into a spreadsheet brought along some errors as typing errors. As these uncertainties usually do not show regular patterns, correcting such errors becomes more difficult when comparing data with other neighboring station data, where different conditions apply, data values might differ immensely (Kasei, 2009). For example, the daily rainfall accumulation at one location may surpass 150 mm (corresponding to roughly 10% percent of mean yearly accumulation), with 80 mm falling within two hours, while slight or no rainfall may occur at a point only 20 km away from that location (Diederich & Simmer, 2010). Most of the hydrometeorological data used in this study have been used in previous studies during different projects implemented in Ouémé basin and the discharge and rainfall data quality has been judged acceptable based on the different publications (see for instance (Judex & Thamm, 2008, Speth *et al.*, 2010)).

In this study, a year is considered missing if the percentage of missing data is greater than 10% during the rainfall season. This is equivalent to 37 days of missing data from March to the end of November and it was mainly applied for the computation of annual rainfall. The statistic of the percentage of missing data (years) for each station is shown on table 2-3. It can be observed that only three stations show more than 25% of missing years. The percentage of missing years (data) is the number of missing years divided by the number of years of data including the missing years. For the computation of the annual precipitation, these years (with more than 10% of missing data during the rainfall season) were simply removed from the data sample. During the hydrological modelling, missing rainfall data (for each day) were filled using the weather generator incorporated in SWAT (this model attributes to each subbasin one rainfall station). Since WaSiM is a spatially distributed model, no data gap filling was carried out. Instead, WaSiM interpolates, at daily time step the rainfall using the inverse distance weighting method (others methods are available). The other climate variables (temperature, global radiation, sunshine duration, wind speed, relative humidity) measured at synoptic stations did not have missing data. The flood frequency analysis (FFA) based on heavy rainfall was carried out exclusively on available data without any data gap filling. For the discharge data used during hydrological modelling, model performance was evaluated only using the available data during the simulation.

3 NON-STATIONARY FLOOD FREQUENCY ANALYSIS IN THE OUÉMÉ RIVER BASIN

In view of the magnitude and ubiquity of the hydroclimatic change apparently now under way, however, we assert that stationarity is dead and should no longer serve as a central, default assumption in water-resource risk assessment and planning. Finding a suitable successor is crucial for human adaptation to changing climate.
Milly et al. 2008

Abstract

A statistical model to predict the probability and magnitude of floods in non-stationary conditions is presented. The model uses a time-dependent and/or covariate-dependent generalized extreme value (GEV) distribution to fit the annual maximal (AM) discharge, and it is applied to five gauging stations in the Ouémé River Basin in Benin Republic, West Africa. Different combinations of the model parameters, which vary with respect to time and/or climate covariates, were explored with the stationary model based on three criteria of goodness of fit. The non-stationary model more adequately explains a substantial amount of variation in the data. The GEV-1 model, which incorporates a linear trend in its location parameter, surpasses the other models. Non-stationary return levels for different return periods have been proposed for the study area. This case study tested the hypothesis of stationarity in estimating flood events in the basin and it demonstrated the strong need to account for changes over time when performing flood frequency analyses.

Keywords: break points; non-stationary extreme value; climate indexes; flood frequency analysis; Ouémé basin

3.1 Introduction

Recently, many countries in West Africa have suffered from catastrophic floods (Burkina Faso, Senegal, Togo, Benin, Cote d'Ivoire, and Niger). These floods affected thousands of people through property damage and fatalities (EM-DAT, 2010). From population perception, floods have become increasingly frequent, and it is unknown whether they are caused by an increasing frequency in heavy rainfall, consequent change in discharge magnitude, or changes in land use. These devastating floods call for improvement in hydrological forecasts to reduce the vulnerability of local communities (Amoussou *et al.*, 2014).

Di Baldassarre *et al.* (2010) examined the recent flooding events over Africa and concluded that most of the recent deadly floods have occurred where the population has

been increasing. They note that while the total population has increased by a factor of 4, the urban population has increased by one order of magnitude; approximately the same magnitude as the increase in fatalities caused by floods. In fact, the intensive and unplanned urbanization and populations living in floodplains that are unwilling to relocate have increased flood vulnerability. The government's failure to provide appropriate maintenance for public infrastructure, such as highways, secondary roads, and bridges, can contribute to flood vulnerability (WMO, 2009). An analysis of the Ivory Coast (Goula *et al.*, 2011) reveals that the recrudescence of the inundation over the last three recent decades is due to nonexistent land use planning and unregulated urbanization. Similar conclusions were attained regarding the 2012 inundation in Niamey, the capital of the Niger Republic (Sighomnou *et al.*, 2013), and in Lusaka, the capital of Zambia (Nchito, 2007), where the flood risk has strongly increased because of the fast growth of the city in a flood-prone area.

Within the context of global warming, more intense and frequent heavy rainfall events are expected at the global scale as a result of enhanced water vapor in the atmosphere (Kunkel, 2003). Therefore, traditional statistical tools for flood risk assessments and infrastructure designs that are based on stationary heavy rainfalls series are inadequate; these tools should be adapted to climate projections and trends (Re & Barros, 2009).

A stationary series is relatively easy to forecast: one simply predicts that statistical properties will be the same in the future as they were in the past (Kiang *et al.*, 2010). However, these authors highlight that anthropogenic climate change and a better understanding of decadal and multi-decadal climate variability challenge the validity of this assumption. There is a need to update stationary risk assessment models for more robust and resilient predictions. For more than a decade, non-stationary distributions have been used to overcome these issues and provide accurate results. Non-stationary extreme value distributions are a powerful and useful tool for characterizing extremes in a changing climate (Brown *et al.*, 2008). If the rate of climate change increases, as is expected in the future, the need for such approaches will increase, and accurate information on the changing risk of extremes must be provided.

Through comparative studies, many researchers (Aissaoui-Fqayeh *et al.*, 2009, Katz *et al.*, 2002, Re & Barros, 2009, Tramblay *et al.*, 2013) show that non-stationary models are more suitable for the data than classical stationary models based on the deviance test. In another catchment situated in the same climate conditions, Tramblay *et al.* (2014) show that the non-stationary distribution surpasses the stationary distribution. Some authors (Alamou, 2011, Avahounlin *et al.*, 2013) focus on flood frequency analysis (FFA) in the Ouémé catchment, but non-stationarity was not considered in their analyses. Based on current knowledge, it is essential to account for non-stationarity when studying flood frequency.

To account for the non-stationarity in the GEV model, different expressions of the parameters have been proposed and analyzed in the literature (Conway & Mah, 2009, El-Adlouni & Ouarda, 2008, Hanel *et al.*, 2009, Khaliq & Ha, 2006, Lopez & Frances, 2013, Osorio & Galiano, 2012, Ribereau *et al.*, 2008, Sugahara & Porf, 2009, Tramblay *et al.*,

2013, Zenoni *et al.*, 2013). Let us recall here that the GEV model has three parameters: the location, scale and shape parameters. Mostly, the shape parameter is assumed to be constant (see, for instance, (Aissaoui-Fqayeh *et al.*, 2009, Katz *et al.*, 2002, Lopez & Frances, 2013)), while the location and shape parameters are assumed to be time- or covariant-dependent (the covariant also depends on time). Different expressions of the location parameter have been proposed in the literature, such as linear, quadratic, and exponential functions, sine wave functions of time, and covariates. As far as the scale parameter is concerned, few expressions are used in the literature. This is mainly because this parameter must be positive; to preserve the value, the exponential function is widely used (Aissaoui-Fqayeh *et al.*, 2009, Coles & Davison, 2008, Hanel *et al.*, 2009, Katz *et al.*, 2002, Kharim & Zwiers, 2004).

A comparison of these models based on statistical tests of the standard deviation show that the quadratic form of the location parameter more appropriately represents the standard deviation in the annual maximal rainfall (El-Adlouni & Ouarda, 2008). In contrast, at 5% of the significance level and based on the deviance statistical test, it was found that the linear function in the location parameter more accurately represents the dependency between the annual maximal precipitation and the covariant SOI (Southern Oscillation Index) than the quadratic form or the constant location parameter (Aissaoui-Fqayeh *et al.*, 2009). Brown *et al.* (2008) used a location parameter that depends on time, covariates when investigating stationary and non-stationary extreme value distributions fitted to observations of daily maximum and minimum temperatures to determine whether such extreme daily temperatures have changed since 1950. They found that the introduction of a trend covariate does not have a significant effect on the magnitude of the NAO (North Atlantic Oscillation) coefficient. Accounting for the diversity of the results obtained by these authors, we propose several model parameter combinations to cover the possible variance in the data.

An important research question is whether non-stationary probabilistic models can be suitably used while assessing extreme events in a changing climate. The objective of this research is to improve modeling tools for flood events in the context of climate change and to investigate possible changes in extreme discharges, which may explain the recent flooding events observed in the basin.

3.2 Materials and Methods

3.2.1 Study Area and Data

Benin is located in the inter-tropical zone (between 06°10' N and 12°25' N), and has a wet and dry tropical climate. Depending on the latitude and the distance from the Atlantic Ocean, the degree of aridity increases from south to north and, to a lesser extent, from west to east (Fink *et al.*, 2010).

The Ouémé Basin, which is approximately 49,256 km² (at the Bonou gauging station, see Figure 3-1) and 500 km in length, has a tropical climate that can be subdivided into three climatic zones according to the different rainfall regimes (Deng, 2007): (1) the

unimodal rainfall regime in North Ouémé comprising two seasons, *i.e.*, the rainy season from May to October, and the dry and hot season; (2) the bimodal rainfall regime in South Ouémé comprising two wet seasons, *i.e.*, a long season between March and July and a short season between September and mid-November, and a long dry season between November and March; and (3) the transitional rainfall regime in Central Ouémé comprising a rainy season between March and October, with or without a short dry season in August. The rain mostly originates from the Guinean Coast. The average annual precipitation varies between 960 mm in the north and 1340 mm in the south. Thus, the rainfall decreases northward and results in a strong natural vegetation gradient.

The Ouémé Basin flows southward, where it is joined by its main effluents, the Okpara on the left bank and the Zou on the right (Figure 3-1). Rainfall-runoff variability is high in this basin and leads to runoff coefficients that vary from 0.10 to 0.26 (of the total annual rainfall), with the lowest values in the savannahs and forest landscapes (Diekkrüger *et al.*, 2010). For all studied sub-catchments, the highest runoff coefficients were obtained in the years with the highest annual rainfall.

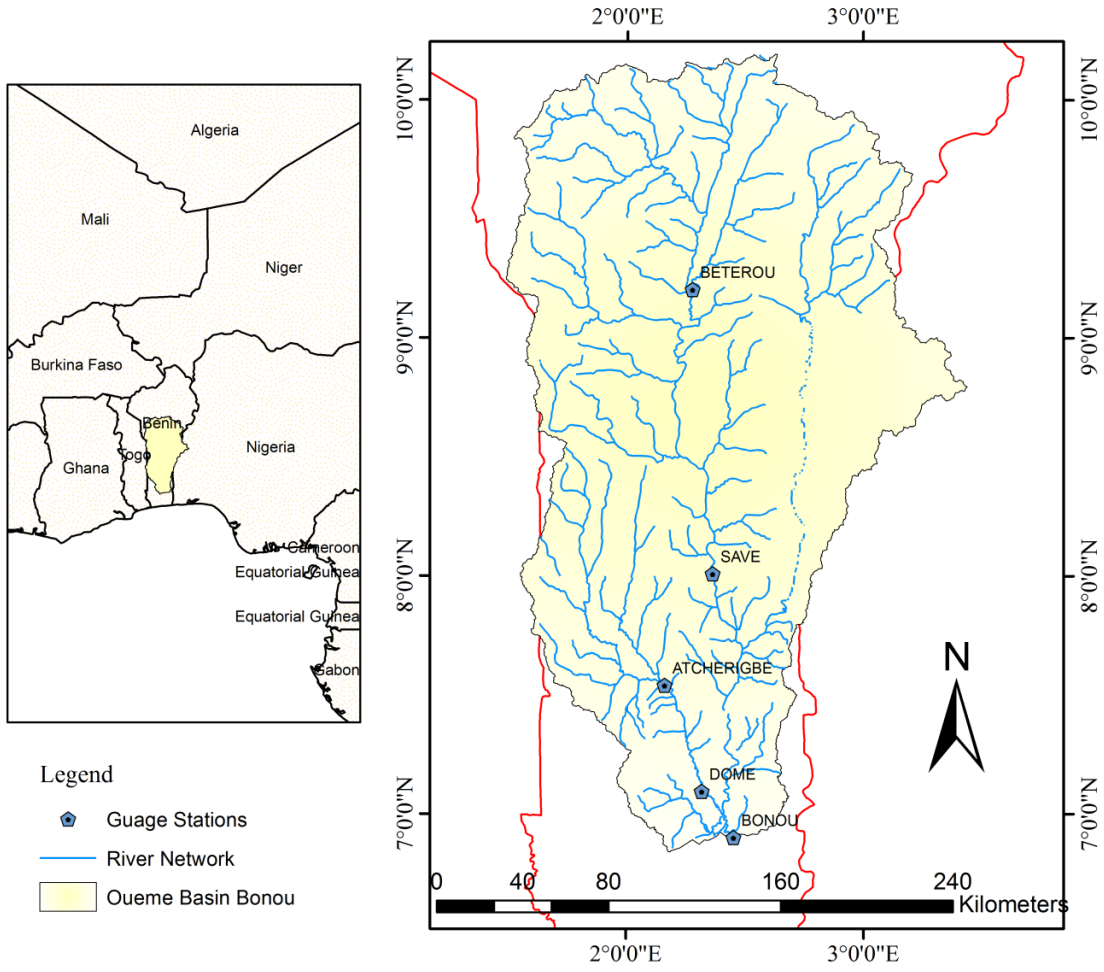

Figure 3-1: Ouémé River Basin at Bonou and the five gauging stations.

The data used in this part of the work are from the National Water Directorate (Direction Générale de l'Eau, DGEau). Twenty river gauges are available from the national observatory network in the Ouémé catchment (including the French Institute for Research and Development (IRD) river gauges). Five of the gauges that have at least 50 years of records and minimal missing data (particularly in the high discharge period) are considered in this study. In this study, discharge data for the period 1952–2009 are used.

3.2.2 Preliminary Analysis

As a first approach to study trends in extreme discharges during the study period 1952–2009, the Mann–Kendall and Spearman's rho trend tests were applied. A trend is considered to be present if it has been detected by both tests. The results show that at the 10% significance level, the annual maximum flood series of Bonou station (the main outlet of the basin) exhibited a statistically significant trend (Figure 3-2), while the other stations did not have any statistically significant trend when we considered the entire study period. Similar results were obtained by Robson et al., (1998) where any trend in the annual peak flow was not detected for a dataset of the U.K.

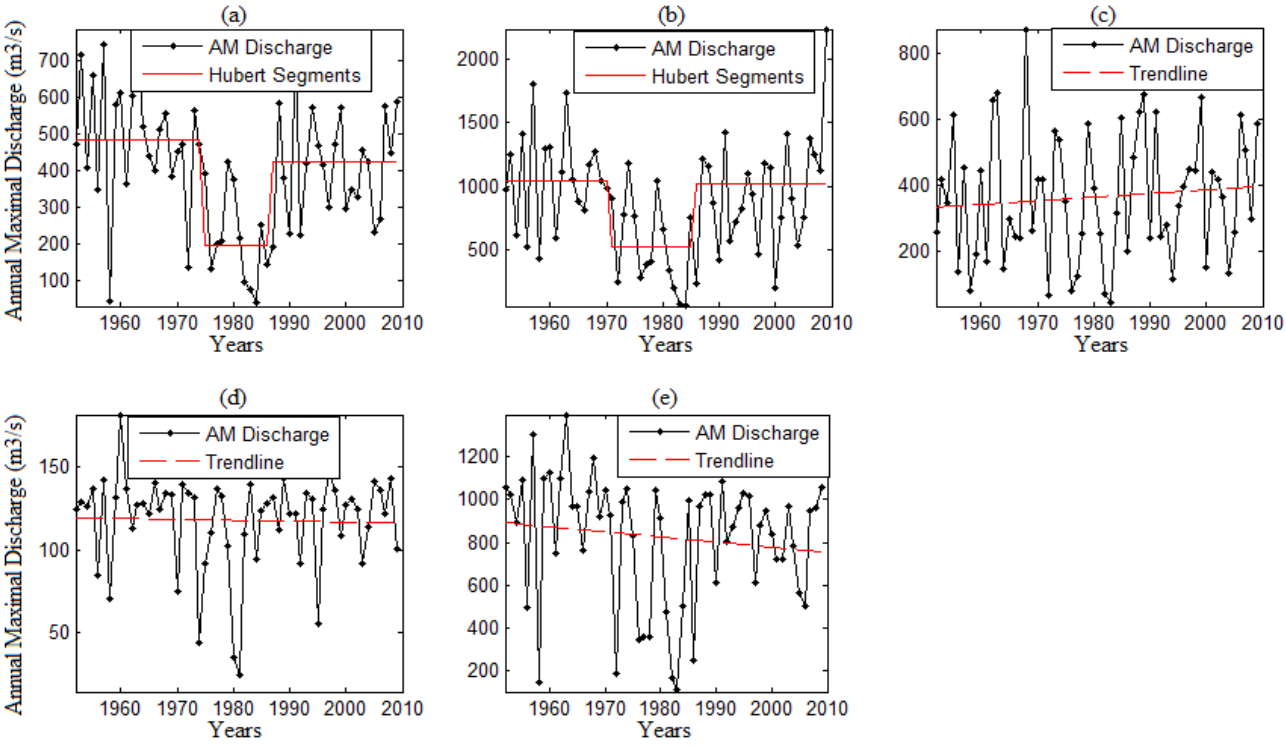

Figure 3-2: Plot of the annual maximal discharge and the corresponding linear trend line or Hubert segments at each station: (a) Bétérou, (b) Savè, (c) Atchérigbé, (d) Domè, and (e) Bonou.

Similarly, no site in Canada was found with upward trends (but they did detect some downward trends) in the annual peak flow or high quantiles of daily mean flow (Katz *et al.*, 2002). Likewise, no statistically significant trend was observed in the annual maximal series of the Yangtze River at the Yichang hydrological station (Xiong & Guo, 2004). In the work performed by Amoussou et al. (2014) on a basin with almost the same climatic conditions, no trend was found in annual maximal discharge over the period of 1988–2010, which is in accordance with our findings. However, as noted by Di Baldassarre *et al.* (2010), trend testing based on the statistical significance is questionable and less value should be given to the intended 'significance' rather than their direction and magnitude.

Another approach was to assess change points. The breakpoint analysis in the annual maximal discharge using the non-parametric Pettitt test (Pettitt, 1979) shows that there is a break point at 1974 in the data for Bétérou and Bonou, but there is no clear pattern for the other gauging stations. Considering the segmentation test of Hubert (Hubert *et al.*, 1989), which verifies whether differences in averages and standard deviations among periods are significant, we found change points in the data of Bétérou and Savè in somewhat similar periods (Figure 3-2a,b). The three sub-periods found by the Hubert segmentation for the Bétérou and Savè gauge stations are in accordance with the three rainfall periods in West Africa (Servat *et al.*, 1999, Vissin *et al.*, 2003): the wet period (up to 1970), the dry period 1971–1989, and the recovery period (1990 to present), assuming that land use is not the main driver of the discharge. Similar results were obtained in the Beninese part of the Niger Basin (Vissin *et al.*, 2003). In fact, the Bétérou and Savè gauging stations are the closest to the Niger Basin and share nearly the same climatic pattern. The important runoff deficit during the period of 1971–1989 corresponds to the drought period in West Africa. There are many different ways in which changes in hydrological series can take place (Kundzewicz & Robson, 2000): a change may occur abruptly (Bétérou and Savè, Figure 3-2 a,b) or gradually (Bonou, Figure 3-2e), or may take more complex forms. The most widely used tests for changes look for one of the following: trend in the mean or median of a series; or step-change in the mean or median of a series. The existence of abrupt changes or trends is a valid hypothesis for introducing non-stationarity into the estimation (Lopez & Frances, 2013).

3.2.3 Climate Indexes

Floods are influenced by the climate, and the connection between annual maximum floods and leading indicators of the current climate can be identified (Jain & Lall, 2001). Previous studies have applied the generalized extreme value (GEV) distribution, among other methods, to analyze extreme stream flow (Katz *et al.*, 2002, McKerchar *et al.*, 1994, Yang & Hill, 2012), and the results suggest that parameters of the GEV distribution can be a function of covariates, such as climate indexes and time. In this study, the correlation between different sets of climate indexes and AM discharge were explored to evaluate the strength of the relationship between the two variables and to study the conditional distribution of the annual maximal discharge as a function of climate indexes.

Among other regions, the Gulf of Guinea (GG) climate indexes—sea surface temperature (SST) and sea level pressure (SLP) (Mitchell, 2006)—were found to be significantly well correlated at the 5% level with the observed data (Table 3-1). In fact, there is a well-known teleconnection between the GG climate conditions and the West Africa monsoon dynamics (and the associated precipitation) (Janicot *et al.*, 2008). Positive SST (or Positive SLP) anomalies in the eastern equatorial Atlantic are accompanied by a southward shift of the inter-tropical convergence zone, along with positive (negative) rainfall anomalies in the Guinean region (Table 3-1) except for Domè station. This is consistent with the results previously obtained (Janicot *et al.*, 1998, Losada *et al.*, 2010) for West African monsoon dynamics and eastern equatorial Atlantic SST anomalies. More information on the climate indexes used as covariates can be found in the appendixes or in (Hounkpè, Afouda, & Diekkrüger, 2015).

Table 3-1: Correlation (significant at the 5% level) between Ouémé River annual maximum discharge series and climate indexes. The longitude and latitude are given for the SST (sea surface temperature) and SLP (sea level pressure) grid cell (4 by 6-degree latitude-longitude resolution, see Mitchell (2006) for more explanation).

Stations	**Bonou**	**Bétérou**	**Savè**	**Atchérigbé**	**Domè**
SST or SLP	SLP	SLP	SLP	SST	SST
Period	Annual Average	Annual Average	August	July	August
Longitude	357°	357°	357°	351°	3°
Latitude	−4°	−4°	−4°	−4°	4°
Correlation coefficient	−0.6	−0.6	−0.5	0.6	−0.3

3.2.4 Method for Modeling Extreme Stream Flows

The generalized extreme value (GEV) distribution is a flexible three-parameter model that combines the Gumbel, Fréchet, and Weibull extreme value distributions. Its cumulative distribution function is (Eq. 3-1):

$$f(x) = \begin{cases} \exp\left(-\left(1+\kappa\frac{x-\mu}{\sigma}\right)^{-\frac{1}{\kappa}}\right) & \kappa \neq 0 \\ \exp\left(-\exp(1-\frac{x-\mu}{\sigma})\right) & \kappa = 0 \end{cases}, \qquad \text{(Eq. 3-1)}$$

where μ, σ and κ are location, scale and shape parameters, respectively. The location parameter μ indicates where the distribution is centered; the scale parameter $\sigma \neq 0$ indicates the spread of the distribution; and the shape parameter κ indicates the behavior of the distribution's upper tail (Coles, 2001). Distributions associated with $\kappa < 0$ are

called Fréchet, and they include well-known long-tailed distributions, such as the Pareto, Cauchy, Student-t, and mixture distributions. If $\kappa = 0$, the GEV distribution is the Gumbel class and it encompasses the normal, exponential, gamma, and lognormal distributions where the lognormal distribution has a moderately heavy tail (Markose & Alentorn, 2011). Finally, in the case where $\kappa > 0$, the distribution class is Weibull. These are short-tailed distributions with finite lower bounds and include distributions such as uniform and beta distributions. To estimate a design value (or return level), the quantile function $f^{-1}(1-p)$ with $0 < p < 1$ can be expressed as (Coles, 2001):.

$$f^{-1}(1-p) = \begin{cases} \mu + \left(\frac{\sigma}{\kappa}\right)\{[-\ln(1-p)]^{-\kappa} - 1\}; & \kappa \neq 0 \\ \mu + \sigma\{-ln[-\ln(1-p)]\}; & \kappa = 0 \end{cases} . \quad \text{(Eq. 3-2)}$$

If the shape parameter $\kappa > 0$, then the GEV distribution is said to be heavy tailed (Katz *et al.*, 2002). Because its probability density function decreases at a slow rate in the upper tail, moments of the GEV are infinite for orders greater than $1/\kappa$ (e.g., the variance is infinite if $\kappa > 1/2$; and the mean is infinite if $\kappa > 1$). If $\kappa < 0$, then the distribution has a bounded upper tail. The case of $\kappa = 0$ (Eq. 3-2), obtained by taking the limit of the general expression as $\kappa \to 0$, is called the Gumbel distribution (*i.e.*, an unbounded, thin tail).

Seven GEV models are considered in this study to cover a variety of combinations of model parameters. The shape parameter for all models is constant. Table 3-2 shows the different GEV models and their parameters. It is interesting that GEV-0 is nested in GEV-1, which is also included in GEV-2. Similarly, the GEV-0 model is nested in GEV-3, which is also included in GEV-4.

Table 3-2: Different GEV model parameters. *Cov* (*t*) represents the covariate, which may be SST (sea surface temperature) or SLP (sea level pressure) (Adapted from (Hounkpè, Afouda, Diekkrüger, *et al.*, 2015)).

Models	Location Parameter	Scale Parameter	Shape Parameter
GEV-0	μ = constant	σ = constant	κ = constant
GEV-1	$\mu(t) = \mu_0 + \mu_1 * Cov(t)$	σ = constant	κ = constant
GEV-2	$\mu(t) = \mu_0 + \mu_1 * Cov(t)$	$\log(\sigma) = \sigma_0 + \sigma_1 * Cov(t)$	κ = constant
GEV-3	$\mu(t) = \mu_0 + \mu_1 * t$	σ = constant	κ = constant
GEV-4	$\mu(t) = \mu_0 + \mu_1 * t$	$\log(\sigma) = \sigma_0 + \sigma_1 * t$	κ = constant
GEV-5	$\mu(t) = \mu_0 + \mu_1 * t + \mu_2 * Cov(t)$	σ = constant	κ = constant
GEV-6	$\mu(t) = \mu_0 + \mu_1 * Cov(t)$	$\log(\sigma) = \sigma_0 + \sigma_1 * t$	κ = constant

The parameters were estimated in this study using the Maximum Log-likelihood Estimator (MLE) from R (R Core Team, 2014) and the Extremes Toolkit (Gilleland & Katz, 2005). The Nelder-Mead algorithm was used as the optimization method. Three criteria of goodness of fit were chosen to identify the optimum model: the likelihood ratio

Test (LRT) (Coles, 2001), the Akaike Information Criterion (AIC) (Akaike, 1974), and the Bayesian Information Criteria (BIC) (Schwarz, 1978). Lower the AIC and BIC, better the fit and consequently the model.

Additionally, Latin Hypercube sampling (McKay *et al.*, 2000), which is a statistical method for generating a sample of plausible collections of parameter values from multidimensional distribution, is used to determine the non-stationary return levels from the different parameters ranges of the non-stationary GEV distribution obtained for each station. Five hundred parameter samples were obtained for each fitted GEV distribution and the different return levels corresponding to each sample computed for a given return period. Since the return level is a function of the year, an ensemble of 500 × 58 years = 29,000 realizations obtained for each return period. The uncertainty bounds of the computed return level is derived based on 0.05 and 0.95 posterior probability intervals of the ensemble (Cheng *et al.*, 2014). In this study, the 50th percentile is considered as high risk, the 75th percentile (high quartile) is medium risk and the 95th percentile is low risk. If the return level computed for a given return period is underestimated (for instance the 50^{th} percentile), higher will be the risk (the likeliness of getting flooded) associated to that estimation. This is why the 95^{th} percentile is associated with a low risk meaning lesser chance (low probability) for the infrastructure designed to be underestimated.

3.3 Results and Discussions

The synthesis of the non-stationary model performances compared to the stationary case is given in Table 3-3. The models are ranked according to the goodness of fit and "ns" (non-significant) is used to note that the model did not show significant and strong improvement compared to GEV-0 (the stationary model). The classification is performed for models that have *p*-values less than or equal to 0.01 (1% significance level). The rank "1" is given to the model with the smallest value of AIC and BIC. According to these criteria, the GEV-1 model, whose location parameter is a linear function of covariates (SST or SLP) and whose other parameters are constant, is the best model for explaining change in the extreme AM streamflow at the different stations. This finding is explained by the high correlation between the annual maximum discharge (AMD) and the climate index.

Table 3-3: Model ranking; "ns" (non-significant) is used to note that the model did not show significant and strong improvements compared with GEV-0.

Model	GEV-0	GEV-1	GEV-2	GEV-3	GEV-4	GEV-5	GEV-6
Atchérigbé	ns	1	ns	ns	ns	2	3
Bétérou	3	1	ns	ns	ns	2	ns
Bonou	3	1	ns	ns	ns	2	ns
Domè	2	1	ns	ns	ns	ns	ns
Savè	4	1	ns	ns	ns	2	3

When incorporating a linear time trend into the location parameter (GEV-3) and/or a linear covariate-dependent trend into the scale parameter (GEV-2), the model performances are not satisfactory; they exhibit the highest values of the AIC and BIC and the *p*-value is nearly 1. The same conclusion can be drawn for the GEV-4 model. The GEV-5 model, whose location parameter depends on both time and covariates, exhibits an improvement compared with the stationary case except in one station out of six. For the different stations, except for Domè, the *p*-values were small, similar to the results of GEV-1. The second rank given to this model (GEV-5) was due to its number of parameters (five) compared with GEV-1, which has four parameters. The basic principle is parsimony, *i.e.*, obtaining the simplest model that explains as much of the variation in the data as possible. The addition of one or more parameters must be justified in terms of the performance and accuracy in describing variations in the observed data compared with the model with fewer parameters. The model requires a description of the process that generated the data, rather than the actual data; thus, it is necessary to assess the strength of the evidence for the more complex model structures (Coles, 2001). Therefore, if the evidence is not particularly strong, the simpler model should be chosen.

Table 3-4 presents the model parameters and values of the performance criteria for all of the stations. The location and scale parameters are high for Savè and Bonou.

Table 3-4: Parameters of the GEV-1 model and the performance criteria; AIC: Akaike Information Criteria and BIC: Bayesian Information Criteria. Values in bracket are the standard deviations of the corresponding parameter and $-ln(L)$ is the log-likelihood.

Stations (1952-2009)	Models	Location		Scale	Shape	Performance Criteria				
		μ_0 ($\Delta\mu_0$)	μ_1 ($\Delta\mu_1$)	σ_0 ($\Delta\sigma_0$)	κ ($\Delta\kappa$)	$-ln(L)$	Deviance Statistic	*p*-value	AIC	BIC
Atchérigbé	GEV-1 4par.	317.7 (22.5)	148.0 (28.8)	151.2 (16.1)	−0.2 (0.1)	376	22	3e−06	760	768
Bétérou	GEV-1	347.5 (21.2)	−270 (49.3)	149.6 (14.7)	−0.3 (0.1)	370	27	<1e−06	749	757
Bonou	GEV-1	749.2 (36.8)	−389 (75.7)	259.7 (27.0)	−0.5 (0.1)	399	24	1e−06	805	813
Domè	GEV-1	122.6	−24.6	34.2	−1.2	260	30	<1e−06	528	537
Savè	GEV-1	812.4 (57.7)	−357 (88.5)	374.2 (36.1)	−0.2 (0.1)	427	17	3.5e−05	862	870

An analysis of the shape parameter obtained for all of the models and all of the gauge stations shows that this parameter is negative everywhere, even when considering the uncertainty bounds ($\kappa \pm \Delta\kappa$) (see table 3-4); thus, the distribution class corresponding to the data is the Fréchet distribution. This parameter varies very slowly from −0.5 (GEV-1 at Bonou) to −0.2 (GEV-1 at Atchérigbé), *excluding the case of Domè*. A greater absolute value of this parameter corresponds to a greater extreme discharge. This is the case with the Bonou gauge station, which is located at the principal outlet of the Ouémé River Basin.

3.3.1 GEV-1 Model

The GEV-1 model presents a linear trend in the covariates of the location parameter while the other parameters remained constant. The likelihood ratio test is a more analytical method of determining the best fit. The GEV-1 model is said to be appropriate to the detriment of GEV-0 for a given station if the *p*-value is less than or equal to 0.01 and if the deviance statistic is greater than the χ_1^2 distribution, which is 3.8. The deviance statistic D for comparing these models for all stations varies from 17 to 26 (Table 3-4), while the 95% quantile of the χ_1^2 distribution is only 3.8. Thus, GEV-0 is rejected at the 0.05 level of significance and GEV-1 is preferred. These values are overpoweringly large, meaning that the model with a location parameter that is linearly related to SST or SLP explains a substantial amount of the variation in the data. Strong evidence supports the use of the GEV-1 model, *i.e.*, the statistic of the *p*-value varies from nearly 0 to 3.5e–05 (Table 3-4), *versus* the null hypothesis that the GEV-0 model is a fit better for the data than GEV-1. Furthermore, the Akaike Information Criteria (AIC), as well as the Bayesian Information Criteria (BIC), applied to all the models produced the lowest values for GEV-1 and confirmed that GEV-1 is the most appropriate model for analyzing flood data in the study area. The SST and SLP in the Gulf of Guinea appear to have a significant teleconnection with the AM discharge, and the use of related climate indexes could help explain the behavior of the extreme discharge. These results are consistent with previous findings (Aissaoui-Fqayeh *et al.*, 2009), where it was stated that the linear function of the location parameter more accurately represents the dependency between the annual maximal precipitation and the SOI covariant than the quadratic form or constant location parameter.

Figure 3-3 displays the probability and quantile plots, the return-level plot, and the density estimate plot for the GEV-0 fit to the Bétérou station. In the case of a perfect fit, the data would line up on the diagonal of the probability and quantile plots. The quantile plot compares the model quantiles against the data (empirical) quantiles. A quantile plot that deviates greatly from a straight line suggests that the model assumptions may be invalid for the data plotted (Gilleland & Katz, 2005). In the present case, the data mostly line up on the first diagonal of the probability and quantile plot, with some deviations from the straight line. The return level plot shows the return period compared with the return level with an estimated 95% confidence interval.

When incorporating covariates in the location parameter (GEV-1, GEV-3), the fit appears to be better (Figure 3-4), with the residual probability plot and quantile plot adjusting satisfactorily to the diagonal at the Bétérou station.

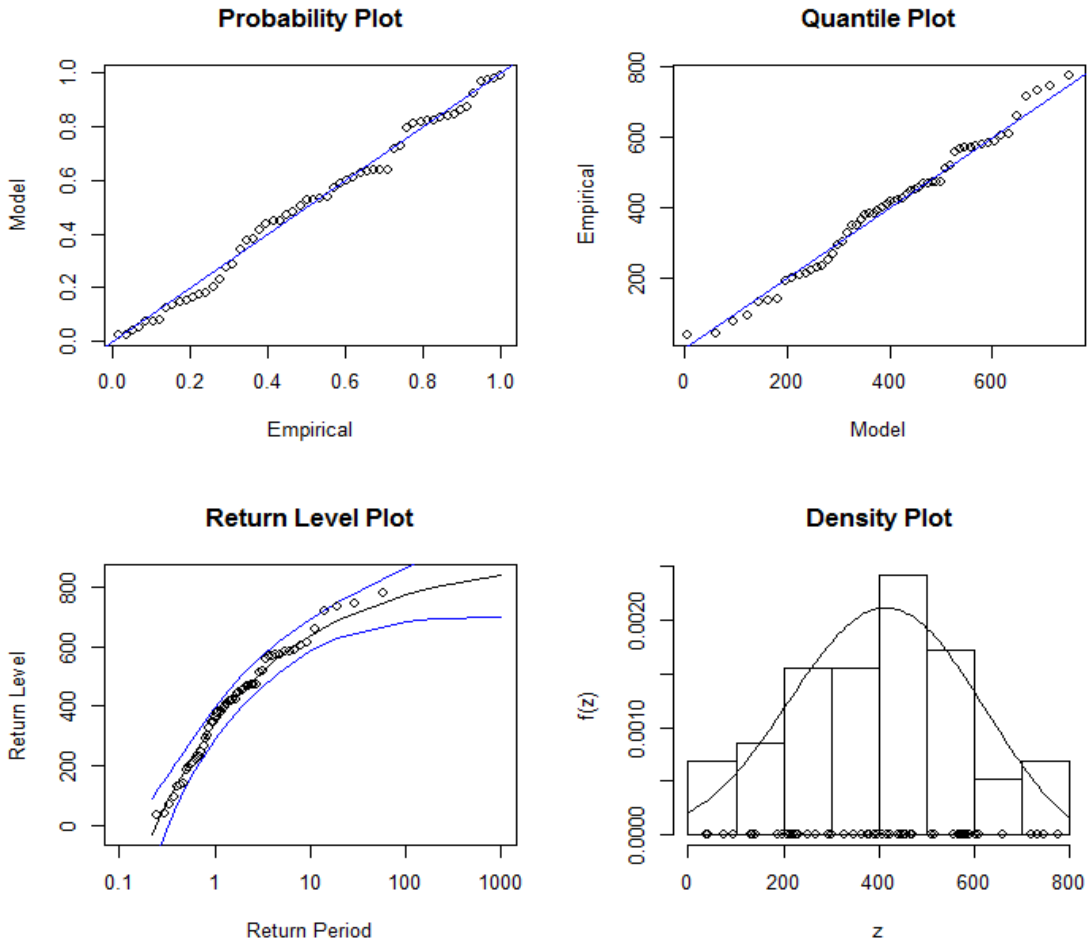

Figure 3-3: Diagnostic plots for the GEV-0 fit to the Bétérou station annual maximum discharge.

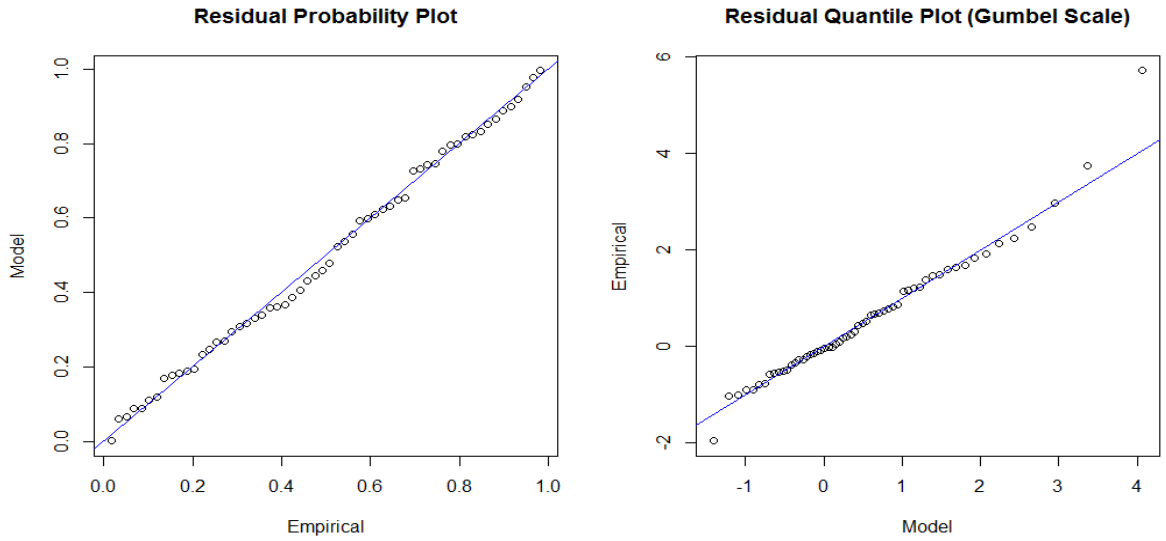

Figure 3-4: GEV fit diagnostics for the GEV-3 to the Bétérou station's annual maximal discharge.

3.3.2 Non-Stationarity in the Location Parameter

The evolution of the location parameter and its trend at the Atchérigbé and Bétérou stations as a function of time is displayed in Figure 3-5. In fact, the location parameter is a function of SST or SLP, which are also, functions of time. To facilitate the understanding of the location parameter, which specifies where the distribution is centered, it is plotted as a function of time. Notably, there is high variation in the location parameter with time. This finding is an improvement compared with the work previously performed by Alamou (2011), where this parameter was assumed to be constant.

Linear regression was used to describe the possible linear trend in the location parameter series quantitatively. The linear regression method used is the non-parametric Sen's slope estimator. It is a robust method that selects the median slope among all lines through pairs of two-dimensional sample points (Sen, 1968). The slopes, *i.e.*, the change per unit time, obtained are negative, except for Atchérigbé, and vary from −3.0 at Savè to −0.3 at Domè. Therefore, the parameter experiences a downward trend. Considering the study period, the mean value of the location parameter or the mean value of the AM discharges decreased by $2.98 \times (2009 - 1952) = 169.9\, m^3/s$ (equivalent to $7.2\ 10^{-3}\ m^3/s/\ km^3$ reported at the basin area) at Savè to $0.26 \times (2009 - 1952) = 14.8\, m^3/s$ (equivalent to $2.1\ 10^{-3}\ m^3/s/\ km^3$ reported at the basin area) at Domè. To test the significance of this trend, we applied the Mann-Kendall and Spearman Rho trend tests. At the 5% significance level, the downward trends observed in the location parameter series are statistically significant for the study period. The significance of the trend in the location parameter should be carefully considered because the relationship between the AM Discharge and the SST or the SLP is not perfect. Atchérigbé is the only station where a significant upward trend in the location parameter was observed.

This result also introduces the possibility for the future prediction of floods in the study area. In fact, using a climate model, it is possible to obtain SLP or SST data in the Gulf of Guinea for a future time period. Knowing that a statistical distribution is characterized by its parameters, the use of covariates in a given statistical distribution is effective by writing its parameters as a function of the covariates. Modeling the parameters as functions of time or covariates helps us to better understand the trends regarding extreme climate events, and it allows predictions to be made (for example, up to 2020) regarding the probability of future occurrences of a particular flood event. In doing so, the non-stationary distribution model can be an efficient tool to (1) account for dependencies between extreme value randomness and temporal evolution of the climate and (2) forecast the future evolution of the random variable. This finding justifies the use of climate indexes to predict seasonal forecasts of precipitation and discharge over West Africa (Philippon, 2002). The evaluation of possible future change in flood frequencies analyses using future climate data is beyond the scope of this study. Nevertheless, this evaluation will be done in future studies.

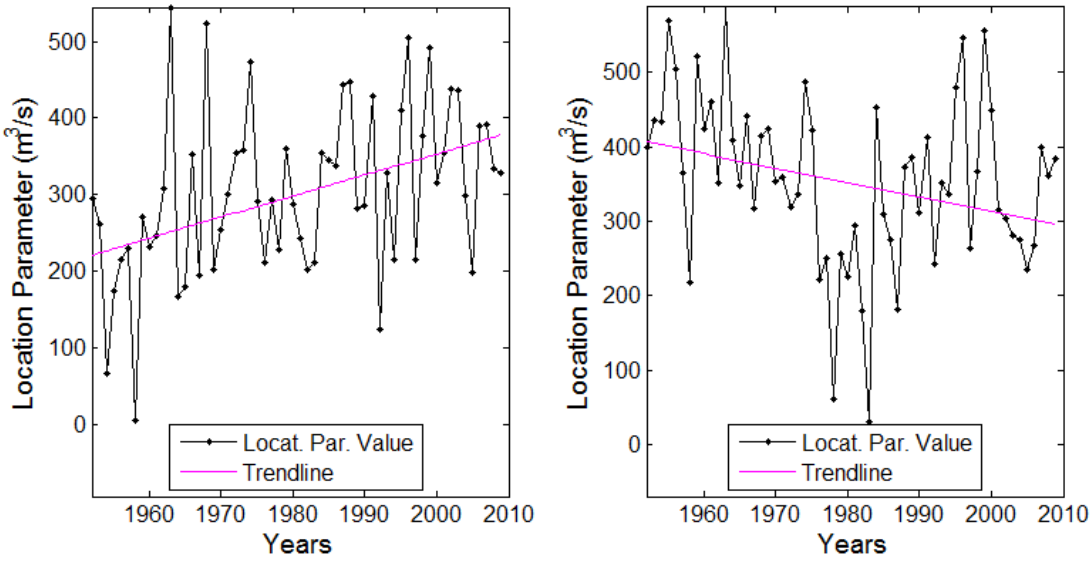

Figure 3-5: Evolution of the location parameter and its trend as a function of time at the Atchérigbé (left) and Bétérou (right) stations. The trend line is plotted using a non-parametric Sen's slope estimator.

3.3.3 Stationary and Non-Stationary Effective Return Level Estimation

The study of floods in operational hydrology aims to estimate flood events for a given *a priori* probability to obtain flood maps, design protective measures, or plan flood risk management (Lopez & Frances, 2013). It is possible to find the quantile corresponding to a specified probability of exceedance or return period for the non-stationary case, except here the return value varies depending on the year. These estimated return values are obtained by substituting the parameter estimates into Equation (2) for the quantile function of the GEV distribution. Figure 3-6 shows the effective design value for the 25-year return period under non-stationary conditions (GEV-1) at different stations. Generally, the plots of the return values preserve the initial trend in the AM discharge. It is interesting to note that the non-stationarity models indicate the existence of periods when the flood risk experiences upward or downward trends following different rainfall regimes during the second half of the century over West Africa (Servat *et al.*, 1999). For example, until the 1990s, there is a decreasing flood risk, which may be due to the droughts in the early 1980s; after the 1990s, there is a recovery to the normal conditions. In contrast, for Atchérigbé, an increase was observed during the entire study period. This was already observed in the annual maximal discharge series. This station was the only one with an increase in the AM discharge. The high variability in the 25-year and 50-year design floods shows that using a constant return discharge could lead to high errors in the estimations. This approach is an improvement compared with previous works performed on the same basin (Avahounlin *et al.*, 2013).

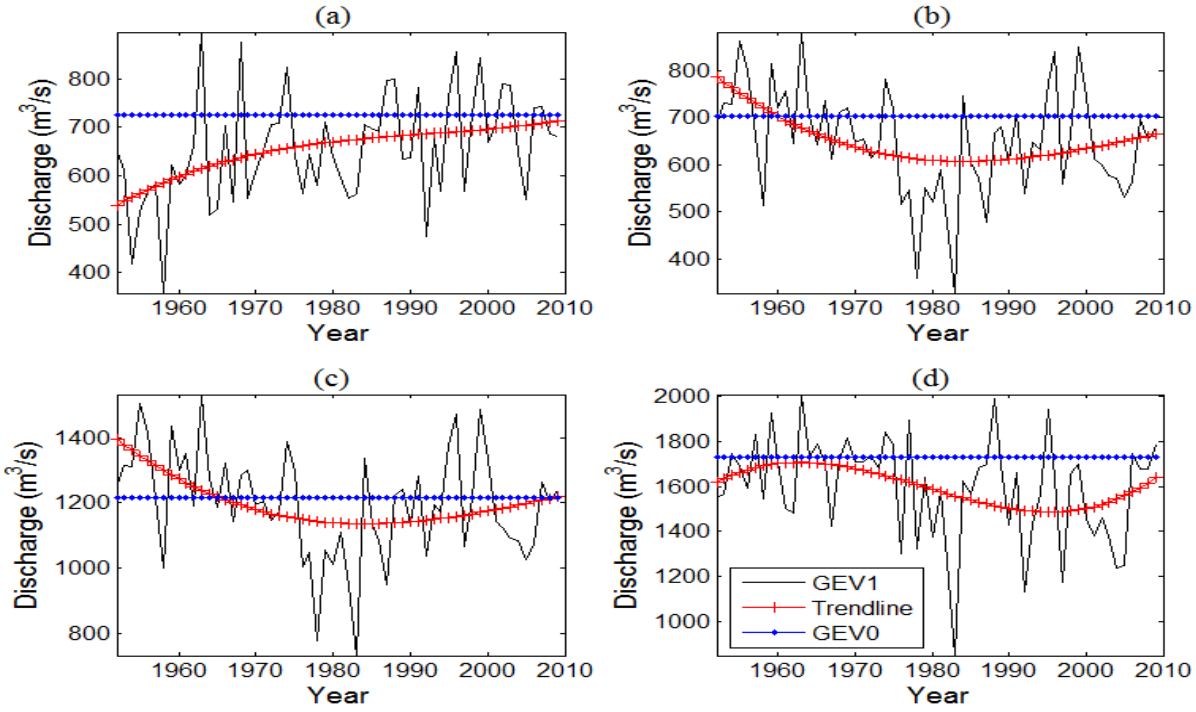

Figure 3-6: The 25-year effective flood values of the annual maximal discharge for the study period (1952–2009) at (a) Atchérigbé, (b) Bétérou, (c) Bonou, and (d) Savè based on the GEV1 (non-stationary) and GEV0 (stationary) models.

This result shows that treating the flood events as stationary may lead to high uncertainties, which may be manifested in two ways: underestimation of the flood risk or over-sizing of the flood design structures. At the Savè station, during the 58 years in the records, the 25-year flood has varied from 846 m^3/s to 2009 m^3/s. The maximal value recorded is much greater than that estimated for stationary conditions (1727 m^3/s). A similar conclusion was found for the other stations. The trend lines exhibited by Bétérou and Bonou were similar with a decreasing flood risk around the year 1980. For Savè station, there is a shift for the decreasing flood risk in comparison with the previous stations. Atchérigbé station is the only one exhibiting clearly an increasing trend for all the study period. These results test the hypothesis of stationarity in estimating flood events and show the strong need to account for the change over time in the flood frequency analysis. Because of the probability of excess changes from year to year in the context of non-stationarity, the concept of "return period" should be re-examined.

3.3.4 Non-Stationary Design Values Estimation

For design and risk assessment purposes under environmental change, estimates of the non-stationary return periods are needed. The plot of the return levels *versus* the corresponding return periods at four stations is displayed in figure 3.7. This is computed from an ensemble of 29,000 realizations for each return period. As can be seen on this

figure, the interquartile bounds encompass the empirical return levels, indicating acceptable simulation. Cheng et al. (2014) used the median of an ensemble as a measure of non-stationary return temperature. As can be seen in Figure 3.7, the median of the ensemble is representative of the trend in the empirical quantile and could be used as a measure for the non-stationary return discharge. For infrastructure design purposes, using the median of the ensemble may result in underestimation of the flood risk. Therefore, to minimize the flood risk, the high quartile of the ensemble is used as the final return level. This choice is also supported by the fact that the high discharges are often underestimated when using the rating curve (Di Baldassarre & Claps, 2010). The estimated return level should therefore be slightly higher than the empirical return values. This approach is similar to the stationary approach but it has the advantage of accounting for change in the location parameter.

Table 3-5: Stationary and non-stationary return levels for Atchérigbé, Bétérou, Bonou, and Savè under different risk levels.

Return Period	2	5	10	15	25	30	40	45	50	60	Risk Level
Non-stationary return level											
	353	495	572	635	653	667	689	697	704	717	High Risk
Atchérigbé	423	567	648	714	734	749	772	781	789	802	Medium Risk
	551	693	772	840	860	875	898	908	916	930	Low Risk
	408	537	602	652	666	676	692	698	703	711	High Risk
Bétérou	480	610	674	725	739	750	767	773	779	788	Medium Risk
	599	728	793	844	858	869	886	892	897	907	Low Risk
	849	1037	1114	1166	1179	1189	1202	1207	1211	1218	High Risk
Bonou	953	1141	1219	1272	1285	1294	1308	1313	1317	1324	Medium Risk
	1123	1311	1390	1443	1456	1465	1479	1484	1489	1496	Low Risk
	922	1270	1459	1614	1658	1693	1745	1766	1784	1814	High Risk
Savè	1014	1372	1573	1743	1793	1833	1892	1915	1936	1970	Medium Risk
	1210	1565	1763	1936	1988	2031	2092	2118	2139	2178	Low Risk
Stationary return level											
Atchérigbé	348	521	619	702	726	745	774	786	796	813	
Bétérou	406	560	634	689	704	716	732	738	743	752	
Bonou	853	1094	1195	1265	1282	1295	1313	1320	1326	1335	
Savè	851	1253	1480	1671	1727	1771	1837	1863	1886	1924	

For Atchérigbé and Bonou, the 75 quantile curve is similar to the one of the stationary approach but for Bétérou and Savè, the 75 quantile overtakes the stationary curve. Table 3-5 shows some stationary and non-stationary return values for different return periods. Domé is not considered in the rest of the work giving that its covariate explains less than 50% of the behavior of the annual maximal discharge at this station. Due to the limited length of data, it was not possible to carry out a proper validation of the stationary and non-stationary models (e.g., by splitting the observation period into calibration and validation).

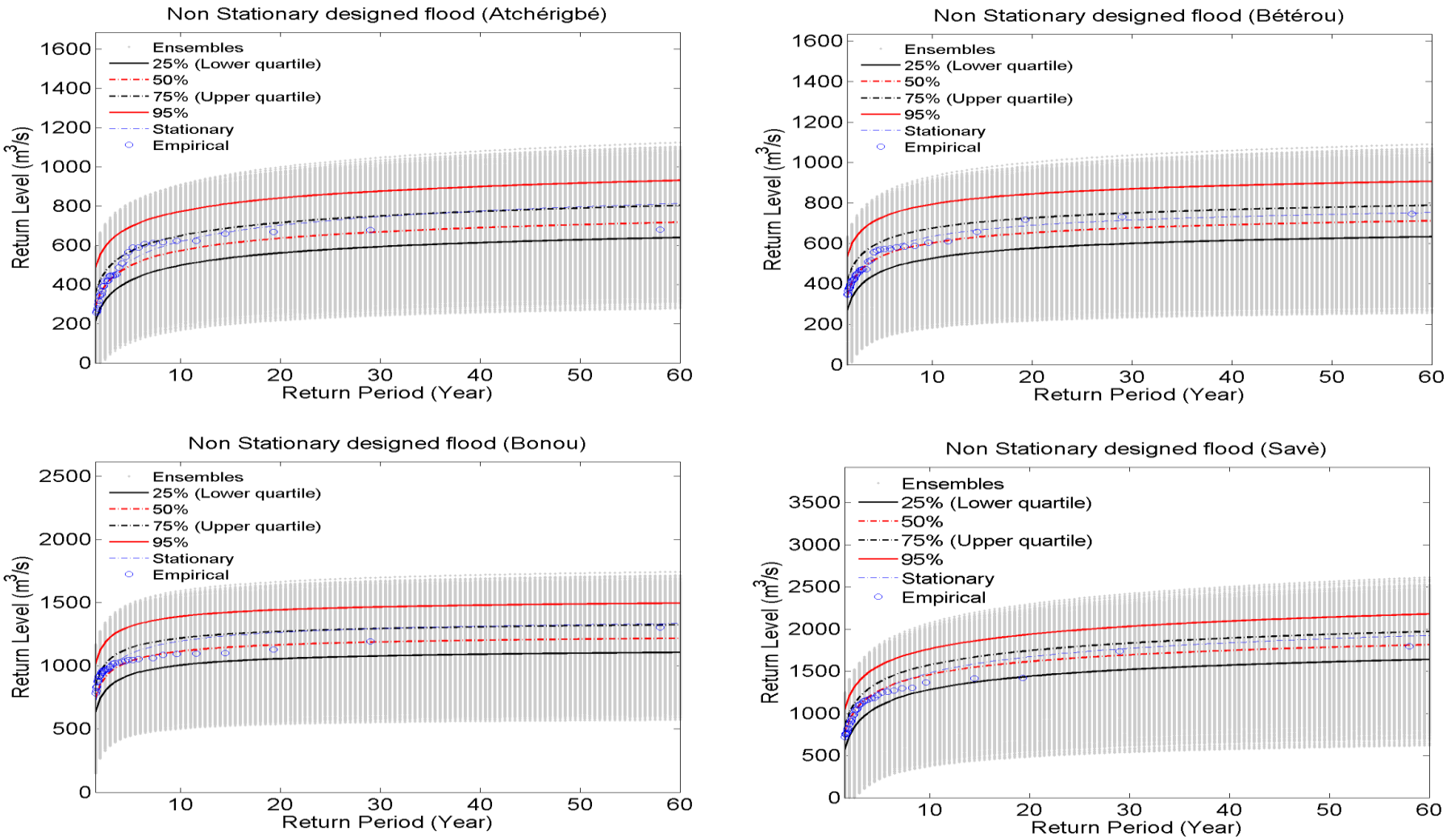

Figure 3-7: Annual maximal discharge (return levels) *versus* return period for Atchérigbé, Bétérou, Bonou, and Savè for the period 1952–2010. Plotted are the ensemble, the median, the upper and lower quartiles (25 and 75 percentiles), the 95 percentiles of the ensemble, the stationary and empirical return levels.

3.4 Conclusions

An extreme-value non-stationary probabilistic model was improved in this study to assess its suitability for frequency analysis of floods in the main sub-basins of the Ouémé River and to investigate possible changes in the extreme discharge, which may explain the recent flooding events observed throughout the country.

Different GEV models have been applied to estimate the quantiles at five gauging stations in the Ouémé Basin. A comparative study of these models based on three performance criteria showed that GEV-1 is the most adequate model for explaining the variance in discharge observations over the Ouémé Basin. These criteria were the deviance statistic, the AIC, and the BIC. This case study shows that it is necessary to incorporate non-stationarity into extreme flood frequency analyses by linking climate variables or time with the distribution parameters to improve estimations.

An analysis of 25- and 50-year floods shows that considering flood events as stationary leads to high uncertainties, which can have two effects: underestimation of the flood risk or over-sizing of the flood design structures. Structural measures remain important elements, and their designs should be updated by considering non-stationarity to reduce the vulnerability of human beings and goods exposed to flood risks. Based on the previously achieved results, non-stationary return values have been proposed for the basin base on the 75 percentile of an ensemble of 29,000 realizations using the Latin hypercube sampling method. Strategic options to reduce the flooding risk in Benin must strike a balance between infrastructural and non-infrastructural interventions, including cross-cutting measures, plans for their implementation, and updates over time based on available resources (World Bank, 2011b). In particular, introduction of flood forecasting systems, improving population awareness and preparedness, urban planning, and discouraging human settlements in flood-prone areas, along with the development of local institutional capacities, are effective and socially sustainable actions that should be pursued (Di Baldassarre *et al.*, 2010). Strengthening the capacities of the various actors concerned with the implementation of the strategy, as well as the integration of flood and disaster risk management, could help reduce flood impacts on the population. Structural measures will remain important elements, and their design should be updated by considering non-stationarity to reduce the vulnerability of human beings and goods exposed to flood risks. Taking into account the evolution of this natural hazard and its trends, one must shift from defensive action against hazards to management of the risk and living with floods. Further, flood prevention should not be limited to flood events, which occur often, but should also consider rare hydrological events.

This generalization of the classical model based on the hypothesis of stationarity and normality allows climate change to affect the evolution of the distribution parameters and provides predictions of the probability of future occurrences of a particular flood event. Further investigations that consider land use change are required for a better understanding of flood risks in the basin.

4 ASSESSING POTENTIAL CLIMATE CHANGE IMPACT ON EXTREME RAINFALL OVER OUÉMÉ RIVER BASIN

Changes to the magnitude, character and spatial distribution of extreme rainfall may have serious impacts upon many sectors such as agriculture, industry, transport, power generation, the built environment and ecosystems.
Fowler et al., 2005

Abstract

Climate change has severe impacts on natural resources, food production and consequently on food security especially in developing countries. Likely accentuated by climate change, flooding is one of the disasters that affect people and destroies agricultural land and products. At different governance levels and scales, appropriate responses are needed. Cluster analysis using scaled at-site characteristics was used to determine homogeneous rainfall regions. A methodology for detecting change was applied to heavy daily rainfall of 34 stations across the Ouémé basin, Benin, in order to assess potential change in its characteristics. The spatial variability of the detected changes in return periods was analyzed using the kriging interpolation method. For this analysis, up to 92 years (1921–2012) of rainfall data were used. Three homogeneous regions were found by the cluster analysis. For all studied return periods, 82% of the stations showed statistically significant change in daily precipitation, among which 57% exhibited a positive change and 43% negative change. A positive change is associated with an increase in heavy rainfall over the area of concern. An analysis of the interpolated change in heavy rainfall of different return periods revealed an east–west gradient from negative to positive along the lower Ouémé basin (Region 2). From the middle to the upper Ouémé (Region 1 and 3), a decreasing tendency of heavy rainfall is dominant mainly for the non-homogeneous period. This result of the complex pattern of changes could be veritable information for decision makers and consequently for development of appropriate adaptation measures.

Keywords: extreme rainfall; climate change; Ouémé basin

4.1 Introduction

Heavy rainfall events are one of the natural hazards that lead to degradation processes like flash floods or flooding as well as severe soil erosion, which can have regional devastating power and pose a serious hazard to lives and property. From 1900 to 2006, floods in Africa killed nearly 20,000 people and affected approximately 40 million more, and caused damage estimated at about US$4 billion (Davidson *et al.*, 2007). In Benin, a

number of extreme floods has occurred over the last 30 years and caused great economic losses. Between 1980 and 2009, there have been 14 major floods affecting a total of 2.26 million peoples (EM-DAT, 2010). According to the World Health Organization, an estimated 500,000 people are at risk of flooding (UNOCHA, 2008). The floods in 2008 and 2009 caused widespread damage and displacement, affecting around 158 thousand and 120 thousand people respectively (EM-DAT, 2010). Floods have become increasingly frequent leading to the question of whether this was due to the increasing frequency of heavy rainfall or changes in land use patterns (Hounkpè, Diekkrüger, *et al.*, 2015).

It is widely accepted that with the increase of temperature, the water cycling process will speed up, which in consequence will possibly result in the increase of precipitation amount and intensity (W. Wang *et al.*, 2008). Worldwide, efforts have been made to study the change direction of extreme rainfall as, for instance, in South America (Carvalho *et al.*, 2002, Re & Barros, 2009), in North America (Feng & Hu, 2007, Karl & Knight, 1998, Kunkel & Andsager, 1999), in Europe (Beguería *et al.*, 2011, Burt & Weerasinghe, 2014, Frei *et al.*, 2006, Klein Tank & Koennen, 2003, Kyselý & Beranová, 2009, Ramos & Martínez-Casasnovas, 2006), in Asia (Hossain *et al.*, 2014, May, 2004, Panthi *et al.*, 2015, W. Wang *et al.*, 2008, Q. Zhang *et al.*, 2011), in Australia (Y. Li *et al.*, 2005) among other regions in the world. The results of the previously cited works indicate that different directions of change in the frequency of heavy rainfall are possible.

Some areas of the globe have experienced an upward trend in extreme rainfall. For instance, Karl & Knight examined by a variety of methods how precipitation has changed over the United States and found that since 1910, precipitation has increased by about 10% (Karl & Knight, 1998). They explained this fact by an increase in the frequency of days with precipitation and by an increase in intensity of the extremely heavy precipitation events. These results were confirmed by a study done by Kunkel and Andsager which was extended to Canada where an upward trend was observed in extreme precipitation events (Kunkel & Andsager, 1999). All Europe-average indices of wet extremes increase in the 1946–1999 period, although the spatial coherence of the trends is low (Klein Tank & Koennen, 2003). The same upward trend was observed in South America (Re & Barros, 2009). Significant increases in the intensity of extreme rainfall events between 1931–1960 and 1961–1990 are identified over about 70% of South Africa and the intensity of the 10-year high rainfall events has increased by more than 10% over large areas of this country, except in parts of the north-east, north-west and in the winter rainfall region of the south-west (Mason *et al.*, 1999). A combined work for Southern and West Africa performed by New et al. shows and confirms that regionally averaged rainfall on extreme precipitation days and maximum annual 5-day and 1-day rainfall amounts increase, but only the trend for the latter is statistically significant (New *et al.*, 2006).

While evidences of increasing trends are presented for many regions, statistically significant decreasing trends in extreme rainfall events have also been found in other areas like the south of Europe (Frei *et al.*, 2006), the southeast Asia and parts of the central Pacific (Manton *et al.*, 2001), and in northern Nigeria (Tarhule & Woo, 1998).

In other parts, like China (Su *et al.*, 2005), no statistically significant change in heavy rain intensity is found. This is confirmed by the work of Wang et al. where little change is observed in various annual extreme precipitation indices, but significant changes are observed in the precipitation processes on a monthly basis, although the seasonal variations are not uniform even in a medium-sized basin such as the Dongxiang River Basin (W. Wang *et al.*, 2008).

Until now, little is known about extreme rainfall over Benin. Yabi and Afouda (2012) examined recent years' rainfall extremes and their socioeconomic and environmental impacts in Benin. Their analysis showed strong incidence of extreme rainfall during the 1950s and 1960s, particularly in the south, while the 1970s and 1980s recorded very dry years. Hountondji and Ozer (2000) studied trends in extreme rainfall events in Benin for the period 1960-2000 by using 12 rainfall indices. They found that only the annual total precipitation, the annual total of wet days and the annual maximum rainfall recorded during 30 days present a significant decreasing trend while the other nine rainfall indicators appear to remain stable. Even though some efforts have been made to study extreme rainfall across the country, no study, as far as we know, investigated change in extreme rainfall over the country especially in the Ouémé basin by emphasizing on its frequency and its magnitude. The main objective of this work is to improve understanding of the heavy rainfall characteristics as key factor to support flood risk management in the Ouémé basin. This objective was split into three specific objectives which are: (a) identification of homogeneous regions in the study area through cluster analysis, (b) assessment of the frequency and/or intensity of extreme rainfall causing floods over the identified regions, (c) interpolation of the point scale results to analyze the spatial pattern of change in heavy rainfall over the entire Ouémé basin. The Ouémé basin covers an area of about 50,000 km² and 90% of this basin is located in Benin, West Africa.

4.2 Materials and Methods

The section presents the methodology used to analyze the heavy rainfall frequency and magnitude. It includes the data sampling approach, the determination of homogeneous regions though K-means clustering and the Principal Component Analysis (PCA), the extreme value distribution used namely the generalized Pareto distribution for quantile estimation, the kriging method for interpolation of the changes in return periods of heavy rainfall and some statistical tests.

4.2.1 Data Sampling

The daily rainfall data used in this study were obtained from the Benin national weather service (DMN: Direction Nationale de la Météorologie) and cover the period of 1921 to 2012. Two approaches were investigated. As a first approach, only the stations having continuous record from 1951-2010 were selected for analysis. This period is referred to as 'homogeneous period'. The term 'homogeneous period' implies that all the stations have the same data length (60 years) and are within the same range 1951-2010. Only the data of 17 stations were within this range (see Figure 4-1). This number of stations was not enough to perform statistical analysis and the regionalization (see section 3.1.) over the area of about 50,000 km^2 because using few stations could lead to high variance in the estimation. The minimum sample size required to have accurate results from statistical test is 30 (David & Sutton, 2011). Nevertheless, an analysis of the impact of the homogeneity in the study period on the results has been performed in section 3-3.

The second approach was to consider the available data length for each station. In doing so, 34 stations with data length varying from 44 to 92 years have been chosen. This is referred to as 'non-homogeneous period' due to the difference in data lengths. The data records are within 1921-2012 (Figure 4-1).

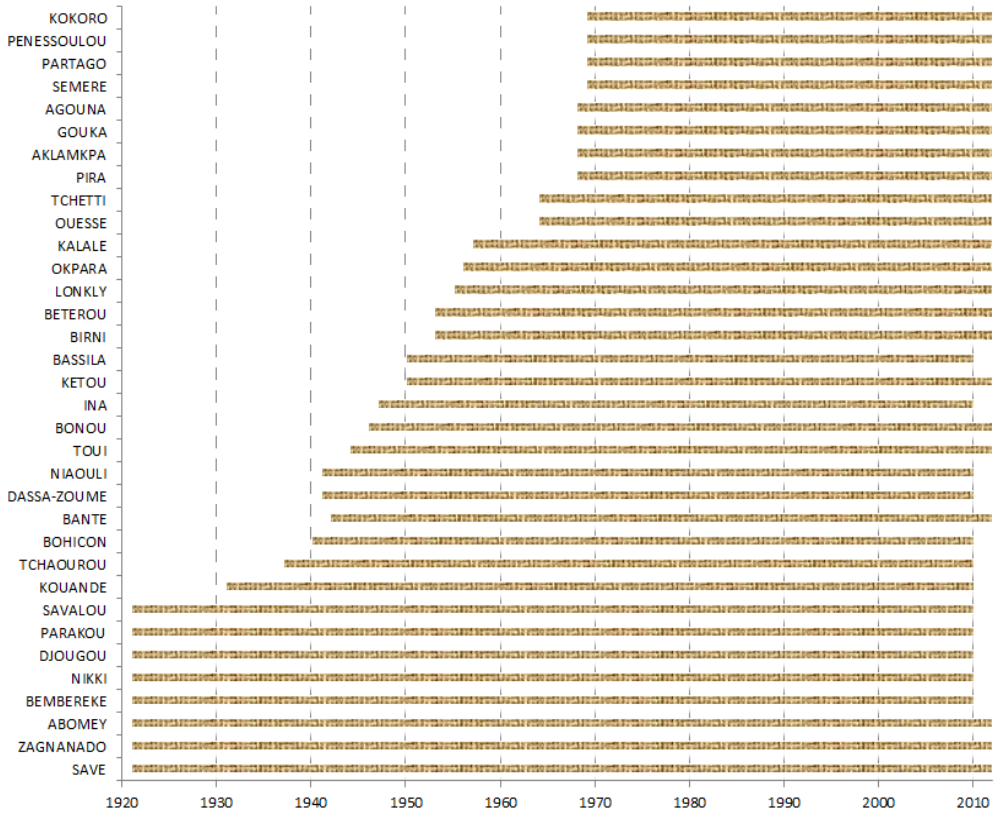

Figure 4-1: Data range for each station. For the spatial distribution of the stations see **Figure 4-2**.

For the non-homogeneous period, the data of each station is split into two sub-samples of equal length. Let X_j be the extreme values for one station such that X_j can be divided into two sub periods A_j and B_j with j varying from 1 to 34 (the number of stations). If we take

$X_j = x_i, x_{i+1}, ..., x_N$ where $i >= 1921$ and $N <= 2012$, we can define:

$A_j = x_i, x_{i+1}, ..., x_m$ and $B_j = x_{m+1}, x_{m+2}, ..., x_N$

with $m = (N + i)/2$ and this is rounded down to the nearest integer. This method was used for instance by Frich et al. (2002). x_i are extreme values corresponding to the year *i*.

4.2.2 Homogeneous clusters

K-means clustering method combined with the principal component analysis (PCA) was used to determine homogeneous regions and their corresponding stations. This approach was choosing due to their successful application in other rainfall regionalization studies (Ngongondo *et al.*, 2011).

Different variables are influencing rainfall characteristics such as large-scale atmospheric variables of air temperature, geopotential height, specific humidity, zonal and meridional wind velocities, precipitable water and surface pressure in addition to latitude/longitude location, elevation and mean annual rainfall (MAR), at-site Mean Annual Precipitation (MAP), station latitude/longitude location, elevation are proposed in the literature (Ngongondo *et al.*, 2011, Satyanarayana & Srinivas, 2008). Due to the limited availability of some data, four of them available for the study area were used namely the geographical location (latitude, longitude and altitude) and the MAP. Each variable was rescaled using the mean and the standard deviation of the corresponding variable in order to avoid bias of variables with large absolute values:

$$X_{i,j} = \frac{\left(Y_{i,j} - \overline{Y_j}\right)}{\sigma_j} \; for \; 1 \le j \le n \quad and \;\; 1 \ll i \ll N \qquad \text{(Eq. 4-1)}$$

with $X_{i,j}$ and $Y_{i,j}$ the scaled and non-scaled values of the i^{th} station and the j^{th} variable, n is the total number of variables and N the number of stations or elements. The K-means algorithm minimizes the function F defined below through an iterative procedure by moving the element from one cluster to another (Ngongondo *et al.*, 2011):

$$F = \sum_{k=1}^{K} \sum_{j=1}^{n} \sum_{i=1}^{N_k} d^2\left(X_{i,j}^k - X_j^k\right) \qquad \text{(Eq. 4-2)}$$

where the number of clusters K is set a priori; N_k is the number of feature vectors (stations) in cluster k; $X_{i,j}^k$ denotes the rescaled value of attribute (variable) in the feature

vector i assigned to cluster k; X_j^k is the mean value of attribute j for cluster k, computed as:

$$X_j^k = \frac{\sum_{i=1}^{N_k} X_{i,j}^k}{N_k} \quad \text{(Eq. 4-3)}$$

The number of clusters was determined using the Principal Component Analysis (PCA). The procedure first requires computation of the principal components of the sites' precipitation records; i.e. the transformation of the sites' precipitation records into a set of linearly uncorrelated (orthogonal) vectors (Irwin, 2015). The loadings indicate the degree of variance of the sites' precipitation records that are described by each component; higher loadings are representative of greater variances. The loadings are contoured and the contoured areas that exceed a predefined threshold value are classified as coherent precipitation regions.

4.2.3 The Generalized Pareto Distribution

Two sampling methods are normally used in extreme events analysis: the annual maximal series (AMS) and the peak over threshold (POT) methods. The AMS considers only the greatest events in each year so the length of the AMS is equal to the number of record years. In contrast, the POT method considers all data in the series which are above a given threshold. Nevertheless, the issue of threshold choice implies a balance between bias and variance. A low threshold is likely to violate the asymptotic basis of the model, leading to a bias; a high threshold will generate few excesses with which the model can be estimated, leading to a high variance (Coles, 2001). The standard practice is to adopt the threshold as low as possible that the model provides a reasonable approximation. Two methods are available for this purpose (Coles, 2001): one is an exploratory technique carried out prior to model estimation; the other is an assessment of the stability of parameter estimates, based on the fitting of models across a range of different thresholds. In this study, the Peak over Threshold (POT) was adopted as sampling method. This choice was imposed by the data which length was not sufficient to perform an analysis using the annual maximal approach for some of the stations.

The probability distribution of a POT variable with random occurrence times belongs to the Generalized Pareto family (Leadbetter *et al.*, 1983) which cumulative distribution *F* and quantile functions are:

$$\begin{cases} F(X \le x|\,\sigma,\kappa) = 1 - \left[1 + \kappa\left(\frac{x}{\sigma}\right)\right]^{\frac{-1}{\kappa}}; \ \kappa \neq 0 \ \ and \ \ \ 1 + \kappa\left(\frac{x}{\sigma}\right) > 0 \\ F(X \le x|\,\sigma,\kappa) = 1 - exp\left(-\frac{x}{\sigma}\right) \ \kappa = 0 \qquad \sigma > 0 \end{cases} \quad \text{(Eq. 4-4)}$$

$$\begin{cases} x_{1-p} = F^{-1}(1-p;\sigma,\kappa) = \left(\frac{\sigma}{\kappa}\right)(p^{-\kappa}-1), \quad 0<p<1, & \kappa \neq 0 \\ x_{1-p} = F^{-1}(1-p;\sigma,\kappa) = \sigma \log\left(\frac{1}{p}\right) & \kappa = 0 \end{cases} \quad \text{(Eq. 4-5)}$$

$p$is the exceedance probability and $(1-p)$ is the non-exceedance probability derived from the cumulative distribution function.σ, κ are respectively scale and shape parameters distribution, and *x* are the excesses over a selected threshold *u* (Katz *et al.*, 2002). The real quantile y_{1-p}will be $y_{1-p} = x_{1-p} + u$. If $\kappa > 0$, then the Generalized Pareto Distribution (GPD) is heavy tailed. By convention, $\kappa = 0$ refers to the limiting case obtained as $\kappa \to 0$ of the exponential distribution (i.e., an unbounded, thin tail).

Different thresholds were selected based on the minimum of the annual maximal sample of each station and the GPD fitted at each time by looking for stability in the estimated parameter values as suggested by Coles (Coles, 2001). This condition is nearly satisfied for a daily rainfall amount of about 50mm for the different data sets (see Appendix B). Therefore the threshold of 50mm is adopted for the following analysis.

The GPD was accordingly fitted to the data of each sub period A_j and B_j. The Maximum Likelihood method was used for parameter estimation. For each station, the intensities ($I_{i=1:9}$) of 2-, 3-, 5-, 7-, 10-, 15-, 20-, 25-, 30- years return period were then obtained from the fitted distribution for each A_j and B_j periods and the percentage change $D_i^{(j)}$ ($j^{\text{-th}}$ station and $i^{\text{-th}}$ return period) in the intensities of the two periods was calculated using the following formula:

$$D_i^{(j)} = \frac{\left(I_i(B_j) - I_i(A_j)\right)}{I_i(A_j)} * 100 \quad \text{(Eq. 4-6)}$$

with $I_i(A_j)$ the $i^{\text{-th}}$ intensity computed for the first sub-period of the j$^{\text{-th}}$ station and $I_i(B_j)$ the i$^{\text{-th}}$ intensity computed for the second sub-period of the $j^{\text{-th}}$ station.

The significance of changes in rainfall extremes was then assessed by comparing the mean of the difference in the intensity of heavy rainfall events with the difference expected under the null hypothesis. The null hypothesis states that there is no difference in the intensity of high rainfall events between A_n and B_n periods. Two statistical tests were used for testing this significance: the Paired samples t-test (L. Zhang & Han, 2009) and the Wilcoxon test (paired samples) (Wilcoxon, 1945). For detail about the computation of these tests, the reader can refer to the reference to (L. Zhang & Han, 2009) and (Wilcoxon, 1945).

4.2.4 Hubert Segmentation, Kriging, standardized precipitation and extreme precipitation indexes

To determine change points in the number of heavy rainfall days above some thresholds per year, we applied the Hubert Segmentation Test. Its principle is to split the data into m segments (m>1) in such a way that the mean computed over a segment is different from the mean of the neighboring segment.

Let $X_i\ \{i = i_1, i_2\ ; 1 < i_1\ and\ \ i_2 < N\ with\ i_1 < i_2\}$ be a segment of the initial series of data. Form a particular segmentation of order m done on the initial data, we can define (Lubes-Niel *et al.*, 1998):

$i_{k\{k=1,2,..m\}}$, the rank of the initial series extremity of the k[th] segment; $\overline{x_k}$, the mean of the k[th] segment;

D_m, the square of the difference between the data and the segmentation considered;

$$D_m = \sum_{k=1}^{m} d_k\ \ with\ \ d_k = \sum_{i=i_{k-1}+1}^{i_k} (x_i - \overline{x_i})^2 \qquad \text{(Eq. 4-7)}$$

The algorithm tries to minimize D_m and the means of continuous segments must be significantly different. This later constrain is satisfied by applying the test of Scheffé (see (Lubes-Niel *et al.*, 1998)).

The interpolation of change in heavy rainfall magnitude was done using the kriging method. Kriging is a linear interpolation method allowing to estimate areal values as a weighted mean of the point observations (Laurent, 2005). The weights attributed to the different observations depend on the variability structure of the variable. This variability structure is taken into account using the variogram function which is the difference between the variance and the covariance function. Empirical variograms are calculated using the observation data sets and then a variogram model is fitted. For each grid cell, using the variogram model, a linear system yields the interpolation weights attributed to the observation points. For a detailed presentation of theoretical and practical issues related to kriging, see for example reference (Isaaks & Srivastava, 1989, Lawin, 2007).

The standardized precipitation index (SPI) and the standardized extreme precipitation index (SEPI) was used to analysis the correlation between the annual rainfall and the extreme rainfall. The SPI is defined as:

$$X_{i,j} = \frac{Y_{i,j} - \overline{Y_i}}{\sigma_i} \qquad \text{(Eq. 4-8)}$$

With $X_{i,j}$ the SPI of the year j at the station i, $Y_{i,j}$ the annual rainfall of the year j at the station i, $\overline{Y_i}$ the mean annual rainfall at the station i and σ_i the standard deviation of the mean annual rainfall at the station i. The SEPI is computed in a similar manner by considering the series of maximum annual rainfall at each station.

4.3 Results and Discussion

4.3.1 Identification of homogeneous regions

In the application of K-means clustering the number of clusters or groups must be set at priori. The PCA was used to find the number of components based on the longitude, the latitude, the altitude and the mean annual rainfall (MAR) of each station. Table 4-1 shows the importance of each principal component (PC). The three first components explained more than 97% of the variance of the data. This suggests that using three groups was sufficient to reproduce the most of the variance in the data set. Based on this, the number of clusters was set to three during the K-means clustering. Figure 4-2 shows the stations of each group.

Table 4-1: Importance of principal components (PC)

	PC1	PC2	PC3	PC4
Standard deviation	1.4	1.0	0.9	0.3
Proportion of Variance	0.5	0.28	0.21	0.02
Cumulative Proportion	0.49	0.76	0.98	1

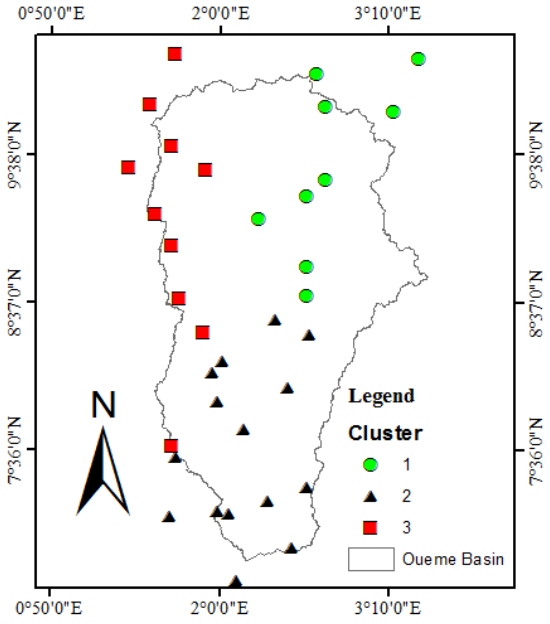

Figure 4-2 Location of rainfall sites of the three clusters in the Ouémé basin

The group 1 had nine stations located in the north-east of the basin with a mean annual rainfall of 1084 mm and an average altitude of 360 m above sea level. Most of the stations of this group are located in a unimodal rainfall regime. The group 2 was comprised of fifteen stations located in the south of the basin with mean annual rainfall of 1079 mm and an average altitude of 169 m. This group was located in a bimodal rainfall regime. The third group had ten stations located in the western part of the basin with mean annual rainfall of 1187 mm and a mean altitude above sea level of 378m. The mean annual rainfall was computed for the period 1970 to 2010 ignoring the years having more than 10% of missing data.

The Paired samples t-test and Wilcoxon test (paired samples) were both applied to the difference in the rainfall intensities of each station. A change is considered if it has been detected by both tests. Considering the results obtained from the non-homogeneous period and for all studied return periods, 82% of the stations show statistically significant change at 99% confidence level (correspond to alpha=1% significance level). This means that heavy rainfall over the study area has statistically changed at 82% of the stations. Among the statistically significant change, 57% of the stations exhibit a positive change and 43% a negative change. Considering the mean percentage change for all return periods, the highest positive change was observed at the station of Tchètti while the highest negative change was observed at Savè.

Analysis of the spatial variation of change was done based on the three rainfall regions found during the cluster analysis. Figure 4-3 shows the maximum, the minimum and the averages of positive and negative changes by region for each return quantile. There is not clear pattern about the change direction of heavy rainfall in the different regions since positive as well as negative changes were found. Nevertheless, for all regions, the maximum negative percentage changes were greater in magnitude than the maximum positive changes for most of the return periods. The highest negative changes were found in region 2 while the highest positive changes were observed in region 3 similarly to what was obtained for the mean annual rainfall of these regions. In region 1, for all the studied return period, the average negative change varied between -15% and -17% while the maximum positive change varied between 7% (2-year) and 13% (30-year). The average negative changes were stable for the different return periods compared to the average positive changes which increased with the return periods. In region 2, the average negative changes varied between -13% (5-year) to -17% (15-year) when the average positive changes varied between 9% (10-year) and 15% (2-year). For the positive percentage change, there was a decreasing trend from 30-year to 10-year before increasing up to 2-year return period. No clear trend was found in the average negative changes in this region. In region 3, the average negative changes varied between -14% (20-year) to -18% (3-year) and the average positive changes varied between 13% (3-year) and 21% (20-year). A decreasing trend is observed from 20-year to 2-year return period for the average positive percentage change.

Overall, positive as well as negative changes are balanced in the basin. This kind of mixed pattern of changes is observed also in other parts of world. Bates *et al.*(2008) report that generally, the frequency of occurrence of more intense rainfall events in many parts of Asia has increased, causing severe floods, landslides, and debris and mud flows, while the number of rainy days and total annual amount of precipitation have decreased. However, they also report that the frequency of extreme rainfall in some countries of Asia has exhibited a decreasing tendency. Increased precipitation intensity and variability can increase the risks of flooding. The frequency of heavy precipitation events (or proportion of total rainfall from heavy falls) will be very likely to increase over most areas during the 21st century, with consequences for the risk of rain-generated floods.

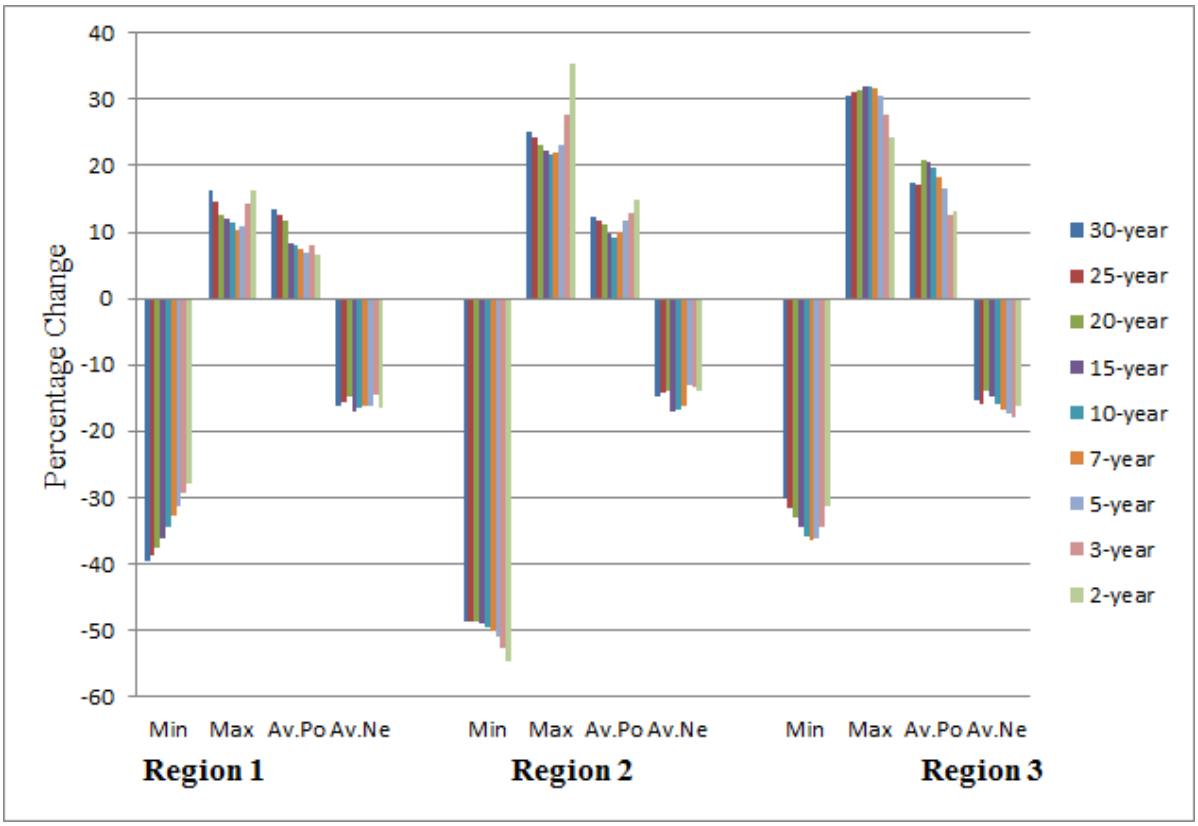

Figure 4-3: Percentage change in heavy rainfall for each region with the maximum (max), the minimum (min) and the averages of positive (Av.Po) and negative (Av.Ne) changes for different return periods.

4.3.2 Spatial pattern of change in heavy rainfall in the study area

Spatial interpolation of change in heavy rainfall was done using the kriging method. Different models used to approximate the variogram corresponding to each return period were the spherical, circular and stable models (see Appendix B for the model variograms). Figure 4-4 shows the map of change in different return periods of heavy rainfall over the Ouémé basin. Generally, the rainfall change-based map shows a mixed pattern of positive and negative changes for the different return periods plotted. Firstly, an east-west gradient from negative to positive was observed along the region 2. Along the western part of this region, high increases in the intensity of heavy rainfall events have been experienced despite the negative rainfall index meaning decreasing in annual rainfall since 1970 over West Africa (Servat *et al.*, 1999). This case study shows that, depending on the threshold used to define dry period, the increase in the frequency of dry spell (statistically significant) observed in large part of Sub-Saharan Africa particularly in Benin (Paeth *et al.*, 2007) does not necessarily mean a decrease in the frequency of extreme heavy-rainfall events. In the eastern part of region 2, decreases in heavy rainfall were observed for the different return periods and it is accentuated around the eastern part of the region. This change at the east-south of the basin is to be taken with precaution

since we do not have enough stations in this region to better represent the spatial variability.

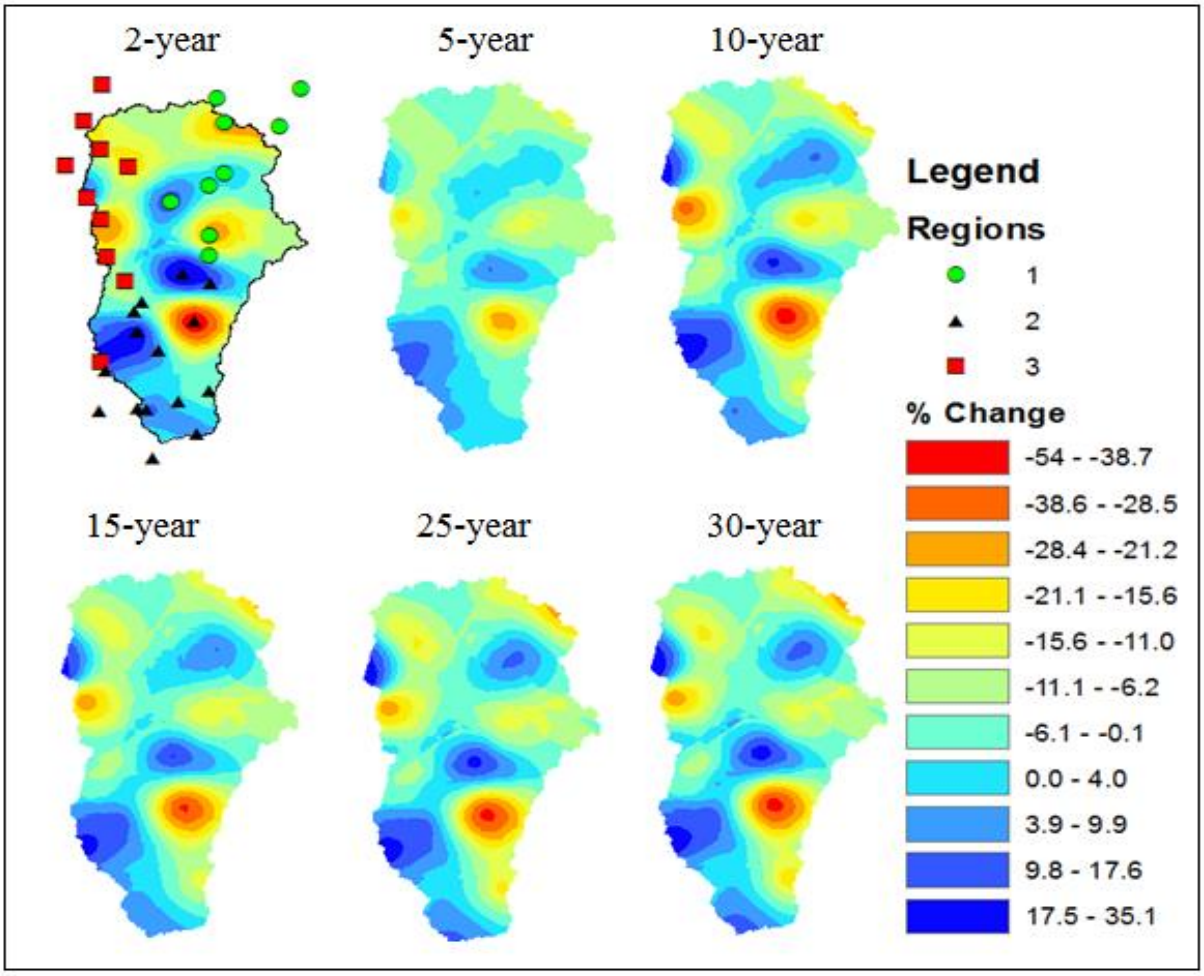

Figure 4-4: Regionalization of the percentage change in heavy rainfall over the Ouémé basin using the Ordinary Kriging method for the non-homogeneous period.

For regions 1 and 3, no general pattern was found. Nevertheless, the decreasing tendency was dominant sprinkled with some local increase in heavy rainfall for the different return periods. This is in accordance with the finding of Hountondji & Ozer (2000) about the annual maximum rainfall recorded during 30 days in Benin. Similarly, downward trend in the extreme rainfall was observed by Soro across part of Ivory Coast (Soro, 2011), and by Tarhule & Woo in Nigeria (Tarhule & Woo, 1998) which were located in almost the same climate region of the study area (golf of guinea). Groisman et al. (2005) show that a general decreasing trend in heavy rainfall exists over West Africa. This downward trend, even if it is not over all the basin is in accordance with the finding of Goula et al. for Ivory Coast (Goula *et al.*, 2011) and Masonet al. for South Africa (Mason *et al.*, 1999) where the direction of changes in extreme rainfall follows the one of total annual rainfall (see section 4.3.6).

Overall, similar spatial patterns of change were found for the different return periods analyzed but the magnitude and the spatial extent of change differed from one return period to another mostly for region 1 and region 3. As reported by Bates *et al.*, changes in extremes, including floods and droughts, are projected to affect water quality and exacerbate many forms of water pollution from sediments, nutrients, dissolved organic carbon, pathogens, pesticides and salt, as well as thermal pollution, with possible negative impacts on ecosystems, human health, and water system reliability (Bates *et al.*, 2008). So, different adaptation measures should be implemented in order to reduce the negative impact this change could have in different sectors such agriculture, health, transportation etc. Some areas in the different homogeneous regions showed very high change in term of magnitude of positive and negative percentage change. The frequency of rainfall in these areas has been analyzed in the next section.

4.3.3 Frequency of heavy rainfall at stations with highest changes

More investigation was done about the areas showing the highest positive and negative changes in heavy rainfall. We concentrated on the rainfall stations having the 2 highest negative changes and the 2 highest positive changes (Region 1: Nikki, Region 2: Savè and Ouèssè, Region 3: Tchètti). We computed the number of days with rainfall greater or equal to 50mm over the available data length and applied the Hubert segmentation test (Hubert *et al.*, 1989) to each sample. The choice of this index is justified by the fact that it helps to better understand the frequency of extreme rainfall (Goula *et al.*, 2011). Figure 4-5 shows the plot of the number of days with daily rainfall greater or equal to 50mm at Savè and Nikki (highest negative change stations), Ouèssè and Tchètti (highest positive change stations) with the Hubert segments. A break point was found in 1936 for the station of Savè. The number of heavy rainfall days during the period 1921-1936 was very high with an average of 13 heavy rainfall days per year compared with an average of 3 days during the period of 1937-2012. This implies that the first period received more extreme rainfall than the second period. At Tchètti, the Hubert segmentation test found a break in 2004 with an average of 4 heavy rainfall days per year during the period 1964-2004 while the period 2005-2012 experienced on average more than 7 heavy rainfall days per year. This shows that less heavy rainfall fell during the first period in comparison with the second period. For Nikki and Ouèssè, the similar changes are found in comparison respectively with Savè and Tchètti (see Figure 4-5).

When we consider the sub-periods used under the 'non-homogeneous period' for the station of Savè, the average of high rainfall days per year was 6.41 during the period 1921-1966 and 2.63 during the period 1967-2012. The first was more than the double of the second period. This shows that the first period was very wet compared with the second period and explains largely the high negative percentage change found for this station. Similarly, under the non-homogeneous period, Nikki exhibited an average of 3.8 high rainfall days per year during the first sub period and 2.5 heavy rainfall days per year during the second sub period (Figure 4-6). Indeed, the heavy rainfalls were becoming less

frequent than previously observed in that region. In the same way, the high decrease in the heavy rainfall could be explained by the reduction in the number of heavy rainfall days per year.

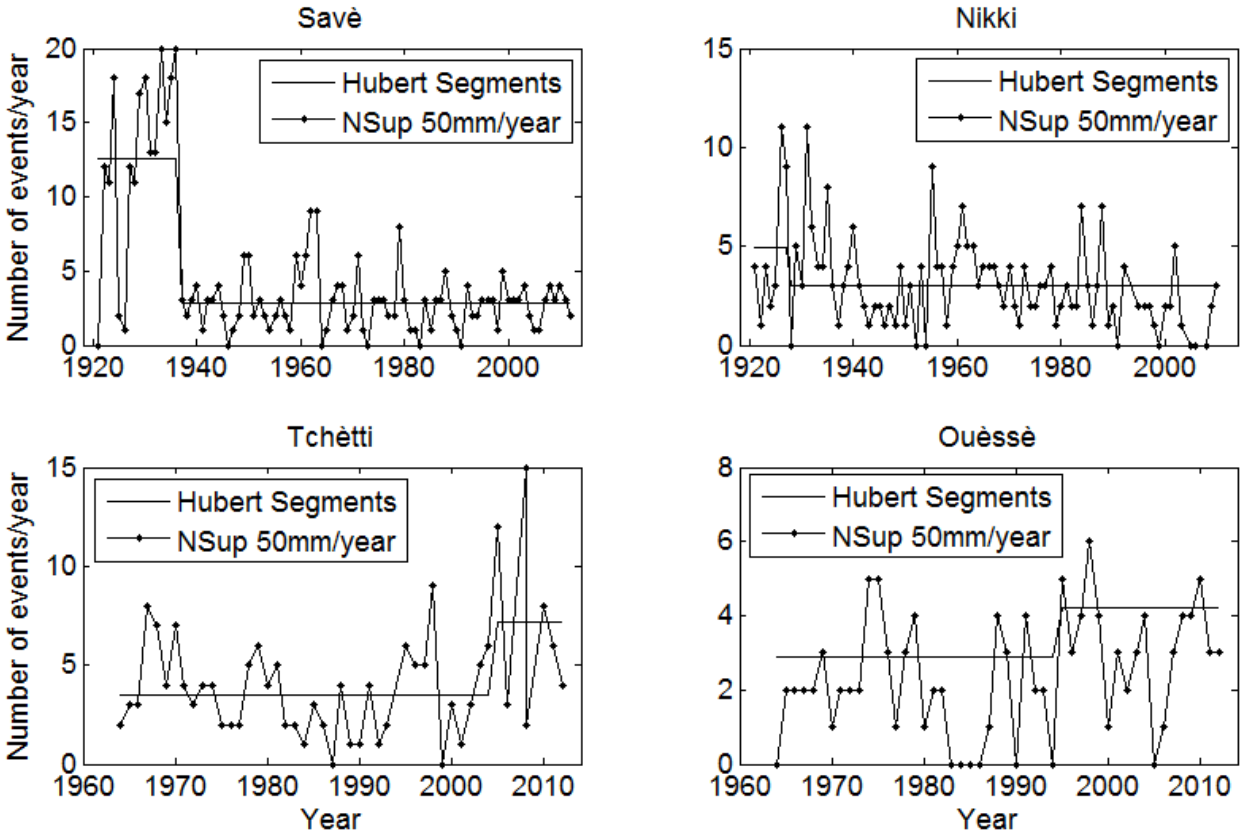

Figure 4-5: Number of heavy rainfall days per year with Hubert segmentation for 4 stations showing highest changes (negative (Savè and Nikki) and positive (Ouèssè and Tchètti)) at a threshold of 50mm (NSup 50mm/year).

As far as the other two stations were concerned and considering the threshold of 50mm, an average of 3.7 and 1.9 heavy rainfall days were found for Tchètti and Ouèssè respectively for the first period. For the second period, 5.4 and 2.9 are respectively the number of rainfall days for Tchètti and Ouèssè. Contrary to what has been found for the first two stations, the second period was wetter than the first period for these stations. There was an increase in the number of heavy rainfall days per year in these areas which explains the positive change in heavy rainfall found.

In addition, two thresholds (40 and 30mm) were added to investigate whether the change direction (sign of the change) would vary depending on the threshold. Low thresholds were chosen since such amounts (less than 50mm) of rainfall may lead to flash flood depending on the morphology of the region and precedent soil moisture condition. As it can be seen on the Figure 4-6, the change direction remained the same when we vary the

threshold meaning that the results obtained were independent of the choice of the threshold.

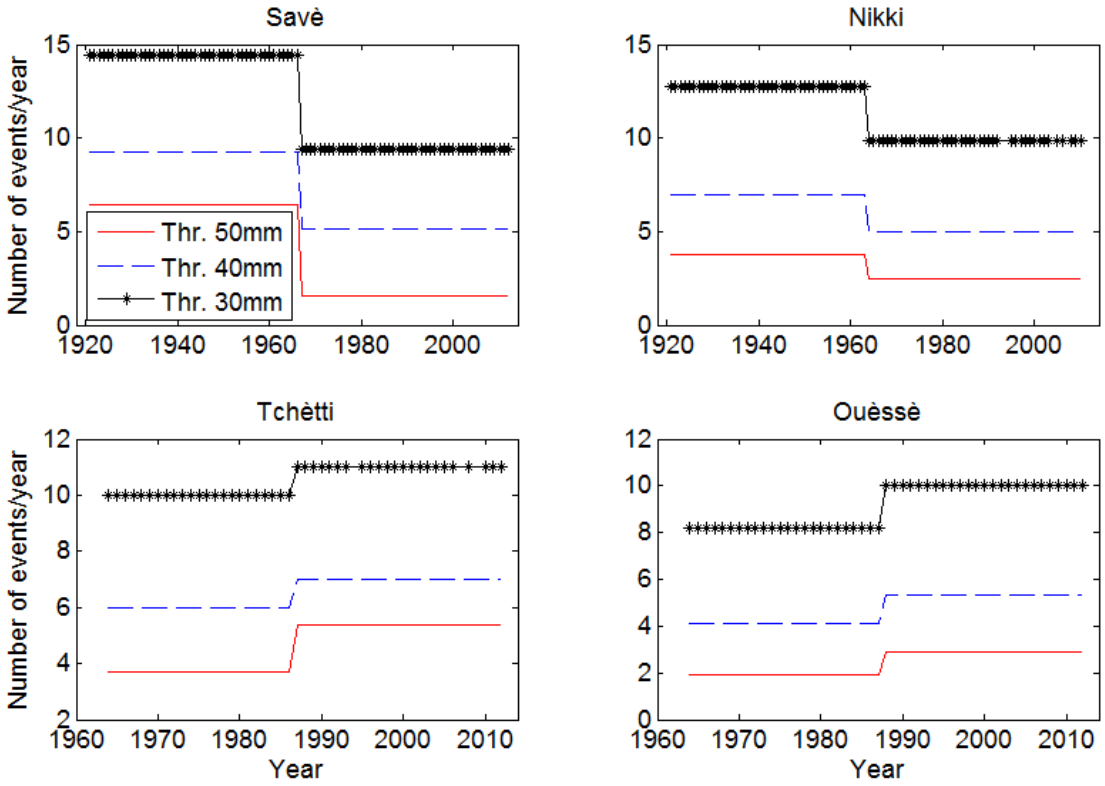

Figure 4-6: Mean number of days with rainfall greater or equal to 50, 40 and 30mm per year at Savè, Nikki, Tchètti and Ouèssè stations for two sub periods used in computed change.

4.3.4 Influence of homogeneity of the study period on the change

In the study of climate change impact, homogeneous periods (same data length and the same range) are required. In data scarce regions like West Africa, satisfying this condition is sometimes not easy making the results of the study uncertain. Through this, a homogeneous period (1951-2010) has been used to compare the results with the non-homogeneous period (different data length) used before. The previous methodology was applied considering the same data length (1951-2010) for all stations. 73% of the stations show a statistically significant change at 99% confidence level compared to the 82% in the non-homogeneous period. Considering the non-homogeneous period with length up to 92 years which was much longer than the one of homogeneous period, the difference in the number of stations showing significant change means that, long term changes in heavy rainfall is stronger than recent changes. **Figure 4-7** shows the percentage change of 2-, 5- and 10-years heavy rainfall for homogeneous period as well as for the non-homogeneous period. As it can be seen, there was a high difference between the spatial patterns of the two sets of map. For the homogeneous period, most of the changes for the

different return periods were negative meaning that there was a decreasing tendency in heavy rainfall. Nevertheless, positive changes were partially observed in the northern and south-western parts of the basin. Due to the limited number of stations used for the homogeneous period, the result of this interpolation should be taken with caution. For the non-homogeneous period, there was a mixed pattern of positive and negative changes. In the south-west of the basin, there was higher increase in heavy rainfall for the non-homogeneous (>17%) than the homogeneous (<10%) periods. In the same way, the maximum negative change for the non-homogeneous period is greater in magnitude than the maximum negative change for the homogeneous period. In comparison with the non-homogeneous period which length was longer (1921-2012), this homogeneous period helps to quantify recent change in extreme rainfall (1951-2010). Whatever the chosen period (homogeneous or non-homogeneous) and return periods were, it was found that the decreasing tendency was dominant in term of spatial distribution. The major difference was in the intensity of this change which was less accentuated with the homogeneous period than the non-homogeneous one.

There is a contract between the station-based results and the interpolation. Indeed, for the at-site based results, the number of stations showing statistically positive change was greater than the one showing negative change for the non-homogeneous period. In contrast, after the spatial interpolation, the area covered by positive change is lesser than the corresponding area for the negative change. This may be due the fact that the maximum of positive change is low sometimes lower than 1/3 of the absolute maximum negative for all return periods. This gave more weight to the negative values during the interpolation than the positive values. The model variogram (see appendix B) for the kriging was an approximation of the observed variogram and this approximation became more accurate with the number of observation sites (network). Due to the limited number of stations used, the uncertainties in the estimation may be high.

4.3.5 Extreme rainfall and annual total rainfall

We computed the correlation coefficient between the annual rainfall and the annual maximal rainfall considering for each station, the years having less than 10% of missing data. Over the 34 rainfall stations in the study area, we found 29 stations showing statistically significant correlation coefficient at 95% confidence level. These coefficients vary from 0.3 at Kétou station to 0.75 at Savè station (Table 4-2). Eleven stations have a correlation coefficient greater 0.5. This implies that the increase in annual total rainfall is due to an increase in annual maximal rainfall and generally in heavy rainfall. A typical example was the station of Savè where the trend in extreme rainfall was similar to the one of annual rainfall.

Additionally, we found high and statistically significant (at 5% significance level) correlation between the number of heavy rainfall days per year and the total annual

rainfall for all stations except Pénéssoulou (Table 4-2). Precipitation seems to be concentrated in more intense events, with more or less longer periods of lower precipitation in between. Therefore, intense and heavy episodic rainfall events with high runoff amounts were interspersed with longer relatively dry periods with increased evapotranspiration.

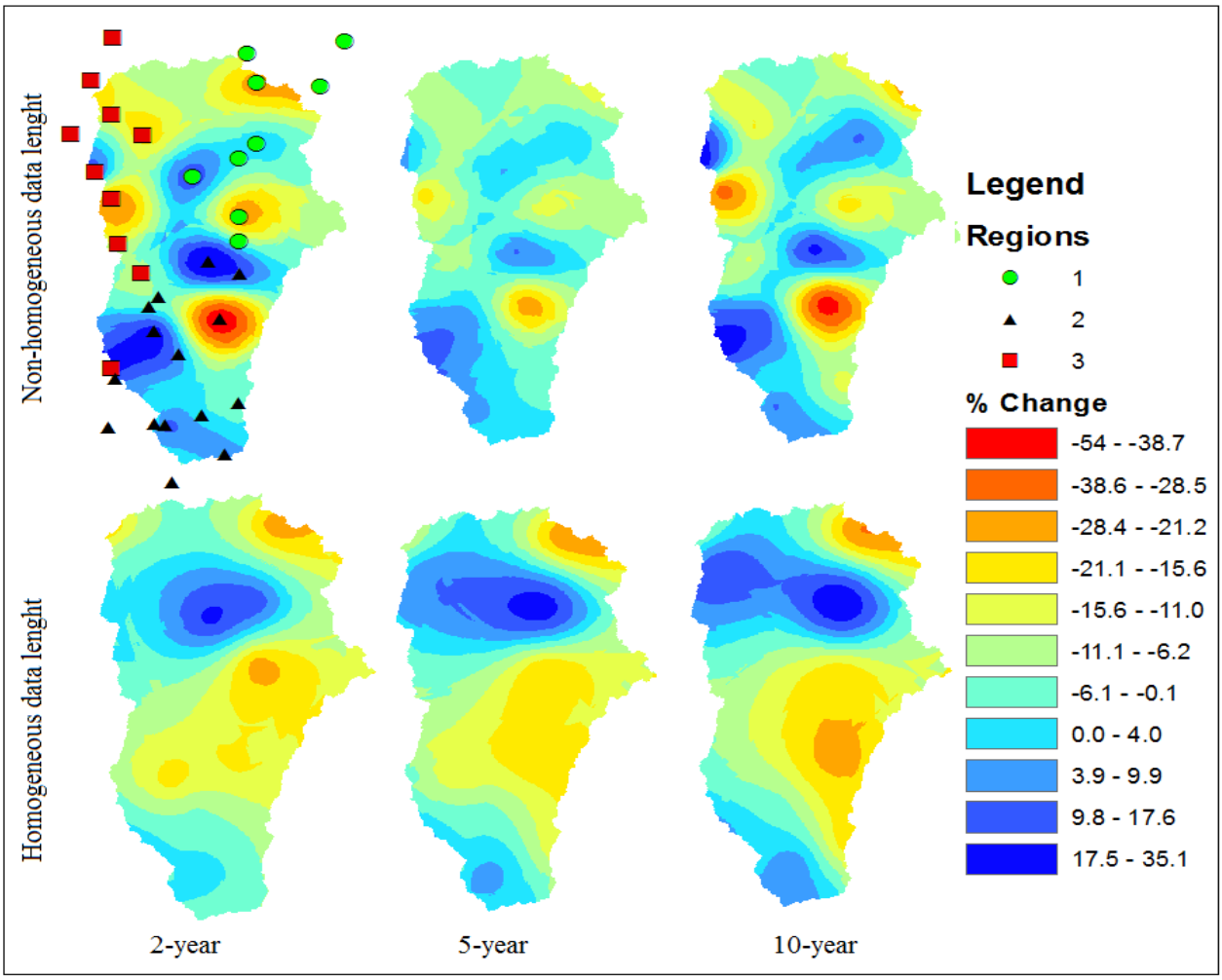

Figure 4-7: Comparison of the percentage changes in heavy rainfall for homogeneous (1950-2010) as well as for non-homogeneous (variable data length) periods considering 2-, 5- and 10-year return periods (R.P.). All maps are put to same scale.

In order to better capture the dynamic between the two variables, we computed the standardized precipitation index (SPI) and the standardized extreme precipitation index (SEPI). Figure 4-8 show the SPI and the SEPI for three stations. It is interesting to notice that for all stations, a positive SPI is mostly accompanied by a positive SEPI and a negative SPI is mostly accompanied by a negative SEPI. In other words, an increase in annual rainfall leads to an increase in extreme rainfall.

Table 4-2: Correlation coefficient between the annual maximal rainfall and the annual rainfall and the corresponding p-value in one hand and the correlation coefficient between the annual rainfall and the number of rainy days with rainfall amount greater or equal to 50mm in other hand. * no statistically significant correlation at 5% significance level

	Annual maximal rainfall and annual total rainfall		**Number of rainy days >50mm and annual total rainfall**	
Stations	**Correlation**	**P-value**	**Correlation**	**P-value**
Abomey	0.50	7.84E-07	0.52	1.57E-07
Agouna*	0.20	2.41E-01	0.76	9.56E-08
Aklankpa	0.68	9.54E-04	0.72	3.03E-04
Bantè *	0.19	1.21E-01	0.54	2.30E-06
Bassila	0.52	5.45E-04	0.68	8.77E-07
Bembèrèkè	0.50	5.81E-07	0.71	3.58E-15
Bétérou	0.45	1.18E-03	0.70	2.25E-08
Birni	0.39	9.43E-03	0.68	4.04E-07
Bohicon	0.46	5.36E-05	0.64	2.66E-09
Bonou	0.32	3.90E-02	0.72	1.20E-07
DassaZoumé	0.44	3.07E-04	0.75	2.67E-12
Djougou	0.50	3.93E-06	0.80	9.31E-19
Gouka	0.38	1.59E-02	0.68	1.54E-06
Ina	0.38	5.41E-03	0.62	6.98E-07
Kalalé	0.68	1.68E-07	0.69	9.59E-08
Kétou	0.30	2.42E-02	0.74	1.42E-11
Kokoro	0.43	7.83E-03	0.81	1.56E-09
Kouandé	0.44	7.44E-05	0.68	1.42E-11
Lonkly	0.43	1.06E-03	0.71	1.10E-09
Niaouli	0.47	4.67E-05	0.76	7.91E-14
Nikki	0.46	2.90E-05	0.64	5.10E-10
Okpara*	0.19	1.73E-01	0.65	1.24E-07
Ouèssè	0.60	6.01E-06	0.62	2.44E-06
Parakou	0.35	7.53E-04	0.63	8.39E-11
Patargo	0.73	2.49E-04	0.81	1.69E-05
Pénéssoulou *	0.42	5.12E-02	0.38	8.17E-02
Pira	0.49	1.37E-03	0.72	1.32E-07
Savalou	0.51	3.87E-06	0.79	7.66E-17
Savè	0.75	1.76E-17	0.94	1.64E-41
Sèmèrè	0.51	7.96E-03	0.82	3.43E-07
Tchaourou	0.46	2.36E-04	0.76	5.80E-12
Tchètti *	0.24	1.89E-01	0.79	5.67E-08
Toui	0.41	1.40E-03	0.49	8.50E-05
Zagnanado	0.36	9.76E-04	0.77	1.52E-17

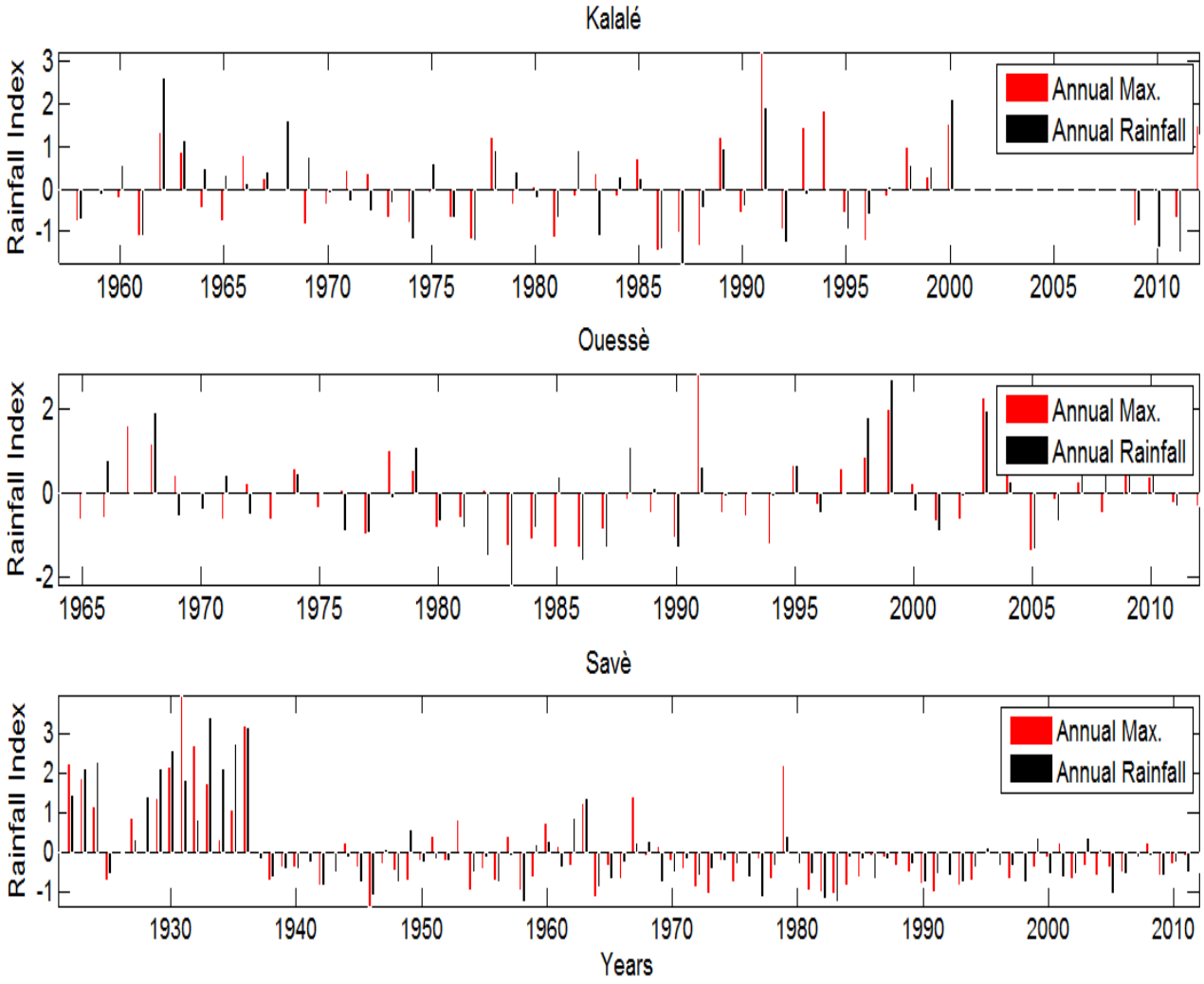

Figure 4-8: Standardized precipitation index (SPI) and standardized extreme precipitation index (SEPI) for three stations (Kalalé, Ouèssè, and Savè).

When we consider the case of Savè (Figure 4-8), between 1922 and 1936, SPI and SEPI were all positive (except the year 1925) and most values exceeded the standard deviation of the corresponding variable with the highest index (for SPI) being almost 4 times the standard deviation of the annual rainfall. The high and positive indexes found reveal that this period was very wet accompanied with very heavy rainfall. From 1936 to 2012, most of the SPI and SEPI had the same sign. An overall, 75% of the SPI and SEPI between 1922 and 2012 exhibited a change of the same direction at Savè station. At Kalalé station, 66% of the SPI and SEPI showed the same direction changes while for Ouèssè, it was 63%.

4.4 Conclusions

In this paper, K-means and PCA clustering analyses were done and three homogeneous rainfall regions were found in the Ouémé basin. We then explored changes in heavy rainfall following the peak over threshold approach using the generalized Pareto distribution. The data of each station were split into two sub-periods and the model is then fitted to the data of each sub-period. Change in extreme rainfall was then assessed by computing the difference in the intensities of the two sub-periods. As it has been observed in other part of the word, the frequency of extreme rainfall has changed over the study area. Significant negative as well as positive changes have been found throughout the basin. For the non-homogeneous period, 82% of the stations show a statistically significant change among which 57% exhibit a positive change and 43% negative change. A positive change is associated to an increasing heavy rainfall over the area of concerned. A spatial interpolation of heavy rainfall corresponding to different return periods was done and it was found that the south-western part of the basin shows an increasing tendency in heavy rainfall while the decreasing tendency was observed in the middle and upper parts sprinkled with some upward trend. It was also found that whatever the chosen period (homogeneous or non-homogeneous) and return periods were, the decreasing tendency is dominant in term of spatial distribution. The major difference was in the intensity of this change which was accentuated with the non-homogeneous period than the homogeneous one. Another difference is in the intensity of the positive change which was more pronounced with the non-homogeneous period than the homogeneous one. Additionally, we found high and statistically significant (at 5% significance level) correlation between the number of heavy rainfall days per year and the total annual rainfall for all stations except Pénéssoulou. The impacts of changes in the frequency of floods could be tempered by appropriate infrastructure investments, and by changes in water and land-use management. Change in flood frequency and magnitude can have positive and negative impacts. It is important, therefore, to be aware of its consequences at local and national levels and to plan accordingly. The expected continuation of rapid population growth will increase human exposure to flooding and adequate adaptation measure must be implemented.

With the mixed pattern of change (increase and decreasing tendency) observed at different return periods for the heavy rainfall, we can deduce that climates factors may not be the main element contributing to increasing flood risk in this basin. This is in line with previous research on high discharge over the same basin which revealed no significant increase in the annual maximum discharge at 5% significance level (Hounkpè, Afouda, Diekkrüger, *et al.*, 2015). More investigations are needed to explain the recent flood inundation observed over the Ouémé basin and at the national level. This may be an analysis of whether this situation (flooding condition) is accentuated by changes in land use patterns and/or by the vulnerability of the population. This is the central theme of chapters 5 and 6.

5 CALIBRATION AND VALIDATION OF DISTRIBUTED AND SEMI-DISTRIBUTED HYDROLOGICAL MODELS FOR ANALYZING LAND USE CHANGE IMPACT ON HIGH DISCHARGE IN ZOU CATCHMENT AT ATCHÉRIGBÉ GAUGING STATION

'All models are wrong, but some models are useful'
George Box, 1979

Abstract:
In the context of climate and land use changes, water cycle is expected to be intensified. This will likely result in frequent hydro-meteorological extremes events such as droughts and floods. Two hydrological models (SWAT and WaSiM) were calibrated and validated on the Zou catchment, gauging station Atchérigbé (area: 7035 km^2) for the period 1991-2010 as part of the assessment of the environmental change impacts on flood regime in the catchment area. The uncertainties related to the simulations were assessed. The preliminary results show that both models predict satisfactorily streamflow on the Atchérigbé basin with the Kling and Gupta efficiency (KGE) between 0.6 and 0.85 and the Nash Sutcliffe efficiency (NSE) between 0.5 and 0.76 for calibration and validation periods. By considering the discharge above the threshold of 120m^3/s (1.5mm/day) for the calibration and validation, the model performances were acceptable with regards to the uncertainties in discharge measurement mainly in peak discharge. The overall water balances predicted by the models are consistent with the hydroclimatic condition of the basin with the runoff coefficient being around 16% and the real evapotranspiration varying between 67 and 87% of the total annual rainfall. Hence, the models are able to reproduce satisfactorily the hydrological processes in the study area and could be used for flood risk assessment.

5.1 Introduction

Changes in land use/land cover and climate systems are expected to speed up the water cycle. At hydrological scale, potential impacts of these changes can be evaluated through watershed models. A number of hydrological model types have been developed in the last decades. The simplest type is the lumped model which describes the watershed as a single entity and it globalizes the hydrological process to its main features and has as input mean or representative values for the parameters. The more complex models are distributed models which consider spatial distribution of variables and reproduce the process in a watershed at a fine spatial resolution. In between these two types of models, are the semi-distributed models. These are models that subdivide the watershed into homogeneous units to which the models principles are applied in a lumped manner. Lumped, semi-distributed or distributed models can be conceptual (meaning that the

process description is not based on physical principles but on simplified descriptions) or physically based (most of its parameters are or can be derived from field measurement). Due to the increasing availability of data (soil, land use, DEM, etc) and numerical facilities, more and more semi-distributed and distributed models are used. In recent years, distributed watershed models have been used increasingly to implement alternative management strategies in the areas of water resources allocation, flood control, land use and climate change impact assessments and pollution control (Shi *et al.*, 2011). To assess land use impact on floods, a semi-distributed (SWAT) (Arnold *et al.*, 1998) and a distributed (WaSiM) (Schulla, 2012) models have been considered. These models are widely used to assess water balance, climate change impact on hydrological cycle and water resources in West Africa (D'Orgeval, 2006; Wagner, 2008; Kasei, 2009; Bossa *et al.*, 2012). Besides, WaSiM model is designed for flood simulation - single event as well as continuous simulation of floods - (Schulla, 2012) and is successfully applied by some authors for flood modelling purpose (Jasper et al. 2002; Cullmann et al. 2006; Kunstmann et al. 2006; Herbst et al. 2009; Crochet 2012). SWAT and WaSiM simulate water quantity and evaluate the effects of land use change and human activities but the use of SWAT is an attempt to evaluate its capability of simulating high discharge over the study area.

The calibration consists of getting the set of model parameters that outputs match as well as possible the observed data based on objective functions and visual inspection. The calibration of hydrological models can be done using manual or automatic approach or a combination of both methods. The manual calibration involves a choice of a set of parameters to run the model and then to assess the output graphically and numerically using an objective function. If acceptable simulations are not found based on the goodness of fit, the model is run with another set of parameters repeatedly until satisfactory simulations are found. During this process, parameters ranges are kept to realistic ranges and the description of hydrological processes must be taking into account. This method has the advantage to get familiar with the model parameters, (i) to encourage a deeper understanding of model structure and its applicability to catchment hydrology, rather than treating as a black box, (ii) to allow hydrologist to consider performance against a broad range of performance metrics, and make appropriate adjustments, (iii) to take into account understanding of the data and the catchment, (iv) to allow a logical checking at each change and (v) to produce a greater appreciation of strengths and limitations of calibrated result (Vaze *et al.*, 2011). The manual calibration of hydrological models has also some weaknesses. It becomes difficult when the number of model parameters is high and when the number of discharge gauges exceeds one, more efforts and running time is needed. To overcome these limitations, the automatic calibration can be used. It has the advantage to operate on one or more objective functions, to undertake calibrations for multiple catchments in a short period of time and can be repeated automatically (Vaze *et al.*, 2011). In other hand, the calibration results using this method are linked to the algorithm of optimization. Unrealistic and physically

meaningless parameters combination may be used during automatic optimization and the optimization may fail in considering the hydrological process on the basin. For instance, the optimum set of parameters automatically found may not necessary reproduce the water balance component and the runoff components correctly. The modelling experiences and the author's knowledge on the basin are required and for that purpose, hybrid optimization strategies (manual and automatic calibrations) are recommended. Experience suggests that uncertainty in both measurements and predictions of flood peaks increases with peak magnitudes (Beven, 2012). In addition, even if a model has been calibrated for a certain range of discharges, uncertainty is bound to increase as predictions are made outside this calibration range for extreme events. An experiment on 216 Australian catchments by Coron *et al.* (2012) indicated that "the transfer of model parameters in time may introduce a significant level of errors in simulations, meaning increased uncertainty in the various practical applications of these models (flow simulation, forecasting, design, reservoir management, climate change impact assessments, etc.)".

Managing risk in the short term is one of the most important applications of rainfall–runoff modelling, particularly for flood forecasting which requires decisions to be made as to whether flood warnings should be issued on the basis of the data coming in from rain gauges, radar rainfall images, stream gauges and the model predictions as the event happens in "real time" (Beven, 2012). The aim of this chapter is to calibrate and validate SWAT and WaSiM models on the Zou catchment and then to evaluate their capability in simulating high discharge over the study area using the hybrid optimization method.

5.2 Study area

Benin Republic is located in West Africa between 06°00' to 12°00' northern latitude and 01°00' to 03°40' eastern longitude. The study area, Atchérigbé basin, is a sub basin of the Ouémé basin (located at about 90% in Benin) and it has an area of 7035 km^2 (Figure 5-1).
Benin lies entirely in the tropical sub-Saharan region with a wet and dry climate. In the north of Benin, a semi-arid environment can be found, made up of savannahs and small mountains, while the south consists of a low coastal plain with marshlands, lakes and lagoons. Its climatic condition is typical for the West African climate, which alternates between the monsoon (from the ocean) during the cool and wet season, and the high thermal amplitude Harmattan wind that blows during the dry season from the Sahara (Aregheore, 2009).
The Ouémé Basin is subdivided into three climatic zones (see figure 2.2) according to different rainfall regimes: the north which has unimodal rainfall regime, the south which has bimodal rainfall regime and the middle which is a transition zone between the two previous regimes. The study area is located in this transition zone (between unimodal and bimodal rainfall regime). Rains mostly originate from the Guinean coast. Situated in a wet (Guinean coast) and a dry (Northern Soudanian zone) tropical climate, the Ouémé catchment records annual mean temperatures of 26 °C to 30 °C, annual mean rainfalls of 1280 mm (from 1950 to 1969) and 1150 mm (from 1970 to 2004) at a climatic station

close to 9° N latitude (Speth *et al.*, 2010). In Atchérigbé catchment, the average annual rainfall is 1161.6 mm for the period 1991:1998 and 1218.5mm for 1999:2010.

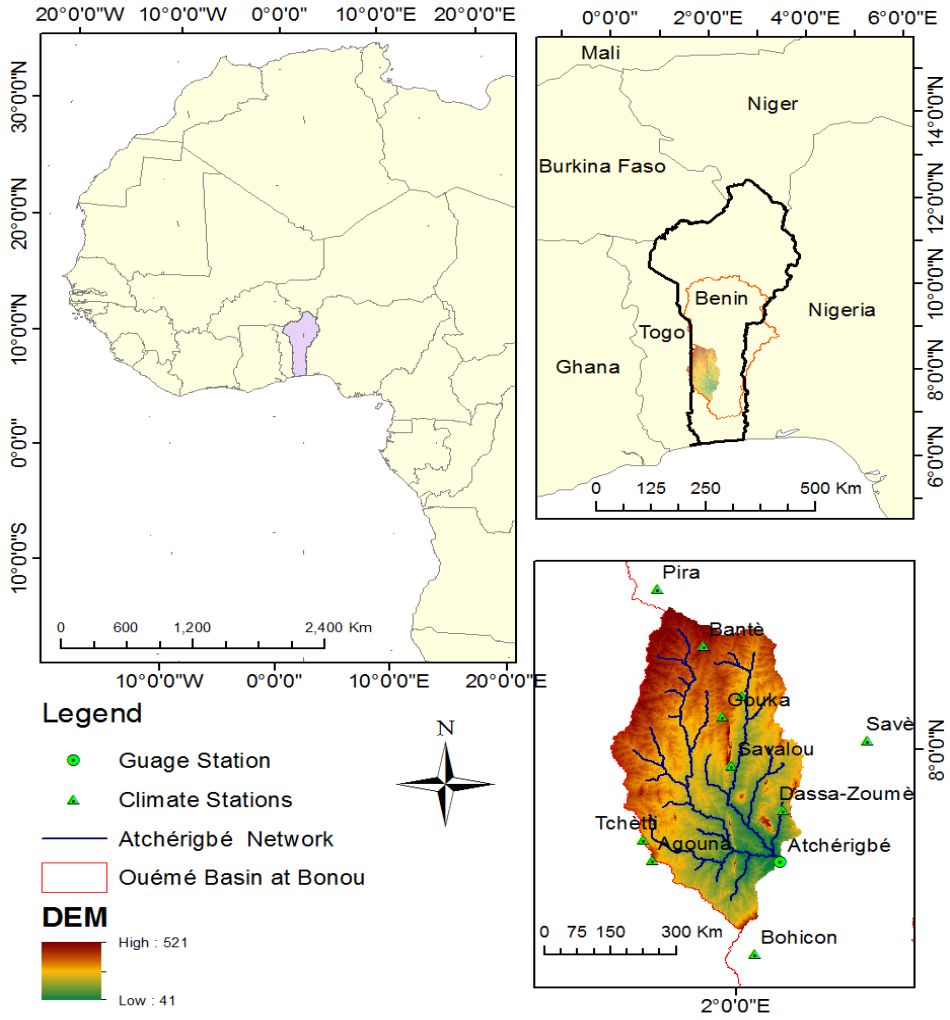

Figure 5-1: Overview of the Ouémé and Atchérigbé Catchments: (A) location of Benin in Africa; (B) location of the Ouémé and Atchérigbé Catchments in Benin and (C) Atchérigbé Catchment, its relief and the climate stations.

5.3 Material and method

5.3.1 Model Inputs, model description and model setup

Three data types (geographic, meteorological and hydrologic) are required for this study and they are compiled from different sources. The geographic data are required to represent spatial structures and time-invariant characteristics of the modelled area. They include the following: digital elevation model (DEM) SRTM at 90m resolution (Jarvis *et al.*, 2008), land use data (see section 6.2 for more explanation) obtained from Rivertwin project (RIVERTWIN, 2007) at 250 m resolution based on both satellite and in situ data,

and soil data obtained from SOil and TERrain (SOTER) database established at a scale: 1:200,000 the whole Ouémé catchment, in corporation with INRAB (Institut National de la Recherche Agricole du Bénin) (Bossa *et al.*, 2014). This soil database was obtained through a combined approach of in situ measurement and remote sensing (satellite). The DEM is the basis for generating other derived data sets like sub-basins, river network, elevation, overland, channel lengths, channel slopes, etc. The soil data serve for deriving soil hydraulic properties like saturated conductivity, organic carbon, bulk density, texture, soil available water content, etc. The hydraulic properties were obtained from field work (Bossa, 2012, Sintondji, 2005) and using the pedo-transfer functions of Van Genuchten (1980) and Brooks & Corey (1964). 40 different soil types have been identified in that basin. The dominant soil types are Albic Plinthosol (22%), Mollic Gleysol (20%), Ferric Luvisol (20%) and Haplic Arenosols (15%) (Figure 5-2a).

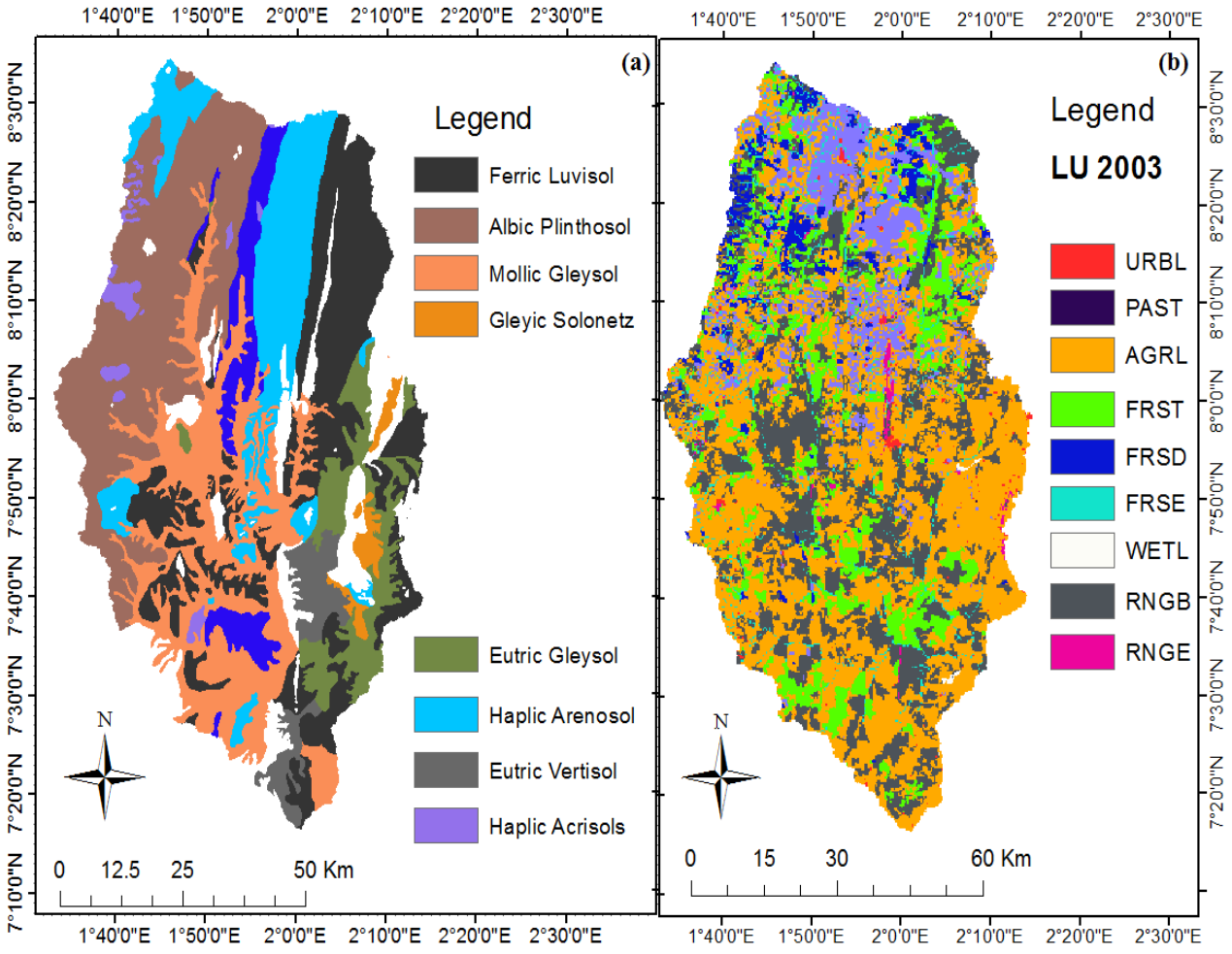

Figure 5-2: Main soil types (van Engelen & Ting-tiang, 1995) and land use types (RIVERTWIN, 2007) in the study area. For the land use, the abbreviations are defined as: URBL: Residential; PAST: Barren lands; AGRL: Agricultural Land-Generic; FRST: Forest-

mixed; FRSD: Forest-deciduous; FRSE: Forest-evergreen; WETL: Wetlands; RNGB: Range-brush; RNGE: Range-grasses.

The catchment landscape is characterized by forest islands, gallery forest, savannah, woodlands, agricultural lands and pastures (Figure 5-2b). Agriculture and other human activities have led to large-scale deforestation and fragmentations leaving only small relicts of the natural vegetation types within a matrix of degraded secondary habitats (Bossa, 2012, P.10).

The meteorological data used are rainfall, air temperature, global solar radiation and/or sunshine duration, wind speed, relative humidity obtained from the national directorate of meteorology (Direction Nationale de la Météorologie, DMN). Global radiation was computed based on Amoussa (1992) using the sunshine duration and other parameters. For WaSiM, the spatial interpolation of the climatic variable was done using the inverse distance weighting methods or the Thiessen polygon. In addition, discharge data were received from Benin national water directorate (Direction Générale de l'Eau, DGEau). The geographic location of the stations is displayed on Figure 5-1.

SWAT is a semi-distributed, deterministic, mainly physically based and time continuous watershed model operating on a daily basis (Arnold *et al.*, 1998). Its main components include hydrology, weather, erosion, plant growth, nutrients, pesticides, land management, and stream routing. It subdivides the catchment into sub-catchments based on a DEM. Each sub-catchment consists of a number of Hydrological Response Units (HRUs) which are homogeneous concerning soil, relief, and vegetation. Surface runoff from daily rainfall is estimated using a modified SCS curve number method (Neitsch *et al.*, 2011), which estimates the amount of runoff based on land use, soil type, and antecedent moisture condition. Peak runoff predictions (see appendix A section a) are based on a modification of the Rational Formula (Chow *et al.*, 1988). The watershed concentration time is estimated using Manning's formula, considering both overland and channel flow (Abbaspour *et al.*, 2007). SWAT was run with 2076 HRUs within 49 subbasins. It should be mentioned that the high number of HRUs makes it possible to take into account almost all land use types. SWAT assigns one rainfall station (the nearest) to each subbasin. Figure 5-3 shows the SWAT model description based on the vertical and horizontal fluxes and an example of repartition of the input rainfall data. The simulated processes include surface runoff, lateral flow, infiltration, exfiltration, evaporation, plant water uptake and percolation to shallow and deep aquifers.

WaSiM is a distributed, deterministic, mainly physically based hydrologic model (Schulla, 2012). It uses physically based algorithms for the vertical fluxes and lateral groundwater fluxes. Other lateral fluxes like surface runoff and interflow are treated in a conceptual manner. It can be applied from event-based to continuous simulations. An important model component is the module for spatial interpolation of meteorological data, which allows interpolations with different methods. The interpolation of rainfall was done using inverse distance weighting method and a value is automatically assigned

to each grid cell based on the interpolated rainfall. As WASIM is a spatially distributed model, it was run at 0.25km^2 resolution. Hydrological processes considerations of each model are described in Table 5-1.

In WaSiM, there are number of tools available for pre and post processing. The main tool used during the pre-processing is the topographic analyzing tool Tanalys. It performs a complex analysis of the digital elevation model to derive slope, flow time, sub-catchment, etc. Afterwards a control file is set up together with the hydrometeorological and soil data for running WaSiM in a command line mode. In SWAT, after preparing all the required data input, a new project is set up using the following steps. From the DEM, the network and sub-catchments delineation are performed. Then, the soil and land use data are uploaded to the project to define the HRUs. Next, we proceed to the climate stations definition and execute the 'write all Input-files' command. After specifying the time period and time step, the model is run. The threshold for HRU delineation was chosen in such a way that all the land use types are considered. More details about each model are giving in the appendix A.

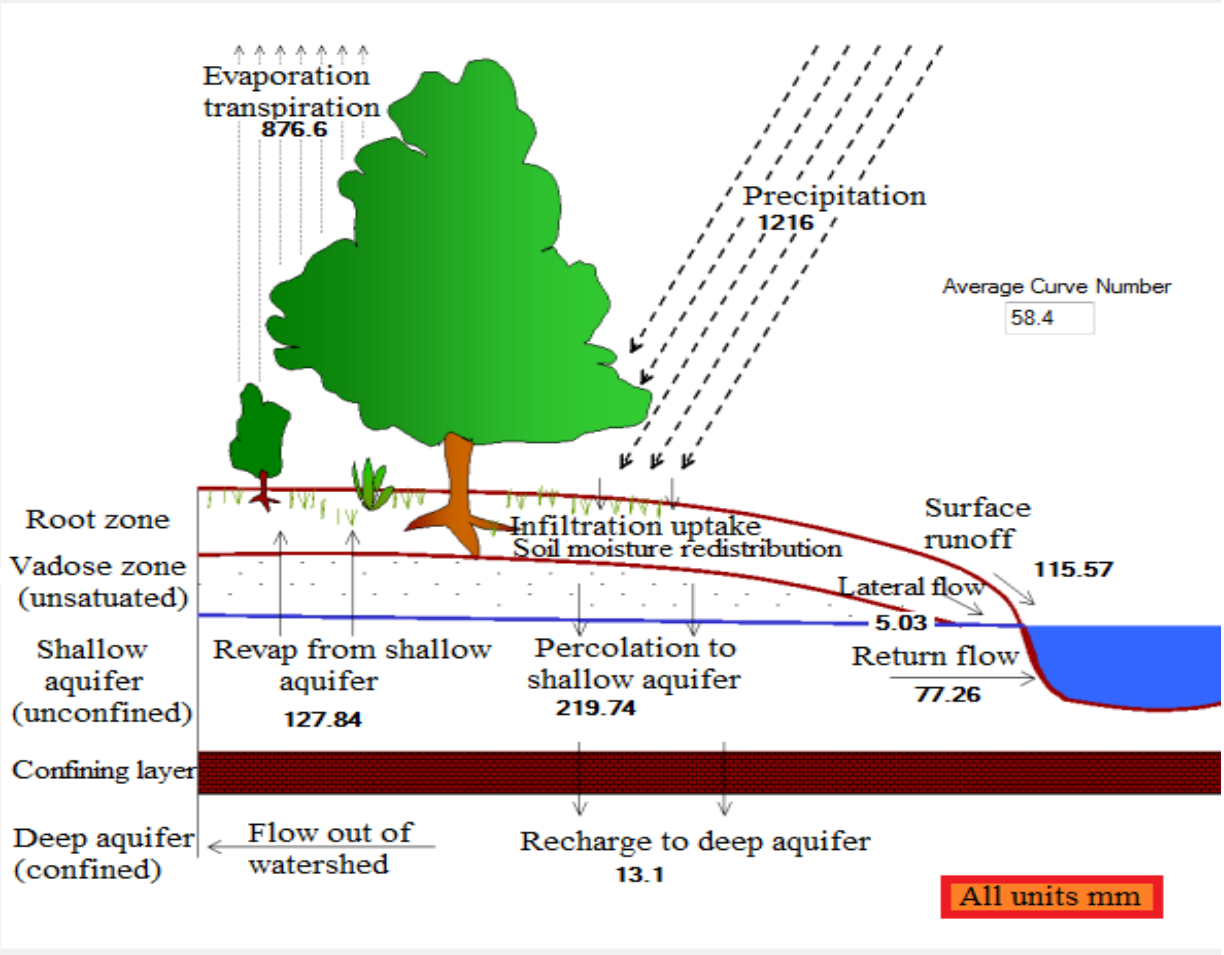

Figure 5-3: SWAT model description adapted from Arnold et al. (1998)

Table 5-1: Hydrological processes and process representation of the two models used in this study (LAI = leaf area index; PET = potential evapotranspiration); adapted from Cornelissen *et al.* (2013).

	WaSiM (Schulla & Jasper, 2007)	SWAT (Arnold *et al.*, 1998)
Interception	Storage approach; function of LAI	Storage approach; function of LAI
Potential Evapotranspiration	Penman-Monteith (J. Monteith, 1975)	Penman-Monteith (Monteith, 1975)
Actual Evapotranspiration	Separate calculation of evaporation from vegetated soils considering all soil layers and from bare soil for the first soil layer; both reduced by soil water content of the first layer	Separate calculation of evaporation from vegetated soils considering all soil layers and from bare soil for the first soil layer; both reduced by soil water content of the first layer
Soil module	Richards equation	Reservoir, Soil is divided into several numerical layers
Infiltration	Richards equation	SCS curve number (SCS, 1972) Green and Ampt (1911)
Overland flow	Horton overland flow	SCS curve number (SCS, 1972)
Percolation	Function based on soil saturation and saturated conductivity	Storage routing; water content must be above field capacity
Interflow	Storage approach; comparing maximum and actual rate	Kinematic storage model
Base flow	Linear storage approach	Linear storage model
Routing	Kinematic wave approach considering retention and translation	Continuity equation using Manning's equation

5.3.2 Model calibration, sensitivity and uncertainty analyses

A time period of 20 years were used for this simulation (1991-2010) at a daily time step. The calibration was done for 1999-2010 with four years of warm up. Thus, the computation of model performance during the calibration was done for the period 2003-2010. This corresponds to the period where we have less missing data compared to the validation period which is 1991-1998. For SWAT model, complex algorithms are used to perform the parameter optimization, the sensitivity analysis, and the uncertainty prediction. It is a computer code called SUFI-2 algorithm in SWAT-CUP program developed by Abbaspour *et al.* (2007). As explained by Abbaspour (2007), in SUFI-2, all uncertainties (parameter, conceptual model, input, etc.) are mapped onto the parameter ranges as the procedure tries to capture most of the measured data within the 95% prediction uncertainty. This means that the parameters have to compensate all uncertainties in the whole model setup. This can be criticized although this is common in

hydrological modelling. The overall uncertainty in the output is quantified by the 95% prediction uncertainty (95PPU) calculated at the 2.5% and 97.5% levels of the cumulative distribution of an output variable obtained through Latin hypercube sampling. The same procedure was applied to WaSiM. Latin hypercube sampling (LHS) is a statistical method for generating a near-random sample of parameter values from a multidimensional distribution (https://en.wikipedia.org/wiki/Latin_hypercube_sampling). The sampling method is often used to construct computer experiments or for Monte-Carlo integration. The LHS was described by McKay in 1979 (McKay *et al.*, 2000).

The sensitivity analysis was done using the partial correlation coefficient {between the set of parameters in one hand and which are sensitivity indexes based on linear (resp. monotonic) assumptions, in the case of (linearly) correlated factors. It is a measure of 'standardized' partial relation between a model result y (water balance components and the models performances) and each of the parameters in $x = (x_1, \ldots, x_K)$ involved in the calibration procedure.

For both models, two indices are used to quantify the goodness of calibration/ uncertainty performance, the P-factor, which is the percentage of data bracketed by the 95PPU band (maximum value 100%), and the R-factor, which is the average width of the band divided by the standard deviation of the corresponding measured variable. Values of 100% for the P-factor and 0 for the R-factor correspond to a perfect simulation where the observed and the simulated data are identical. An R-factor value less than 1 is generally a desirable measure (Abbaspour *et al.*, 2009).

5.3.3 Evaluation of model performance

For model performance evaluation, three criteria are used. In the following equation, $Q_{sim}^{(thr)}$ is the simulated discharge above the threshold thr, $Q_{obs}^{(thr)}$ is the observed discharge above the threshold thr, N is the total number of observation points and i is a counter.

- The Kling and Gupta Efficient (KGE) (Gupta *et al.*, 2009) has the property to account for the linear correlation coefficient r between observed and simulated discharge, the ratio α of the standard deviation of simulated discharge over the standard deviation of observed discharge and the ratio β of the mean simulated discharge over the mean observed discharge.

$$KGE = 1 - \sqrt{(r-1)^2 + (\alpha-1)^2 + (\beta-1)^2} \qquad \text{(Eq. 5-1)}$$

- For long term simulation evaluation, the absolute percentage bias (APB) which is a measure for total volume differences between measured and observed data was used.

$$APB = \frac{\left|\sum_{i=1}^{N}\left(Q_{obs}^{(thr)} - Q_{sim}^{(thr)}\right)\right|}{\sum_{i=1}^{N} Q_{obs}^{(thr)}} \qquad \text{(Eq. 5-2)}$$

- The Nash and Sutcliffe Efficiency (NSE)

$$NSE = 1 - \frac{\sum_{i=1}^{N}\left(Q_{sim}^{(thr)} - Q_{obs}^{(thr)}\right)^2}{\sum_{i=1}^{N}\left(Q_{obs}^{(thr)} - \overline{Q_{obs}^{(thr)}}\right)^2} \quad \text{(Eq. 5-3)}$$

5.4 Model results for current land use distribution

5.4.1 Models performance for threshold $thr = 0$

The calibration of the hydrological process in this catchment was done using daily observed river discharge for comparison. The observed runoff coefficient (quotient of the mean annual discharge and the mean annual rainfall) referred to as CoefRun and the coefficient of real evapotranspiration (ETR) (quotient of mean annual ETR and the mean annual rainfall) referred to as CoefETR derived from previous works done in similar climate conditions to our study area were used as qualitative information. Both models predicted satisfactorily streamflow on the Atchérigbé basin with KGE between 0.6 and 0.85 for the calibration as well as for the validation periods (Table 5-2). The absolute percentage errors (APB) between observed and simulated daily flows for calibration and validation for both models were less than 15% with the minimum reaching the value of 0.01. During both calibration and validation periods, the APB obtained with WaSiM were between 2.01 and 14.81% while with SWAT, this criterion was between 0.01 and 12.52%. Further agreement between observed and simulated flows is shown by the NSE which was between 0.5 and 0.76 during calibration and validation of SWAT. The performance of each model depends on the criteria used (Figure 5-4).

$$\boldsymbol{CoefRun = \frac{Mean\ Annual\ total\ runoff}{Mean\ annual\ rainfall} * 100,\ CoefETR = \frac{mean\ annual\ ETR}{Mean\ annual\ rainfall} * 100}$$

For instance, according to the NSE, SWAT is the best model during calibration while according to the KGE; it is WaSiM the best model during calibration. During validation period, whatever the chosen criteria, SWAT performed better than WaSiM. Higher performance criteria were achieved when we decrease the data length. For instance, using the period 2007:2009 during the calibration period, the KGE is greater than 0.8 and the NSE is greater than 0.7 for $thr = 0\ m^3$.

Table 5-2: Models Performance criteria. The conditions to be fulfilled by simulation to be considered are the Nash and Sutcliffe Efficiency (NSE) should be greater or equal to 0.50, the Kling and Gupta Efficiency (KGE) greater or equal to 0.6 and the absolute percentage bias (APB) should be less to 15%. *Std* stands for standard deviation at threshold $\boldsymbol{thr = 0 m^3/s}$.

		NSE			KGE			APB		
		Mean	Std	Range	Mean	Std	Range	Mean	Std	Range
SWAT	Cal	0.57	0.01	0.54: 0.60	0.65	0.03	0.60: 0.71	6.15	3.42	1.11: 11.17

WASIM	Cal	0.55	0.02	0.50: 0.56	0.72	0.01	0.71: 0.74	11.88	2.42	6.37: 14.30
SWAT	Val	0.73	0.01	0.71: 0.76	0.83	0.01	0.81: 0.85	5.12	3.72	0.01: 12.52
WASIM	Val	0.52	0.02	0.50: 0.57	0.73	0.02	0.71: 0.79	11.49	3.62	2.01: 14.81

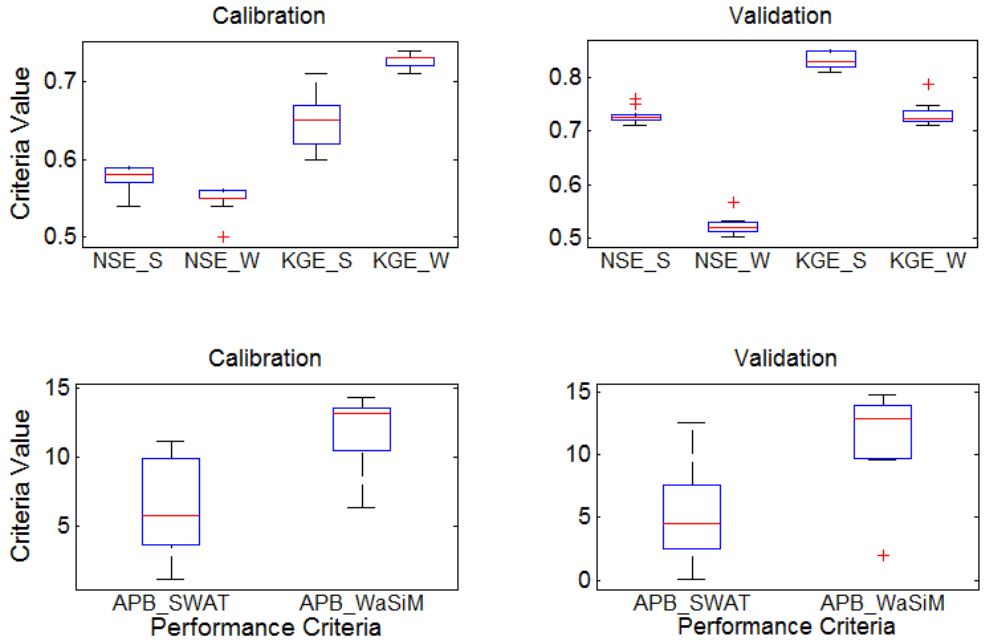

Figure 5-4: Boxplot of the performance criteria for 10 best simulations: Nash and Sutcliffe Efficiency for SWAT (NSE_S) and for WaSiM (NSE_W), the Kling and Gupta Efficiency for SWAT (KGE_S) and for WaSiM (KGE_W) in one hand and in other hand the absolute percentage bias (APB) for SWAT (APB_SWAT) and WaSiM (APB_WaSiM) models at threshold $\boldsymbol{thr = 0\ m^3}$.

5.4.2 Graphical assessment of the models results for threshold $\boldsymbol{thr = 0\ m^3/s}$

Out of the performance criteria for assessing the models, it is important to proceed to graphical inspection of models results. **Figure 5-5** shows the observed and simulated discharges as well as the corresponding rainfall for calibration period by WaSiM. Generally, the high and low discharges have been acceptably reproduced by the models. Nevertheless, some high discharges were not well captured. This may be due to limited quality of rainfall and discharge measurements. Taking individually the models, WaSiM reproduces better the high discharge than the SWAT model. These results show that the models satisfactorily reproduce the hydrological processes of the study area and could be used for impact assessment on the basin. Additionally, we provided the scatter plot of the simulated versus observed discharge (Figure 5-7). Out of the acceptable model performance, the scatter plot reveals that the model was not able to reproduce some of the discharge points. There is some temporal mismatching between observed and simulated discharges leading data points scatted on either sides of the first diagonal. During the

validation period, the graphical performances of the models were also acceptable with some high discharges which were not well captured (**Figure 5-6**)

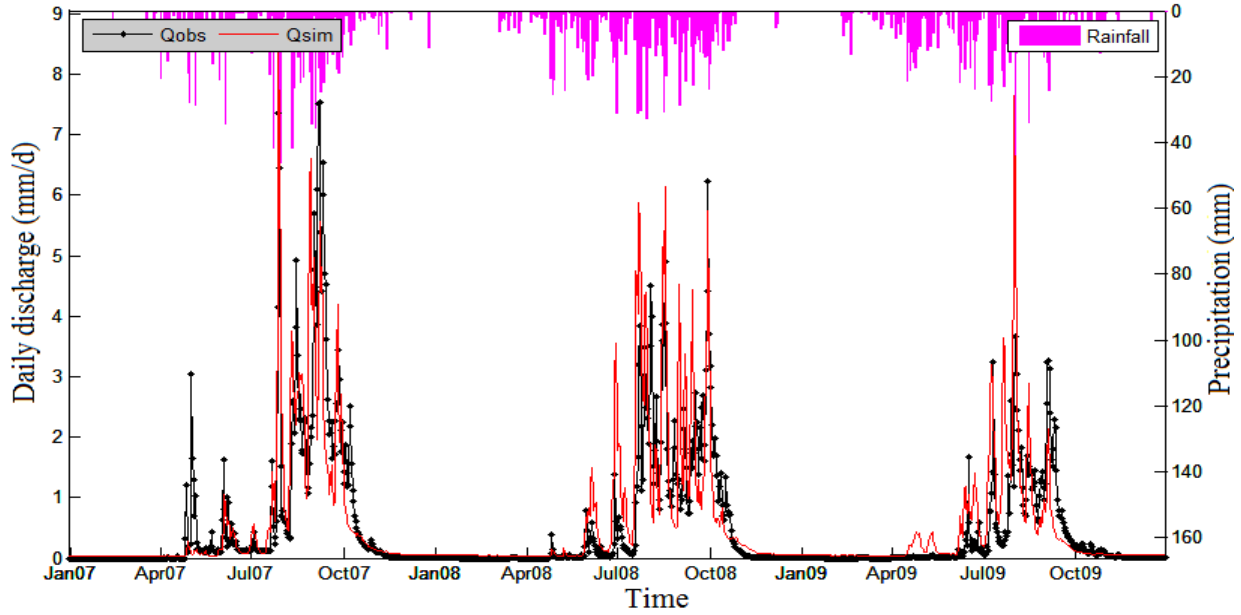

Figure 5-5: Observed and simulated discharges by WaSiM for 2007: 2009 during the calibration period

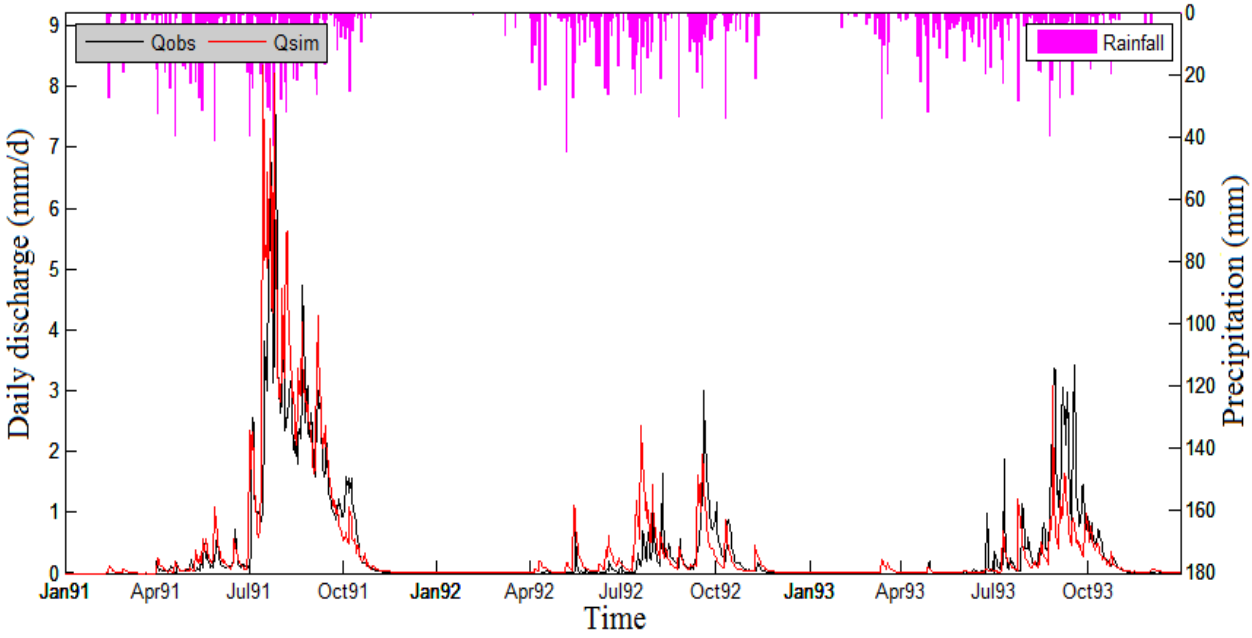

Figure 5-6: Observed and simulated discharges by SWAT for 1991:1993 during validation period

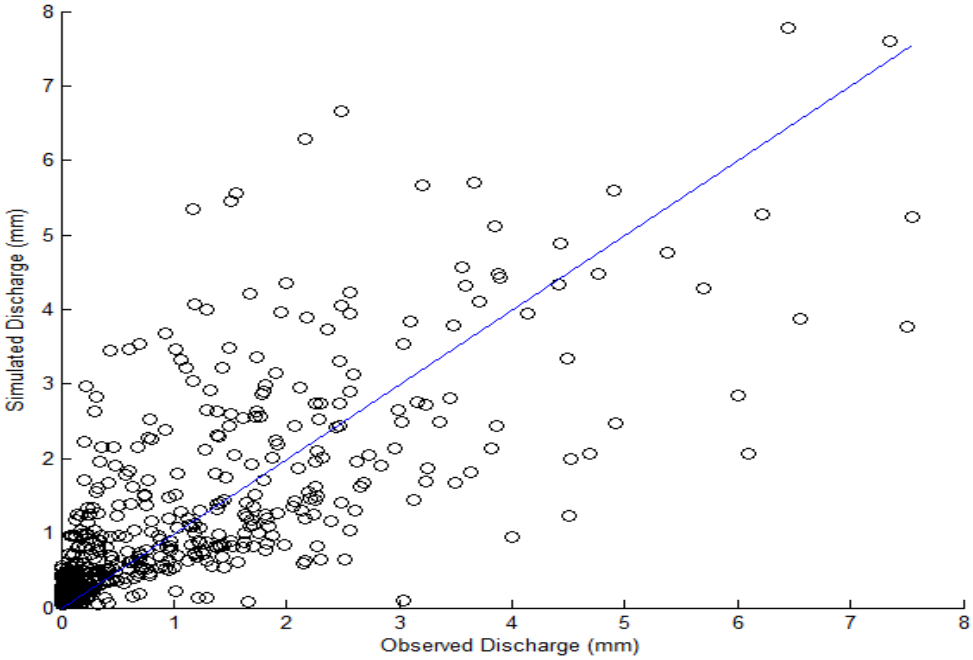

Figure 5-7: Scatter plot of the simulated discharge versus the observed discharge. The blue line represents the diagonal 1:1 with equation y=x.

5.4.3 Models performances for threshold $thr \neq 0\ \mathrm{m}^3/\mathrm{s}$

We computed the performances of WaSiM and SWAT in simulating the discharge above some thresholds (0:10:120m^3/s corresponding to 0:0.125:1.5mm/day) using the discharge data previously calibrated with $thr = 0\ m^3/s$. Figure 5-8 shows the NSE and the KGE values in function of thresholds for the calibration period. It can be observed that the criteria values decrease as the threshold increases. The NSE decreases more rapidly than the KGE reaching in case of WaSiM model negative values. When the NSE is used in optimization, it tends to underestimate the runoff peak. As explained by Gupta *et al.* (2009), the same applies for KGE, but the underestimation will not be as severe. Indeed, more attentions will be paid to the KGE in this section. For both models, KGE is positive for all the selected thresholds reaching 0.74 in the case of WaSiM and 0.71 in the case of SWAT for $thr = 0\ m^3/s$. KGE continued to be greater than 0.50 for the $thr \leq 80\ m^3/s$ (1mm/day) in the case of WaSiM and $thr \leq 30\ m^3/s$ (0.375mm/day) in the case of SWAT. At $thr = 120 m^3/s$ (1.5mm/day), the KGE reach it minimum value of 0.42 in the case of WaSiM and 0.36 in the case of SWAT. Based on these results, it is clear that WaSiM performed better in term of simulating high discharge than SWAT during the calibration period.

During the validation period, for both models, the KGE is positive and according to that criterion, SWAT performed better than WaSiM model (Figure 5-9) in opposition to what was found during the calibration period. This is reflected by a KGE greater than 0.55 for

all thresholds ($\boldsymbol{thr} \leq 120\ m^3/s, 1.5mm/day$) in case of SWAT whereas the minimum KGE for WaSiM is around 0.3 for all thresholds ($\boldsymbol{thr} \leq 120\ m^3/s, 1.5mm/day$). As previously observed during calibration, the maximum value of the criteria is obtained at $\boldsymbol{thr} = \mathbf{0}\ m^3/s$ reaching 0.85 for SWAT and 0.79 for WaSiM.

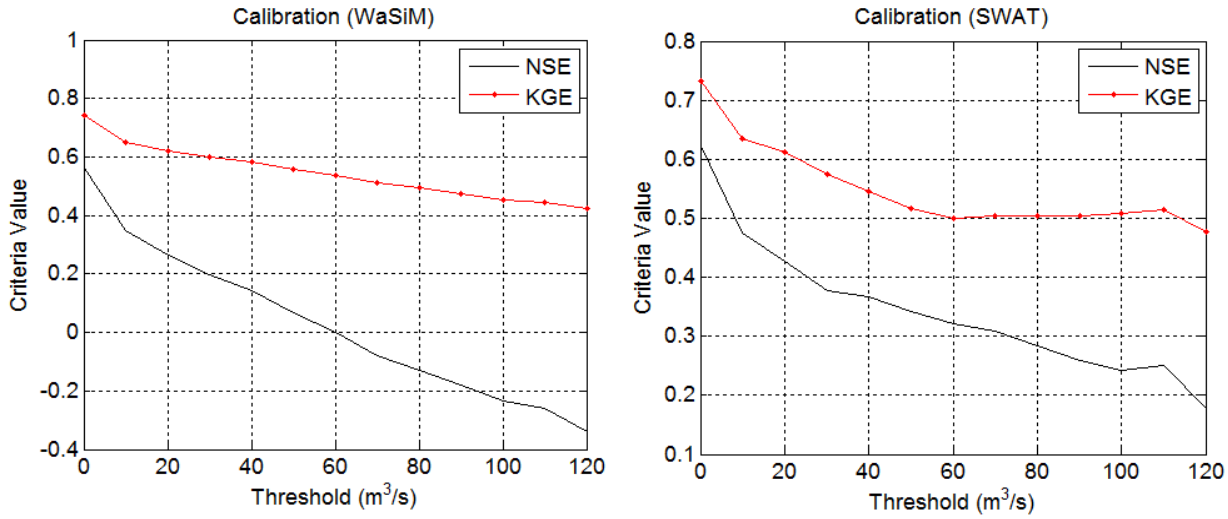

Figure 5-8: Models efficiencies for different thresholds during calibration with $\boldsymbol{thr} = \mathbf{0}\ \boldsymbol{m^3}$

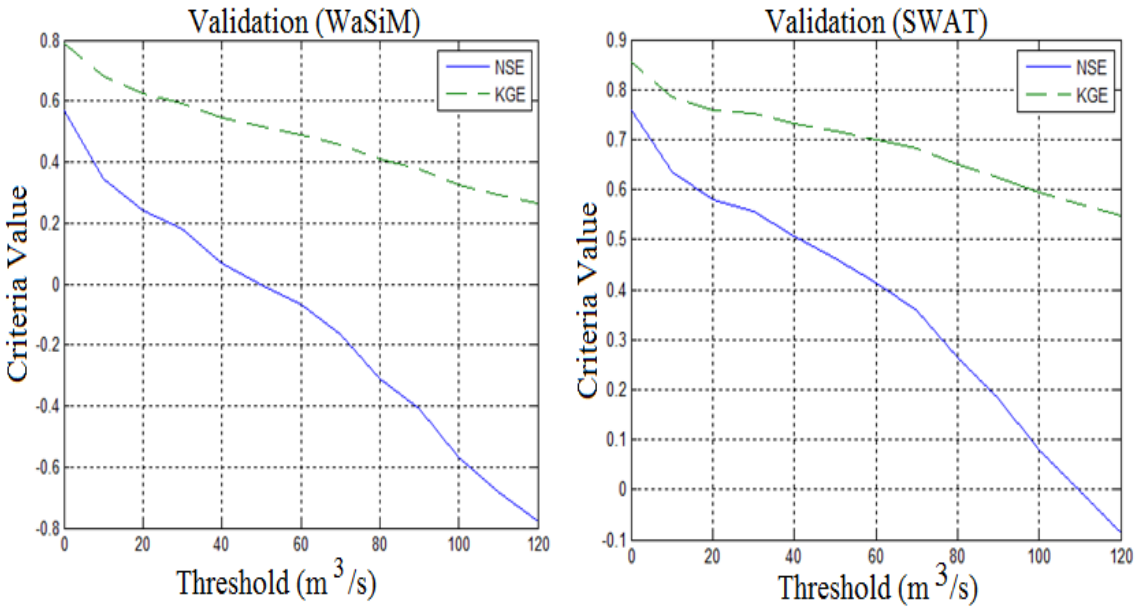

Figure 5-9: Models efficiencies for different thresholds during validation with $\boldsymbol{thr} = \mathbf{0}\ \boldsymbol{m^3}$

We recalibrated the two hydrological models by considering only the observed discharge above the threshold of 120m^3/s (1.5mm/day) which corresponds to 1.5mm/day for the

calibration (Figure 5-10) using KGE for optimization criteria. Acceptable results were found with KGE around 0.61 for WaSiM and 0.48 for SWAT at threshold of 120m^3/s. At the same time, for thresholds lesser than 120m^3/s (1.5mm/day), the KGE is higher reaching a value of 0.81 in the case of WaSiM and 0.73 in the case of SWAT. This implies that by concentrating the calibration on the discharge greater than a threshold, the other parts of the hydrograph are by the same time well simulated. This recalibration gave an added value to the modelling in term of high discharge simulation since better results are obtained in comparison to the calibration done without threshold or with $thr = 0\ m^3/s$ (see Figure 5-8).

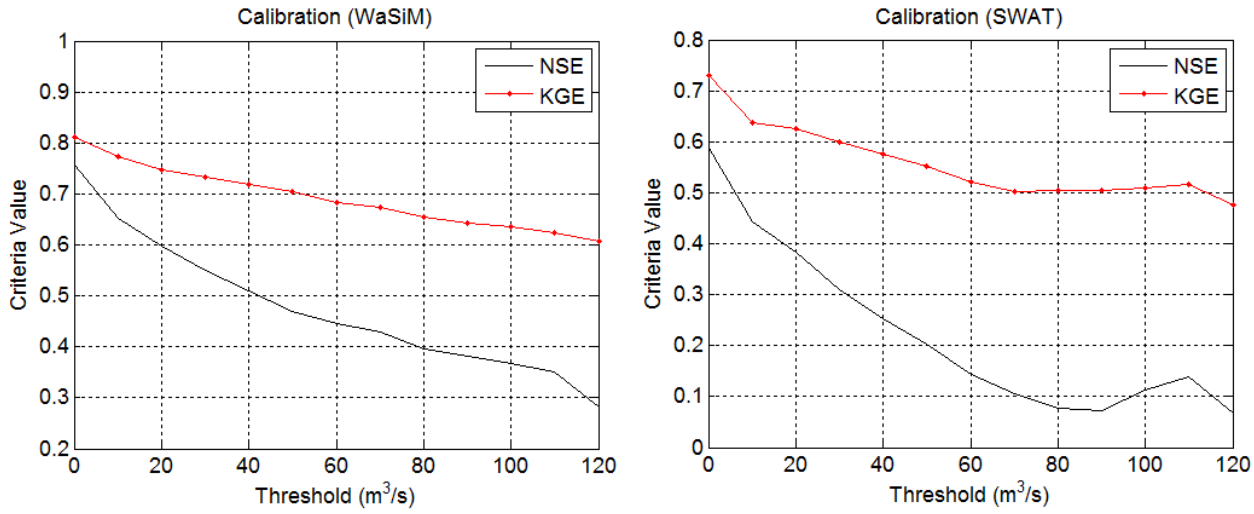

Figure 5-10: Recalibrated model performances using the threshold of 120m^3/s (1.5mm/day) for the calibration.

As far as the validation is concerned, WaSiM performed acceptably with KGE greater than 0.5 at the threshold of $120\ m^3/s$. For SWAT, the parameter set that perform well during the Calibration period did not give good performance during the validation and vice versa. For instance, during the calibration, there are a number of parameter set for which the KGE exceed 0.47 but during the validation the corresponding KGE for the same parameter sets don not exceed 0.3. Similarly, when we used the validation period to calibrate the model, the KGE exceed 0.5 for a number of parameter sets but for the corresponding validation period (previously calibration period), the KGE is very poor for the simulations respecting the water balance. We finally considered, after exploring all the parameter spaces, the simulations (parameter sets) which had good water balance for both calibration and validation periods with KGE less or equal to 0.40 (see Table 5-3) at threshold of 120m^3/s (1.5mm/day). WaSiM reproduced better the high discharge of the study area than SWAT.

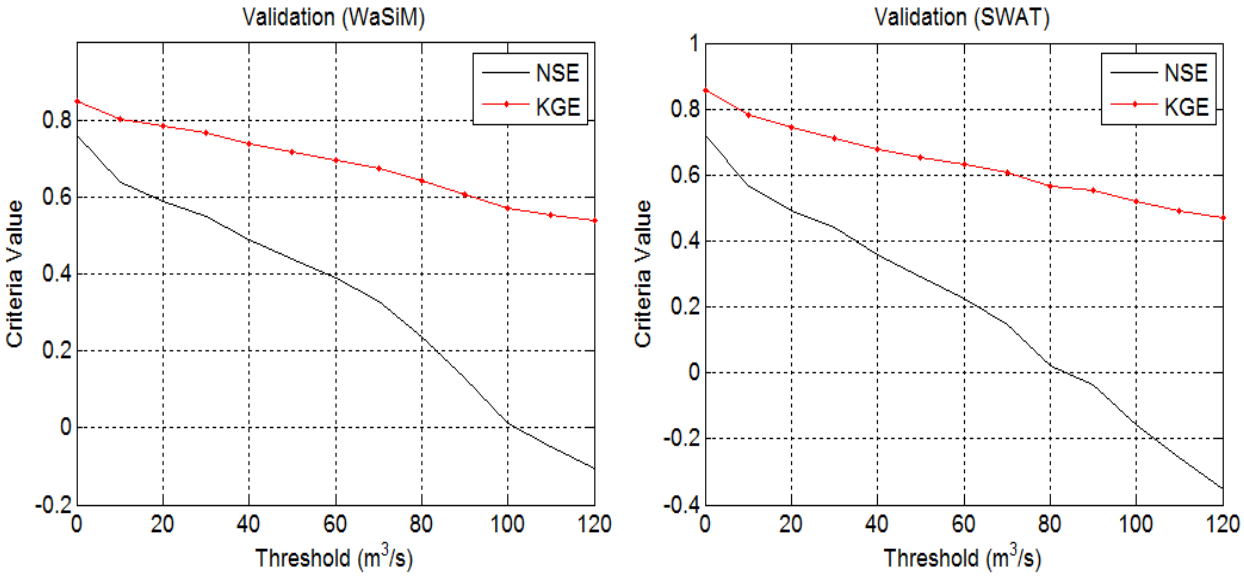

Figure 5-11: Model performance during validation done with the parameters obtained during the recalibration.

The overall water balances predicted by the models were consistent with the hydroclimatic condition of the basin (table 5-3). The interpolated mean monthly rainfall computed by SWAT for the calibration and validation periods were similar for both models. The ETR coefficient predicted by WaSiM was around 84% (87% respectively) of the rainfall and the runoff coefficient was around 16% (12% respectively) during the calibration (validation respectively). In this study, the main water balances components consider by WaSiM model are the rainfall, the ETR, the discharge and the variation of the storage. The calibration and validation of SWAT model was done that groundwater recharge through the deep aquifer recharge coefficient was minimized. In most of the cases, the deep aquifer recharge was less than 2% of the total rainfall. Due to the difference in the model structures, there is not agreement about the repartition of the rainfall in the different water balance components by the models. More ETR was simulated by WaSiM than SWAT during calibration and validation. However, the mean predicted water balance for calibration and validation periods is in line with what is regionally observed (Bossa, 2012). According to Diekkrüger *et al. (*2010), the runoff coefficients within the Ouémé basin vary between 0.10 and 0.26 with the lowest value for savannahs and forests. The results obtained are in line with this funding. In accounting for the uncertainty in discharge measurement particularly in high discharge estimation from rating curve (see section 2.2.2) and the performance criteria, we can deduce that the models reproduce acceptably the runoff and it process over the study area.

Different fractions of discharge components were obtained. The proportion of the three components of the runoff (surface runoff, interflow, and baseflow) depends on the physical characteristics of the watershed, the land use and the soil characteristics.

According to WaSiM, the interflow is the dominant runoff component while less than 5% of the total runoff was simulated by SWAT as interflow. This fact was observed by previous studies in Ouémé Catchment (Sintondji, 2005 Giertz et al., 2006; Cornelissen et al., 2013). The low fraction of interflow calculated by SWAT was explained by the model concept. In this model, the lateral flow depends on the local slope (Cornelissen *et al.*, 2013). The low interflow simulated is compensated by a high overland flow component of about 60 to 73% of the total runoff.

Table 5-3: Mean performance criteria and mean water balance components as simulated by WaSiM and SWAT models during the recalibration period (2005:2009) and the validation period (1991:1998) with a threshold of 120m^3/s (1.5mm/day) based on 10 behavioral simulations. ETR is the real evapotranspiration; ETP, the potential evapotranspiration, SHL_AQ_R is the shallow aquifer recharge and APB is the absolute percentage bias. CoefRun (CoefETR) is the percentage of the mean annual discharge (ETR respectively) to the mean annual rainfall.

	Calibration						Validation					
	WaSiM			SWAT			WaSiM			SWAT		
	Min	Mean	Max	Min	Mean	Max	Min	Mean	Max	Min	Mean	Max
KGE	0.50	0.54	0.60	0.36	0.37	0.40	0.50	0.52	0.54	0.35	0.37	0.39
APB	0.32	3.39	8.21	10.23	12.65	15.42	9.85	16.04	19.44	6.26	8.46	9.98
CoefRun	15.24	16.14	18.00	16.04	16.25	16.69	11.46	12.24	13.68	12.26	12.51	13.03
CoefETR	82.13	83.92	84.86	66.60	66.83	67.09	85.84	87.10	87.81	70.65	70.89	71.14
Rainfall	1179	1179	1179	1193	1193	1193	1158	1158	1158	1166	1166	1166
Total Runoff	180	190	212	191	194	199	133	142	158	143	146	152
Interflow	139	151	164	2	5	15	102	110	122	2	4	12
Overland	13	17	21	125	133	140	10	12	16	101	107	114
Baseflow	12	22	35	43	56	64	10	20	30	25	35	41
ETR	968	989	1000	795	797	801	994	1008	1017	824	827	830
ETP	2239	2306	2344	1509	1509	1509	2248	2317	2357	1514	1514	1514
Storage	-5	-1	2	15	17	18	5	8	9	14	15	16
SHL_AQ_R	-	-	-	177	185	190	-	-	-	170	179	183

The interflow simulated by WaSiM represented respectively 79% and 77% of the total runoff during calibration and validation. The simulated percentages of baseflow which preserves the discharge during the dry season are respectively 12% and 14% of the total discharge during calibration and validation. Similar results were obtained by Legesse et al. (2003) for a catchment located in central Ethiopia (tropical catchment) for which around 10% of the total runoff was simulated as overland flow. The contribution of the overland flow is relatively small and can be explained by the absence of impervious zone in the catchment otherwise the quick flow would have been higher. The mainly cultivated/grazing land in the watershed favors infiltration in the soil zone and thereby lateral subsurface flow along subsurface channels, macro pores, and fractures (Legesse *et*

al., 2003) and this would explain the relatively small contribution of overland flow to the streamflow.

5.4.4 Graphical assessment of the models results for threshold $thr \neq 0\ m^3/s$

The observed and simulated discharges above the threshold of 120m³/s for both models are shown on Figure 5-12. Some of the peaks are well simulated but the models fail to reproduce other peaks. Data quality is a critical issue and even more concerning the high discharge when performing hydrological modelling. The fact that the optimum discharges simulated by both models are well correlated with correlation coefficient of 0.8 with p-value less than 10^{-4} combined with difference in models structure may raise the important issue of the quality of observed discharges mainly the high discharge which required extrapolation from water level using the rating curves.

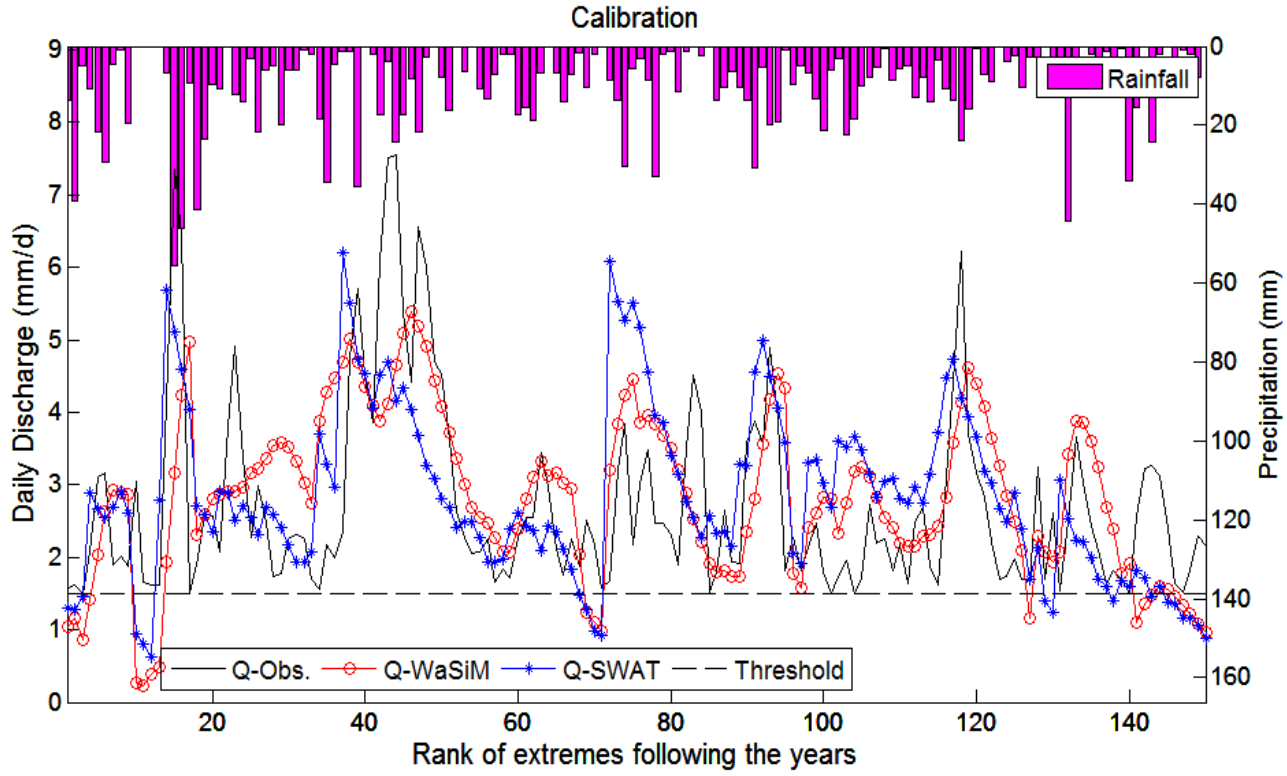

Figure 5-12: Observed and simulated high discharge (greater or equal to 120m3/s or 1.5mm/day) by WaSiM and SWAT during recalibration period of 2005-2009.

Experience suggests that uncertainty in both measurements and predictions of flood peaks increases with peak magnitudes (Beven, 2012). Therefore, it cannot be expected that the simulated discharge peaks will match exactly the observed peaks. The standard practice is to match as well as possible the two signals. Generally, the models acceptably represent the variability in the observed high discharge over the basin.

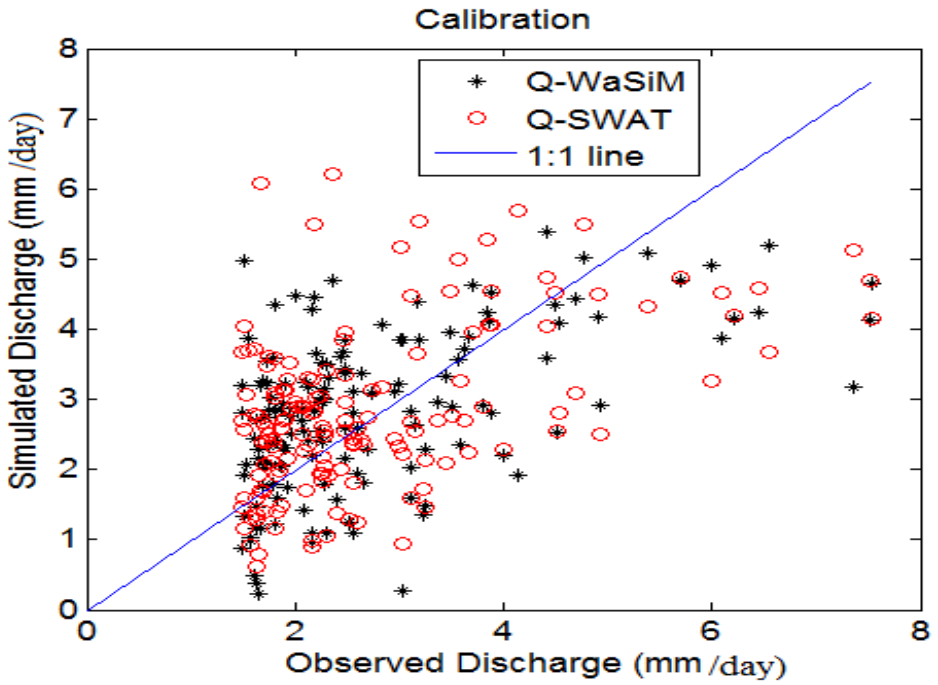

Figure 5-13: Scatter plot of the observed and simulated discharges by WaSiM and SWAT during the recalibration period.

5.4.5 Models sensitivity and uncertainties analysis

For WaSiM (see appendix A-b), a number of parameters (Appendix B, **Error! Reference ource not found.**) were calibrated in the first step. These are the drainage density (DD), the interflow parameter (KI), the direct runoff parameter (KD), the base flow parameters and mainly some land use and soil parameters. The drainage density parameter directly determines the amount of interflow which can be generated per time step. It expresses the drainage density of the (sub-) catchment as well as the anisotropy with regard to the vertical and horizontal hydraulic conductivities. The parameters KD and KI denote the storage coefficients of the surface runoff and the lateral flow, respectively (Schulla & Jasper, 2007, Herbst *et al.*, 2009). The optimization was done mainly on the parameters which are found more sensitive (based on the partial correlation). As defined in Moriasi *et al*. (2007) the sensitivity analysis is a process through which we evaluate the rate of change in the model output (discharge) with respect to changes in model inputs (parameters). The sensitivity analysis of WaSiM shows that the leaf surface resistance RSC, the interflow parameter KI, the drainage density DD, the direct or surface runoff KD and the hydraulic conductivity Ks are the main drivers of high discharge in the basin (**Figure 5-15**). RSC5 corresponds to the leaf surface resistance of agriculture land which is the dominant land use type in the study area. It appears sensitive to the general model performance (KGE) and to the main runoff components with sensitivity index among the highest computed. Higher this parameter, higher is the performance criteria and the interflow, meaning that a better model performance could be achieved by increasing this

parameter. Keeping in mind that increasing this parameter will result in more interflow generated and less direct runoff which evidentially will bias the runoff components, we did not increase this parameter. A compromise between a good simulation of runoff components at the detriment of getting better performance criteria for the total discharge or vice versa is needed. Given that realistic hydrology is the foundation of any model and any hydrological modelling, attention was paid to the simulation of the different water balance components and runoff components. Another parameter which influences highly the runoff generation and the model performance is the drainage density (DD). It behaves like the RSC5 parameter for the model performance and water balance. The water balance components appeared very sensitive to the DD parameter. An increase in this parameter leads to an increase in the interflow (and the total runoff) but a decrease in the overland flow, baseflow and the real evapotranspiration (ETR) (figure 5-15). The model performance and the water balance components were found sensitive to the hydraulic conductivity Ks for Albic Plinthosol and Mollic Gleysol (which are among the dominant soil types with respectively 22% and 20% of the study area).

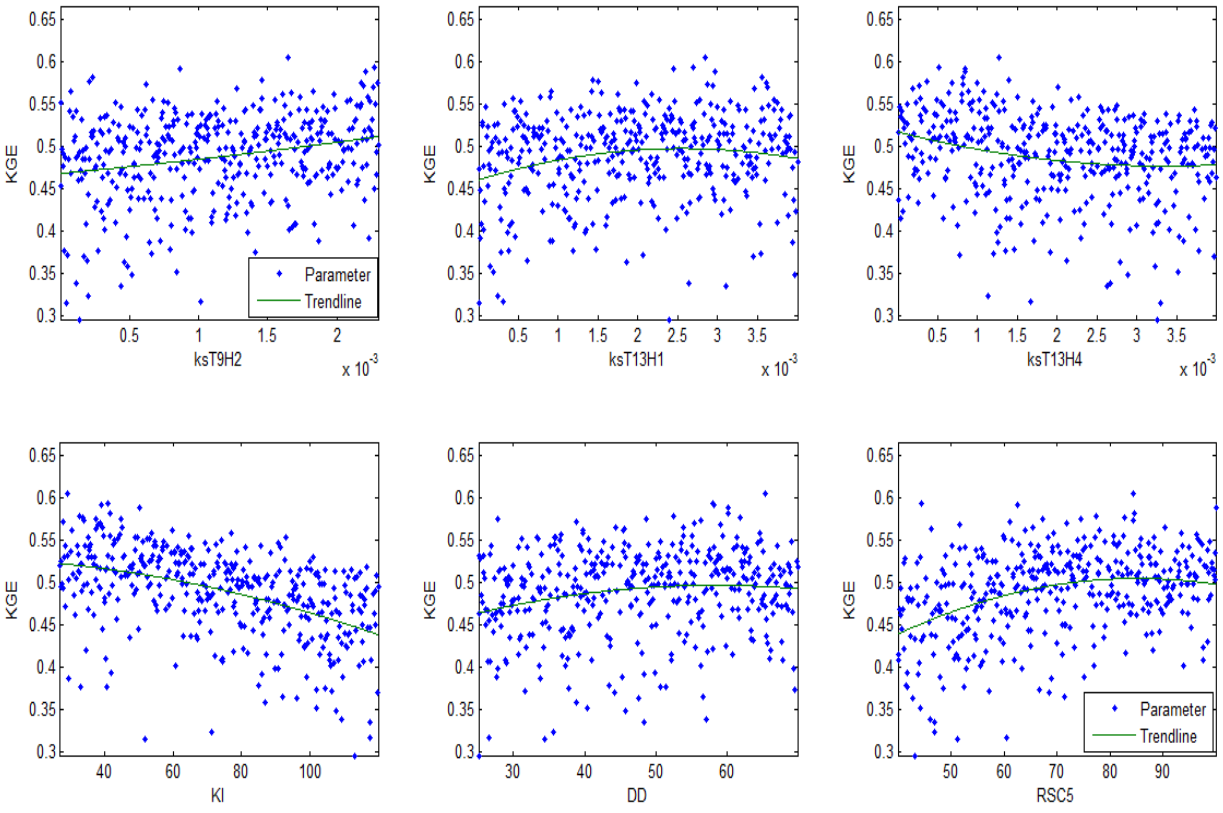

Figure 5-14: Scatter plot of KGE and some parameters detected as sensitives for WaSiM at threshold of 120m^3/s (1.5mm/day) with sensitivity index ≥0.3: the hydraulic conductivity of Albic Plinthosol (KsT9H2) and Mollic Gleysol (KsT13H1, KsT13H4), the interflow parameter KI, the drainage density DD and the leaf surface resistance of agriculture land RSC5.

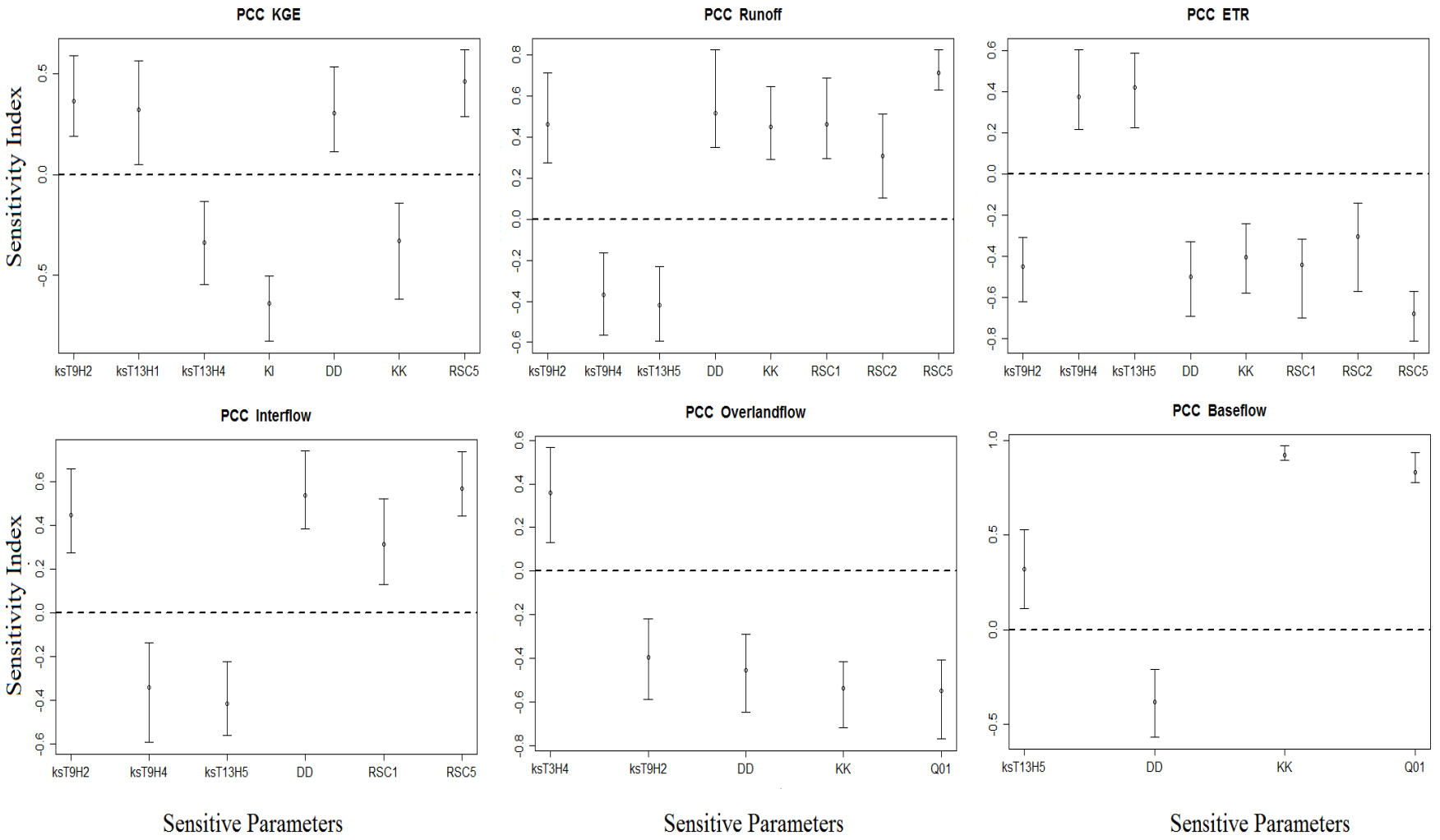

Figure 5-15: Sensitivity Index (corresponding to the partial correlation coefficient (PCC), see sub-section 5.3.2) for the most sensitive WaSiM parameters with absolute PCC greater or equal to 0.3. The uncertainty bounds and the real computed indices are represented for each sensitive parameter. The parameters are: the hydraulic conductivity of Albic Plinthosol (KsT9H2) and Mollic Gleysol (KsT13H1, KsT13H4), the interflow parameter KI, the drainage density DD, the leaf surface resistance of agriculture land RSC5, the baseflow parameters KK and QO1.

Overall, the parameters that were found very sensitives to the total runoff are also sensitives to the real evapotranspiration with evidentially an opposite effect. An increase in total runoff results in a decrease in real evapotranspiration and vice versa.

In SWAT (see appendix A-a), 17 parameters (Appendix B, **Table 0-2**) were included in the calibration procedure: the Curve Number, the soil parameters, groundwater parameters and others. After thousands of runs, some of the parameters were found more sensitive parameters to high discharge (above 120m^3/s, (1.5mm/day)) with significant correlation between these parameters and the KGE (Figure 5-17): (i) SURLAG, the surface runoff lag time. SWAT incorporates a surface runoff storage feature to lag a portion of surface runoff release to the main channel. SURLAG controls the fraction of the total available water that will be allowed to enter the reach on any one day. High correlation was found between this parameter and the KGE. (ii) SOL_K, the saturated hydraulic conductivity. It relates the soil water flow rate (flux density) to the hydraulic gradient and is a measure of the ease of water movement through the soil. (iii) GWQMN, threshold depth of water in the shallow aquifer required for return flow to occur.

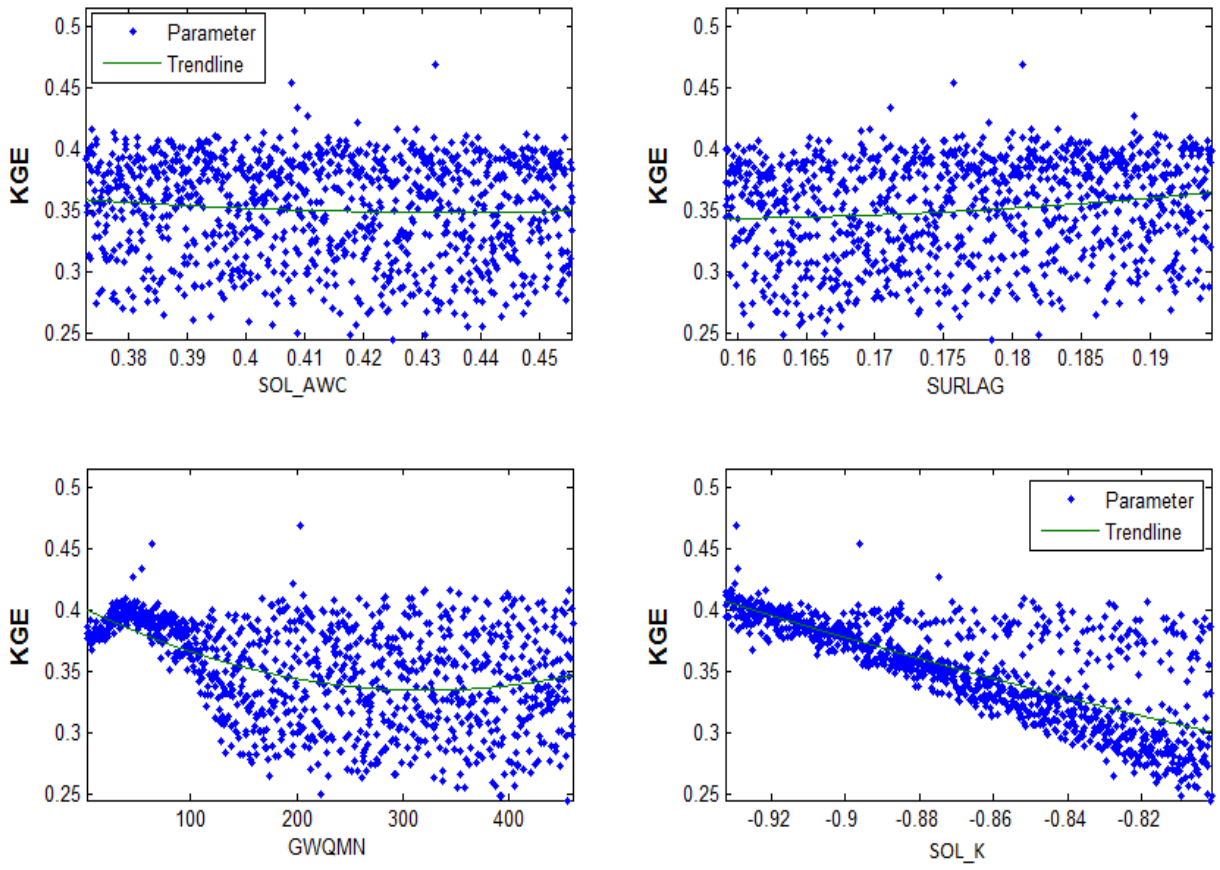

Figure 5-16: Scatter plot of some sensitive parameters and the associated KGE based on the partial correlation coefficient.

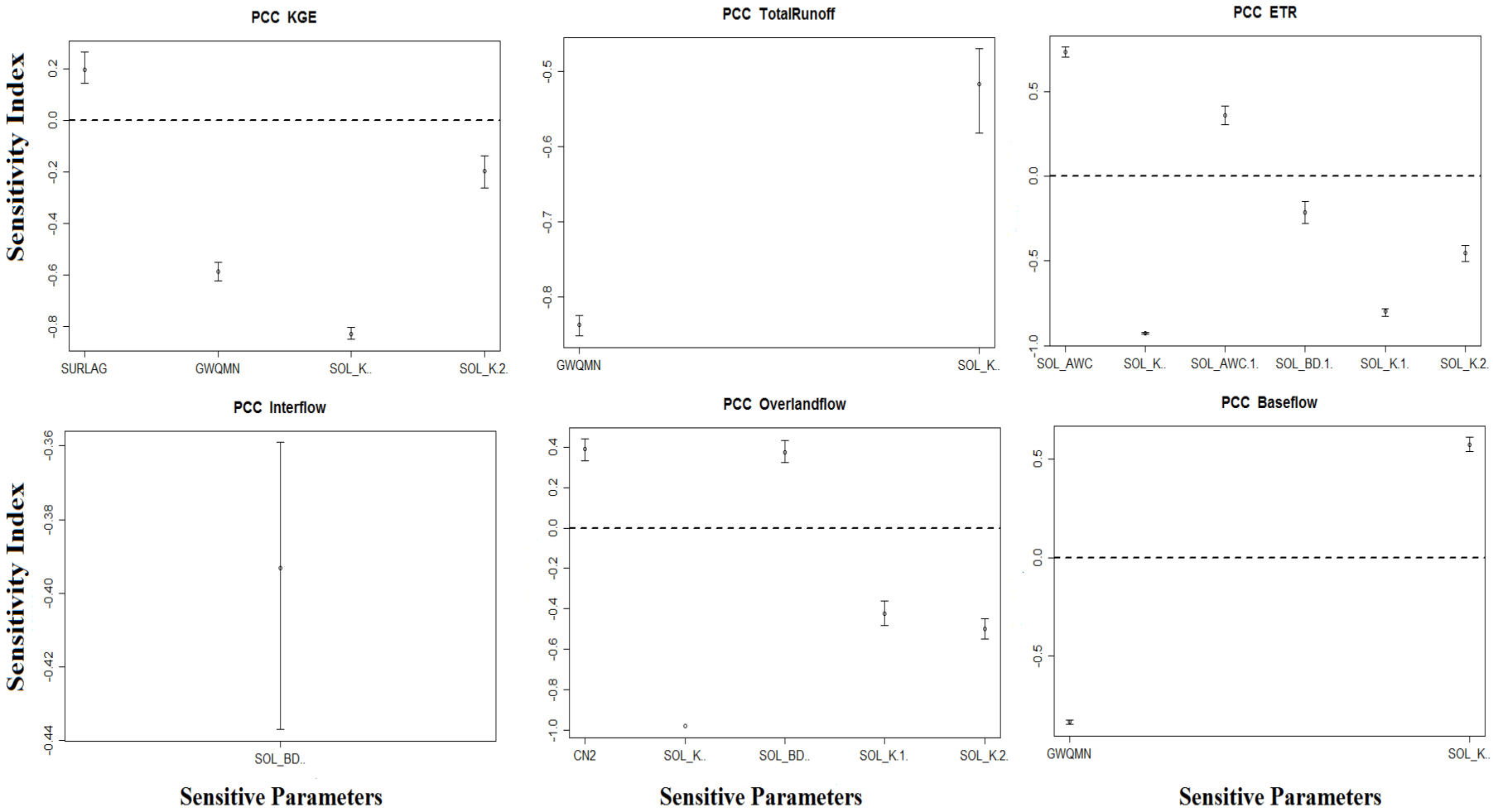

Figure 5-17: Sensitivity Index based on the partial correlation coefficient (PCC) for the most sensitive SWAT parameters with absolute PCC greater or equal to 0.2. The uncertainty bounds and the real competed indices are represented for each sensitive parameter. The surface runoff lag time, SURLAG; threshold depth of water in the shallow aquifer required for return flow to occur, GWQMN; Saturated hydraulic conductivity, SOL_K (if a number is specified, it indicates the corresponding layer); available water capacity of the soil layer, SOL_AWC (if a number is specified, it indicates the corresponding layer); Moisture bulk density, SOL_BD and the SCS runoff curve number, CN2**.**

Quantities used to access the uncertainty measure are the P-factor, which is the percentage of data bracketed by the 95PPU band, and the R-factor, which is the average width of the band divided by the standard deviation of the corresponding measured variable. Figure 5-18 illustrates the 95% prediction uncertainty (95PPU) and the observed discharge for WaSiM and SWAT models during 2005:2009. Large uncertainties are found for both models with R-factor greater than 1 (2.3 for SWAT and 2.9 for WaSiM). Nevertheless, acceptable P-factors were found for both models: more than 80.6% of the observed data are bracket by the 95PPU for SWAT and more than 75% of the observed data are bracket by the 95PPU for WaSiM. A larger P-factor can be achieved at the expense of a larger R-factor.

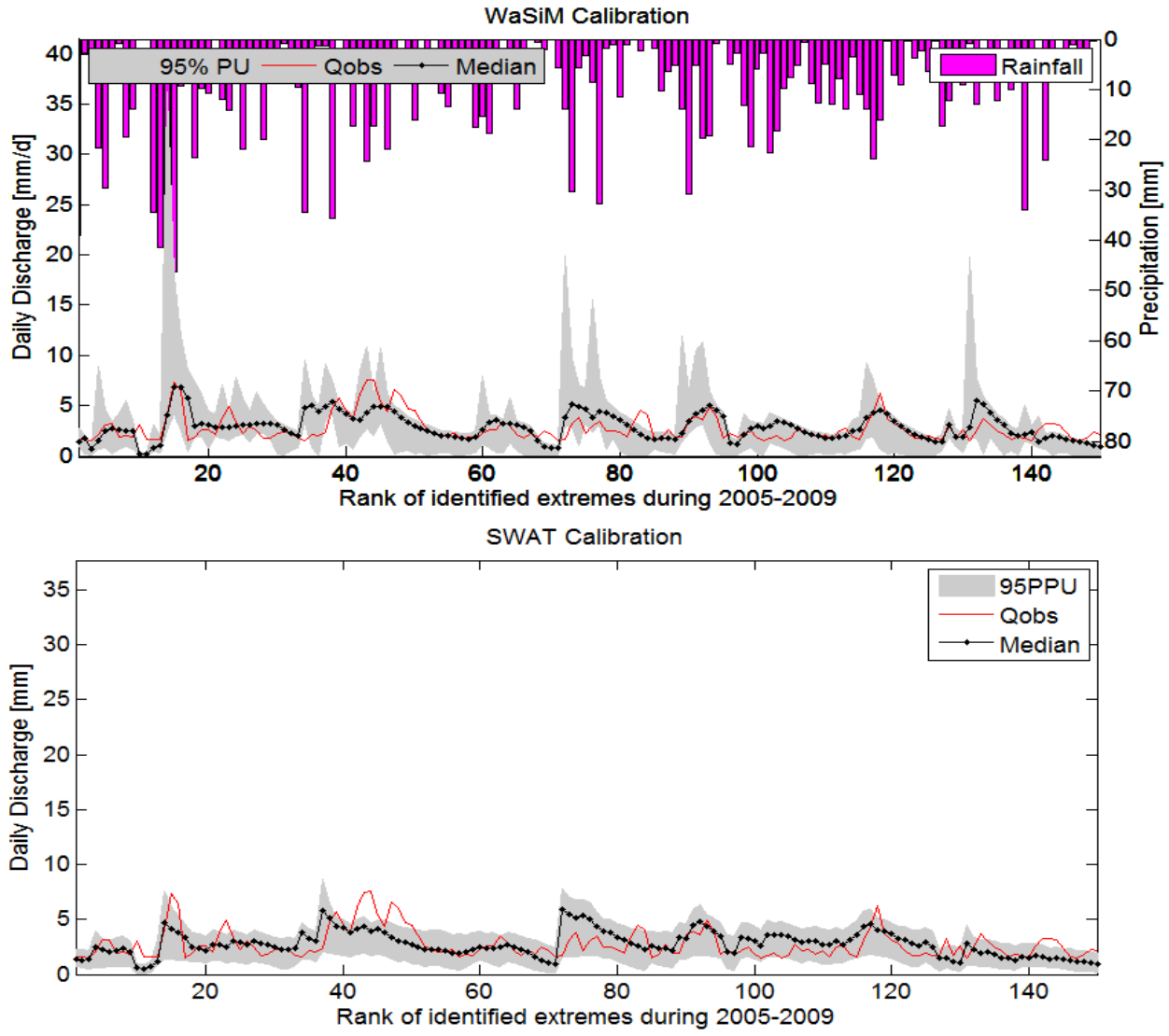

Figure 5-18: 95 percent predictive uncertainty (95PPU) of observed discharge during the calibration period of 2005:2009. Qobs is the observed discharge above 120m^3/s (1.5mm/day).

5.5 Conclusions

In this study, we evaluated the performance of SWAT and WaSiM models in simulating discharge over Atchérigbé basin. The calibration and validation of these models are necessary and prior to their use for any impact assessment. Statistical and graphical methods were used for model performances evaluation. It was found that both models perform satisfactorily in simulating discharge in Atchérigbé basin for the period 1991-2010. In fact, the absolute percentage bias is less than 15%, the NSE value greater than 0.5 and the KGE is greater than 0.6 for calibration and validation periods for both models when using the threshold of $0m^3/s$ to quantify the objective function. After this, we recalibrated the two models by considering only the discharge above the threshold of $120m^3/s$ (1.5mm/day) and acceptable results were found. Due to the uncertainties in discharge measurement and mainly in the peaks estimated from the rating curve, the model performances were not as good for high discharge as for the whole hydrograph. Nevertheless, we realized that by calibrating the models on high discharge above a given threshold, the discharge which are below this threshold are by the same time well simulated. When we compared the performance of both models, WaSiM simulated better the high discharge than SWAT model during the calibration and validation. Notwithstanding their similarity in modelling capacity, a graphical comparative analysis show that WaSiM slightly better predicted high flows than SWAT model.

Generally, stage–discharge rating curves are obtained by extrapolation when a water level is recorded below the lowest or above the highest gauged level. Large errors can result from extrapolation of ratings beyond the range of gauged discharges without consideration of cross-section geometry and controls (Legesse *et al.*, 2003, Mosley & McKerchar, 1993). In fact, during the high discharge period, the water may overflow the stream channel complicating the reliability of the stage-discharge relationship and leading to underestimation of high discharges. Using these discharges during rainfall-runoff modelling will necessarily impact on the performance of the simulation. This may explain the moderate performance of the hydrological models in simulating the high discharge in the Zou catchment.

The sensitivity analysis performed show that the leaf surface resistance RSC, the interflow parameter KI, the drainage density DD, the direct or surface runoff KD and the recession constant Krec are the most sensitive parameters of WaSiM when simulating high discharge over the Zou catchment at Atchérigbé station. For SWAT model, the most sensitive parameters are the surface runoff lag time, SURLAG; threshold depth of water in the shallow aquifer required for return flow to occur, GWQMN; available water capacity of the soil layer, SOL_AWC, Saturated hydraulic conductivity, SOL_K. We also performed the uncertainty analysis for both models using the 95 percent predictive uncertainty band characteristics meaning the p-factor and the r-factor. Very good p-factors were found but the r-factors were greater than 1. Nevertheless, performances of both models are acceptable and they can be used for impact study in the area of interest.

6 SCENARIO BASED LAND USE CHANGES IMPACT ON HIGH DISCHARGE ASSESSED BY DISTRIBUTED (WASIM) AND SEMI-DISTRIBUTED (SWAT) HYDROLOGICAL MODELS.

Due to the complexity of the processes involved, the magnitude of their impact (land use change) on storm-runoff generation and subsequent flood discharge into the river system is still highly uncertain.
Niehoff et al., 2002

Abstract

The present session aims is to assess the effects of land use change on flood regime in one of the tributaries of Ouémé basin. The analysis has been carried out by applying distributed and semi-distributed hydrological models (WaSiM and SWAT) to generate river flow after calibration and validation. Projected land use maps for the time horizon 2015–2019; 2020-2024 and 2025–2029 combined with two socio-economic scenarios have been used as forcing inputs for the hydrological models. The peak over threshold analysis was undertaken to produce flood frequency distributions from which the magnitude and return periods are computed. A methodology to assess change in flood frequency and magnitude relatively to the baseline was then applied. According to the median of all scenarios, the magnitude of flood event is shown to increase for most return periods, changes being greatest for low return periods. Though increase in magnitude of flood events was simulated by both models and for the different scenarios, the magnitude of change is influenced by the model types. The overall combined results from WaSiM and SWAT show that a 5-year event may become a 3.4-year or 4.7-year event depending on the scenario. The more extreme events are projected to most often occur. A 40-year flood event may turn into a 23.4-year or 31.1-year event depending on the scenario. These increases in flood magnitudes are accompanied with increase in mean monthly and mean annual discharges in the study area. However, these results should be interpreted with caution in light with the uncertainty related to the uncertainty in land use scenario and hydrological models.

6.1 Introduction

Environmental changes, such as land use change and climate change are expected to impact water cycle by increasing potential evapotranspiration, rainfall variability and distributions and streamflow. The magnitude and frequency of floods and droughts could be significantly affected as results of the change in rainfall patterns. Changes in land use and land cover have definite and predictable impacts on climate, hydrology, biodiversity and biogeochemical cycles. Changes in land use will happen at high rates in Benin, mainly because of a doubling in the population within the next 30 years (Menz *et al.*, 2010). Located at about 90% in Benin, the Ouémé basin is the largest basin. Some authors have focused on the analysis of land use change impact on the hydrology of the

Ouémé basin. Giertz et al. (2010) analyzed the impact of land use change on the hydrology of the Upper Ouémé catchment using spatially distributed land use change scenarios and found that the model results, particularly surface runoff, are highly sensitive to changes in land use. Scenario-based impacts of land use and climate change on land and water degradation from the meso to regional scale in the Ouémé basin was done by Bossa *et al.* (2014) and they found that surface runoff, groundwater flow, sediment and organic N and P yields were affected by land use change (as major effects) up to +50%, while water yield and evapotranspiration were dominantly affected by climate change of −31% to +2%. Cornelissen *et al.* (2013) assessed the impact of land use and climate change on discharge in the Térou catchment (a sub-catchment of Ouémé basin) by multi-models ensemble simulation. All models simulated an increase in surface runoff due to land use change. It is clear from the previously cited studies that a change in land use will results in change in discharge in the study area. However, no study investigated how change in land use will impact on high discharge over the Ouémé basin. Repeated severe floods and related damages in Benin (EM-DAT, 2010) have raised the concern of how floods have been affected by regional climate variations and by human induced changes in land cover and land-use in the country. To address this concern and related issues it is important to know how climate, land-use and land-cover changes in the region affect the annual and seasonal variations of basin hydrology and streamflow especially the high discharge. This knowledge is essential for long-term planning for land-use to protect water resources and to effectively manage floods (Guo *et al.*, 2008). It also has important ecological and socioeconomic implications for the region.

In previous studies (see chapter 4), potential climate change impacts on extreme rainfall were analysed. We applied a method to detect change in the intensity and frequency of extreme rainfalls. No general upward trend was found. Nevertheless, among the 34 rainfall stations investigated, 57% exhibit an upward trend and 43% a downward trend. Spatial interpolation of 10-year return period of heavy rainfall using the kriging method reveal that there is an west to east gradient in the south of the Ouémé basin while the decreasing tendency is dominant for the other parts of the basin. Nevertheless, more investigations are needed by using long term climate projection to quantitatively assess the impact of climate change on flood regime in the Ouémé basin. This is beyond the scope of this work and will be done in future study. Additionally, we investigated trends in extreme discharge by applying the Mann Kendall trend test and Spearman rho test. It has been found that the extreme discharge data analyzed did not significantly change over the period of 1952-2009 and no general increasing trend was detected. The remaining element that influence flood recurrence is land use. It is important to analyze how the frequency of fixed magnitude events may change in the future. This can help to examine changing frequency of flood protection measures may fail (Prudhomme *et al.*, 2003). Thus, the present study aims to investigate how changes in land use /land cover will affect the frequency and the magnitude of flood events in the study area. To this end, two hydrological models were chosen, WaSiM (Water balance Simulation Model) and SWAT

(Soil and Water Assessment Tool) and they were successfully calibrated and validated in the previous chapter.

After model set-up, model calibration and model validation using the 2003 land use, the next step is the implementation of land use change scenarios. This implies running the two models with the parameters obtained from the current land use condition but with different land use classes (new fraction of land use type with new spatial arrangement). Same parameters are used for the present and future conditions in order to reduce model parameter uncertainty. As stated by Huisman *et al. (*2009) a key factor for the simulation of land use change effects is to account for differences in evapotranspiration (ET) of different land use classes. For that purpose, same method for the computation of ETP was used for both models namely the Penman–Monteith method. In other hand, soil properties (hydraulic conductivity, storage capacity…) are strongly influenced by the vegetation types so change in land use will impact on soil properties especially in WaSiM. In SWAT, this change is covered by the SCN-Curve Number which depends on local land use, soil type. The spatial discretization of the models was done in such a way that all the land use types (9 land use types) were considered in the simulation.

6.2 Land use and land use change scenarios

A land use/land cover map was established within the RIVERTWIN project at a scale of 1/200.000 from satellite images from LANDSAT ETM Plus of 2003 using 3 scenes (Igué *et al.*, 2006). After image treatment, imaged maps were established and interpretation keys were defined. For efficacy reasons, the interpretation was carried out at the scale of 1/50.000 in order to get maximum information and for more than 650 observation points ground data were available. Finally, 17 land use/cover classes were defined. The subsequent accuracy check shows that the overall interpretation accuracy is high (87 %) (Igué *et al.*, 2006, RIVERTWIN, 2007).

In the Ouémé basin, the major driver for land use change is population growth and subsequent conversion of the natural savannah vegetation into settlements, roads and a mosaic of fields by slash and burn. Together with stakeholders, two socio-economic scenarios were set up: LUA is characterized by a stronger economic development, controlled urbanization, the implementation of two large-scale irrigation schemes and by 3.2% population growth per year; LUB is characterized by a weak national economy, uncontrolled settlement and farmland development, and a 3.5% population growth per year (Götzinger, 2007). These scenarios are also used in the national planning administration of Benin. For each scenario, the population growth has been translated into a specific demand for settlements and agricultural area according to the development of the national framework. According to the proximity to roads and existing villages, new settlements and agricultural areas have been created leading to new land use distribution. Therefore, large areas of natural vegetation were also accordingly converted to croplands (Bossa *et al.*, 2014). With respect to the scenarios LUA and LUB, change in the Ouémé

land use/cover is expressed by the conversion of the natural vegetation including savannah into agricultural lands and pastures: 10% to 20% for the scenario LUA and 20% to 40% for the scenario LUB. For Atchérigbé basin, this consists of natural vegetation conversion into agriculture lands and pasture, 18.7% to 48% for the scenario LUA and 19.8% to 55.8% for the scenario LUB. The most noticeable increase is in the pasture land use type varying from 18.7% to 25.7% for both scenarios. Three time windows have been chosen for each land use scenario: 2015–2019; 2020-2024 and 2025–2029. Figure 6-1 shows the mean percentage change of the different land use type for each scenario. It can be observed that the agricultural and pasture lands have increase for the different scenario while the other land use types decrease in percentage.

A combination of the two land use scenarios with the three time horizons lead to six different scenarios (see Table 6-1). For example, LU2017A is the land use scenario A for the time window 2015-2019. Similarly, LU2027B is the land use scenario B for the time horizon 2025-2029.

Table 6-1: Different land use scenarios with the corresponding time horizon.

Time horizons and Land Use scenarios	2015–2019	2020-2024	2025–2029
LUA	LU2017A	LU2022A	LU2027A
LUB	LU2017B	LU2022B	LU2027B

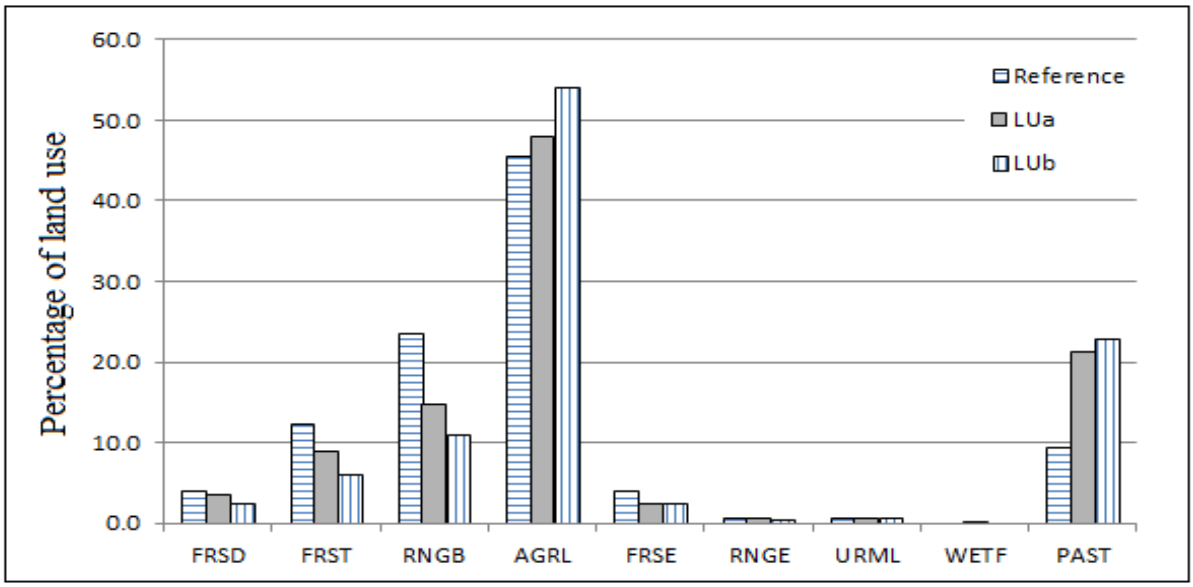

Figure 6-1: Change in land use scenario. The different land use types are forest-deciduous (FRSD), forest-mixed (FRST), range-bush (RNGB), agriculture (AGRI), forest-evergreen (FRSE), range-grasses (RNGE), urban area (URML), wetlands-forest (WETF), and pasture (PAST).

6.3 Flood calculation

Where data are available at long-term gauging stations, it is normal to fit a statistical distribution to either the annual maximum peaks or the peaks over a chosen threshold as a way to define the frequencies of extremes (Beven, 2012).The objective of flood frequency analyses is to link the magnitude of extreme or high discharge to their frequency or probability of future occurrence. This analysis is done by selecting either the most extreme events of each year known as the block maxima approach or by selecting all the events over a given threshold known as the peak over threshold approach. Then, the data are fitted to a selected probability density function to derive the flood frequency distribution. Typically, the estimation of extreme events such as a 100-year flood involves significant extrapolation from the period of observed data, e.g. a 30-year time series, and will be sensitive to the choice of the probability density function (Lehner *et al.*, 2006). Due to the reduced data length, the peak over threshold approach (see section 6.4.2) is adopted in this work and the generalized Pareto distribution (GPD), a flexible and robust distribution, is used for frequency analysis.

The GPD can be described by three parameters: the shape parameter κ, the scale parameter σ and the location parameter ε. Its cumulative distribution function is as follow:

$$\begin{cases} F(X \le x|\, \varepsilon, \sigma, \kappa) = 1 - \left[1 + \kappa\left(\frac{x-\varepsilon}{\sigma}\right)\right]^{\frac{-1}{\kappa}}; & \kappa \neq 0 \ \ and \ \ \ 1 + \kappa\left(\frac{x-\varepsilon}{\sigma}\right) > 0 \\ F(X \le x|\varepsilon, \sigma, \kappa) = 1 - exp\left(-\frac{x-\varepsilon}{\sigma}\right); & \kappa = 0 \qquad \sigma > 0 \end{cases} \quad \textbf{(Eq. 6-1)}$$

Since the location parameter representing the threshold is known in advance, there is no need to estimate again this parameter. Equation 1 can be transformed in the following way:

$$\begin{cases} F(Y \le y|\, \sigma, \kappa) = 1 - \left[1 + \kappa.\left(\frac{y}{\sigma}\right)\right]^{\frac{-1}{\kappa}}; & \kappa \neq 0 \ \ and \ \ \ 1 + \kappa\left(\frac{x}{\sigma}\right) > 0 \\ F(Y \le y|\sigma, \kappa) = 1 - exp\left(-\frac{y}{\sigma}\right) & \kappa = 0 \qquad \sigma > 0 \end{cases} \quad \textbf{(Eq. 6-2)}$$

The occurrence of events is assumed to be a Poisson process. Given a discrete variable N, expressing the annual number of occurrences of a given event and λ, the average rate of occurrence per year, the number n of events occurring in any year constitutes a Poisson variate, with probability (Beguería, 2005):

$$P(N = n|\lambda) = e^{-\lambda} * \frac{\lambda^n}{n!}, n = 1, 2, \ldots \quad \textbf{(Eq. 6-3)}$$

The Poisson assumption implies that the occurrences λ are independent, i.e. the probability of observing an extreme event in time $t + j$ does not depend on the occurrence of an extreme event in time t. The dispersion index DI is defined as the ratio of the variance to the mean. Given that the variance and the mean of a Poisson distribution should be equal, it is expected that DI will be equal to one. This is an important property which can help to find the threshold x_0 from which the selected POT data follows the Poisson process.

Under the assumption of Poisson, the T-year exceedance X_T is defined as the $(1 - 1/\lambda T)$ quantile in the distribution of the exceedances with λ, the frequency parameter of the Poisson process distribution, equalling the average number of exceedances per year and can be estimated from the sample mean (see below). Inverting equation (2) and substituting for X, we obtain the following expression for the T-year event X_T, expressed in the original scale x_0 (Beguería, 2005):

$$\begin{cases} X_T = F^{-1}(1 - 1/\lambda T; \sigma, \kappa) = x_0 + \frac{\sigma}{\kappa} * \left(\left(\frac{1}{\lambda T}\right)^{-\kappa} - 1\right), \quad 0 < \frac{1}{\lambda T} < 1, \quad \kappa \neq 0 \\ X_T = F^{-1}(1 - 1/\lambda T; \sigma, \kappa) = x_0 - \sigma * \log\left(\frac{1}{\lambda T}\right) \qquad\qquad \kappa = 0 \end{cases} \quad \textbf{(Eq. 6-4)}$$

$1 - p = 1 - \frac{1}{\lambda T}$, $p\ is\ the\ probability\ of\ exceedance\ and$ $(1 - p)$ is the probability derive from the cumulative distribution function.

In this study, two flood indicators are investigated: severity of flood events known as change in the magnitude of flood events of a fixed return period and frequency of flood events described by the change in the return period (i.e. frequency of occurrence) of a flood event of fixed magnitude. We analyze events of different return periods and focus on changes instead of quantity. A comparison between quantiles in on hand and return periods in other hand will give an indication on how future land cover will impact on flood regime. We always used the same climate data in this chapter.

6.4 Results and discussions

6.4.1 Change in mean monthly and mean annual discharge

From the daily discharge simulated, the monthly and annual means discharges were computed for each scenario and compared to the baseline meaning the mean monthly and annual discharges computed for the baseline simulation (using the land use map of 2003) not the observed discharge in order to reduce the model structure uncertainties (reducing the variability in the model bias). This way of doing is common in scenarios projection. For example, in IPCC climate change prediction (IPCC, 2001), changes are reported relatively to the simulation of the baseline and not to observed data. Similarly, Huisman

et al. (2009) performed land use change scenario relatively to the baseline simulation. Modelling errors are assumed to be of the same order of magnitude under current and changed conditions when using the same model and can thus be ignored (Prudhomme *et al.*, 2003). Errors from the input data which are propagated to the outputs are assumed to be of the same order of magnitude and can be as well neglected. In WaSiM, changes in land use are described by vegetation parameters. Changes in the distribution of land use parameters result from the usage of different land use maps for the scenarios and cause a change in potential and actual evapotranspiration and, therefore, in total discharge therefore in runoff components (Cornelissen *et al.*, 2013). Figure 6-3 shows changes in mean monthly water balance components as simulated by WaSiM. It is interesting to note that for all scenarios, increases in monthly discharges (total runoff, baseflow, interflow and overland flow) are found.

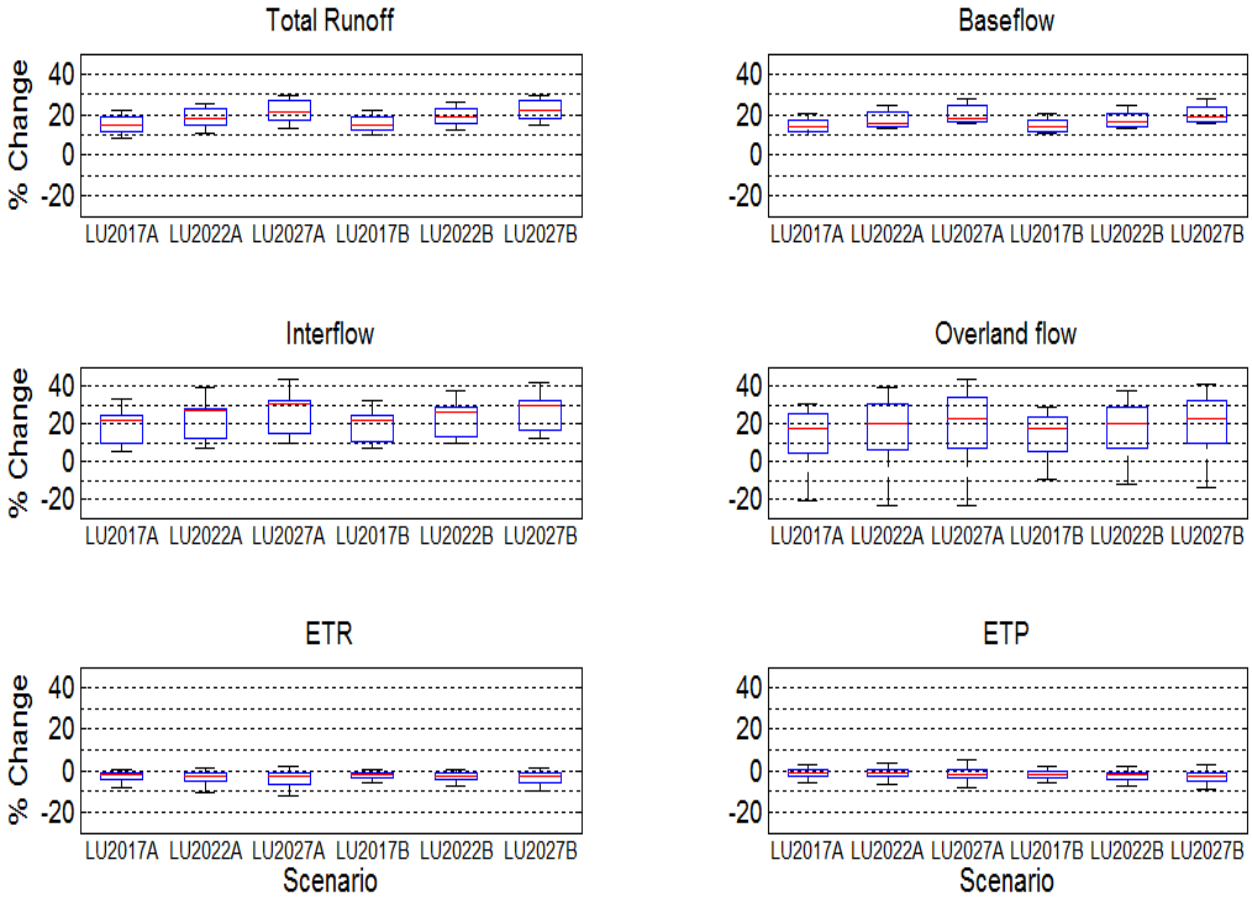

Figure 6-2: Boxplot of the percentage change in mean monthly water balance components simulated by WaSiM. On each box, the central mark is the median, the edges of the box are the 25th and 75th percentiles and the whiskers extend to the most extreme data points not considered outliers. Three time windows have been chosen for each land use scenario: 2015–2019 (LU2017A, LU2017B); 2020-2024 (LU2022A, LU2022B) and 2025–2029 (LU2027A, LU2027B)

Considering the 75th percentile of the changes, an increase up to 27% of the total discharge relatively to the baseline can be expected depending on the time window and the land use scenarios implemented. For the three time horizons considered in the analysis, longer the time period, higher the increase in the mean monthly discharge (and the runoff components) and consequently in the mean annual discharge. There is almost no difference in the simulated runoff components from one scenario to another considering the same time horizon. A decrease in the real evapotranspiration was simulated by WaSiM while the medians of the change in potential evapotranspiration projected by the model are negatives. This is in line with the fact that conversion of natural vegetation into agriculture land, pasture and agglomeration results in less transpiration. Nevertheless, it must be noted that the scenarios implemented in this study does not consider any change in the climate state mainly the temperature which is the principal parameter conditioning the ETP and ETR. Change in runoff components from one scenario to another seems not apprehend by WaSiM model.

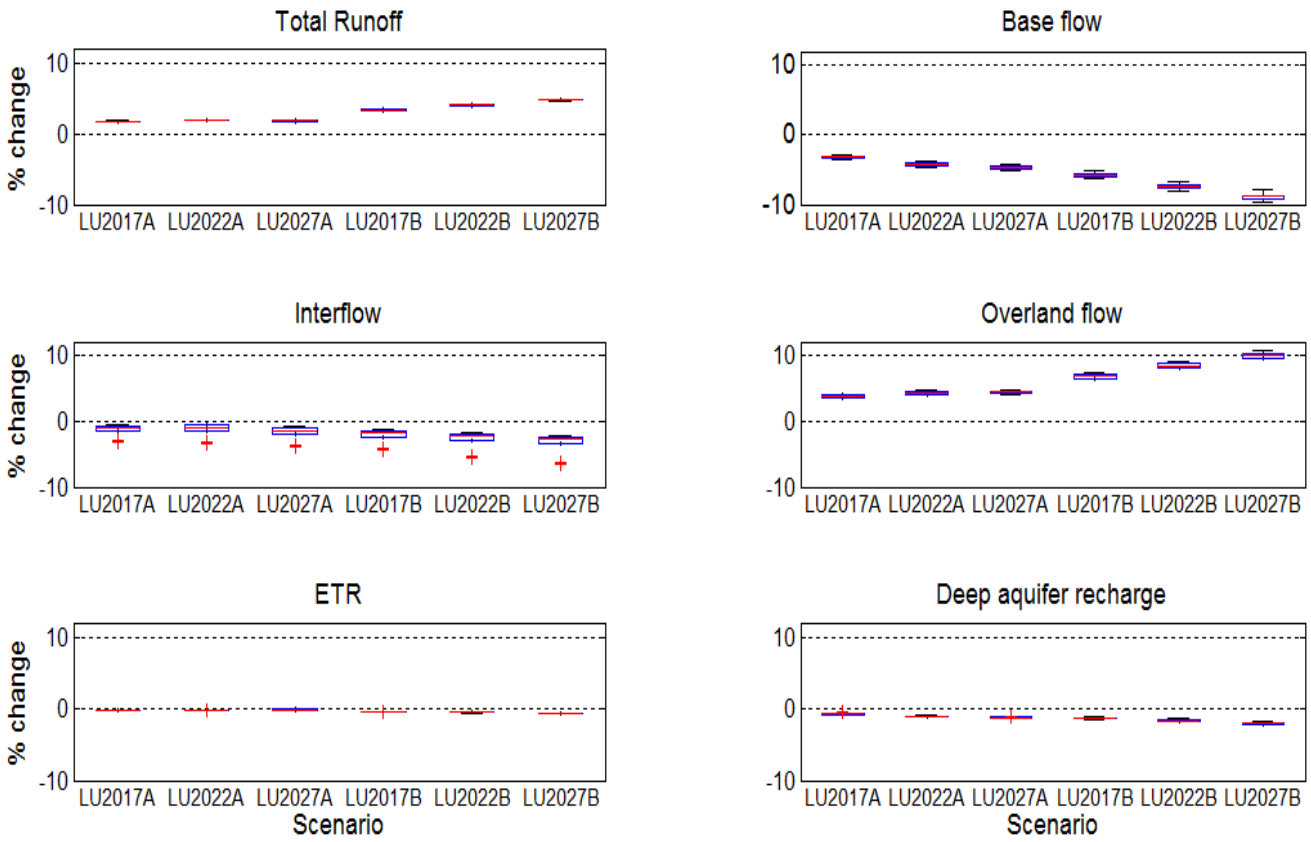

Figure 6-3: Boxplot of the percentage change in mean annual water balance components simulated by SWAT. On each box, the central mark is the median, the edges of the box are the 25th and 75th percentiles and the whiskers extend to the most extreme data points not considered outliers. Three time windows have been chosen for each land use scenario: 2015–2019 (LU2017A, LU2017B); 2020-2024 (LU2022A, LU2022B) and 2025–2029 (LU2027A, LU2027B).

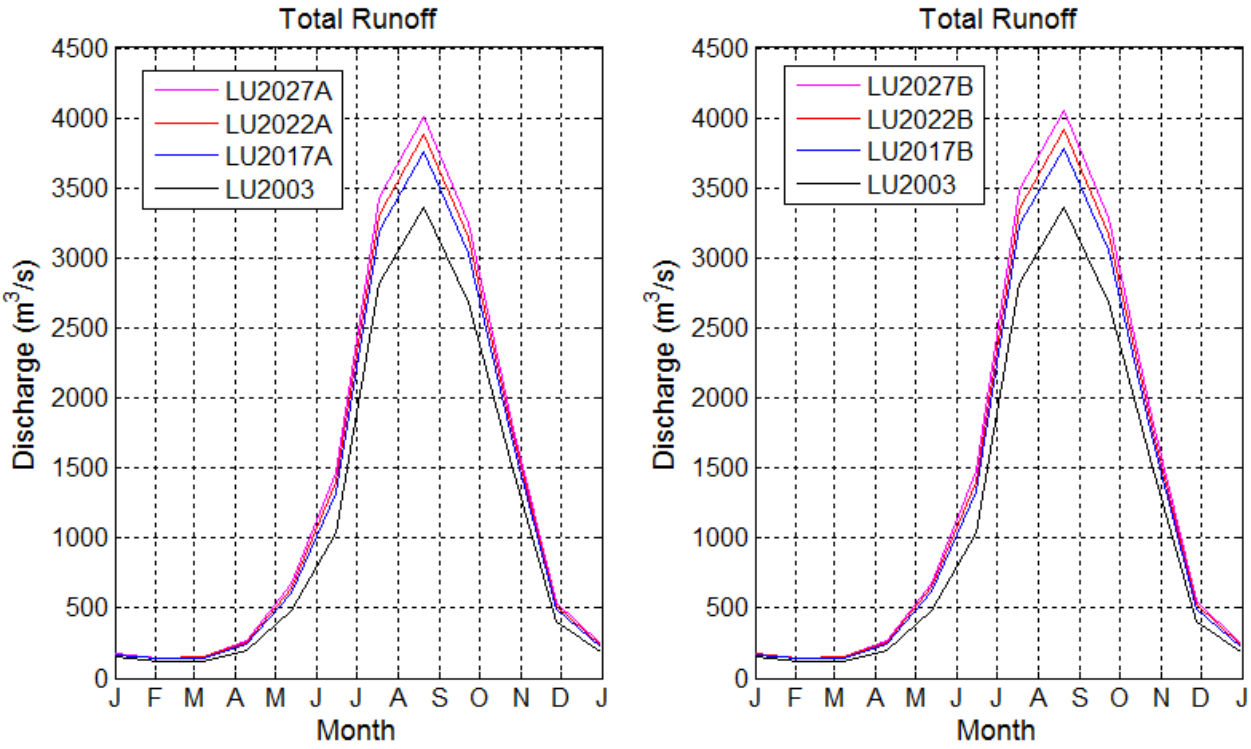

Figure 6-4: Mean monthly discharge simulated by WaSiM for the different land use scenarios.

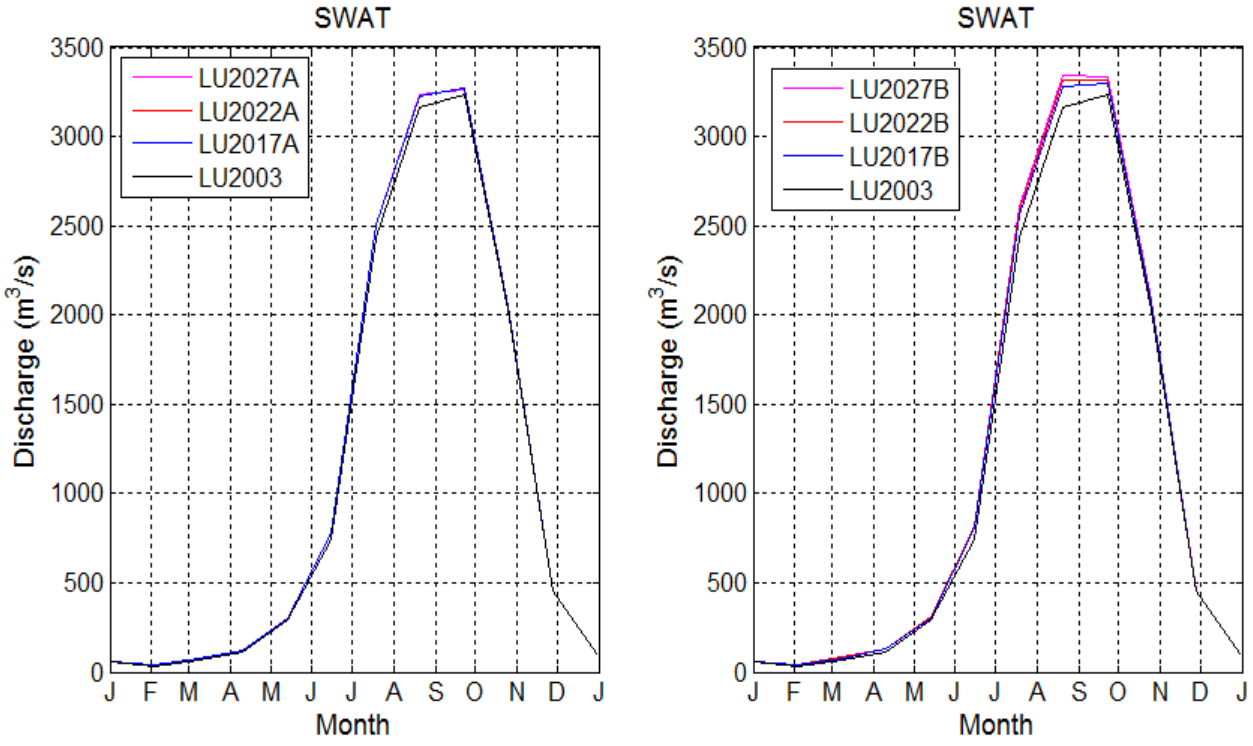

Figure 6-5: Mean monthly discharge simulated by SWAT for the different land use scenarios.

As far as SWAT model is concerned; the overland flow which is the principal runoff component conditioning change in total runoff (water yield) was projected to increase while the other runoff components (lateral flow and baseflow) and water balance components was projected to decrease. Considering each scenario, changes are more important for land use scenario B - which arises from weak national economy, uncontrolled settlement and farmland development with 3.5% population growth per year - than the land use scenario A – which results from stronger economic development, controlled urbanization, two large-scale irrigation schemes with 3.2% population growth per year.

At annual basis, an increase in total runoff was simulated by both models ranging from 15% to 25% for WaSiM and from 4% to 10% for SWAT for both scenario but these changes are more pronounce for the land use scenario B. For WaSiM, the interflow had increased from 13% to 22%, the overland flow from 24 to 37%, the baseflow from 19% to 29%. The ETR (PET respectively) had decreased from -4% to -2% (-3% to -1% respectively).

Both models predicted an increase in total runoff and a decrease in real evapotranspiration. Changes projected by WaSiM were very high, sometimes more than three times what was projected by SWAT. The changes in water balance components from one scenario to another for the same time horizon simulated by SWAT seemed more acceptable than WaSiM results which showed no difference from one scenario to another for the same time horizon. Changes obtained from scenario A should be greater than changes obtained from scenario B. The increase in the overland flow may lead to more erosion which can cause large volumes of soil to come in a river and reduce the river's capacity and results in more flood events. At yearly basis, positive changes are found for all scenarios and all time horizons. The increase in annual basin discharge is associated to a reduction of real evapotranspiration comparatively to the baseline.

6.4.2 The threshold selection and Poisson assumption

Nearly independent peaks were selected using the criteria described by Willems (2014). Two successive peaks can be considered independent when the time p between the two peaks is longer than the recession constant k, and when the minimum discharge in between these two peaks is smaller than a fraction f of the peak discharge. Additionally, the peak must be greater or equal to the selected threshold. For each threshold, the corresponding dispersion index (DI, defined as the ratio of the variance to the mean) was computed for the simulated discharges. For both models (WaSiM and SWAT), the condition of DI=1 was satisfied for many thresholds. Lastly, given that we had 20 years data, the choice of the threshold was done in such a way that the average occurrence per year must be greater or equal to 1.5 to achieve at least 30 data points selected for each simulation. Figure 6-6 shows the median value of the dispersion index for the baseline (with the 25^{th} and 75^{th} bound in green) and average rate of occurrence per year in

function of the thresholds. It reveals that the condition of DI =1 was nearly satisfied around the threshold of 130m^3/s (1.625mm/day) for WaSiM. The corresponding average rate of occurrence per year (Lambda) is 2.43. Therefore, giving that 20 years of discharge data were used in this analysis, the approximate POT data size will be 2.43*20=49 which is sufficient to perform statistical analysis. For SWAT, the condition of DI=1 is nearly satisfied around the threshold of 140m^3/s (1.75mm/day) and the corresponding Lambda is 1.97. This implies that the average number of data above the selected threshold is 1.97*20=39 which is acceptable data sample required in statistical analysis. The highest threshold used in calibrating the models (WaSiM and SWAT) was 120m^3/s which is fortunately lower to the thresholds at which the Poisson assumption was verified. Figure 6-7 (a) and Figure 6-8 (a) show the distribution of DI for overall 70 samples derived from WaSiM and SWAT outputs respectively. Most of the dispersion indexes are between 0.8 and 1.2 (1±0.2) which is acceptable measure in achieving a fundamental property of the Poisson process distribution.

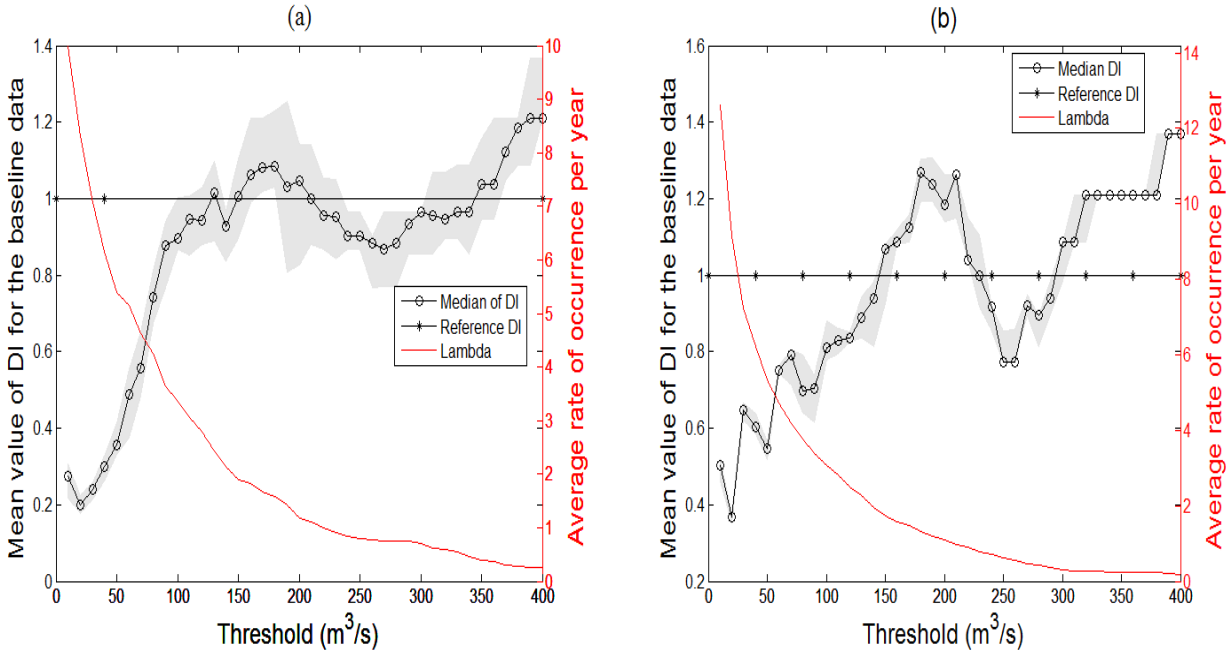

Figure 6-6: Dispersion index (DI) median, the band between the 25th and the 75th percentiles of DI (in blue) and Lambda (the average rate of occurrence per year).

The distribution of the 70 data set used from each simulation in function of their size is shown on Figure 6-7 (b) and Figure 6-8 (b) for both models. We can observe that after applying the threshold selection procedure described above, the data size varies between 33 and 58. In addition, we applied the Mann Kendall trend to test the stationarity of each dataset. This test found no trend in the data.

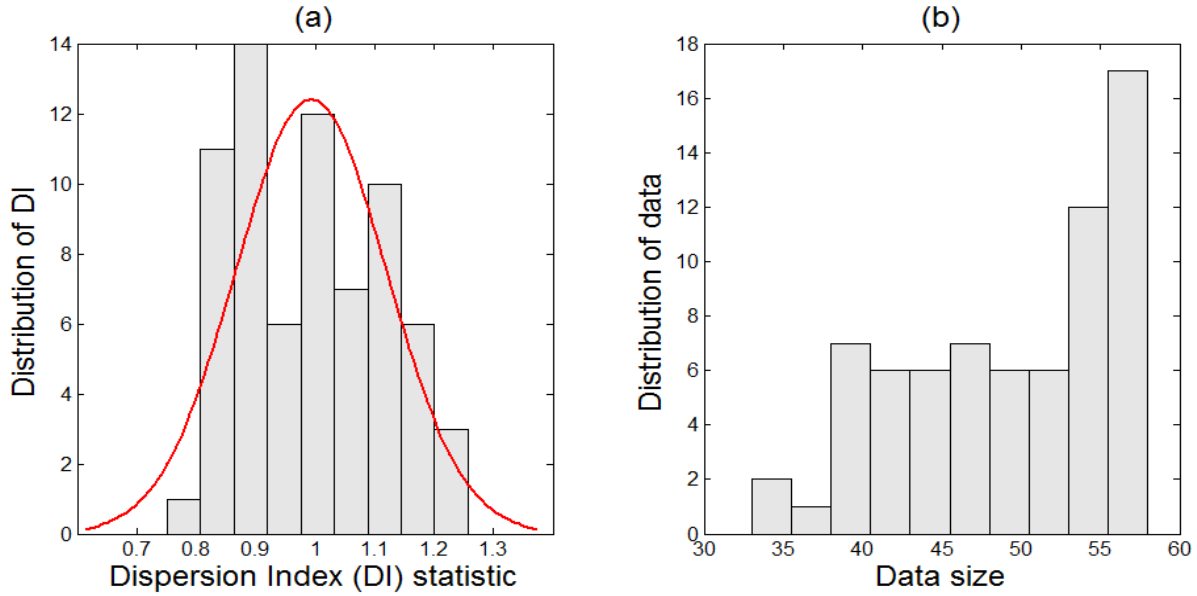

Figure 6-7: Distribution of the dispersion indexes (DI) (a) and of the data size (b) corresponding to the 70 runs (datasets) used in this study for WaSiM.

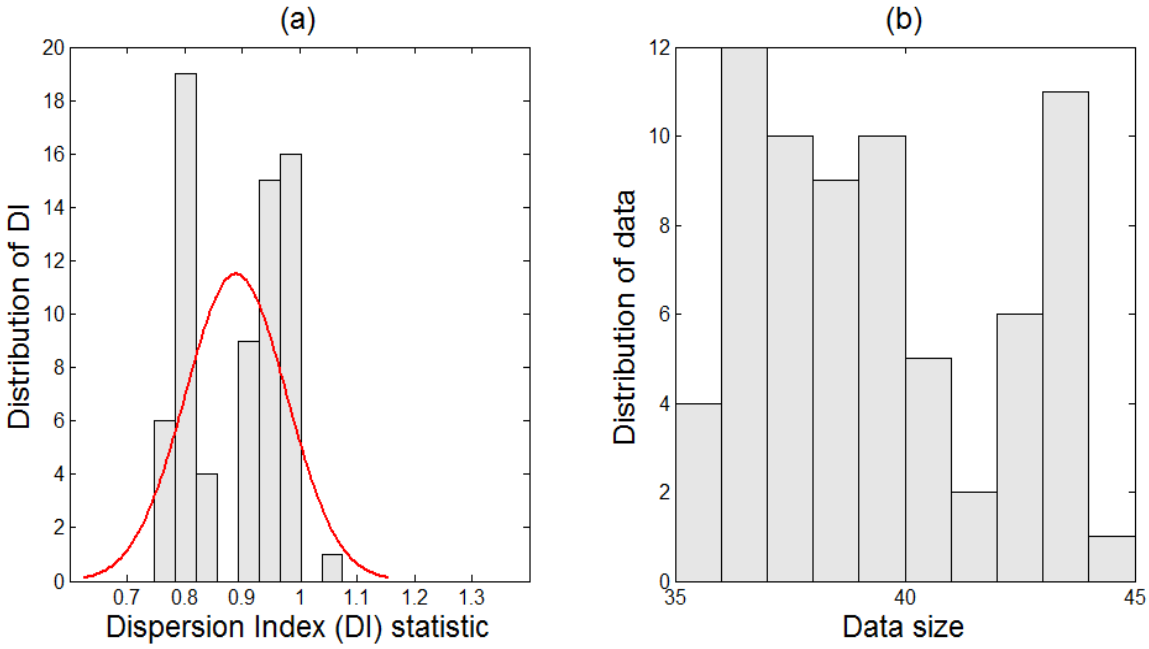

Figure 6-8: Distribution of the dispersion indexes (DI) (a) and of the data size (b) corresponding to the 70 runs (datasets) used in this study for SWAT

After applying the criteria of Willems (2014) for the selection of independent peaks in such a way that the dispersion indexes were nearly equal to 1 with each data size greater or equal to 30 (the minimum sample required for obtaining accurate results from a

statistical distribution) and verifying the stationarity of the selected data, we can proceed to flood frequency analysis based on generalized Pareto distribution for quantile estimation and the associated Poisson distribution for the frequency analysis.

6.4.3 Quantile estimated from SWAT and WaSiM outputs

Quantiles of the simulated discharges for different scenarios and the baseline are shown on Figure 6-9. It is interesting to note that the curve for the future time windows surmount the curve of the baseline in each scenario.

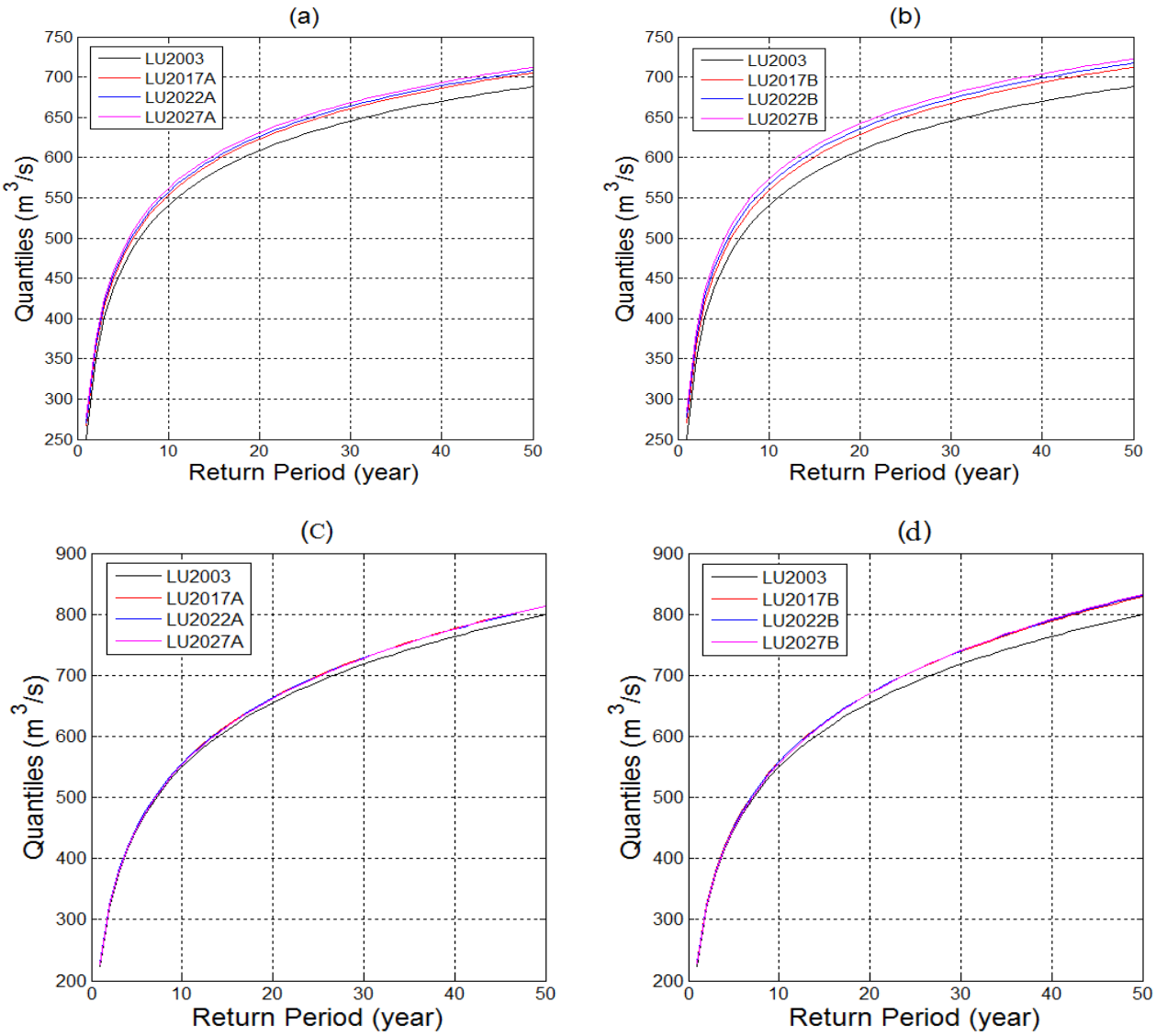

Figure 6-9: Quantile plots of the simulated discharges by WaSiM (a, b) and SWAT (c, d) for the different scenarios and the baseline.

Indeed, there is an increase in quantile of each return period. In other words, for a given return period, the corresponding quantile for the scenarios is greater than the corresponding quantile for the baseline simulation. Both the magnitude and the frequency of floods increased under the different land use scenario. Nevertheless, there is a high difference between the quantile simulated from WaSiM (a, b) and the one simulated from SWAT (c, d). Using for instance the baseline, while 45-year quantile simulated from SWAT was 775m^3/s, the corresponding 45-year quantile simulated by WaSiM was 675m^3/s. Let us recall here that the baseline discharge is not the observed discharge but the simulated discharge by each hydrological model using the land use data of 2003. This difference may be explained by the poor quality of data used in calibrating the models mainly the observed peaks discharge in one hand and the model structure in other hand. In order to reduce these errors (uncertainties due to input data and model structure), we concentrate our analysis on change in quantile which is common in scenario analysis (Arnell, 1999, IPCC, 2001, Huisman *et al.*, 2009, Vaze & Teng, 2011, Teng *et al.*, 2012) rather than absolute values.

6.4.4 Change in quantiles projected from WaSiM and SWAT outputs

Figure 6-10 shows the percentage change in quantile computed relatively to the baseline by WaSiM (a) and SWAT (b). Strictly positive changes were simulated by WaSiM. More changes were found for low return period in comparison to high return period whatever the scenario and time window. For the scenario LUA which is based on stronger economic development, changes were more important for the furthest time horizon. For the time period of 2015–2019 represented by LU2017A, the third quartile of the percentage changes was greater than 8% while for the time horizon of 2025-2029 represented by LU2027A, the 75th percentile of changes is 14% in 1-year quantile. The changes simulated from WaSiM for the scenario A were slightly smaller than the change computed for the scenario B considering the same time window for most of the return periods. Taking for instance LU2027A, the percentage change in 3-year quantile was 5% (median) while the percentage change in 3-year quantile for LU2017B was 7% (median).

As far as SWAT is concerned (b), changes were more important for land use scenario B than land use scenario A. The median of all changes found were positives and more important changes were found for lower quantile and higher quantiles. According to the 75th percentile and the scenario B, the percentage change for 35-year quantile was around 4% for the time window 2015-2019, 4.5% for 2020-2024 and 4.2% for 2025–2029. For the scenario A, changes are of the same order of magnitude like scenario B. There is no clear trend for SWAT. This may be explained by the fact that SWAT failed to reproduce precisely the peaks runoff exhibited from change in land use. This may arise from the modified rational method used to compute the peak discharge in SWAT model based on the assumption that the time of concentration is equal to the rainfall duration, that rainfall

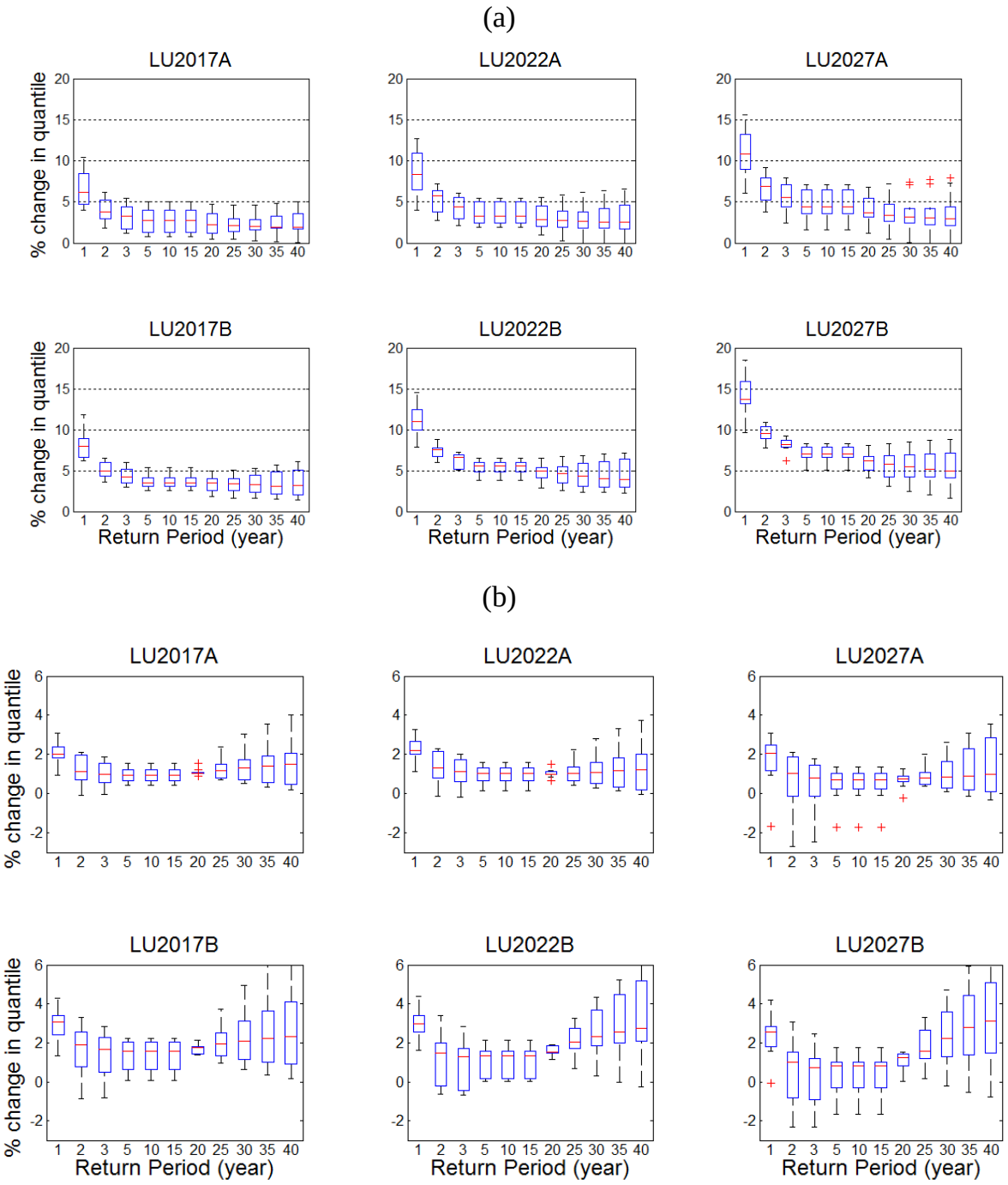

Figure 6-10: Percentage changes in x-year quantile as computed from WaSiM (a) and SWAT (b). On each box, the central mark is the median, the edges of the box are the 25th and 75th percentiles, and the whiskers extend to the most extreme data points not considered outliers and the outliers (the red plus sign). Three time windows have been chosen for each land use scenario: 2015–2019 (LU2017A, LU2017B); 2020-2024 (LU2022A, LU2022B) and 2025–2029 (LU2027A, LU2027B).

intensity over the entire catchment remains constant during the storm duration. However, for large catchment, these assumptions may not be true. Sometimes the peak discharge occurs before all of the drainage area is contributing to the main outlet. For instance, when a significant portion of drainage area within the catchment has very small time of concentration so that a higher rainfall intensity can be used for this portion, the runoff coming solely from this portion is higher than that of the whole catchment in which a lower rainfall intensity is adopted because the remaining part of the catchment has comparatively large time of concentration. Therefore, this results in incorrect estimation of peak runoff of large catchments if the Rational Method is adopted.

Increased in magnitude of flood is simulated by both models based on the different scenarios but changes exhibited by WaSiM are more important than changes simulated from SWAT model despite the difference in the magnitude (see sub-section 6.4.3). According to the median of all scenarios, the magnitude of flood event is shown to increase for most return periods, changes being greatest for low return periods. While changes of about 10% are observed for the third quartile for WaSiM, lesser changes are found by SWAT. Overall, whatever the model used, the flood regime is shown to be influenced by land use changes in term of magnitude.

6.4.5 Return periods estimated from WaSiM and SWAT outputs

Whatever the scenarios and the hydrological models considered, flood events of any given magnitude are expected to become more frequent than currently observed (Figure 6-12). For WaSiM model (a), according to the minimum value of the 25th percentile of all scenarios and the maximum value of the 75th percentile of all scenarios, the current 2-year event may vary between 1.6 and 1.9-year; between 3.7 and 4.8-year for a current 5-year event; between 7.0 and 9.4-year for a current 10-year event; between 13.1 and 18.0-year for a current 20-year event, and between 23.4 and 35.6-year for a current 40-year event. Any given magnitude is likely to occur more frequently. The frequency is more accentuated for scenario B than the scenario A. For SWAT model, using the minimum value of the 25th percentile of all scenarios and the maximum value of the 75th percentile of all scenarios, the current 2-year event may vary between 1.9 and 2.0-year; between 4.7 and 5.0-year for a current 5-year event; between 9.3 and 9.8-year for a current 10-year event; and between 17.5 and 19.8-year for a current 20-year event, between 31.1 and 40.0-year for a current 40-year event. Similarly to WaSiM, any given magnitude is likely to occur more frequently and the frequency is more accentuated for scenario B than the scenario A.

Overall, combining results from WaSiM and SWAT, a 5-year event may become a 3.7-year or 4.7-year event depending on the scenario. The more extreme events are projected to most often occur. For instance, a 40-year flood event may turn into a 23.4-year or 31.1-year event depending on the scenario. Intensified land use such as conversion of natural vegetation into agricultural lands and urban area will result in more flooding. Both the magnitude and the

frequency of the floods increased under land use change conditions as modelled by the WaSiM and SWAT models.

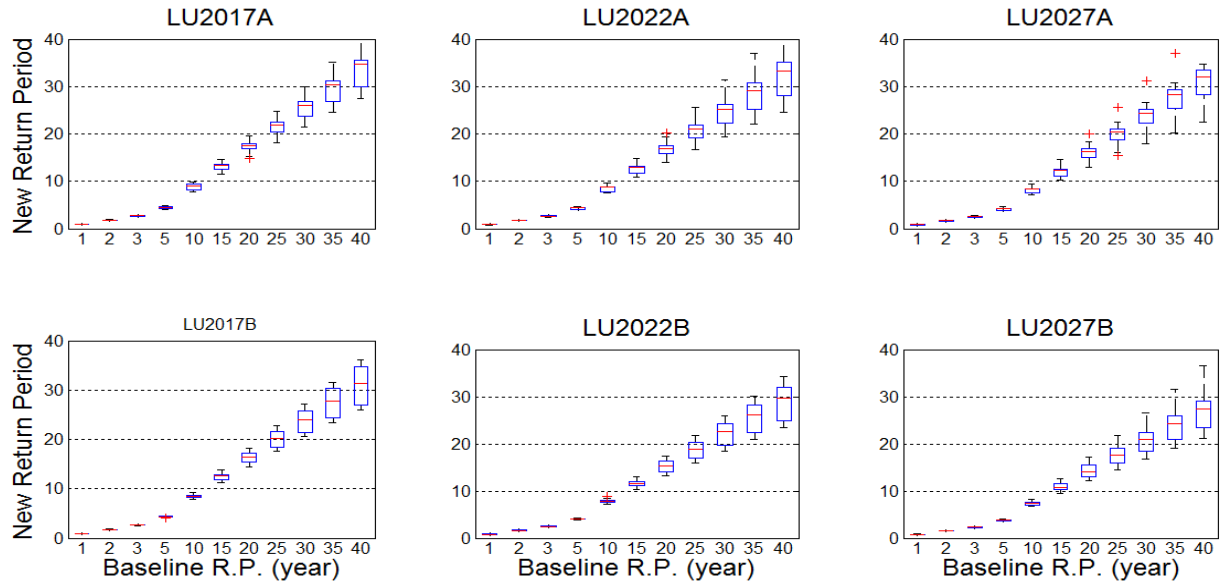

Figure 6-11 Baseline return period and the corresponding return period under the different land use scenarios and time windows for WaSiM

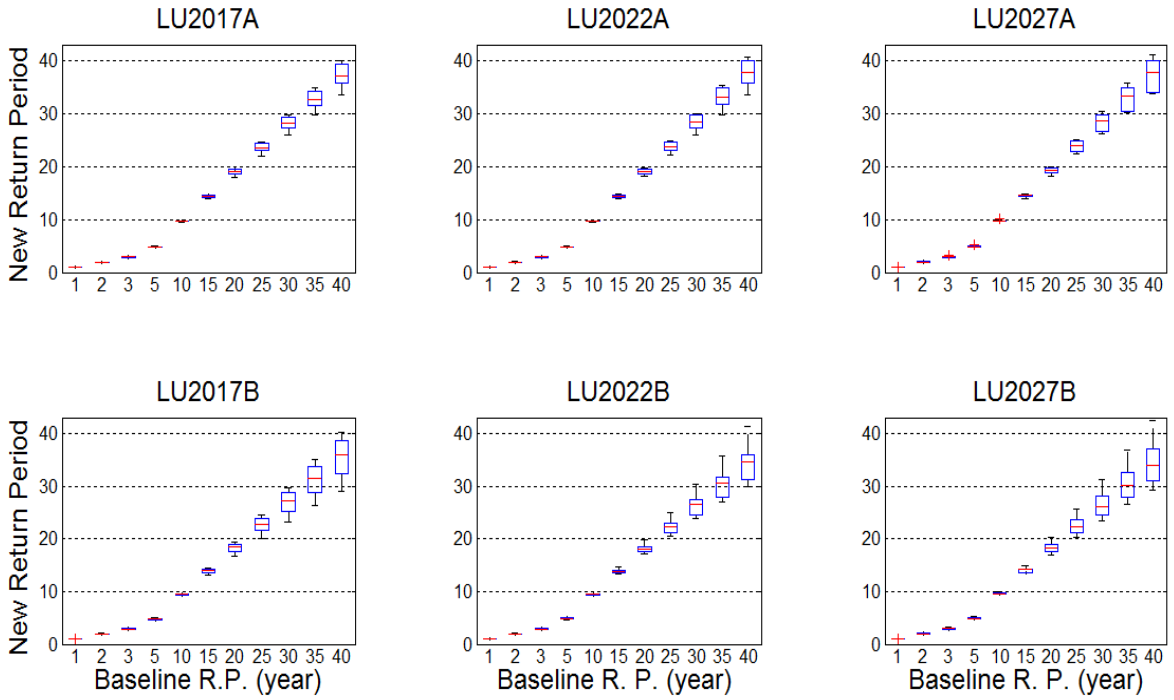

Figure 6-12: Baseline return period and the corresponding return period under the different land use scenarios and time windows for SWAT.

6.4.6 Percentage change in return period estimated from WaSiM and SWAT

In order to evaluate change in return periods among different scenarios and time windows, we computed the percentage change in return period obtained from the different scenarios relatively to the baseline return period (Figure 6-13 and Figure 6-14). According to the median, any given return period is projected to decrease whatever the scenario. Decreases in return period are more important for high return periods than the low return periods. As far as the scenarios are concerned, scenario LUB, based on more anthropogenic action on land use/land cover, exhibit the highest change in magnitude. Using the median, decrease up to -30% (LU2027B) in return period can be expected for scenario B and a decrease up to -20% (LU2027A) for scenario LUA. Flood events are expected to become more frequent than what is currently observed. A consequence of increase of flood events may be the pollution. If the river floods spread into farmland, the water can be polluted by pesticides and other chemicals sprayed onto the farmland. When that water drained back into the river, it can pollute it and kill off wildlife that inhabits the river. If the floodwater is not polluted though, flooding can create wetlands that can help introduce new habitats for many species of animals.

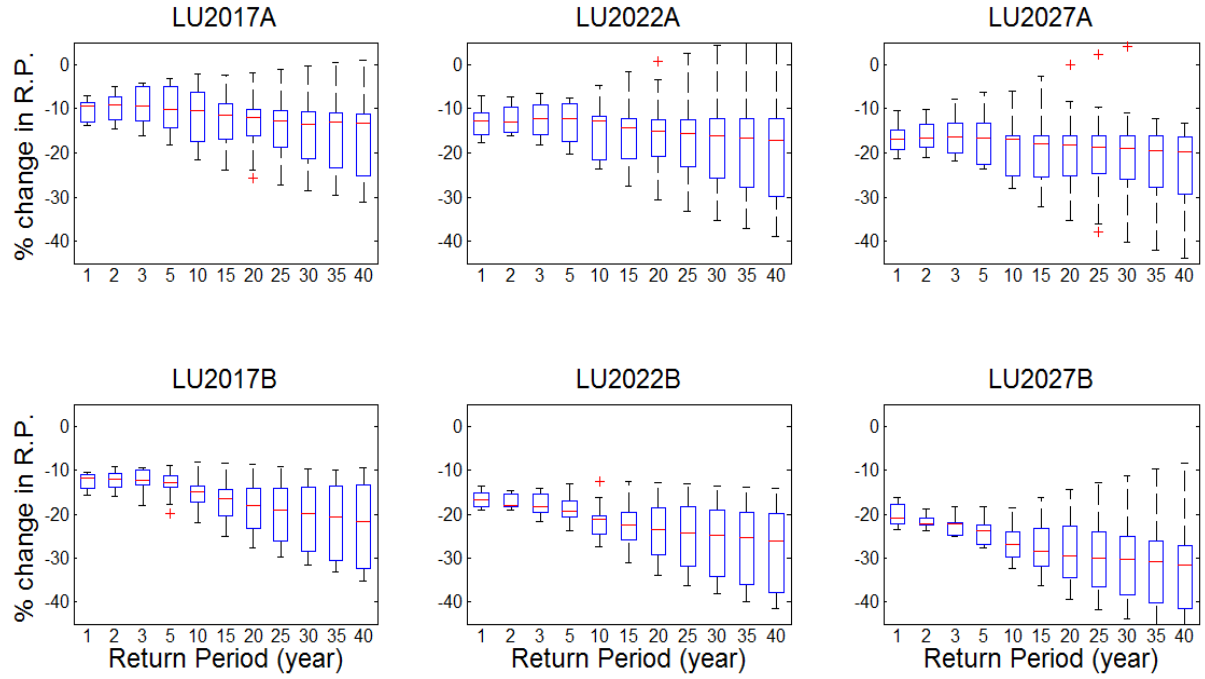

Figure 6-13: Percentage change in return period compared to the baseline as computed from WaSiM for the different scenarios and time windows

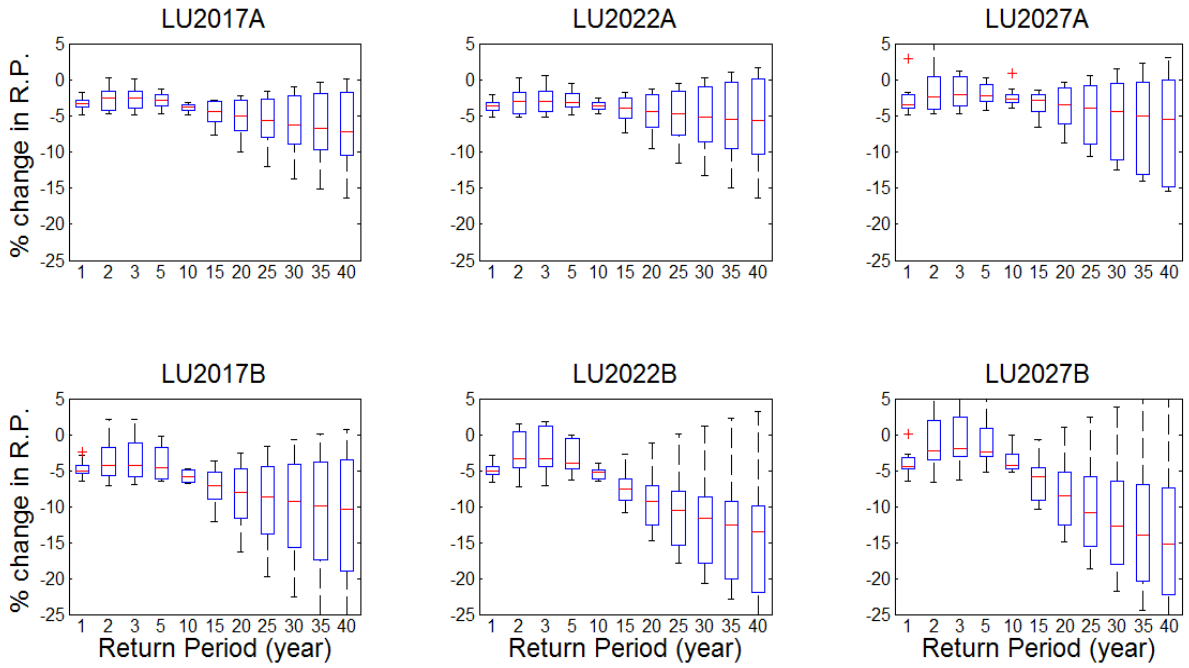

Figure 6-14: Percentage change in return period compared to the baseline as computed from SWAT for the different scenarios and time windows.

6.5 Conclusion

This work using different land use scenarios through rainfall-runoff modelling aims to derive possible changes in flood frequency and magnitude over Zou catchment at Atchérigbé gauge. Most studies use one model to assess the land use and land cover change impact on hydrology (average flow, extreme events such as flood and drought etc.) relying on single run of single model. An added value of this work is the multi-modelling approach. It helps to get a general idea about how flood indicators such its frequency and magnitude may be expected to change in the future. This result should not be treated as prediction of what will happen to flood indicators in the future since we do not consider the how climate change will impact on rainfall which is the primary cause of the flooding. … Due to the uncertainty in the input data, model structure and unknown uncertainties, discharge measurement especially for the high discharge, it was difficult for the models to reproduce correctly the discharge peaks. A compromise was to concentrate on change modelled by the models rather than on the absolute values. Two socio-economic scenarios set up by RIVERTWIN project (RIVERTWIN, 2007) have been used with three time windows: 2015–2019, 2020-2024 and 2025–2029. Applied to baseline climatic series, these scenarios show an overall change of the flood regime both in terms of increase of magnitude and frequency of the extreme events. However, significant differences in the impacts exist stating from lower to higher the return periods and the type of scenario. Flood events are projected to occur more often under scenario B

than scenario A and events of high return periods may occur more often than events of low return periods.

With the projected intensification of rare events due to climate change (IPCC, 2007), more changes in flood occurrence may be expected. These findings highlight the growing challenges for water resources managers and planners and emphases the need to address potential climate and land use changes impact on water resources while developing water management plans. Infrastructural and non-infrastructural actions to reduce the flooding risk must be taking and these include updating current flood infrastructure designed methods; reinforcing flood forecast systems, improving population awareness and preparedness, urban planning, and discouraging human settlements in flood-prone areas. Future studies based on combined effects of climate and land use changes on flood are required to get more accurate projection since the uncertainty related to change in the climate has not been evaluated here.

7 SUMMARY, CONCLUSIONS AND OUTLOOK

It is widely accepted that under the global warning, the hydrological cycle will be sped up leading to more extreme events. This work focuses on understanding how climate change and land use influence on flood frequency and flood magnitude in the Ouémé basin. This is a central task to support the implementation of flood early warning system in the basin. In the following, we revisited the main research questions posed in the introduction.

7.1 Is there an increasing observed annual maximal discharge accompanying the increasing number and/or severity of floods?

The annual maximal discharges were extracted from five gauges stations during the period 1952–2009. The Mann–Kendall and Spearman's rho trend tests were applied. A trend is considered to be present if it has been detected by both tests. The results show that at 95% confidence level, there is no statistically significant trend in the annual maximal discharge. Nevertheless, the annual maximal flood series of Bonou station (the main outlet of the basin) exhibited a statistically significant trend at 10% significance level. Additionally, a break point analysis was performed using the Hubert segmentation test and the non-parametric Pettitt test. We found change points in the data of Bétérou and Savè in somewhat similar periods. The three sub-periods found by the Hubert segmentation for the Bétérou and Savè gauge stations are in accordance with the three rainfall periods in West Africa (Figure 3-2). Indeed, there is no increasing trend in the observed annual maximal discharge accompanying the increasing number of flood and its severity.

7.2 What could be the added value of non-stationary modelling approach in the Ouémé basin?

From the previous research question, break points and trends in the annual maximal discharges series of some of the stations have been identified. The existence of abrupt changes or trends is a valid hypothesis for introducing non-stationarity into the estimation (Lopez & Frances, 2013). Different non-stationary generalized extreme value (GEV) models were built using the sea surface temperature (SST) and the see level pressure (SLP) of the gulf of Guinea as covariates. It has been generally found, based on four criteria of goodness of fit ($-ln(L)$, deviance statistic, AIC, BIC), that the non-stationary GEV models outperformed the stationary model. In particular, the non-stationary GEV1 model which incorporates covariate in the location parameter with other parameters constant was the most appropriated for flood frequency analysis in the study. Based on this and through an ensemble modelling, new return values corresponding to the non-stationary approach were proposed. Considering that structural measures are important elements for flood risk management, their design should be updated by considering non-

stationarity to reduce the vulnerability of human beings and goods exposed to flood risks. This generalization of the classical model based on the hypothesis of stationarity and normality allows climate change to affect the evolution of the distribution parameters and provides predictions of the probability of future occurrences of a particular flood event

7.3 How does climate change influence the frequency and severity of extreme rainfall in the Ouémé River Basin or is there any change in the characteristics of extreme precipitation events causing floods?

Increased rainfall intensity and duration is causing more extensive flooding in both rural and urban areas. The primary cause of flood is rainfall and change in the frequency of heavy rainfall can lead to devastating events. 34 rainfall stations which data length is within 1921-2012 were investigated. The available data length of each station was used and it is referred to as 'inhomogeneous period'. First, rainfall data of each station are split into two parts and the peak over threshold approach was applied. Second, the distribution function is then fitted to each part and the intensities corresponding to different return periods are computed for each part. Finally, change in extreme rainfall characteristic (intensity and frequency) are computed and the significance of the change was assessed using the paired t-test and the Wilcoxon paired test. As it has been observed in other part of the word, the frequency of extreme rainfall has changed over the study area. Significant negative as well as positive changes have been found throughout the basin. For the inhomogeneous period, 82% of the stations show statistically significant change among which 57% exhibit a positive change and 43% negative change. A positive change is associated to an increasing heavy rainfall over the area of concerned. Additionally, we found high and statistically significant (at 5% significance level) correlation between the number of heavy rainfall days per year and the total annual rainfall for all stations except Pénéssoulou. The impacts of changes in the frequency of floods could be tempered by appropriate infrastructure investments, and by changes in water and land-use management. Change in flood frequency and magnitude can have positive and negative impacts. It is important, therefore, to be aware of its consequences at local and national levels and to plan accordingly. The expected continuation of rapid population growth will increase human exposure to flooding and adequate adaptation measure must be implemented.

With the mixed pattern of change (increase and decreasing tendency) observed at different return periods for the heavy rainfall, we can deduce that climates factors may not be the main element contributing to increasing flood risk in this basin. The implication for this is to look at how changes in land use affect flood characteristics.

7.4 How does land use change affect flood magnitude and flood frequency in this river? Will the magnitude and frequency of extreme weather events increase in the future?

The modelling methodology consists of four steps: - Hydrological models (WaSiM and SWAT) were calibrated and validated- Land use scenarios for three time horizons (2015–2019; 2020-2024 and 2025–2029) were constructed based on the Rivertwin project - The models with the parameters fitted in step 1 were run to simulate flow series representative of the three time horizons - Change in flood characteristics (severity and frequency) were computed using ensemble modelling approach (ten satisfactory simulations for the calibration and validation periods for each model).

The results show that both models predict satisfactorily streamflow on the Atchérigbé basin with the Kling and Gupta efficiency (KGE) between 0.6 and 0.85 and the Nash Sutcliffe efficiency (NSE) between 0.5 and 0.76 for calibration and validation periods at threshold of $0m^3/s$. The models simulations were also acceptable when we considered the discharge above the threshold of $120m^3/s$ (1.5mm/day) for performance evaluation. The overall water balances predicted by the models were consistent with the hydroclimatic condition of the basin with the runoff coefficient being around 15% and the real evapotranspiration varying between 67 and 84% of the total annual rainfall depending on the model. In addition, the high streamflows were acceptably simulated. Hence, the models are able to reproduce satisfactorily the hydrological processes in the study area and could be used for flood risk assessment.

The peak over threshold analysis was undertaken to produce flood frequency distributions from which the magnitude and return periods are computed. According to the median of all scenarios, the magnitude of flood event is shown to increase for most return periods, changes being greatest for low return periods. Though increase in magnitude of flood events was simulated by both models and for the different scenarios, the magnitude of change is influenced by the model types. The overall combined results from WaSiM and SWAT show that a 5-year event may become a 3.4-year or 4.7-year event depending on the scenario. The more extreme events are projected to most often occur. A 40-year flood event may turn into a 23.4-year or 31.1-year event depending on the scenario. These increases in flood magnitudes are accompanied with increase in mean monthly and mean annual discharges in the study area. However, these results should be interpreted with caution in light with the uncertainty related to hydrological modelling.

With the projected intensification of rare events due to climate change (IPCC, 2007), more changes in flood occurrence may be expected. These findings highlight the growing challenges for water resources managers and planners and emphases the need to address potential climate and land use changes impact on water resources while developing water management plans. Future studies based on combined effects of climate and land use

changes on flood are required to get more accurate projection since the uncertainty related to change in the climate has not been evaluated here.

7.5 Adaptation and mitigation measures

In this work we found that around half of the rainfall stations analyzed show a decreasing trend and the other half show an increasing trend in their heavy rainfall data. So, there is no clear direction about the change in heavy rainfall. In contrast, when we considered the land use scenario, we found exclusively an increasing trend in flood risk over the study area. Based on this, we can conclude that land use change is the main driver of the increasing flood risk in Ouémé basin. Climate change influence on flood risk is less pronounced than the land use change. This is an alarmist results and action to reduce flood risk must be implemented.

Adaptation and mitigation measures must be taking such as updating flood protection infrastructures considering non-stationarity of flood characteristics, revision of hydrological norms since ‘stationarity is dead’, and integration of flood risk into the planning and management of urban area. Hard options include reinforcing riverbanks, dredging rivers, and raising houses; redirecting flood runoff through the use of flood-walls and flood gates.

Soil disturbance after forest removal leads to increase in peak flood because the associated reduction in ETR will cause the soil to be wetter and hence more responsive to rainfall. Ecosystem based adaptation (EBA) has been internationally recognized as effective tool to attenuate the effects of climate and land use change and related hazards. One of the ecosystem based adaptation measures is the sustainable water management, where river basins, aquifers, flood plains and their vegetation are managed to provide water storage and flood regulation. Therefore, ecosystem based adaptation measure can be used to reduce flood risk by afforesting the upper catchment and planting floodplain vegetation, grassland and alfalfa hay land use. This upland afforestation typically provides great benefits because trees not only reduce the damages from flooding but also produce large quantities of monetized ecosystem services such as fruits, firewood, and carbon sequestration. Preserving forests or replanting them in head catchment and river bank can reduce flash flood and delay runoff peaks. Sustainable management of grasslands and rangelands can enhance pastoral livelihoods and increase resilience to drought and flooding and contribute to disaster risk reduction.

Other actions to reduce the flooding risk can be taking such as updating current flood infrastructure designed methods, improving population awareness and preparedness, urban planning, discouraging human settlements in flood-prone areas, reinforcing flood forecast systems, etc.

7.6 Outlook

Some efforts have been made in this study by providing useful information on current flood state in the Ouémé basin. Nevertheless, some aspects need more investigation. The non-stationary approach used in this study was based on the generalized extreme value distribution (GEV) which is the widely used in flood frequency analysis (FFA). Based on the fitness criteria used, satisfactory results were obtained. A comparison of the results obtained using GEV with other non-stationary distributions such as lognormal, log-Pearson type III etc. can be done for improving flood frequency analysis in the basin. This type of study can help to confirm or to ameliorate the findings of this work. Floods are affected by climatic and non-climatic factors. We investigated the non-climatic factor namely the land use effect on flood hazard. The aspect concerning the impact of climate change on extreme events using climate scenario from regional climate models still remained to be assessed and future work should address this and also the combined impacts of climate and land use changes on flood risk in the basin. In fact, based on the increasing temperature, the water cycle will be sped up and a warmer climate will result in an increase in the evapotranspiration. Thus more water will be available in the atmosphere leading to more extreme hydrometeorological events. For these purposes, deep study is needed to assess the impact of environmental change on extreme events in order to provide scientific basis and information for water management and planning. We implemented a methodology to assess change in heavy rainfall over the study area. A comparative study can be done using other trend detection methods such as the Mann Kendal, Spearman Rho trend tests to validate or to improve the findings of this work. Considering that flood risk is defined as combination of flood hazard and vulnerability and we mainly focused on the hazard aspect in this thesis, the vulnerability assessment of population living in the study area need to be addressed to fully determine it contribution relatively to flood hazard and flood risk in the Ouémé basin. The vulnerability can be evaluated through the exposure, susceptibility and resilience using flood vulnerability indices by adapting it to the availability of the data in the study area. Flood vulnerability indices provides a method to systematically express the vulnerability of a river system to disruption factors, such as floods regarding four different components: social, economic, environmental and physical (Florina, 2007). It was found that the current flood forecast method based on multiple regression analysis has some limitations in term of information provided to the probable victims. Based on this finding a new approach was proposed; its theoretical framework has been slightly described below (7.6) after a brief description of the current state of flood forecast. For a real implementation, this approach will be translated into the form of project for Flood Forecast and Early Warning System.

In this global changing world, all fields of research mentioned above are important for society and policy making. It is our task as scientists and engineers to address the most important challenges for a more sustainable development.

7.7 Future work: contribution to the implementation of Ouémé Flood Forecast and Early Warning System (OFFEWS).

After the alarmist results of increasing flood frequency and magnitude in the future, what should be done to reduce it impact on human life, properties and on the ecosystems. In our opinion, mitigation measures as well as adaptation measures should be taking. This can done through the flood control using reservoirs, afforestation to decrease flood spreading speed, and mainly the flood forecast and early warning system. Some efforts have been done to forecast the flood in the Ouémé basin but this forecast system need to be reinforced. After assessing the current flood forecast method, we proposed a theoretical framework which will be evaluated in the future works. The components of the suggested non structure framework for flood forecasting and early warning system are: Data collection center (meteorological data, hydrological data and others), computational center and dissemination center.

7.7.1 Current state on flood forecast and early warning system in Ouémé basin

The flood forecast in Ouémé basin is currently based on linear propagation of discharge waves, a runoff-runoff model. Two types of formulas are used:

- Use of the discharge of upstream stations (if available) to predict the discharge of downstream station with some lag time. For instance, the discharge at Bonou in this case can be predicted using the discharge at the Domè and Zagnanado stations with the following formula:

$$Q_{Bonou}(t) = \alpha * Q_{Dome}(t - t_i) + \beta * Q_{Zagnanado}(t - t_j) + Q_0$$

The parameters (α, β, Q_0) and $(t_i,\ t_j)$ are found using a multiple regression method. The model is calibrated by taking into account different cases (the discharge of Domè and Zagnanado are both available or one of them is available).

- In case none of the discharges of Domè and Zagnanado is available, it is suggested to use the discharge of previous time steps as input to predict the discharges of the current and next coming time steps for Bonou station using the following prediction formula:

$$Q_{Bonou}(t_i) = \alpha * Q_{Bonou}(t_{i-1}) + \beta * Q_{Bonou}(t_{i-2}) + Q_0$$

The same procedure is applied to each of the gauging stations to get the model used to forecast the discharge.

Once the discharge data are collected from the different stations, the previous methodology is used to derive the discharge of the current and next coming days. If the discharges exceeded some thresholds (4 levels previously defined based on the past

inundations), the probable areas to be flooded are identified and decision is taking to communicate the result to appropriate authorities. The technical authorities issue the warning at appropriated time and the message is propagated through a well-established framework (diffusion screens, radio channels, TV, etc). This method applied to different rivers basins in the country can forecast river discharge from 3 to 10 days in advance based on preliminary analysis done by Zannou (2013). It was successfully applied to forecast the 2012 flood on the Ouémé basin and this reduce substantially the damages to properties and loss of life, better protection of the citizens, the environment, properties and cultural heritage.

Nevertheless, the current method flood forecast method can be improved by accounting for the mapping of the potential area to be flooded accompanying inundation characteristics such as flood extent, water level, water velocity, etc. Flood hazard maps shows areas which could be flooded according to three probabilities (low, medium high) complemented with: type of flood, the flood extent; water depths or water level, flow velocity or the relevant water flow direction. The usefulness of those parameters are (EXCIMAP, 2007):

- Flood extent: - Serves as a basic product to establish danger maps and risk maps - Land use planning (legally binding) - City and village planning - Rural planning - Risk management - Awareness building (particularly when combined with past events).
- Flood depth: - Serve as a basic product to establish danger and flood damage maps - City and village Planning - Risk management (evacuation).
- Flow velocity: Planning of flood defense measures or any structure within the flood area. Tool for technicians.
- Flood propagation: - Planning tool for emergency response - Evacuation schemes, implementation of temporal flood protection measures - the information requires a well-functioning early warning and alert system.

7.7.2 Use of the results of the current study in building Ouémé flood forecast early warning system (OFFEWS)

In addition to short-term (real-time) warnings related to a specific, forthcoming flood event, some authors have raised the need of another type of early warning if the projections (predictions) of flood hazards in the more distant future indicate considerable changes in the anticipated risk (Kundzewicz, 2013). Early warnings of increasing flood risk in the decades ahead are necessary to upgrade defense strategies, for example by undertaking the time-consuming and resource-intensive task of strengthening levees. Climatic and non-climatic factors affect future flood risk and adaptation needs. For example, land-cover changes and urbanization can increase flood risk regardless of any change in climate. Observations and climate projections show widespread increases in the

contribution of very wet days to total annual precipitation in the warming atmosphere (Kundzewicz, 2013).

Increasing flood magnitudes are projected in the study area. Since the assumption of stationarity is no longer valid, operational system design need to be updated to account for land use and land cover change, climate change and other relevant future changes in the area of concern. Failure in revising current design procedure may result in over or underestimation of infrastructures which could not be benefic regarding the cost.

For example in Bavaria (Germany), flood design values now take into account projections of a 40–50 % increase in small and medium flood discharges by 2050, and an increase of around 15% in 100-year floods (Kundzewicz, 2013).

7.7.3 Toward an OFFEWS for Ouémé basin

The suggested framework is based on what has been successfully applied in Europe: European Flood Awareness System (EFAS). The European Flood Awareness System (EFAS) produces European overviews of ongoing and forecasted floods up to 15 days in advance and contributes to better protection of the European citizens, the environment, properties and cultural heritage. The components of the suggested framework for flood forecasting and early warning system in Ouémé basin are:

- Data collection center: meteorological data, hydrological data and others
- Computational center
- Dissemination center

7.7.3.1 Data collection center

This center will have the target to collect all data needed to perform the flood forecasting. This starts by the collection of historical climatic (rainfall, temperature etc.) and hydrologic (discharge and water level) data. The implementation of automatic weather stations, automatic discharge and water level stations and collection of these data will be assigned to this center. Contact with international research groups for providing weather forecasts, satellite based rainfall data (TRMM TMI, http://www.remss.com/missions/tmi), Geostationary Satellite data for near real time rainfall estimated from, for instance, the GSMaP_NRT system developed by JAXA (http://sharaku.eorc.jaxa.jp/GSMaP/). *The GSMaP_NRT system is currently capable of producing rainfall maps after four hours of observation* (UNESCO, 2015). It will provide all data to computation center.

7.7.3.2 Computational center

The center runs the forecasts and post-processing calculations as well as the web interface of the OFEWS-Information System. Based on the data collected by the collection center, the computation center will calibrate and validate the hydrological model WaSiM (Schulla, 2012) using available information. Return levels corresponding

to different return periods (20, 5, 2, 1.5-year) will be computed and validated with the one calculated from the historical discharge data. The inundation mapping of water surface profile (inundation depth and floodplain boundary) can be performed using e.g. the HEC-RAS computer program and the result will be compared with historical flood inundation maps (satellite maps of historical floods) for efficiency (calibration and validation of HEC-RAS). Based on the efficiency of the system in predicting the inundation depth and inundation extent, it can be adopted for Ouémé flood early warning system (OFEWS).

For the OFEWS, the parameters previously calibrated are used to get predicted inundation maps (depth, extent, velocity…) based on the weather forecast data and automatic meteorological data recorded, automatic discharge data provided by the data collection center.

The hydrological model for OFEWS should be able to provide up to twice a day early flood warning information. As it has been done for EFAS, results can be based on multiple weather forecasts with different spatial and temporal resolutions including data from different weather services, deterministic and ensemble products, short-range and medium-range products. The majority of information will be based on critical level exceedance and not quantitative discharge forecasts. At the stations where appropriate real-time data are provided, OFEWS can provide bias corrected quantitative discharge forecasts. All information related to the forecast should be freely available online and provided to the dissemination center.

7.7.3.3 Dissemination center

An effective and well-understood protocol for issuing warnings is an essential yet often overlooked element of early warning system (EWS). The activities that define a multi-hazard early warning system (EWS), from the collection of data to the decision to warn to actions taken by constituents, will only protect the people within a forecast center's area of responsibility if individuals and groups receive the warning message in a timely fashion, understand its meaning, and take appropriate action (NOAA, 2010). The center analyses the results on a daily basis, assesses the situation, and disseminate information up to the end users. Information must be provided to government agencies, the media, the public, and other persons and groups that will be affected by the event Flash flood forecasting. Some important Points to Remember about Dissemination are (NOAA, 2010):

- The media play a crucial role in the distribution of warning messages.
- The dissemination processes should be automated as much as possible to decrease the time required to issue warnings.
- Dissemination techniques should take advantage of new communications technology.

- Centers have found that it is important to limit the number of primary dissemination channels and to steer customers to those channels if they are readily available at that customer's location.
- Repeated warning messages ensure those who missed an earlier warning message will have another chance to receive it, and those who ignored an earlier warning message will have another opportunity to act.

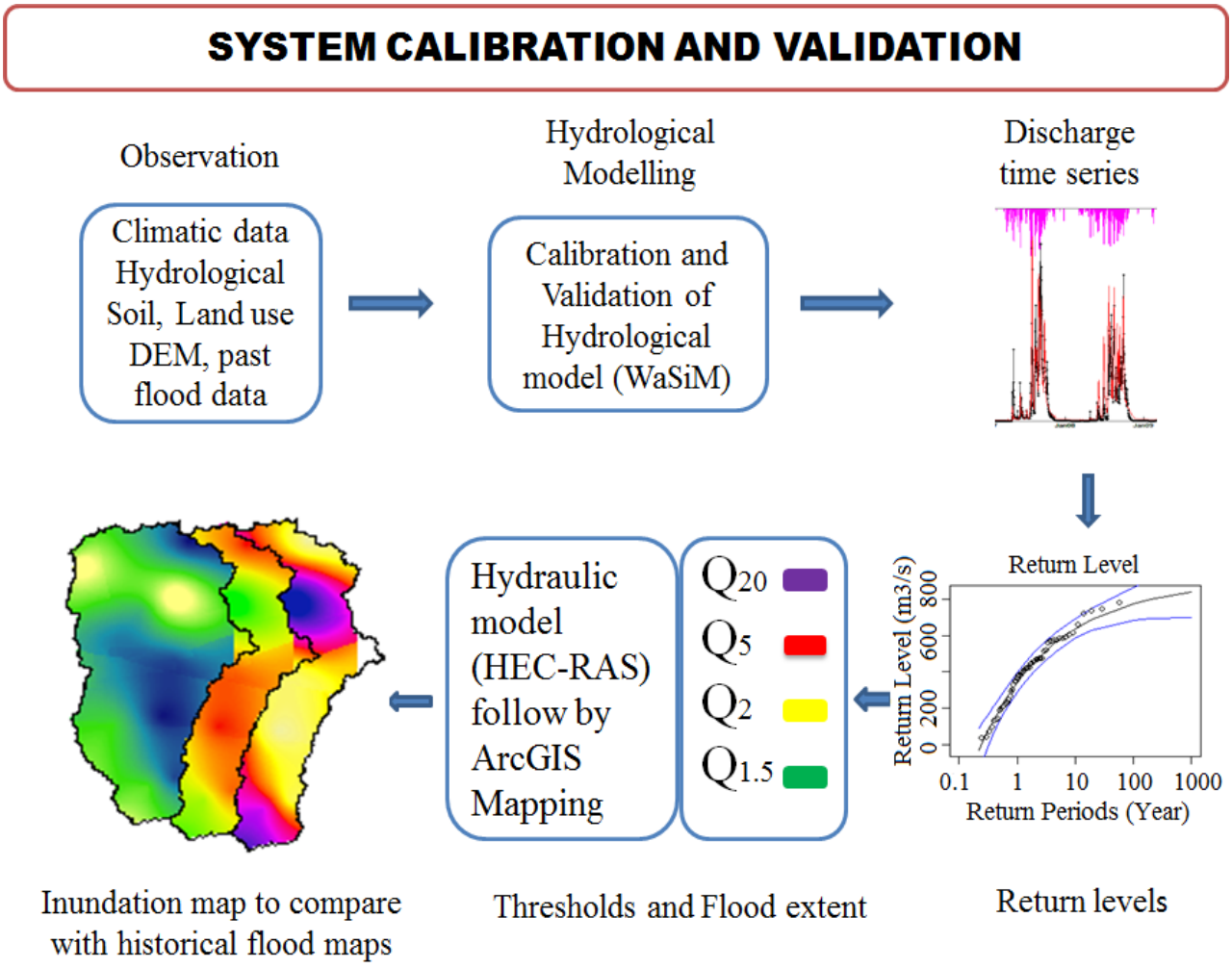

Figure 7-1: System calibration and validation and the different components

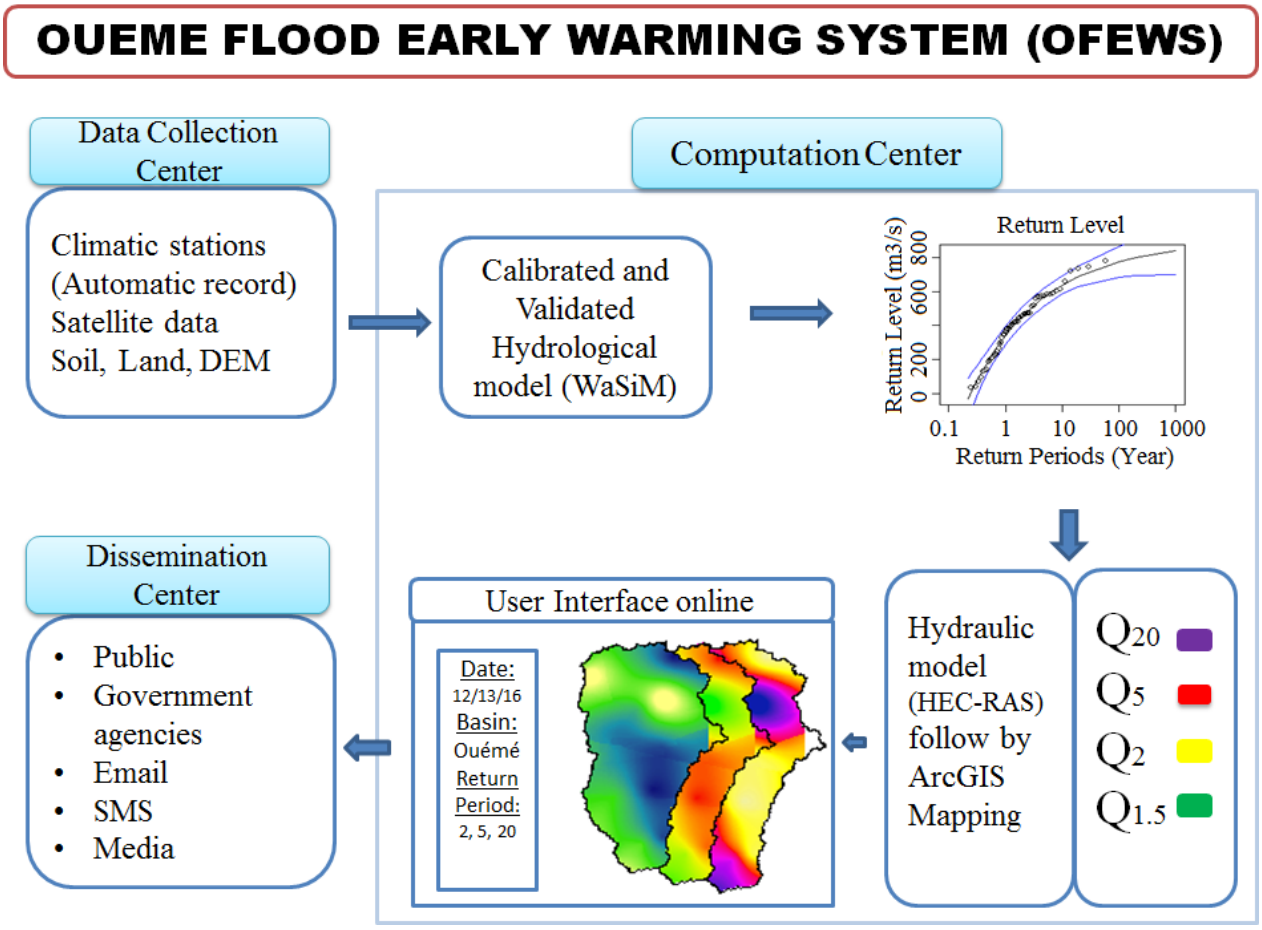

Figure 7-2: The proposed framework for Ouémé flood forecast and early warning system (OFFEWS)

References

Abbaspour, K. C., Faramarzi, M., Ghasemi, S. S. & Yang, H. (2009) Assessing the impact of climate change on water resources in Iran. *Water Resour. Res.* **45**(W10434), 1–16. doi:10.1029/2008WR007615

Abbaspour, K. C., Yang, J., Maximov, I., Siber, R., Bogner, K., Mieleitner, J. & Zobrist, J. (2007) Modelling hydrology and water quality in the pre-alpine / alpine Thur watershed using SWAT. *J. Hydrol.* **333**, 413–430. doi:10.1016/j.jhydrol.2006.09.014

Abdo, G. M. & Nasr, A. E. (2012) An Improved Flood Forecasting Model of the Blue Nile River in Sudan. *Univ. Khartoum Eng. J.* **2**(1), 27–30. doi:10.1017/CBO9781107415324.004

Aissaoui-Fqayeh, I., El-Adlouni, S., Ouarda, T. B. M. J. & St-Hilaire, A. (2009) Développement du modèle log-normal non-stationnaire et comparaison avec le modèle GEV non-stationnaire. *Hydrol. Sci. J.* **54**(6), 1141–1156. doi:10.1623/hysj.54.6.1141

Akaike, H. (1974) A New Look at the Statistical Model Identification. *IEEE Trans. Autom. Control* **ac-19**(6), 716–723.

Alamou, E. (2011) *Application du Principe de Moindre Action à la Modélisation Pluie-débit. Ph.D. Thesis*. Université d'Abomey-Calavi, Abomey Calavi, Benin, 231 p.

Allen, R. G. (1986) Penmann for all season. *J. Irrig. Drain. Eng.* **112**(4), 348–368.

Amoussa, S. (1992) Estimation of global solar radiation in Benin. *Renew. Energy* **2**(3), 311–317.

Amoussou, E., Tramblay, Y., Totin, H. S. V., Mahé, G. & Camberlin, P. (2014) Dynamics and modelling of floods in the river basin of Mono in Nangbeto, Togo/Benin. *Hydrol. Sci. J.* **59**(11), 2060–2071. doi:10.1080/02626667.2013.871015

Aregheore, E. M. (2009) Country Pasture / Forage Resource Profiles, The Republic of Benin. Retrieved from www.fao.org/ag/agp/agpc/doc/counprof/benin/Benin.htm

Arnell, N. W. (1999) The effect of climate change on hydrological regimes in Europe : a continental perspective. *Glob. Environ. Chang.* **9**, 5–23.

Arnold, J. G., Allen, P. M. & Bernhardt, G. (1993) A comprehensive surface-groundwater flow model. *J. Hydrol.* **142**, 47–69.

Arnold, J. G., Srinivasan, R., Muttiah, R. S. & Williams, J. R. (1998) Large area hydrologic modeling and assessment part I: Model development. *J. Am. Water Resour. Assoc.* **34**(1), 73–89.

Artan, G., Gadain, H., Smith, J. L., Asante, K., Bandaragoda, C. J. & Verdin, J. P. (2007) Adequacy of satellite derived rainfall data for stream flow modeling. *Nat. Hazards* **43**(2), 167–185. doi:10.1007/s11069-007-9121-6

Artan, G., Verdin, J. & Asante, K. (2001) A wide-area flood risk monitoring model. *Fifth Int. Work. Appl. Remote Sens. Hydrol.*, 10. Montpellier, France, October 2–5.

Asante, K. O., Macuacua, R. D., Artan, G. a., Lietzow, R. W. & Verdin, J. P. (2007) Developing a flood monitoring system from remotely sensed data for the Limpopo basin. *IEEE Trans. Geosci. Remote Sens.* **45**(6), 1709–1714. doi:10.1109/TGRS.2006.883147

Avahounlin, F. R., Lawin, A. E., Alamou, E., Chabi, A. & Afouda, A. (2013) Analyse Fréquentielle des Séries de Pluies et Débits Maximaux de L' ouémé et Estimation des Débits de Pointe. *Eur. J. Sci. Res.* **107**(3), 355–369.

Bader, J.-C., Piedelievre, J.-P. & Lamagat, J.-P. (2006) Prévision saisonniere du volume de crue du Fleuve Sénégal: utilisation des résultats du modele ARPEGE Climat. *Hydrol. Sci. J.* **51**(3), 406–417. doi:10.1623/hysj.51.3.406

Baldassarre, G. Di & Claps, P. (2010) A hydraulic study on the applicability of flood rating curves. *Hydrol. Res.* **42**(1), 10–19. doi:10.2166/nh.2010.098

Baldassarre, G. Di, Montanari, A., Lins, H., Koutsoyiannis, D., Brandimarte, L. & Blöschl, G. (2010) Flood fatalities in Africa: From diagnosis to mitigation. *Geophys. Res. Lett.* **37**(L22402), 1–5. doi:10.1029/2010GL045467

Bates, B., Kundzewicz, Z. W., Wu, S. & Palutikof, J. (Eds.). (2008) *Climate Change and Water. Technical Paper of the Intergovernmental Panel on Climate Change*. IPCC Secretariat, Geneva, 201 p.

Beguería, S. (2005) Uncertainties in partial duration series modelling of extremes related to the choice of the threshold value. *J. Hydrol.* **303**, 215–230. doi:doi:10.1016/j.jhydrol.2004.07.015

Beguería, S., Angulo-Martínez, M., Vicente-Serrano, S. M., López-Moreno, J. I. & El-kenawy, A. (2011) Trends in extreme precipitation by non-stationary POT analysis. *Int. J. Climatol.* **31**, 2102–2114.

Beven, K. (2012) *Rainfall-Runoff Modelling, the Primer*, 2nd ed. Oxford, UK: JohnWiley & Sons, Ltd, 472 p.

Bormann, H. (2005) Regional hydrological modelling in Benin (West Africa): Uncertainty issues versus scenarios of expected future environmental change. *Phys. Chem. Earth, Parts A/B/C* **30**, 472–484. doi:10.1016/j.pce.2005.07.002

Bormann, H. & Diekkrüger, B. (2004) A conceptual, regional hydrological model for Benin (West Africa): validation, uncertainty assessment and assessment of applicability for environmental change analyses. *Phys. Chem. Earth* **29**, 759–786.

Bormann, H., Fass, T., Giertz, S., Junge, B., Diekkrüger, B., Reichert, B. & Skowronek, A. (2005) From local hydrological process analysis to regional hydrological model application in Benin: concept, results and perspectives. *Phys. Chem. Earth* **30**, 347–356.

Bossa, Y. A. (2012) *Multi-scale modeling of sediment and nutrient flow dynamics in the Ouémé catchment (Benin)– towards an assessment of global change effects on soil degradation and water quality. PhD thesis*. University of Bonn, Bonn, Germany, 110 p. Retrieved from http://hss.ulb.uni-bonn.de/2012/2983/2983.htm

Bossa, Y. A., Diekkrüger, B. & Agbossou, E. K. (2014) Scenario-Based Impacts of Land Use and Climate Change on Land and Water Degradation from the Meso to Regional Scale. *Water* **6**, 3152–3181. doi:10.3390/w6103152

Bossa, Y. A., Diekkrüger, B., Giertz, S., Steup, G., Sintondji, L. O., Agbossou, E. K. & Hiepe, C. (2012) Modeling the effects of crop patterns and management scenarios on N and P loads to surface water and groundwater in a semi-humid catchment (West Africa). *Agric. Water Manag.* **115**, 20–37. Elsevier B.V. doi:10.1016/j.agwat.2012.08.011

Bronstert, A. (2003) Floods and Climate Change : Interactions and Impacts. *Risk Anal.* **23**(3), 545–557.

Brook, F. C. A. & Lash, D. (1983) *A hydrologic simulation model for eastern forests*. Water Resources Research Center, University of New Hampshire, USA, 94 p.

Brown, S. J., Caesar, J. & Ferro, C. T. (2008) Global changes in extreme daily temperature since 1950. *J. Geophys. Res.* **113**(D05115), 1–11. doi:10.1029/2006JD008091

Brutsaert, W. (1982) *Evaporation into the atmosphere*. Kluwer Academic Publishers, 302 p.

Burek, P. (2011) Towards a Pan-African Flood Forecasting and Early Warning System. *GEOSS African Water Cycle Symp. (Addis Ababa, 23 – 25 Febr. 2011)*. Retrieved November 1, 2015, from

ftp://193.194.138.98/documents/meetings/201102_2nd_awcs/Burek_floodfore_addis.pdf, 14 p

Burt, T. & Weerasinghe, K. (2014) Rainfall Distributions in Sri Lanka in Time and Space: An Analysis Based on Daily Rainfall Data. *Climate* **2**(4), 242–263. doi:10.3390/cli2040242

Carvalho, L. M. V., Jones, C. & Liebmann, B. (2002) Extreme Precipitation Events in Southeastern South America and Large-Scale Convective Patterns in the South Atlantic Convergence Zone. *J. Clim.* **15**, 2377–2394.

Cheng, L., Aghakouchak, A., Gilleland, E. & Katz, R. W. (2014) Non-stationary extreme value analysis in a changing climate. *Clim. Change* **127**, 353–369. doi:10.1007/s10584-014-1254-5

Chow, V. T., Maidment, D. R. & Mays, L. W. (1988) *Applied Hydrology*. New York, USA: McGraw-Hill, 570 p.

Coles, S. (2001) *An Introduction to Statistical Modeling of Extreme Values*. Bristol, UK: Springer, 221 p.

Coles, S. & Davison, A. (2008) Statistical Modelling of Extreme Values. Retrieved February 4, 2013, from http://www.cces.ethz.ch/projects/hazri/EXTREMES/talks/colesDavisonDavosJan08.pdf, 70 p

Conway, D. & Mah, G. (2009) River flow modelling in two large river basins with non-stationary behaviour : the Parana and the Niger. *Hydrol. Process.* **23**, 3186–3192. doi:10.1002/hyp.7393

Cornelissen, T., Diekkrüger, B. & Giertz, S. (2013) A comparison of hydrological models for assessing the impact of land use and climate change on discharge in a tropical catchment. *J. Hydrol.* **498**, 221–236. Elsevier B.V. doi:10.1016/j.jhydrol.2013.06.016

Coron, L., Andreassian, V., Perrin, C., Lerat, J., Vaze, J., Bourqui, M. & Hendrickx, F. (2012) Crash testing hydrological models in contrasted climate conditions : An experiment on 216 Australian catchments. *Water Resour. Res.* **48**(5), 1–17. doi:10.1029/2011WR011721

Crochet, P. (2012) Flood-Duration-Frequency modeling Application to ten catchments in Northern Iceland. Report. Retrieved from http://www.vedur.is/media/2012_006.pdf, 50 p

Cullmann, J., Mishra, V. & Peters, R. (2006) Flow analysis with WaSiM-ETH – model parameter sensitivity at different scales. *Adv. Geosci.* **9**, 73–77.

D'Orgeval, T. (2006) *Impact du changement climatique sur le cycle de l'eau en Afrique de l'Ouest : Modélisation et incertitudes, PhD thesis*. Universite Paris 6, Paris, France. Retrieved from http://dods.ipsl.jussieu.fr/orchidee/WEBORCHIDEE/ANOTER/These_dOrgeval.pdf, 187 p

David, M. & Sutton, C. (2011) *Social Research: An Introduction*. London, UK: SAGE, 235-236.

Davidson, O., Chenene, M., Kituyi, E., Nkomo, J., Turner, C. & Sebitosi, B. (2007) Sustainable Energy in sub-Saharan Africa. *ICSU Reg. Off. Africa*. Retrieved October 11, 2015, from http://www.icsu.org/icsu-africa/publications/ICSUROASciencePlanonSustainableEnergy.pdf, 22 p

Deng, Z. (2007) *Vegetation Dynamics in Oueme Basin, Benin, West Africa*. Göttingen, Germany: Cuvillier Verlag, 156 p.

DGEau. (2008) Annales hydrologiques des années 2003 a 2007. Cotonou, Benin. Retrieved from http://www.hydrosciences.fr/sierem/produits/biblio/annales/Benin/annale hydrologique de 2003 a 2007 de tous les bassins versants du Benin.pdf, 210 p

Diederich, M. & Simmer, C. (2010) Weather and climate monitoring in Benin. In: *Impacts of Global Change on the Hydrological Cycle in West and Northwest Africa* (P. Speth, M. Christoph & B. Diekkrüger, eds.), 114–121. Springer Heidelberg Germany.

Diekkrüger, B., Busche, H., Giertz, S. & Steup, G. (2010) Hydrology. *Impacts of Global Change on the Hydrological Cycle in West and Northwest Africa* (P. Speth, M. Christoph & B. Diekkrüger, eds.), 60–69. Springer, Heidelberg, Germany.

Diop, M. & Grimes, D. I. F. (2003) Satellite-based rainfall estimation for river flow forecasting in Africa. II: African Easterly Waves, convection and rainfall. *Hydrol. Sci. J.* **48**(4), 567–584. doi:10.1623/hysj.48.4.567.51410

El-Adlouni, S. & Ouarda, T. (2008) Comparaison des méthodes d'estimation des paramètres du modèle GEV non stationnaire. *Rev. des Sci. l'eau* **21**(1), 1–35. doi:10.7202/017929ar

El-Fahem, T. & Kocher, A. (2008) Geology of the Ouémé Catchment. *IMPETUS Atlas Benin. Res. Results 2000–2007. 3rd Ed.* (M. Judex & H.-P. Thamm, eds.). Department of Geography, University of Bonn, Germany, 65 p.

El-Fandy, M. G., Ashour, Z. H. & Taiel, S. M. M. (1994) Time series models adoptable for forecasting Nile floods and Ethiopian rainfalls. *Bull. - Am. Meteorol. Soc.* **75**(1), 83–94.

EM-DAT. (2010) The OFDA/CRED international disaster database. Available online: Retrieved September 23, 2013, from www.emdat.be

Engelen, V. van & Ting-tiang, W. (1995) Global and National Soils and Terrain Digital Databases (SOTER). *World Resour. Rep.* Retrieved March 12, 2012, from http://www.isric.org/isric/webdocs/Docs/ Soterep.PDF, 74 p

EXCIMAP. (2007) Handbook on good practices for flood mapping in Europe. Retrieved November 13, 2015, from http://ec.europa.eu/environment/water/flood_risk/flood_atlas/pdf/handbook_goodpractice.pdf, 57 p

Faure, P., Volkoff, B., Eschner, A. R., Trimble, S. W. & Angeles, L. (1998) Some factors affecting regional differentiation of the soils in the Republic of Benin (West Africa). *Catena* **32**, 281–306.

Feng, S. & Hu, Q. (2007) Changes in winter snowfall / precipitation ratio in the contiguous United States. *J. Geophys. Res.* **112**, 1–12. doi:10.1029/2007JD008397

Fink, A., Christoph, M., Born, K., Bruecher, T., Piecha, K., Pohle, S., Schulz, O., et al. (2010) Climate. *Impacts of Global Change on the Hydrological Cycle in West and Northwest Africa* (P. Speth, M. Christoph & B. Diekkrüger, eds.), 54–59. Heidelberg, Germany: Springer.

Florina, B. S. (2007) *Development and Application of Flood Vulnerability Indices for Various Spatial Scales*. UNESCO-IHE Institute for Water Education, Delft, the Netherlands, 157 p.

Fowler, H. J., Kilsby, C. G. & Jones, P. D. (2005) New estimates of future changes in extreme rainfall across the UK using regional climate model integrations . 2 . Future estimates and use in impact studies. *J. Hydrol.* **300**, 234–251. doi:10.1016/j.jhydrol.2004.06.019

Frei, C., Scho, R., Fukutome, S. & Vidale, P. L. (2006) Future change of precipitation extremes in Europe : Intercomparison of scenarios from regional climate models. *J. Geophys. Res.* **111**(D06105), 1–22. doi:10.1029/2005JD005965

Frich, P., Alexander, L. V, Gleason, B., Haylock, M., Tank, A. M. G. K. & Peterson, T. (2002) Observed coherent changes in climatic extremes during the second half of the twentieth century. *Clim. Res.* **19**, 193–212.

Giertz, S., Diekkrüger, B. & Höllermann, B. (2012) Impact of global change on water resources in the Ouémé catchment, Benin. *Conf. Glob. Catchment Initiat. (GCI). Glob. Dimens. Chang. River Basins* (E. J. J. Bogardi, J. Leentvaar & H. Nachtnebel, eds.), 34–40. Delft, The netherlands: UNESCO-IHE.

Giertz, S., Hiepe, C., Höllermann, B. & Diekkrüger, B. (2010) Impacts of Global Change on water resources and soil degradation in Benin. *Impacts of Global Change on the Hydrological Cycle in West and Northwest Africa* (P. Speth, M. Christoph & B. Diekkrüger, eds.), 484–511.

Giertz, S., Steup, G. & Schönbrodt, S. (2012) Use and constraints on the use of inland valley ecosystems in central Benin: Results from an inland valley survey. *Erdkunde* **66**(3), 239–253. doi:10.3112/erdkunde.2012.03.04

Gilleland, E. & Katz, R. W. (2005) Extremes Toolkit (extRemes): Weather and Climate Applications of Extreme Value. Retrieved December 23, 2014, from www.isse.ucar.edu/extremevalues/extreme.pdf, 130 p

Götzinger, J. (2007) *Distributed Conceptual Hydrological Modelling - Simulation of Climate , Land Use Change Impact and Uncertainty Analysis, PhD Thesis*. University of Stuttgart, Stuttgart, Germany, 144 p. Retrieved from http://elib.uni-stuttgart.de/opus/volltexte/2007/3349/pdf/Diss_Goetzinger_ub.pdf

Goula, B. T. A., Soro, E. G., Kouassi, W. & Srohourou, B. (2011) Tendances et ruptures au niveau des pluies journalières extrêmes en Côte d ' Ivoire (Afrique de l'Ouest). *Hydrol. Sci. J.* **57**(6), 1067–1080.

Grimes, D. I. F. & Diop, M. (2003) Satellite-based rainfall estimation for river flow forecasting in Africa. I: Rainfall estimates and hydrological forecasts. *Hydrol. Sci. J.* **48**(4), 567–584. doi:10.1623/hysj.48.4.567.51410

Groisman, P. Y., Knight, R. W., Easterling, D. R. & Karl, T. R. (2005) Trends in intense precipitation in the climate record. *J. Clim.* **18**(8), 1326 – 1349.

Gumbel, E. J. (1958) It's impossible that the improbable will never happen. (Il est impossible que l'improbable n'arrive jamais). Retrieved March 8, 2015, from http://www.azquotes.com/quote/699855

Guo, H., Hu, Q. & Jiang, T. (2008) Annual and seasonal streamflow responses to climate and land-cover changes in the Poyang Lake basin. *J. Hydrol.* **355**, 106–122. doi:10.1016/j.jhydrol.2008.03.020

Gupta, H. V., Kling, H., Yilmaz, K. K. & Martinez, G. F. (2009) Decomposition of the mean squared error and NSE performance criteria: Implications for improving hydrological modelling. *J. Hydrol.* **377**, 80–91. Elsevier B.V. doi:10.1016/j.jhydrol.2009.08.003

Hanel, M., Buishand, T. A. & Ferro, C. A. T. (2009) A non-stationary index-flood model for precipitation extremes in transient Regional Climate Model simulations. *J. Geophys. Res. Atmos.* **114**(D15), 1–61. Retrieved from http://cdn.knmi.nl/

Hargreaves, G. H. (1975) Moisture availability and crop production. *Am. Soc. Agric. Biol. Eng.* **18**(5), 0980–0984. doi:10.13031/2013.36722

Herbst, M., Casper, M. C., Grundmann, J. & Buchholz, O. (2009) Comparative analysis of model behaviour for flood prediction purposes using Self-Organizing Maps. *Nat. Hazards Earth Syst. Sci.* **9**(2), 373–392. doi:10.5194/nhess-9-373-2009

Höllermann, B. (2008) *Water : A Scarce Resource in Benin ? Modeling the water balance of the Ouémé catchment. PhD Thesis*. Rheinischen Friedrich – Wilhelms – Universität Bonn, 116 p.

Höllermann, B., Giertz, S. & Diekkrüger, B. (2010) Benin 2025 — Balancing Future Water Availability and Demand Using the WEAP ‘ Water Evaluation and Planning ’ System. *Water Resouces Manag.* **24**, 3591–3613. doi:10.1007/s11269-010-9622-z

Hossain, M., Roy, K. & Datta, D. (2014) Spatial and Temporal Variability of Rainfall over the South-West Coast of Bangladesh. *Climate* **2**(2), 28–46. doi:10.3390/cli2020028

Hounkpè, J., Afouda, A. A. & Diekkrüger, B. (2015) Use of climate indexes as covariates in modelling high discharges under non stationary condition in Ouémé River. *E-proceedings 36th IAHR World Congr.*, 1–5. Retrieved from http://89.31.100.18/~iahrpapers/85339.pdf

Hounkpè, J., Afouda, A. A., Diekkrüger, B. & Hountondji, F. (2015) Modelling extreme streamflows under non-stationary conditions in Ouémé river basin, Benin, West Africa. *Hydrological Sciences and Water Security: Past, Present and Future*, 143–144. Paris, France: IAHS (International Association of Hydrological Sciences). doi:10.5194/piahs-366-143-2015

Hounkpè, J., Diekkrüger, B., Badou, D. & Afouda, A. (2015) Non-Stationary Flood Frequency Analysis in the Ouémé River Basin, Benin Republic. *Hydrology* **2**(4), 210–229. doi:10.3390/hydrology2040210

Hountondji, Y. & Ozer, P. (2000) Trends in extreme rainfall events in Benin (West Africa), 1960-2000. *1 st Int. Conf. Energy , Environ. Clim. Chang.* Retrieved October 23, 2014, from http://orbi.ulg.be/bitstream/2268/96112/1/ICEC2011_Full_Hountondji-etal.pdf, 8 p

Hubert, P., Carbonnel, J.-P. & Chaouche, A. (1989) Segmentation des séries hydrométéorologiques — application à des séries de précipitations et de débits de l’afrique de l'ouest. *J. Hydrol.* **110**, 349–367. doi:10.1016/0022-1694(89)90197-2

Huisman, J. A., Breuer, L., Bormann, H., Bronstert, A., Croke, B. F. W., Frede, H.-G., Gräff, T., et al. (2009) Assessing the impact of land use change on hydrology by ensemble modeling (LUCHEM) III: Scenario analysis. *Adv. Water Resour.* **32**(2), 159–170. doi:10.1016/j.advwatres.2008.06.009

Igué, A. M., Houndagba, C. J., Gaiser, T. & Stahr, K. (2006) Land Use/Cover Map and its Accuracy in the Oueme Basin of Benin (West Africa). *Conf. Int. Agric. Res. Dev. L.*, 1:4. Bonn, Germany: University of Bonn. Retrieved from http://www.tropentag.de/2006/abstracts/links/Igue_EuSf9GlR.pdf

IPCC. (2001) *Climate change, 2001: The scientific basis. Contribution of Working Group I to the Third Assessment Report of the Intergovernmental Panel on Climate Change.* (J. T. Houghton, Y. Ding, D. J. Griggs, M. Noguer, P. J. van der Linden, X. Dai, K. Maskell, et al., Eds.). Cambridge, UK: Cambridge University Press, 881 p.

IPCC. (2007) *Climate Change 2007: The Physical Science Basis*. (S. Solomon, D. Qin, M. Manning, Z. Chen, M. Marquis & K. B. Averyt, Eds.). New York, NY, USA: Cambridge University Press, 996 p.

IPCC. (2012) Glossary of terms. In: *Managing the Risks of Extreme Events and Disasters to Advance Climate Change Adaptation. A Special Report of Working Groups I and II of the Intergovernmental Panel on Climate Change (IPCC).* (C. B. Field, V. Barros, T. F. Stocker, D. Qin, D. J. Dokken, K. L. Ebi, Mastrandrea, et al., eds.), 555–564. Cambridge University Press, Cambridge, UK, and New York, NY, USA.

Irwin, S. E. (2015) *Assessment of the Regionalization of Precipitation in Two Canadian Climate Regions : A Fuzzy Clustering Approach. Master Thesis*. University of Western Ontario, Ontario, Canada, 126 p. Retrieved from http://ir.lib.uwo.ca/cgi/viewcontent.cgi?article=4574&context=etd

Isaaks, E. H. & Srivastava, R. M. (1989) *Applied Geostatistics*. Oxford, UK: Oxford University Press, 561 p.

Jain, S. & Lall, U. (2001) Floods in a changing climate: does the past represent the future? *Water Resour. Res.* **37**(12), 3193–3205. doi:10.1029/2001WR000495

Janicot, S., Ali, H., Fontaine, B. & Vincent, M. (1998) West African Monsoon Dynamics and Eastern Equatorial Atlantic and Pacific SST Anomalies (1970 – 88). *J. Clim.* **11**, 1874–1883.

Janicot, S., Thorncroft, C. D., Ali, A., Asencio, N., Berry, G., Bock, O., Bourles, B., et al. (2008) Large-scale overview of the summer monsoon over West Africa during the AMMA field experiment in 2006. *Ann. Geophys.* **26**(9), 2569–2595. doi:10.5194/angeo-26-2569-2008

Jarvis, A., Reuter, H. I., Nelson, A. & Guevara, E. (2008) Hole-filled seamless SRTM data V4, International Centre for Tropical Agriculture (CIAT). Retrieved May 4, 2013, from www.cgiar-csi.org/data/srtm-90m-digital-elevation-database-v4-1

Jasper, K., Gurtz, J. & Lang, H. (2002) Advanced flood forecasting in Alpine watersheds by coupling meteorological observations and forecasts with a distributed hydrological model. *J. Hydrol.* **267**, 40–52. doi:10.1016/S0022-1694(02)00138-5

Judex, M. & Thamm, H.-P. (2008) *IMPETUS Atlas Benin. Research Results 2000 – 2007*, 3rd ed. Department of Geography, University of Bonn, Germany, 130 p.

Kamagaté, B. (2006) *Ecoulements sur un bassin versant de milieu tropical de socle au Bénin : bassin versant de la Donga (haute vallée de l'Ouémé). Thèses de Doctorat*. Université de Monpellier II, Montpellier, France. 320 p.

Karl, T. R. & Knight, R. W. (1998) Secular Trends of Precipitation Amount, Frequency, and Intensity in the United States. *Bull. Am. Meteorol. Soc.* **79**(2), 231–241. doi:10.1175/1520-0477(1998)079<0231:STOPAF>2.0.CO;2

Kasei, R. A. (2009) *Modelling impacts of climate change on water resources in the Volta Basin , West Africa, PhD Thesis*. University of Bonn, Bonn, Germany. Retrieved from http://hss.ulb.uni-bonn.de/2010/1977/1977.htm, 185 p

Katz, R. W., Parlange, M. B. & Naveau, P. (2002) Statistics of extremes in hydrology. *Adv. Water Resour.* **25**, 1287–1304.

Khaliq, M. N. & Ha, C. (2006) Frequency analysis of a sequence of dependent and / or non-stationary hydro-meteorological observations : A review. *J. Hydrol.* **329**, 534–552. doi:10.1016/j.jhydrol.2006.03.004

Kharim, Vi. V. & Zwiers, F. W. (2004) Estimating Extremes in Transient Climate Change Simulations. *J. Clim.* **18**, 1156–1173.

Kiang, J., Rolf, O. & Waskom, R. (2010) Workshop on Nonstationarity, Hydrologic Frequency Analysis, and Water Management. Colorado, USA. Retrieved from http://www.usbr.gov/research/climate/Workshop_ Nonstat.pdf, 309 p

Klein Tank, A. M. G. & Koennen, G. P. (2003) Trends in Indices of Daily Temperature and Precipitation Extremes in Europe. *J. Clim.* **16**, 3665–3680.

Kloos, J., Asare-Kyei, D., Pardoe, J. & Renaud, F. G. (2015) Towards the Development of an Adapted Multi-hazard Risk Assessment Framework for the West Sudanian Savanna Zone. *UNU-EHS Publ.* **11**, 1–37.

Kundzewicz, Z. W. (2013) Floods : lessons about early warning systems. *Emerg. lessons from Ecosyst.*, 379–400. Retrieved from http://www.eea.europa.eu/publications/late-lessons-2/late-lessons-chapters/late-lessons-ii-chapter-15

Kundzewicz, Z. W. & Robson, A. (Eds.). (2000) *Detecting trend and other changes in hydrological data*. Geneva, Swtherland. Retrieved from http://www.wmo.ch/web/wcp/wcdmp/wcdmp.html, 168 p

Kunkel, K. E. (2003) North American Trends in Extreme Precipitation. *Nat. Hazards* **29**, 291–305.

Kunkel, K. E. & Andsager, K. (1999) Long-Term Trends in Extreme Precipitation Events over the Conterminous United States and Canada. *J. Clim.* **12**(1998), 2515–2527.

Kunstmann, H., Marx, A., Werhahn, J. & Smiatek, G. (2006) Early Flood Warning for Alpine catchments through Coupled Precipitation / River Runoff - Forecasts. Retrieved May 4, 2015, from http://www.univie.ac.at/IMG-Wien/meetings/map_d-phase/abstracts/20-floodwarn-marx.pdf, 4 p

Kyselý, J. & Beranová, R. (2009) Climate-change effects on extreme precipitation in central Europe : uncertainties of scenarios based on regional climate models. *Theor Appl Clim.* **95**, 361–374. doi:10.1007/s00704-008-0014-8

Lane, L. J. (1982) Distributed Model for Small Semi-Arid Wathersheds. *J. Hydraul.* **108**(HY10), 1114–1131.

Lane, L. J. (1983) Transmission Losses. In: *National Engineering Handbook*, 36 p. New York, USA: USDA.

Laurent, H. (2005) *Contribution à l'étude des systèmes convectifs en régions tropicales. Mémoire pour l'obtention du diplôme 'Habilitation à diriger les recherches'.* Université Joseph Fourier, Grenoble I, Grenoble, France, 177 p.

Lawin, A. E. (2007) *Analyse climatologique et statistique du regime pluviométrique de la haute vallee de l'Ouémé à partir des données pluviographiques AMMA-CATCH Bénin. Thèse de Doctorat*. Institut National Polytechnique de Grenoble, Grenoble, France, 211 p.

Lay, M. Le. (2006) *Modelisation hydrologique dans un contexte de variabilite hydroclimatique. Une approche comparative pour l'étude du cycle hydrologique à méso-échelle au Bénin. These de Doctorat*. Institut National Polytechnique de Grenoble, Grenoble, France, 254 p.

Leadbetter, M., Lindgren, G. & Rootzén, H. (1983) *Extremes and related properties of random sequences and series*, Springer-V. New York, USA, 336 p.

Lebel, T., Cappelaere, B., Galle, S., Hanan, N., Kergoat, L., Levis, S., Vieux, B., et al. (2009) AMMA-CATCH studies in the Sahelian region of West-Africa : An overview. *J. Hydrol.* **375**(1-2), 3–13. Elsevier B.V. doi:10.1016/j.jhydrol.2009.03.020

Legesse, D., Vallet-Coulomb, C. & Gasse, F. (2003) Hydrological response of a catchment to climate and land use changes in Tropical Africa : case study South Central Ethiopia. *J. Hydrol.* **275**, 67–85. doi:10.1016/S0022-1694(03)00019-2

Lehner, B., Oll, P. D., Henrichs, T. & Kaspar, F. (2006) Estimating the impact of global change on flood and drought risks in Europe: a continental, integrated analysis. *Clim. Change* **75**, 273–299. doi:10.1007/s10584-006-6338-4

Li, L., Hong, Y., Wang, J., Adler, R. F., Policelli, F. S., Habib, S., Irwn, D., et al. (2009) Evaluation of the real-time TRMM-based multi-satellite precipitation analysis for an operational flood prediction system in Nzoia Basin, Lake Victoria, Africa. *Nat. Hazards* **50**(1), 109–123. doi:10.1007/s11069-008-9324-5

Li, Y., Cai, W. & Campbell, E. P. (2005) Statistical Modeling of Extreme Rainfall in Southwest Western Australia. *J. Clim.* **18**, 852–863.

Lopez, J. & Frances, F. (2013) Non-stationary flood frequency analysis in continental Spanish rivers, using climate and reservoir indices as external covariates. *Hydrol. Earth Syst. Sci.* **17**(8), 3189–3203. doi:10.5194/hess-17-3189-2013

Losada, T., Rodriguez-Fonseca, B., Janicot, S., Gervois, S., Chauvin, F. & Ruti, P. (2010) A multimodel approach to the Atlantic ecuatorial mode. Impact on the West African monsoon. *Clim. Dyn.* **35**, 29–43. doi:10.1007/s00382-009-0625-5

Loster, T. (2002) Flood Trends and Global Change. Retrieved April 2, 2014, from http://fp.arizona.edu/kkh/hwrs/pdfs/trends/T-loster-Flood-Trends-summary-Reinsureance-Co.pdf, 7 p

Lubes-Niel, H., Masson, J. M., Paturel, J. E. & Servat, E. (1998) Variabilité climatique et statistiques . Étude par simulation de la puissance et de la robustesse de quelques tests utilisés pour vérifier l'homogénéité de chroniques. *Rev. des Sci. l'eau* **3**, 383–408.

Manton, M. J., Haylock, M. R., Hennessy, K. J., Nicholls, N., Chambers, L. E., Collins, D. A., Daw, G., et al. (2001) Trends in extreme daily rainfall and temperature in southeast Asia and the south Pacific : 1961 - 1998. *Int. J. Climatol.* **284**, 269–284.

Markose, S. & Alentorn, A. (2011) The Generalized Extreme Value (GEV) Distribution , Implied Tail Index and Option Pricing. *J. Deriv.* **18**(3), 35–60. doi:10.3905/jod.2011.18.3.035

Mason, S., Waylen, P., Mimmack, G., Rajaratnam, B. & Harrison, J. M. (1999) Changes in extreme rainfall events in South Africa. *Clim. Change* **41**, 249–257.

May, W. (2004) Variability and extremes of daily rainfall during the Indian summer monsoon in the period 1901–1989. *Glob. Planet. Change* **44**(1-4), 83–105. doi:10.1016/j.gloplacha.2004.06.007

McKay, M. D., Beckman, R. J. & Conover, W. J. (2000) A comparison of three methods for selecting values of input variables in the analysis of output from a computer code. *Technometrics* **42**(1), 55–61.

McKerchar, M. E., Moss, C. P. & Pearson, A. (1994) The Southern Oscillation index as a predictor of the probability of low streamflows in New Zealand. *Water Resour. Res.* **30**(10), 2717–2723. doi:10.1029/94WR01308

Menz, G., Judex, M., Orékan, V., Kuhn, A., Heldmann, M. & Thamm, H.-P. (2010) Land use and land cover modeling in Central Benin. *Impacts of Global Change on the Hydrological Cycle in West and Northwest Africa* (P. Speth, M. Christoph & B. Diekkrüger, eds.), 512–535. Springer-Verlag Berlin Heidelberg.

Milly, P. C. D., Betancourt, J., Falkenmark, M., Hirsch, R. M., Kundzewicz, Z. W., Lettenmaier, D. P. & Stouffer, R. J. (2008) Stationarity is dead: whither water management? *Science (80-.).* **319**, 573–574. doi:10.1126/science.1151915

Mitchell, T. (2006) 4 by 6-degree latititude-longitude resolution anomalies of ICOADS SST, SLP, surface air temperature, winds, and cloudiness. Retrieved July 17, 2014, from http://jisao.washington.edu/data_sets/sstanom_4by6/

Monteith, J. (1975) *Vegetation and the Atmosphere 1. Prinicples*. Academic Press, London, UK, 278 p.

Monteith, J. L. (1965) Evaporation and the environment. *state Mov. water living Org. XIX Symp. Soc. Exp. Biol.*, 205–234. Swansea, Cambridge University Press.

Moriasi, D. N., Arnold, J. G., Liew, M. W. Van, Bingner, R. L., Harmel, R. D. & Veith, T. L. (2007) Model evaluation guidelines for systematic quantification of accuracy in watershed simulations. *Am. Soc. Agric. Biol. Eng.* **50**(3), 885–900.

Mosley, M. & McKerchar, A. (1993) Streamflow. In: *Handbook of Hydrology* (D. Maidment, ed.), 8.1–8.39. McGraw-Hill Inc., New York.

Nchito, W. S. (2007) Flood risk in unplanned settlements in Lusaka. *Environ. Urban.* **19**(2), 539–551. doi:10.1177/0956247807082835

Neitsch, S. L., Arnold, J. G., Kiniry, J. R. & Williams, J. R. (2011) *Soil & Water Assessment Tool Theoretical Documentation Version 2009. Grassland, Soil, Water Res. Labaoratory*. Texas, USA: Texas Water Resources Institute, 647 p.

New, M., Hewitson, B., Stephenson, D. B., Tsiga, A., Kruger, A., Manhique, A., Gomez, B., et al. (2006) Evidence of trends in daily climate extremes over southern and west Africa. *J. Geophys. Res.* **111**(D14102), 1–11. doi:10.1029/2005JD006289

Ngongondo, C. S., Xu, C. Y., Tallaksen, L. M., Alemaw, B. & Chirwa, T. (2011) Regional frequency analysis of rainfall extremes in Southern Malawi using the index rainfall and L-moments approaches. *Stoch. Environ. Res. Risk Assess.* **25**(7), 939–955. doi:10.1007/s00477-011-0480-x

Niehoff, D., Fritsch, U. & Bronstert, A. (2002) Land-use impacts on storm-runoff generation : scenarios of land-use change and simulation of hydrological response in a meso-scale catchment in SW-Germany. *J. Hydrol.* **267**, 80–93.

Nigg, J. (1995) Risk communication and warning systems. In: *Natural Risk and Civil Protection* (T. Hotlick-Jones, A. Amendola & R. Casale, eds.), 369–382. E & FN Spon.

NOAA. (2010) *Flash Flood Early Warning System Reference Guide*. USA: U.S. Departement of Commerce. Retrieved from http://www.meted.ucar.edu/hazwarnsys/haz_fflood.pdf, 204 p

Oboubie, E. (2008) *Estimation of groundwater recharge in the context of future climate change in the White Volta River Basin , West Africa, PhD Thesis*. University of Bonn, Bonn, Germany. Retrieved from http://hss.ulb.uni-bonn.de/2008/1616/1616.pdf, 165 p

Osorio, J. D. G. & Galiano, S. G. G. (2012) Non-stationary analysis of dry spells in monsoon season of Senegal River Basin using data from Regional Climate Models (RCMs). *J. Hydrol.* **450-451**, 82–92. Elsevier B.V. doi:10.1016/j.jhydrol.2012.05.029

Paeth, H., Born, K. & Heuer, K. O. (2007) Changes in Benin's Monsoon Climate. In: *IMPETUS Atlas Benin. Research Results* (M. Judex & H.-P. Thamm, eds.), 3rd ed., 23–24. Department of Geography, University of Bonn, Germany.

Panthi, J., Dahal, P., Shrestha, M., Aryal, S., Krakauer, N., Pradhanang, S., Lakhankar, T., et al. (2015) Spatial and Temporal Variability of Rainfall in the Gandaki River Basin of Nepal Himalaya. *Climate* **3**(1), 210–226. doi:10.3390/cli3010210

Pettitt, A. N. (1979) A Non-Parametric Approach to the Change-Point Problem. *J. R. Stat. Soc. Ser. C. Appl. Stat.* **28**(2), 126–135.

Peyre De Fabregues, B. (1980) Végétation. In: *Atlas du Niger*, 20–21. Paris, France: édition jeune afrique.

Philippon, N. (2002) *Une nouvelle approche pour la prévision statistique des précipitations saisonnières en Afrique de l' Ouest et de l'est: méthodes, diagnostics et application, PhD Thesis*. Universté de Bourgogne, Bourgogne, France, 241 p. Retrieved from http://climatologie.u-bourgogne.fr/perso/nphilipp/thesis/Thesis.pdf

Pitman, W. V. (1973) *A Mathematical Model for Generating Monthly River Flows from Meteorological Data in South Africa*. South Africa: University of the Witwatersrand, Department of Civil Engineering, Hydrological Research Unit, 56 p.

Priestley, C. H. B. & Taylor, R. J. (1972) On the Assessment of Surface Heat Flux and Evaporation Using Large-Scale Parameters. *Mon. Weather Rev.* **100**(2), 81–92. doi:10.1175/1520-0493(1972)100<0081:OTAOSH>2.3.CO;2

Prudhomme, C., Jakoba, D. & Svenssona, C. (2003) Uncertainty and climate change impact on the flood regime of small UK catchments. *J. Hydrol.* **277**, 1–23. doi:10.1016/S0022-1694(03)00065-9

R Core Team. (2014) R: A language and environment for statistical computing. R Foundation for Statistical Computing. Vienna, Australia. Retrieved November 12, 2014, from http://www.r-project.org

Rallison, R. E. & Miller, N. (1981) Past, Present, and Future SCS Runoff Procedure. *Rainfall Runoff relationship, Water Resour. Publ.* (V. P. Singh, ed.), 1–14. Littleton, CO.

Ramos, M. C. & Martínez-Casasnovas, J. (2006) Trends in Precipitation Concentration and Extremes in the Mediterranean Penedès-Anoia Region, Ne Spain. *Clim. Change* **74**, 457–474. doi:10.1007/s10584-006-3458-9

Re, M. & Barros, V. R. (2009) Extreme rainfalls in SE South America. *Clim. Change* **96**, 119–136. doi:10.1007/s10584-009-9619-x

Ribereau, P., Guillou, A. & Naveau, P. (2008) Nonlinear Processes in Geophysics Estimating return levels from maxima of non-stationary random sequences using the Generalized PWM method. *Nonlinear Process. Geophys.* **15**, 1033–1039.

Ritchie, J. T. (1972) Model for predicting evaporation from a crop with incomplete cover. *Water Resour. Res.* **8**, 1204:1213.

RIVERTWIN. (2007) Regional Model for Integrated Water Management inTwinned River Basins. Adapted and Integrated Model for the Ouémé River Basin, Institute for Landscape Planning and Ecology: Stuttgart, Germany, Final Report. Retrieved June 3, 2015, from http://cordis.europa.eu/publication/rcn/11810_de.html

Robson, A. J., Jones, T. K., Reed, D. W. & Bayliss, A. C. (1998) A study of national trend and variation in UK floods. *Int. J. Climatol.* **18**, 165–182.

Sandholt, I., Nyborg, L., Fog, B., Lô, M., Bocoum, O. & Rasmussen, K. (2013) Remote sensing techniques for flood monitoring in the Senegal River Valley. *Geogr. Tidsskr. J. Geogr.* **103**(1), 71–81. doi:10.1080/00167223.2003.10649481

Satyanarayana, P. & Srinivas, V. (2008) Regional frequency analysis of precipitation using large-scale atmospheric variables. *J Geophys Res* **113**(D24110), 1–16. doi:10.1029/2008JD010412

Schoenau, S., Thapa, P. & Bárdossy, A. (2008) Erosion and sediment yield estimation for flood protection. *4th Int. Symp. Flood Def. Manag. Flood Risk, Reliab. Vulnerability*, 1–8. Toronto, Ontario, Canada. Retrieved from http://gfzpublic.gfz-potsdam.de/pubman/item/escidoc:6060:7/component/escidoc:6061/82_Schoenau.pdf

Schulla, J. (2012) *Model Description WaSiM*. Zurich, Swetherland. Retrieved from http://www.wasim.ch/downloads/doku/wasim/wasim_2012_en.pdf, 300 p

Schulla, J. (2014) *Model Description WaSiM*. Zurich, Swetherland. Retrieved from http://www.wasim.ch/downloads/doku/wasim/wasim_2013_en.pdf, , 316 p

Schulla, J. & Jasper, K. (2007) Model description WaSiM-ETH. Zurich, Swetherland. Retrieved from http://www.wasim.ch/downloads/doku/wasim/wasim_2007_en.pdf, 181 p

Schwarz, G. (1978) Estimating the Dimension of a Model. *Ann. Stat.* **6**(2), 461–464. Retrieved from http://www.jstor.org/stable/2958889

SCS. (1972) *Estimation of Direct Runoff from Storm Rainfall. National Engineering Handbook, Section 4 – Hydrology. USDA*. USA, 24 p.

Séguis, L., Kamagaté, B., Favreau, G., Descloitres, M., Seidel, J., Galle, S., Peugeot, C., et al. (2011) Origins of streamflow in a crystalline basement catchment in a sub-humid Sudanian zone : The Donga basin (Benin , West Africa) Inter-annual variability of water budget. *J. Hydrol.* **402**, 1–13. doi:10.1016/j.jhydrol.2011.01.054

Sen, P. K. (1968) Estimates of the Regression Coefficient Based on Kendall's Tau. *J. Am. Stat. Assoc.* **63**, 1379–1389. doi:10.1080/01621459.1968.10480934

Seneviratne, S. I., Nicholls, N., Easterling, D., GoodSeneviratne, C. M. S. I., Nicholls, N., Easterling, D., Goodess, C. M., et al. (2012) Changes in climate extremes and their impacts on the natural physical environment. In: Managing the Risks of Extreme Events and Disasters to Advance Climate Change Adaptation. In: *A Special Report of Working Groups I and II of the Intergovernmental Panel on Climate Change (IPCC)* (C. B. Field, V. Barros, T. F. Stocker, D. Qin, D. J. Dokken, K. L. Ebi, M. D. Mastrandrea, et al., eds.), 109–230. Cambridge University Press, Cambridge, UK, and New York, NY, USA.

Servat, E., Paturel, J.-E., Lubes-Niel, H., Kouamé, B., Masson, J. M., Travaglio, M. & Marieu, B. (1999) Des différents aspects de la variabilité de la pluviométrie en Afrique de l'ouest et centrale non sahélienne. *Rev. des Sci. l'eau* **12**(2), 363 – 387.

Shamseldin, A. Y., Abdo, G. M. & Elzein, A. S. (1999) Real-Time Flood Forecasting on the Blue Nile River. *Water Int.* **24**(1), 39–45. doi:10.1080/02508069908692132

Shi, P., Chen, C., Srinivasan, R., Zhang, X., Cai, T., Fang, X., Qu, S., et al. (2011) Evaluating the SWAT Model for Hydrological Modeling in the Xixian Watershed and a Comparison with the XAJ Model. *Water Resour. Manag.* **25**(10), 2595–2612. doi:10.1007/s11269-011-9828-8

Sighomnou, D., Descroix, L., Genthon, P., Gil, M. & Emmanuele, G. (2013) La crue de 2012 a Niamey : un paroxysme du paradoxe du Sahel ? *Secheresse* **24**, 3–13.

Simonovic, S. P. (2012) *Floods in a changing climate: Risk Management*. Cambridge University Press, New York, United States of America, 179 p: Cambridge University Press, Cambridge, UK, and New York, NY, USA.

Sintondji, L. O. C. (2005) *Modelling the rainfall-runoff process in the Upper Ouémé catchment (Terou in Bénin Republic) in a context of global change : extrapolation from the local to the regional scale, PhD thesis*. University of Bonn, Bonn, Germany, 205 p.

Smith, K. & Ward, R. (1998) *Floods. Physical Processes and Human Impacts*. John Wiley & Sons, Chichester 382 p.

Soro, E. G. (2011) *Modelisation statistique des pluies extremes en Cote d'Ivoire. PhD Thesis*. Université d'Abobo-Adjamé, Abidjan, Côte d'ivoire, 193 p.

Speth, P., Christoph, M. & Diekkrüger, B. (Eds.). (2010) *Impacts of Global Change on the Hydrological Cycle in West and Northwest Africa*, Springer-V. Germany, 675 p.

Su, B. D., Jiang, T. & Jin, W. B. (2005) Recent trends in observed temperature and precipitation extremes in the Yangtze River basin, China. *Theor. Appl. Climatol.* **83**(1-4), 139–151. doi:10.1007/s00704-005-0139-y

Sugahara, S. & Porf, R. (2009) Non-stationary frequency analysis of extreme daily rainfall in Sao Paulo , Brazil. *Int. J. Climatol.* **29**(December 2008), 1339–1349. doi:10.1002/joc

Tarhule, A. & Woo, M. (1998) Changes in rainfall characteristics in northern Nigeria. *Int. J. of. Climatol.* **18**(11), 1261–1271.

Teegavarapu, R. S. V. (2012) *Floods in a Changing Climate: Extreme Precipitation*. New York, USA: Cambridge University Press, 294 p.

Teng, J., Chiew, F. H. S., Timbal, B., Wang, Y., Vaze, J. & Wang, B. (2012) Assessment of an analogue downscaling method for modelling climate change impacts on runoff. *J. Hydrol.* **472-473**, 111–125. Elsevier B.V. doi:10.1016/j.jhydrol.2012.09.024

Thiemig, V., Pappenberger, F., Thielen, J., Gadain, H., Roo, A. de, Bodis, K., Medico, M. Del, et al. (2010) Ensemble flood forecasting in Africa: A feasibility study in the Juba-Shabelle river basin. *Atmos. Sci. Lett.* **11**(2), 123–131. doi:10.1002/asl.266

Tramblay, Y., Amoussou, E., Dorigo, W. & Mahé, G. (2014) Flood risk under future climate in data sparse regions: Linking extreme value models and flood generating processes. *J. Hydrol.* **519**, 549–558. Elsevier B.V. doi:10.1016/j.jhydrol.2014.07.052

Tramblay, Y., Neppel, L., Carreau, J. & Kenza, N. (2013) Non-stationary frequency analysis of heavy rainfall events in Southern France. *Hydrol. Sci. J.* **58**(2), 1–15.

Tucci, C. E. M. (2007) *Urban Flood Management*. *WMO/TD -No. 1372*. APFM, 303 p. Retrieved from http://www.wmo.int/apfm/

UNESCO. (2015) *Increasing Resilience to Floods in South Sudan*. South Sudan: UNESCO-IHE, 7 p. Retrieved from http://en.unesco.org/system/files/South Sudan Juba Increasing Resilience to Floods_final_0.pdf

UNOCHA. (2008) Benin: Half million potential flood victims : WHO. IRIN online news service. UN Office for the Coordination of Humanitarian Affairs. *IRIN*. Retrieved from http://www.irinnews.org/report/80153/benin-half-million-potential-flood-victims-who

UNOCHA. (2009) Affairs BENIN: Flooding prompts state of emergency. *IRIN online news Serv. UN ie Coord. Humanit. Af airs*. Retrieved December 29, 2013, from http://

Vaze, J., Jordan, P., Beecham, R., Frost, A. & Summerell, G. (2011) Guidelines for rainfall-runoff modelling Towards best practice model application. *eWater Coop. Res. Cent.* Retrieved March 8, 2014, from http://ewater.org.au/uploads/files/eWater-Guidelines-RRM-(v1_0-Interim-Dec-2011).pdf, 50 p

Vaze, J. & Teng, J. (2011) Future climate and runoff projections across New South Wales , Australia : results and practical applications. *Hydrol. Process.* **25**, 18–35. doi:10.1002/hyp.7812

Vissin, E., Boko, M., Houndenou, C. & Perard, J. (2003) Recherche de ruptures dans les séries pluviométriques et hydrologiques du bassin beninois du fleuve niger (Bénin, Afrique de l'ouest). *Publ. l 'Association Int. Climatol.* **15**, 368–376.

Walsh, R. P. D., Davies, H. R. J. & Musa, S. B. (1994) Flood Frequency and Impacts at Khartoum since the Early Nineteenth Century. *Geogr. J.* **160**(3), 266–279.

Wang, G. & Eltahir, E. a B. (1999) Use of ENSO information in medium- and long-range forecasting of the Nile floods. *J. Clim.* **12**(6), 1726–1737.

Wang, W., Chen, X., Shi, P. & Gelder, P. H. A. J. M. Van. (2008) Detecting changes in extreme precipitation and extreme streamflow in the Dongjiang River Basin in southern China. *Hydrol. Earth Syst. Sci.* **12**, 207–221.

Wang, X., Melesse, A. M. & Yang, W. (2006) Influences of potential evapotranspiration estimation methods on swat's hydrologic simulation in a northwestern Minnesota watershed. *Trans. ASABE* **49**(6), 1755–1772.

Wendling, U. (1975) Zur Messung und Schätzung der potentiellen Verdunstung. *Zeitschrift für Meteorol.* **25**(2), 103–111.

Wilcoxon, F. (1945) Individual comparisons by ranking methods. *Biometrics Bull.* **80**(1), 80–83.

Willems, P. (2014) WETSPRO : Water Engineering Time Series PROcessing tool. Retrieved July 16, 2015, from http://www.kuleuven.be/hydr/pwtools.htm

Williams, J. R. (1969) Flood routing with variable travel time or variable storage coefficients. *Transations ASAE* **12**(1), 100:103.

Williams, J. R. & Hann, R. W. (1973) HYMO: Problem oriented language for hydrologic modelling- Users' manual.

WMO. (2007) *Applying environmental assessment for flood management. A Tool for Integrated Flood Management*. APFM Technical Document No. 8, 33 p.

WMO. (2009) Flood management in a changing climate: A Tool for Integrated Flood Management. Associated Programme on Flood Management. Retrieved October 13, 2013, from http://www.apfm.info/publications/tools/Tool_09_FM_in_a_changing_climate.pdf, access on 23/09/13

Wolski, P., Savenije, H. H. G., Murray-Hudson, M. & Gumbricht, T. (2006) Modelling of the flooding in the Okavango Delta, Botswana, using a hybrid reservoir-GIS model. *J. Hydrol.* **331**(1-2), 58–72. doi:10.1016/j.jhydrol.2006.04.040

World Bank. (2011) World Bank provides support to address vulnerability and resilience issues in benin. Retrieved April 3, 2014, from http://www.banquemondiale.org/fr/news/press-release/2011/04/26/world-bank-provides-support-to-address-vulnerability-and-resilience-issues-in-benin

World Bank. (2011) *Inondation au Benin: Rapport d'evaluation des Besoins Post Catastrophe*. Cotonou, Benin, 84 p. Retrieved from www.gfdrr.org/sites/gfdrr.org/files/GFDRR_Benin_PDNA_2010.pdf, access on 01/12/2013

Xiong, L. & Guo, S. (2004) Trend test and change-point detection for the annual discharge series of the Yangtze River at the Yichang hydrological station. *Hydrol. Sci. J.* **49**(1), 99–112.

Yabi, I. & Afouda, F. (2012) Extreme rainfall years in Benin (West Africa). *Quat. Int.* **262**, 39–43. Elsevier Ltd and INQUA. doi:10.1016/j.quaint.2010.12.010

Yang, C. & Hill, D. (2012) Modeling stream flow extremes under non-time-stationary conditions. *XIX Int. Conf. Water Resour.*, 1–8. University of Illinois at Urbana-Champaign. Retrieved from http://cmwr2012.cee.illinois.edu/Papers/Special Sessions/Data-driven Approaches for Water Resources Forecasting and Knowledge/Yang_Ci_CMWR2012_Final version.pdf

Yawson, D. K., Kongo, V. M. & Kachroo, R. K. (2005) Application of linear and nonlinear techniques in river flow forecasting in the Kilombero River basin, Tanzania. *Hydrol. Sci. J.* **50**(5), 37–41. doi:10.1623/hysj.2005.50.5.783

Young, P. C. (2002) *Advances in real time forecasting*. Phil. Trans. R. Soc. Lond. (360) 1433–1450.

Zannou, A. B. (2013) Prévision/Suivi des inondations et cartographie des zones inondables au niveau national (Présentation orale). *Atelier Natl. Renf. Capacit. préparation d'un Program. Natl. Prévision Gest. des inondations*. Cotonou, Benin.

Zenoni, E., Pecora, S., Michele, C. De & Vezzoli, R. (2013) Maximum annual flood peaks distribution in non-stationary conditions. In: *Comprehensive Flood Risk Management Research for Policy and Practice*. (Poster Presentation). Retrieved from http://www.floodrisk2012.net/author/assets/posters/23-19-PO_1_84_FR12.pdf

Zhang, L. & Han, K. (2009) How to Analyze Change from Baseline : Absolute or Percentage Change ? Retrieved April 9, 2014, from http://www.statistics.du.se/essays/D09_Zhang Ling & Han Kun.pdf

Zhang, Q., Sun, P., Chen, X. & Jiang, T. (2011) Hydrological extremes in the Poyang Lake basin, China : changing properties , causes and impacts. *Hydrol. Process.* **25**, 3121–3130. doi:10.1002/hyp.8031

Zhao, R. & Liu, X. (1995) The Xinanjiang model. In: *Computer models of watershed hydrology* (V. P. Singh, ed.), 215–232. Water Resources Publications, USA.

Appendixes

Appendix A : Hydrological models SWAT and WaSiM description

a) SWAT model

The simulation of hydrological cycle by SWAT is based on water balance equation:

$$SW_t = SW_0 + \sum_{i=1}^{t}\left(R_{day} - Q_{surf} - \text{ETR} - w_{seep} - Q_{gw}\right) \quad \text{Eq. 0-1}$$

Where SW_t is the final soil water content (mm H_2O), SW_0 is the initial soil water content on day i (mm H_2O), t is the time (days), R_{day} is the amount of precipitation on day i (mm H_2O), Q_{surf} is the amount of surface runoff on day i (mm H_2O), ETR is the amount of real evapotranspiration on day i (mm H_2O), w_{seep} is the amount of water entering the vadose zone from the soil profile on day i (mm H_2O), and Q_{gw} is the amount of return flow on day i (mm H_2O). Indeed, six main elements are involved in the simulation of water balance and there are described in the following section based on Neitsch et al. (2011).

i) Surface Runoff

Surface runoff occurs when the rate of water coming on the ground exceeds infiltration rate. The infiltration rate depends on initial soil state. On a dry land, the infiltration rate is higher and it decreases as long as the soil became wet. If the infiltration rate continues to be higher than the water application rate and all the surface depressions have been filled, the surface runoff commences. SWAT provides two methods for computing the surface runoff (Neitsch *et al.*, 2011): the SCN Curve number procedure (SCN, 1972) and the Green & Ampt infiltration method (1911). The SCN Curve Number is an empirical model developed to provide a consistent basis for estimating the amounts of runoff under varying land uses and soil types conditions (Rallison & Miller, 1981).

The SCN Curve Number equation is (SCN, 1972):

$$Q_{surf} = \frac{\left(R_{day} - I_a\right)^2}{\left(R_{day} - I_a + S\right)} \quad \text{Eq. 0-2}$$

Where Q_{surf} is the accumulated runoff or rainfall excess (mm); R_{day} is the amount of precipitation on a given day (mm); I_a (with $I_a = 0.2 * S$) is the initial abstractions which includes surface storage, interception and infiltration prior to runoff (mm); and S is the retention parameter (mm). The retention parameter varies due to change in soil types, land use, management, slope and temporally due to soil water content (Neitsch *et al.*, 2011). The retention parameter is defined as:

$$S = 25.4\left(\frac{1000}{CN} - 10\right) \quad \text{Eq. 0-3}$$

where CN is the curve number for the day. The initial abstractions is commonly approximated as $0.2S$ and Q_{surf} equation will become:

$$Q_{surf} = \frac{\left(R_{day} - 0.2S\right)^2}{\left(R_{day} + 0.8S\right)} \quad \text{Eq. 0-4}$$

It can be deduced from the previous equation that surface runoff occurs when $R_{day} > I_a$. Tables of typical curve numbers for various soil types and land covers that are appropriate for a land slope of 5 % can be obtain from the SCS Engineering Division (1986). In SWAT, the runoff is calculated separately for the individual HRUs and routed to obtain the total runoff for each sub-basin. The sub-basin runoff is then routed to obtain the total runoff for the entire basin.

- Peak runoff

The peak runoff rate is the maximum runoff flow rate that can be reach with a given rainfall event. The peak runoff rate is an indicator of the erosive power of a storm and it is used to predict sediment transport. SWAT computes the peak runoff with a modified form of the rational method. This method is based on the assumption that if a rainfall of intensity I begin at time t=0 and continues indefinitely, the rate of runoff will increase until the time of concentration, t=tconc when the entire basin is contributing entirely to outlet of the basin. The modified rational formula is (Neitsch *et al.*, 2011):

$$q_{peak} = \frac{\alpha_{tc} \cdot Q_{surf} \cdot Area}{3.6 t_{conc}} \quad \text{Eq. 0-5}$$

where: q_{peak} is the peak runoff rate (m^3/s); Q_{surf} is the surface runoff (mm); $Area$ is the sub-basin area (km^2); $tconc$ is the time of concentration for a sub-basin (h); α_{tc} is the fraction of daily rainfall that occurs during the time of concentration; and 3.6 is a unit conversion factor.

The time of concentration $(tconc)$ in $t_{conc} = t_{ov} + t_{ch}$ Eq. 0-6 is a summation of overland flow time and channel flow time. Overland flow time is defined as the time it takes for water to travel from the furthest point in the sub-basin to reach the stream channel, and channel flow time is the time it takes for flow in the upstream channel to reach the outlet (Oboubie, 2008). The overland and channel flow time are calculated using Manning's formula.

$$t_{conc} = t_{ov} + t_{ch} \quad \text{Eq. 0-6}$$

where: t_{conc} is the time of concentration; t_{ov} is the overland flow time; and t_{ch} is the channel flow time. The overland flow time is:

$$t_{ov} = \frac{n^{0.6} \cdot L_{slp}^{0.6}}{18 \cdot slp^{0.3}} \quad \text{Eq. 0-7}$$

where: L_{slp} is the average sub-basin slope length (m); slp is the average sub-basin slope (m/m); and n is the Manning's roughness coefficient.

The channel flow time is:

$$t_{ch} = \frac{0.62 \cdot L \cdot n^{0.75}}{Area^{0.125} \cdot slp_{ch}^{0.375}} \quad \text{Eq. 0-8}$$

where: t_{ch} is the time of concentration for channel flow (hr); L is the channel length from the most distant point to the sub-basin outlet (km); n is the Manning's roughness coefficient for the channel; $Area$ is the sub-basin area (km^2); and slp_{ch} is the channel slope (m m^{-1}).

ii) Surface runoff lag time

In large sub-basins with a time of concentration greater than 1 day, only a portion of the surface runoff will reach the main channel on the day it is generated. SWAT incorporates a surface runoff storage feature to lag a portion of the surface runoff release to the main channel (Neitsch *et al.*, 2011). After computing the surface runoff, the amount released to the main channel is (Neitsch *et al.*, 2011):

$$Q_{surf} = \left(Q'_{surf} + Q_{stor,\ i-1}\right) \cdot \left(1 - exp\left[\frac{-surlag}{t_{conc}}\right]\right) \quad \text{Eq. 0-9}$$

where: Q_{surf} is the amount of surface runoff discharged to the main channel on a given day (mm); Q'_{surf} is the amount of surface runoff generated in the sub-basin on a given day (mm); $Q_{stor,\ i-1}$ is the surface runoff stored or lagged from the previous day (mm); $surlag$ is the surface runoff lag coefficient; and t_{conc} is the time of concentration for the sub-basin (hrs).

It can be deduced Eq. 9-9 that as $surlag$ decreases, more water is held in storage. A delay in the release of surface runoff will smooth the streamflow hydrograph simulated in the channel (Neitsch *et al.*, 2011).

iii) Transmission losses

Many arid and semi-arid zone watersheds have ephemeral channels that abstract large quantities of streamflow and the abstraction or transmission losses reduce runoff volume as floods waves travel downstream (Lane, 1982). Transmission losses are assumed to percolate into the shallow aquifer. SWAT uses the procedure describe by (Lane, 1983) to estimate transmission losses. Reader can referred to Neitsch et al. (2011) for more details.

iv) Evapotranspiration

Evapotranspiration can be understood as the sum of the evaporation and the transpiration of plants from the earth surface to the atmosphere. The evapotranspiration accounts for

the evaporation from plant canopy, transpiration, sublimation and evaporation from the soil. Evapotranspiration is the main mechanism by which water is removed from the basin and roughly, 62% of the precipitation that fall on the continent is evapo-transpirated (Neitsch *et al.*, 2011). In SWAT, evaporation from soils is computed separately from transpiration from plants (Neitsch *et al.*, 2011). The difference between evapotranspiration and rainfall is the water available for human use and management. For that raison, an accurate estimation of ET is critical for water resources management. There are two way of characterizing the evapotranspiration: the potential evapotranspiration and the actual or real evapotranspiration.

Potential evapotranspiration (PET) is defined as the rate at which evapotranspiration would occur from a large area completely and uniformly covered with growing vegetation, which has access to an unlimited supply of soil water and that was not exposed to advection or heat storage effects (Neitsch *et al.*, 2011). Three methods for estimating PET are implemented in SWAT model (Neitsch *et al.*, 2011). The Penman-Monteith method (Allen, 1986, J. L. Monteith, 1965) requires solar radiation, air temperature, relative humidity and wind speed, the Priestly-Taylor method (Priestley & Taylor, 1972) requires solar radiation, air temperature and relative humidity and the Hargreaves method (Hargreaves, 1975) requires only air temperature as input data. The Penman-Monteith method was chosen for estimating the PET in the study area.

The real or actual evapotranspiration (ETR) is the amount of water that is actually removed from a surface through the processes of evaporation and transpiration. The ETR is equal to the PET when there is no limitation in term of water availability. After computing the evapotranspiration, SWAT first evaporates any rainfall intercepted by plant canopies and then calculates the maximum amount of transpiration and sublimation or soil evaporation using an approach similar to that of Ritchie (1972). In SWAT, ETR is usually computed based on the PET. Soil water evaporation is estimated as an exponential function of soil depth and water content based on PET and a soil cover index based on the aboveground biomass. Transpiration is simulated as a linear function of the leaf area index, root depth, soil water content, and PET (X. Wang *et al.*, 2006).

v) Soil water

When water enters the soil, it can be removed through the process of evapotranspiration or percolate through the bottom of the soil profile and ultimately becomes groundwater recharge, or may move laterally in the soil profile and contribute to streamflow (Neitsch *et al.*, 2011).

The percolation is computed for each soil layer. Water is allowed to percolate if the water content of the soil layer exceeds field capacity and the soil layer below is not saturated. The amount of water that is allowed to percolate from one layer to another is calculated using the storage routing layer which equation is as follow (Neitsch *et al.*, 2011):

$$W_{perc,ly} = SW_{ly,excess} \cdot \left(1 - exp\left[\frac{-\Delta t}{TT_{perc}}\right]\right) \quad \text{Eq. 0-10}$$

Where: $W_{perc,ly}$ is the amount of water percolating to the underlying soil layer on a given day (mm of water); $SW_{ly,excess}$ is the drainable volume of water in the soil layer on a given day (mm of water); Δt is the length of the time step (hrs); and TT_{perc} is the travel time for percolation (hrs). If the HRU has a seasonal high water table, percolation is not allowed if $SW_{ly+1} \leq FC_{ly+1} + 0.5 \cdot (SAT_{ly+1} - FC_{ly+1})$ where: SW_{ly+1} is the water content of the underlying soil layer (mm); FC_{ly+1} is the water content of the underlying soil layer at field capacity (mm); and SAT_{ly+1} is the amount of water in the underlying soil layer when completely saturated (mm). The water will instead stay ponded in the upper layer. The travel time for percolation is unique for each layer (Neitsch *et al.*, 2011):

$$TT_{perc} = \frac{SAT_{ly} - FC_{ly}}{K_{sat}} \quad \text{Eq. 0-11}$$

Where K_{sat} is the saturated hydraulic conductivity (mm/h) and the other variables are defined above. The water that percolates out of the lowest soil layer enters into the vadose zone. The vadose zone is the unsaturated zone located between the lowest soil layer and the top of the aquifer.

Lateral water flow is the lateral movement of water in the soil profile. When rainfall is received in an area that has soils with high hydraulic conductivities in the surface layers and an impermeable or semi-permeable layer at a shallow depth, the water percolates vertically until it reaches the impermeable layer and cannot percolate any further. The water then pond above the impermeable layer forming a saturated zone of water that leads to lateral subsurface flow (Neitsch *et al.*, 2011). SWAT uses the kinematic storage model for computing subsurface flow in a two-dimensional cross-section along a flow path down a steep hillslope. This model is based on the mass water balance or continuity equation. A soil layer can be considered saturated whenever the water content of the layer exceeds the field capacity water content. The lateral flow is computed using the formula (Neitsch *et al.*, 2011):

$$Q_{lat} = 0.024 \cdot \left(\frac{2 \cdot SW_{ly,excess} \cdot K_{sat} \cdot slp}{\emptyset_d \cdot L_{hill}}\right) \quad \text{Eq. 0-12}$$

where: Q_{lat} is lateral flow (mm/d); $SW_{ly,excess}$ is the drainable volume of soil water (mm); K_{sat} is the saturated hydraulic conductivity (mm/h); slp is slope (m/m); $\emptyset_d$ is the drainable porosity (mm/mm); and L_{hill} is the hillslope length (m).

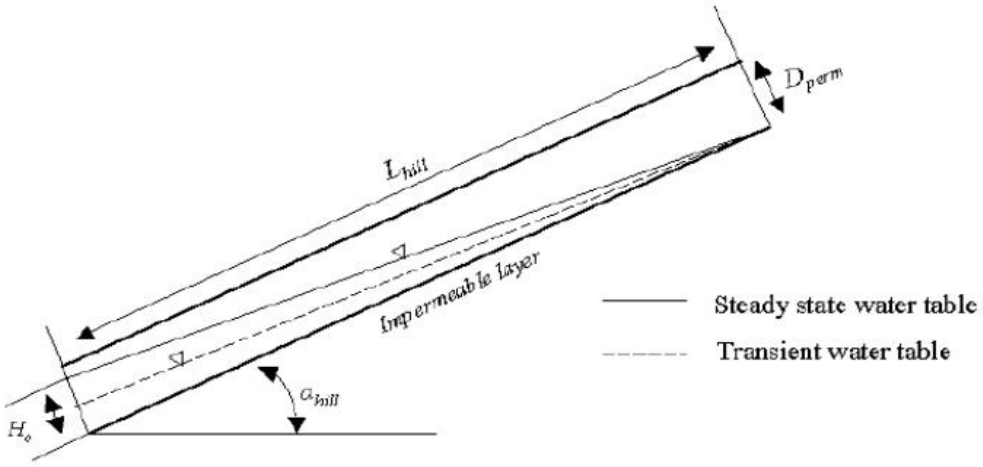

Figure 0-1: Behavior of the water table as assumed in the kinematic storage model.

In large sub-basins with a time of concentration greater than 1 day, only a portion of the lateral flow will reach the main channel on the day it is generated. A lateral flow storage feature has been built into the SWAT model to lag a portion of lateral flow released to the main channel. The amount of lateral flow released to the main channel is calculated as (Neitsch *et al.*, 2011):

$$Q_{lat} = \left(Q'_{lat} + Q_{latstor,i-1}\right) \cdot \left(1 - exp\left[\frac{-1}{TT_{lag}}\right]\right) \quad \text{Eq. 0-13}$$

where: Q_{lat} is the amount of lateral flow discharged to the main channel on a given day(mm); Q'_{lat} is the amount of lateral flow generated in the sub-basin on a given day (mm); $Q_{latstor,i-1}$ is the lateral flow stored or lagged from the previous day (mm); and TT_{lag} is the lateral flow travel time (days).

SWAT can calculate the lateral flow travel time or use a user-defined value. Nevertheless, Neitsch et al. (2011) receommended the users to allow SWAT to calculate this parameter. It uses this formula (Neitsch *et al.*, 2011):

$$TT_{lag} = \frac{tile_{lag}}{24} \quad \text{Eq. 0-14}$$

where: TT_{lag} is the lateral flow travel time (days); and $tile_{lag}$ is the drain tile lag time (hr). In HRUs without drainage tiles, lateral flow travel time is calculated as:

$$TT_{lag} = 10.4 \cdot \frac{L_{hill}}{K_{sat,mx}} \quad \text{Eq. 0-15}$$

where: TT_{lag} is the lateral flow travel time (days); L_{hill} is the hillslope length (m), and $K_{sat,mx}$ is the highest layer saturated hydraulic conductivity in the soil profile (mmhr-1).

vi) Groundwater

Groundwater is the water in the saturated zone. Water enters the groundwater storage primarily by infiltration/percolation, although recharge from surface water body by seepage may occur. Water leaves the groundwater storage primarily by discharge into rivers and lakes. Two types of groundwater aquifers are simulated in each sub-basin in the SWAT model. They are the shallow unconfined aquifer that contributes to flow in the main channel or reach of the sub-basin and the deep confined aquifer that is assumed to contribute to streamflow outside of the basin (Arnold *et al.*, 1993). SWAT simulates the shallow aquifer contribution to the main stream channel or to the reach within the sub-basin.

The water balance of the shallow aquifer as simulated in SWAT is (Neitsch *et al.*, 2011):

$$aq_{sh,i} = aq_{sh,i-1} + w_{rchrg,sh} - Q_{gw} - w_{revap} - w_{pump,sh} \qquad \text{Eq. 0-16}$$

where: $aq_{sh,i}$ is the amount of water stored in the shallow aquifer on day i (mm); $aq_{sh,i-1}$ is the amount of water stored in the shallow aquifer on day i-1 (mm); $w_{rchrg,sh}$ is the amount of recharge entering the shallow aquifer on day i (mm); Q_{gw} is the groundwater flow or baseflow into the main channel on day i (mm); w_{revap} is the amount of water moving into the soil zone in response to water deficiencies on day i (mm); and $w_{pump,sh}$ is the amount of water removed from the shallow aquifer by pumping on day i (mm).

Baseflow is allowed to enter the channel only if the amount of water stored in the shallow aquifer exceeds a threshold value specified by the user. The groundwater flow discharge into the main channel is computed using (Neitsch *et al.*, 2011):

$$Q_{gw,i} = Q_{gw,i-1} \cdot exp\left[-\alpha_{gw} \cdot \Delta t\right] + w_{rchrg,sh} \cdot \left(1 - exp\left[-\alpha_{gw} \cdot \Delta t\right]\right); \quad \text{if } aq_{sh} > aq_{shthr,q} \qquad \text{Eq. 0-17}$$

$$Q_{gw,i} = 0 \quad \text{if } aq_{sh} < aq_{shthr,q}$$

where: $Q_{gw,i}$ is the groundwater or baseflow into the main channel on day i (mm); $Q_{gw,i-1}$ is the groundwater flow into the main channel on day i-1 (mm); α_{gw} is the baseflow recession constant; Δt is the time step (1 day), $w_{rchrg,sh}$ is the amount of recharge entering the shallow aquifer on day i (mm); aq_{sh} is the amount of water stored in the shallow aquifer at the beginning of day i (mm) and $aq_{shthr,q}$ is the threshold water level in the shallow aquifer for groundwater contribution to the main channel to occur (mm).

For the computation of the other component of the shallow aquifer water balance, the reader can referred to (Neitsch *et al.*, 2011).

vii) Flow routing

SWAT uses a command structure similar to that of HYMO (Williams & Hann, 1973) to route the loadings of water, sediment, nutrients and pesticides to the main channel. The user is offered two options for routing streamflow: the variable storage routing method developed by Williams (1969) and the Muskingum River routing method.

b) WaSiM

WaSiM (Schulla, 2014) is a distributed, deterministic, mainly physically based hydrologic model. It can be run from events based to time continuous simulation. The model can be used in various spatial and temporal scales. It is able to model hydrologic processes for basins with sizes of <1 km² up to more than 100,000 km². Detailed simulations for locations are also possible (e.g. habitats). The temporal resolution of the model ranges from minutes to several days. WaSiM can be used for both short-term (floods) and long-term simulations (long-term water balance simulations). WaSiM is available in two basic versions: the conceptual model TOPMODEL and the process-oriented Richards approach based on Richards equation. In this work, the Richards version of WaSiM is used. **Figure 0-2** shows the link between the different model components used for this study and the routine that allows for computing the total runoff and other outputs. In the following section the most important components of the hydrological model WaSiM and the required adaptations for this study are described, following Schulla (2014).

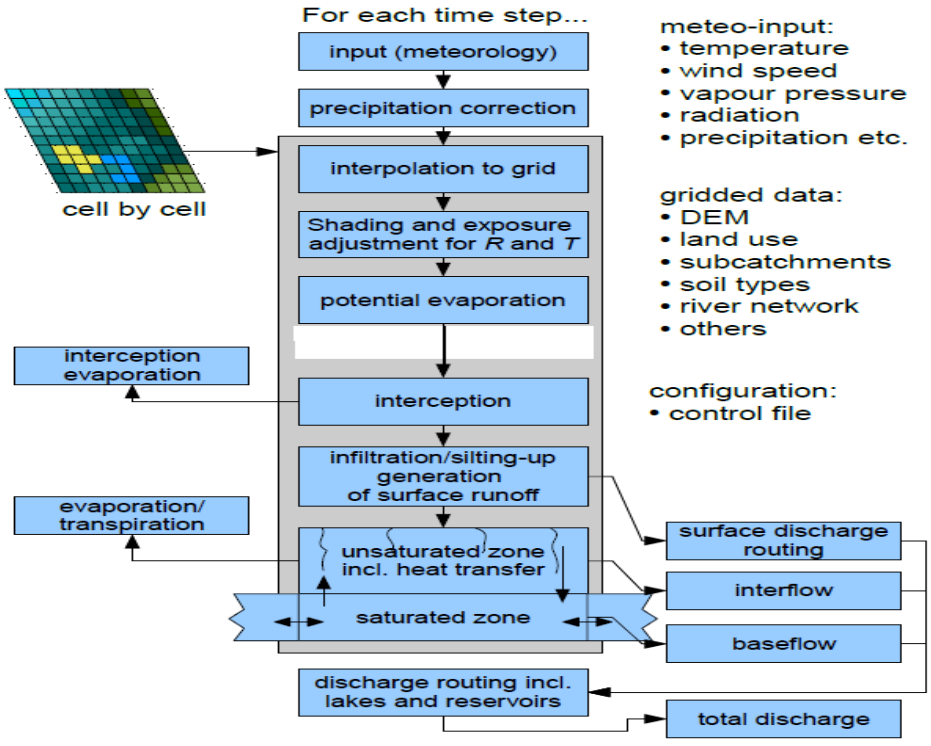

Figure 0-2: WaSiM model structure with the module used in this study (modified from Schulla, 2014)

i) Preprocessing

One of main tools for preprocessing is the Topographic analyzer Tanalys. It performs a complex analysis of the DEM (see figure below) to different set of information that are used during the model running such as flow directions, flow accumulations (specific catchment area), the river network and the subbasin structure etc. Only the shaded data sets are really needed by WaSiM.

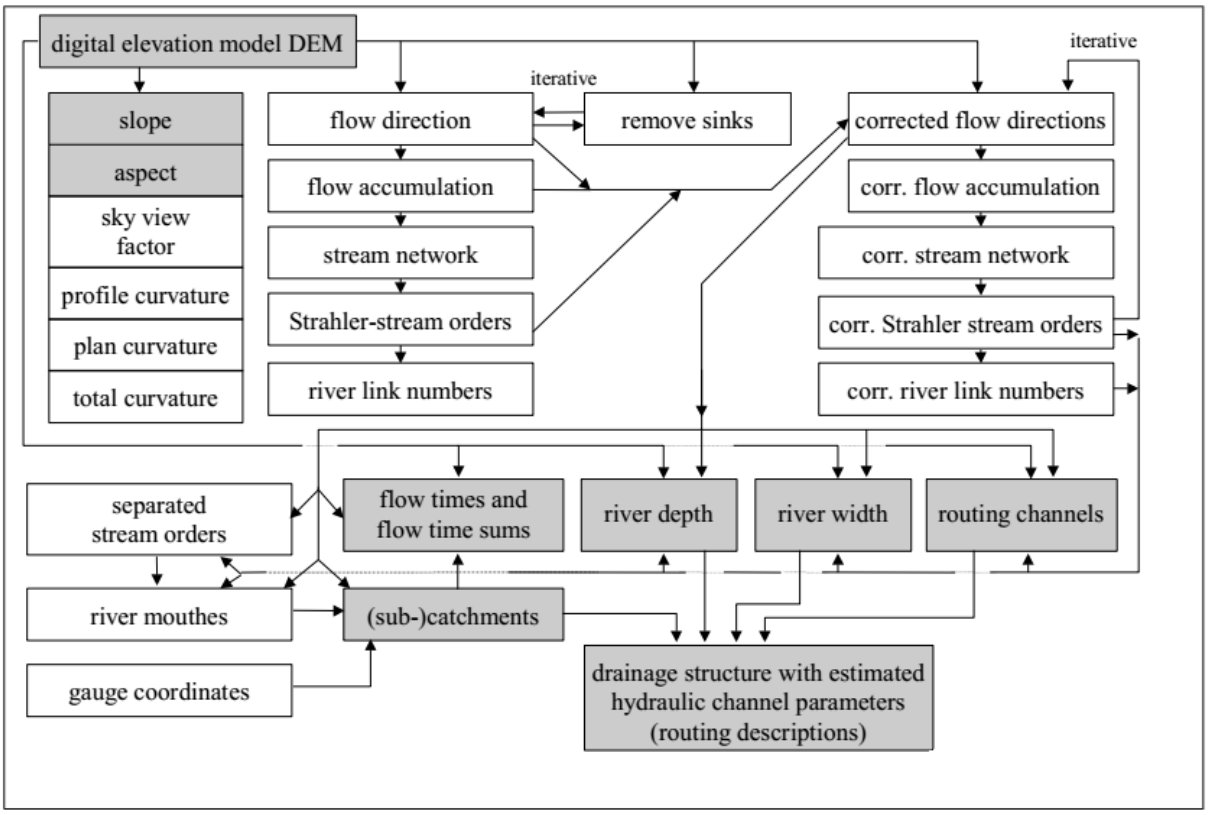

Figure 0-3: Topographic analysis of a digital elevation model by TANALYS (Schulla, 2013)

ii) Interpolation of meteorological input data

Various methods for interpolating meteorological data (from sparse spatial resolution to model grid) are available in WaSiM model. The interpolation can be done by using one or more methods or a linear combination of different methods with a weight given to each method. The available methods are:

1. Inverse Distance Interpolation (IDW). Use: for precipitation, sunshine duration and other data which are not (strongly) dependent on elevation or when modelling flat regions without substantial elevation ranges
2. Elevation Dependent Regression with External Pre-processing (EDREXT). Use: for all elevation dependent types of input data like temperatures, vapor pressure, air

humidity, wind speed. Recommended for basins with a substantial elevation range only

3. A linear combination of IDW + EDREXT. Use: for data that depend only partly on elevation, e.g. precipitation in high mountain areas.
4. Thiessen Polygons. Use: if only one station is available (same results as IDW or EDR but faster)
5. Bi-linear Interpolation (BLI). Use: when using gridded time series from RCM or GCM output (WaSiM-tables containing time series for each grid cell of the GCM run)
6. Bi-linear Interpolation of both gradients and residuals and a linear combination thereof (BIGRES). Use: same as BLI but for data which are separately available as residues and gradients
7. Bi-cubic Spline Interpolation (BSI). Use: same as BLI but with another (smoother) technique
8. Bi-cubic Splice Interpolation of both gradients and residuals and a linear combination thereof (BSIRES). Use: same as BIGRES, but somewhat smoother
9. A pseudo-method: Reading externally interpolated data from grids; Use: when gridded input is already available (in the model raster dimensions!) from external interpolation routines
10. Elevation dependent regression with internal processing (EDRINT); like EDR but without external preprocessing using regr or regress. Use: same as method 2. The main difference between methods 2 and 10 is, that for method 2 the stations to be used can be selected manually in the ini file for the regress tool wheres for method 10 all stations in the input file will be used. Also, the internal preprocessing does not allow the mixing of input files with different temporally resolution as it is possible in regr and regress. To achieve identical results, the input file used for method 10 should only contain the stations which were used in the regress-ini-file, too.
11. A linear combination of IDW and EDRINT, like IDW+EDREXT but without external preprocessing using regr or regress. Use: same as for method 3; read comments on method 10 here above.
12. A combination of nearest neighbor (Thiessen) and a constant lapse rate

iii) Potential evapotranspiration

In WaSiM, 4 methods are available for PET computation: Penman-Monteith (Brutsaert, 1982, J. Monteith, 1975), Hamon (only daily, in (Brook & Lash, 1983)), Wendling (only daily, (Wendling, 1975)) and Haude (Haude, 1955). In this study, the Penman-Monteith method was used as recommended by Schulla (2014).

The potential transpiration from plant leaves, the evaporation from bare soil and the evaporation from interception surfaces (usually leaves, too) are calculated separately in WaSiM. The potential transpiration after Penman-Monteith is given by:

$$\lambda E = \frac{3.6 \cdot \frac{\Delta}{\gamma_p} \cdot (RN - G) + \frac{\rho \cdot C_p}{\gamma \cdot r_a}(e_s - e) \cdot t_i}{\frac{\Delta}{\gamma_p} + 1 + r_s / r_a} \qquad \text{Eq. 0-18}$$

with λ latent vaporization heat; $\lambda = (2500.8 - 2.372 \cdot \mathrm{T}) KJ \cdot Kg^{-1}$, T: temperature in °C; E latent heat flux in $mm \cdot m^{-2} \equiv kg \cdot m^{-2}$ ($\rightarrow [\lambda E] = KJ \cdot m^{-2}$); Δ tangent of the saturated vapor pressure curve $[hPa \cdot K^{-1}]$; RN net radiation, conversion from $Wh \cdot m^{-2}$ *to* $KJ \cdot m^{-2}$ by a factor 3.6 $[Wh \cdot m^{-2}]$; G soil heat flux (here: $0.1 \cdot RN$) $[Wh \cdot m^{-2}]$; ρ density of dry air $= p/(RL \cdot T)$ (at 0 °C and 1013,25 hPa: ρ = 1.29 $[Kg \cdot m^{-3}]$; C_p specific heat capacity of dry air at constant pressure $C_p = 1.005$ [KJ $\cdot$ (Kg $\cdot$ K)$^{-1}$]; e_s saturation vapor pressure at the temperature T [hPa]; e actual vapor pressure (observed) [hPa]; t_i number of seconds within a time step; γ_p psychrometric constant [hPa·K^{-1}]; r_s bulk-surface resistance [s·m^{-1}]; r_a bulk-aerodynamic resistance [s·m^{-1}].

Equation (9-18) has units of energy flux, i.e. the flux of latent heat in $KJ \cdot m^{-2}$. The denominator has no units. Both terms of the nominator are given in units of $KJ \cdot m^{-2}$ ($1\, Wh \cdot m^{-2} = 3.6\, KJ \cdot m^{-2}$). By dividing λE by the latent heat λ $[KJ \cdot Kg^{-1}]$, the unit changes into m^{-2} , which is the height of water in mm. The model uses for each land use type monthly values for a minimum bulk-surface resistance. To get the real evapotranspiration ETR, the potential evapotranspiration is then reduced according to the actual soil moisture. Reader interested in knowing more about the others methods for PET estimation can refer to the references above.

iv) Soil module

WaSiM versions with physically based soil model use the RICHARDS-equation for modeling the fluxes within the unsaturated soil zone. The modeling is done one-dimensional in the vertical direction using a soil with several numeric layers. The continuity equation for this type of problem is given by:

$$\frac{\partial \Theta}{\partial t} = \frac{\partial \mathrm{q}}{\partial z} = \frac{\partial}{\partial z}\left(-k(\Theta)\frac{\partial \Psi(\Theta)}{\partial z}\right) \qquad \text{Eq. 0-19}$$

with Θ water content [m³/m³]; t time [s]; k hydraulic conductivity [m/s]; Ψ hydraulic head as sum of the suction ψ and geodetic altitude h [m]; q specific flux [m/s]; z vertical coordinate [m].

The discretized form of RICHARDS-equation is given by:

$$\frac{\Delta \Theta}{\Delta \mathrm{t}} = \frac{\Delta \mathrm{q}}{\Delta \mathrm{z}} = q_{in} - q_{out} \qquad \text{Eq. 0-20}$$

with q_{in} and q_{out} repectively inflow into the actual soil layer [m/s] and outflow from the actual soil layer (including interflow and artificial drainage) [m/s].

The dependencies of the hydraulic properties on the water content of the soil are considered in a discrete manner. The flux q between two layers with indices u (upper) and l (lower) is then given by:

$$q = k_{eff} \cdot \frac{h_h(\Theta_u) - h_h(\Theta_l)}{0.5 \cdot (d_u - d_l)} \quad with \quad \frac{1}{k_{eff}} = \frac{d_u}{d_u + d_l} \cdot \frac{1}{k(\Theta_u)} + \frac{d_l}{d_u + d_l} \cdot \frac{1}{k(\Theta_l)} \qquad \text{Eq. 0-21}$$

with q flux between two discrete layers [m/s]; k_{eff} effective hydraulic conductivity [m/s] h_h hydraulic head, dependent on the water content and given as sum of suction $\Psi(\Theta)$ after equation (9.19) and geodetic altitude h_{geo} [m]; d thickness of the layers under consideration [m].

For solving equation (9.19) a one dimensional vertical finite difference (FD) scheme is applied. After transforming equation (9.20) into its discrete form as given by equation (9.21) the fluxes between the discrete soil layers are calculated followed by the calculation of interflow, drainage, and exfiltration into or infiltration from rivers.

v) Groundwater recharge and baseflow calculation

The groundwater recharge is the balance of inflows and outflows to that layer which contains the groundwater level. Recharge can be positive or negative. If the groundwater tables moves to another layer, the balances are calculated including the fluxes of all affected layers. The drained or filled porosity is balanced with the lateral net flux change from the groundwater model (the rate of rise or fall of groundwater in terms of mm/time step).

Base flow is generated in WaSiM as exfiltration from the groundwater into the surface river system. It is generated only at that grid cells which are marked in a number of grids as river cells. The output is written not only as a grid but also as an areal average value for subbasins. For this output files the exfiltration into rivers is not balanced with the infiltration from rivers into the groundwater. This is done during the discharge routing.

However, if the model is run without the groundwater module (which is the case in this study), calculation of base flow must be done in a conceptual way, because no lateral exchange between cells is possible. For such cases an approach similar to the TOPMODEL-Approach is used:

$$Q_B = Q_0 \cdot K_s \cdot exp\left[\left(h_{GW} - h_{geo,0}\right)/k_B\right] \qquad \text{Eq. 0-22}$$

with Q_B, base flow [m/s]; Q_0 scaling factor for base flow (or maximum baseflow if the soil is saturated) [-]; K_s saturated hydraulic conductivity [m/s]; h_{GW} groundwater table [m a.s.l.]; $h_{geo,0}$ geodetic altitude of the soil surface (upper limit 1st layer) [m a.s.l.]; k_B recession constant for base flow [m].

vi) Discharge routing

WaSiM does the routing based on a hydraulic calculation of the of the flow velocities. Some channel characteristics are needed for describing the geometry. The approach neglects effects of inertia and diffusion. It is a cinematic wave approach using different flow velocities for different water levels in the channel. After the translation of the wave a single linear storage is applied to the routed discharge in order to consider the effects of diffusion and retardation. The approach can be seen as a three step process: In the first step the translation is done for all channels, in the second step the storage approach is applied and in the third step the discharges from different subbasins are superposed.

Appendix B : Determination of appropriate threshold (for chapter 4) and models parameters used (for Chapter 5)

This appendix provides information on the determination of appropriate threshold for the peak over threshold and Generalized Pareto distribution application in one hand and the modelled variograms for spatial interpolation of change for the analysis performed in chapter 4. About the threshold selection, the method applied looked for stability in the estimated parameters as recommended by Coles (2002). The encircled parts on figure B1 to B10 show the threshold ranges where the stability in the estimated parameters were approximatively reached taking into account the uncertainty in the estimation. The threshold of 50mm was chosen. As far as the spatial interpolation is concerned, the kriging method was used and the figure B11 shows the models and its parameters for the experimental variograms.

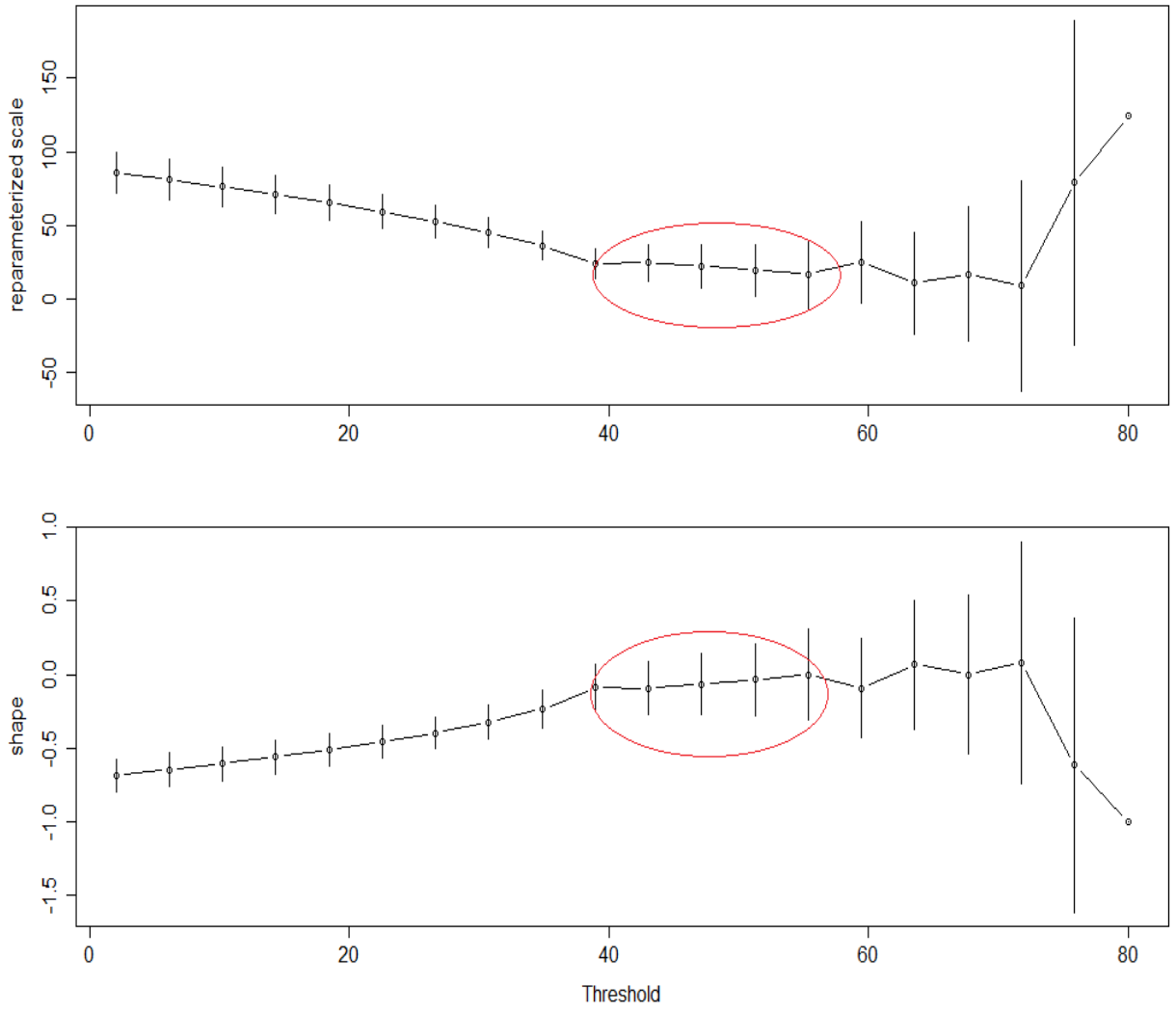

Figure B1. Parameter estimates against threshold for daily rainfall data at Agouna station.

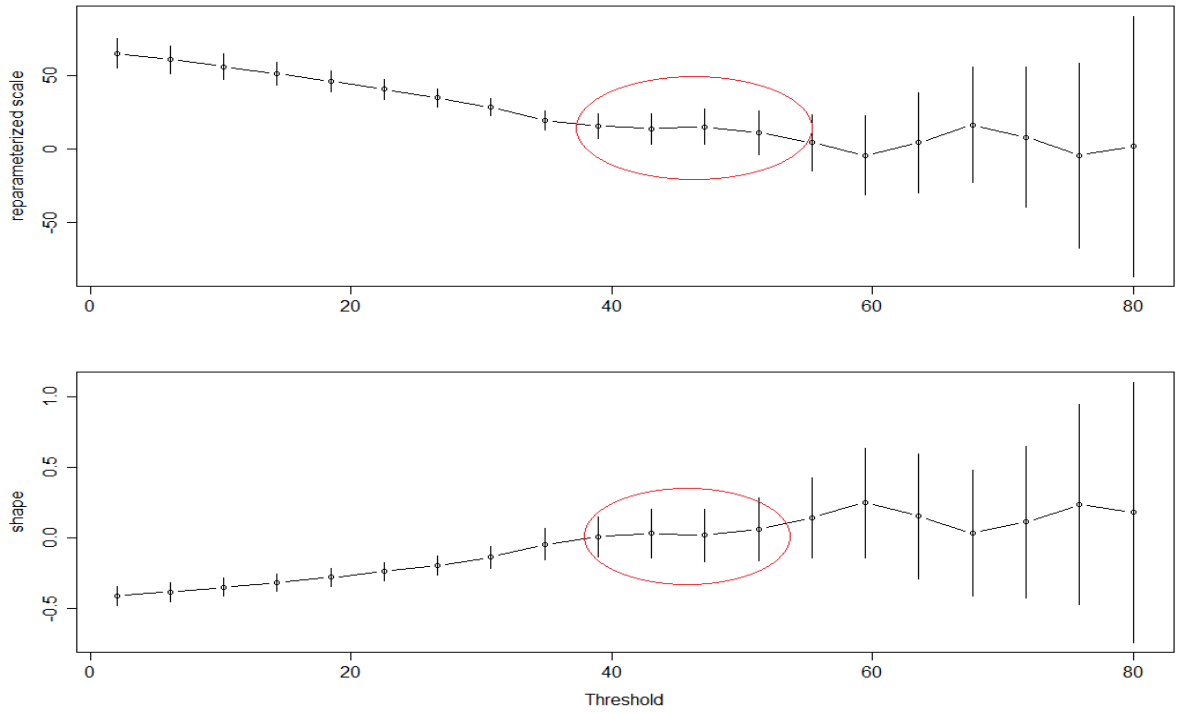

Figure B2. Parameter estimates against threshold for daily rainfall data at Bonou station (first sub-samples).

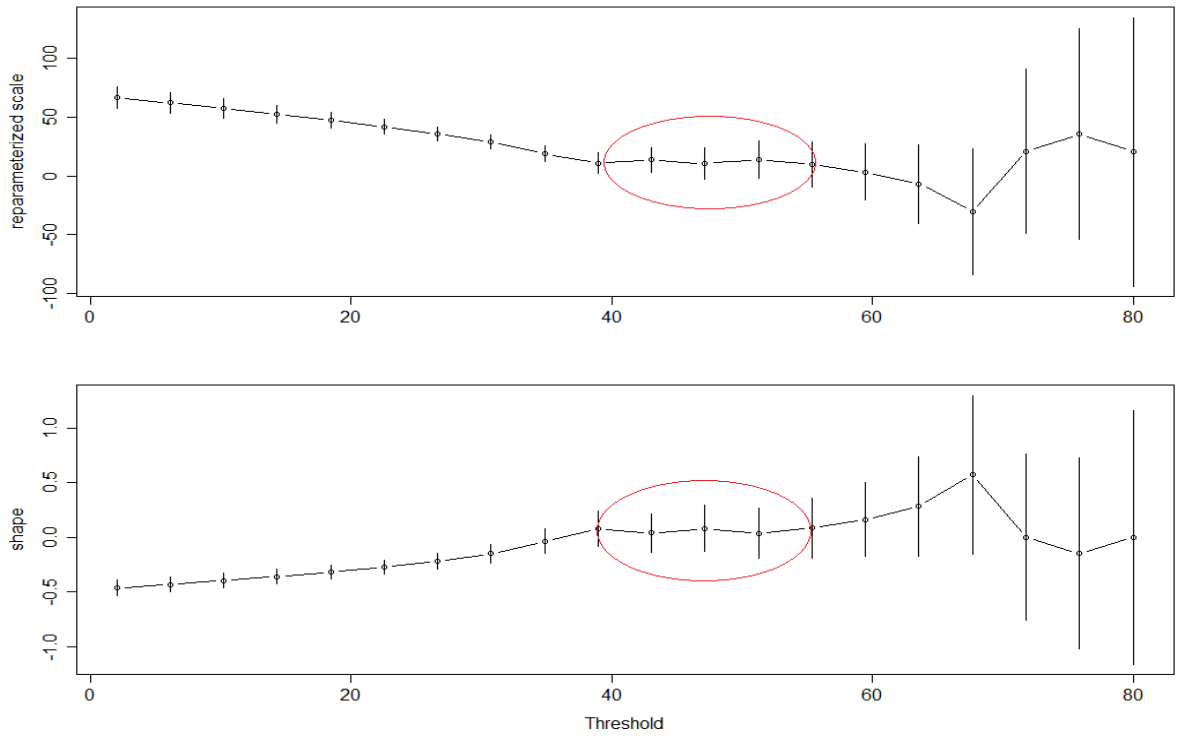

Figure B3. Parameter estimates against threshold for daily rainfall data at Bonou station (second sub-samples)

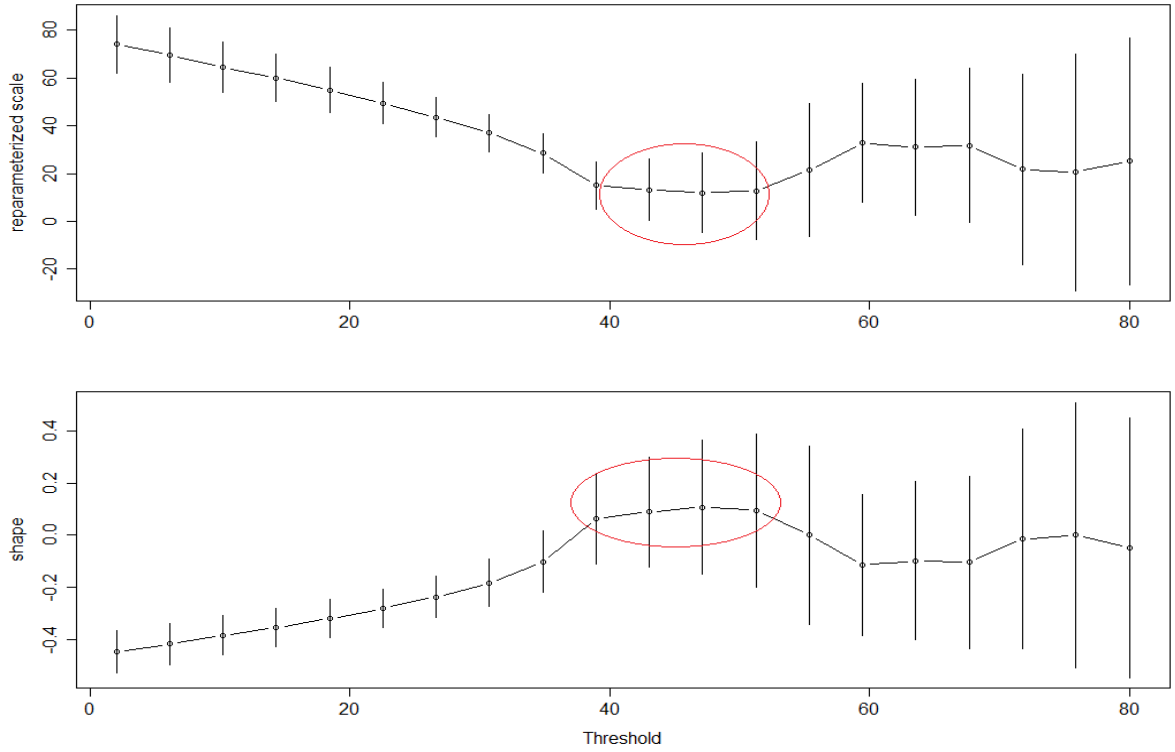

Figure B4. Parameter estimates against threshold for daily rainfall data at Kalalé station.

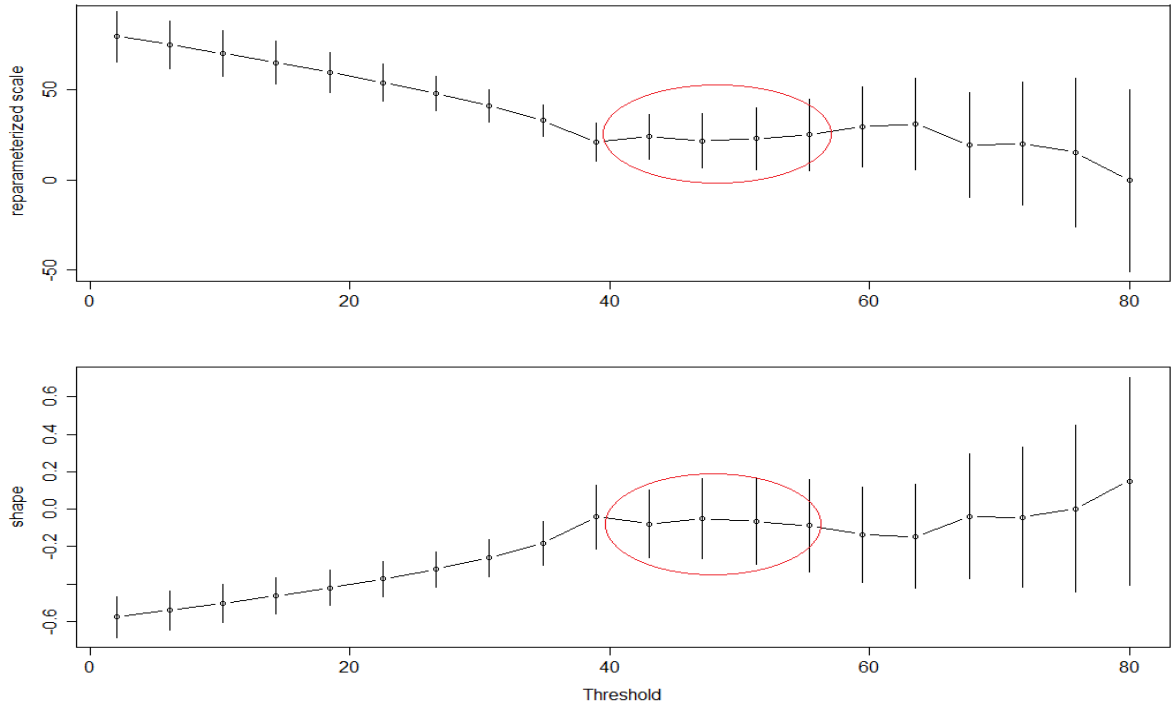

Figure B5. Parameter estimates against threshold for daily rainfall data at Kokoro station (first sub-samples).

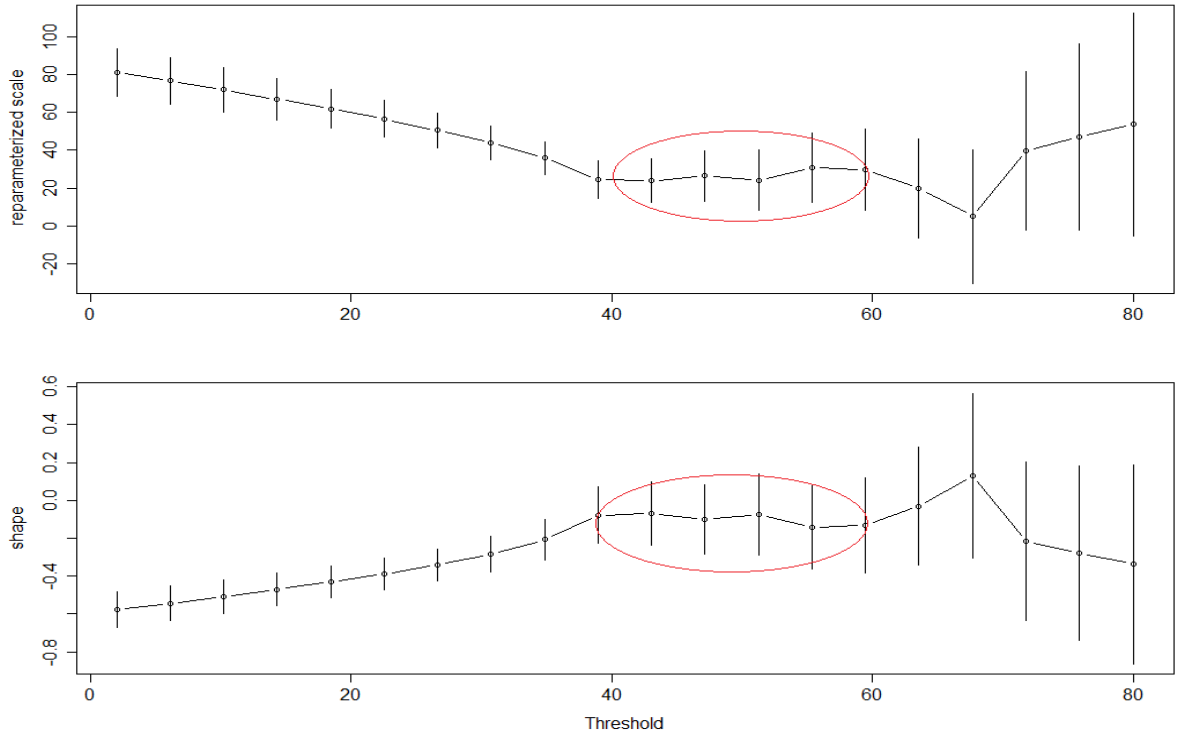

Figure B6. Parameter estimates against threshold for daily rainfall data at Kokoro station (second sub-samples).

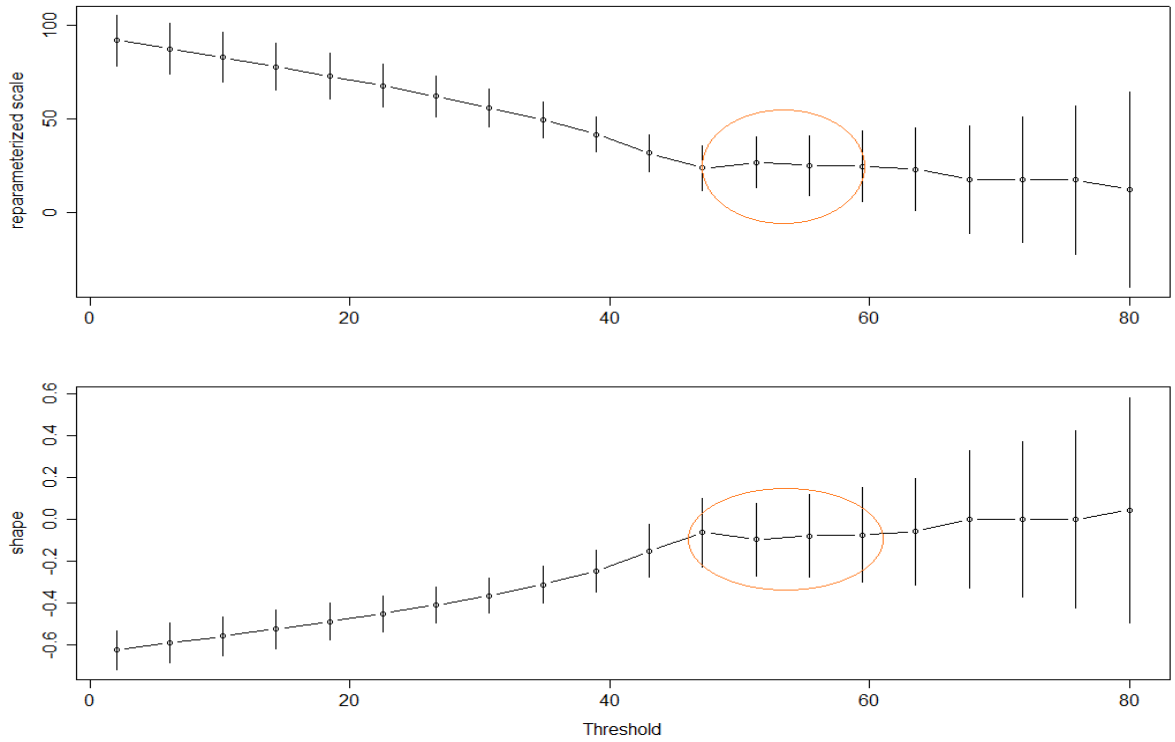

Figure B7. Parameter estimates against threshold for daily rainfall data at Lonkly station.

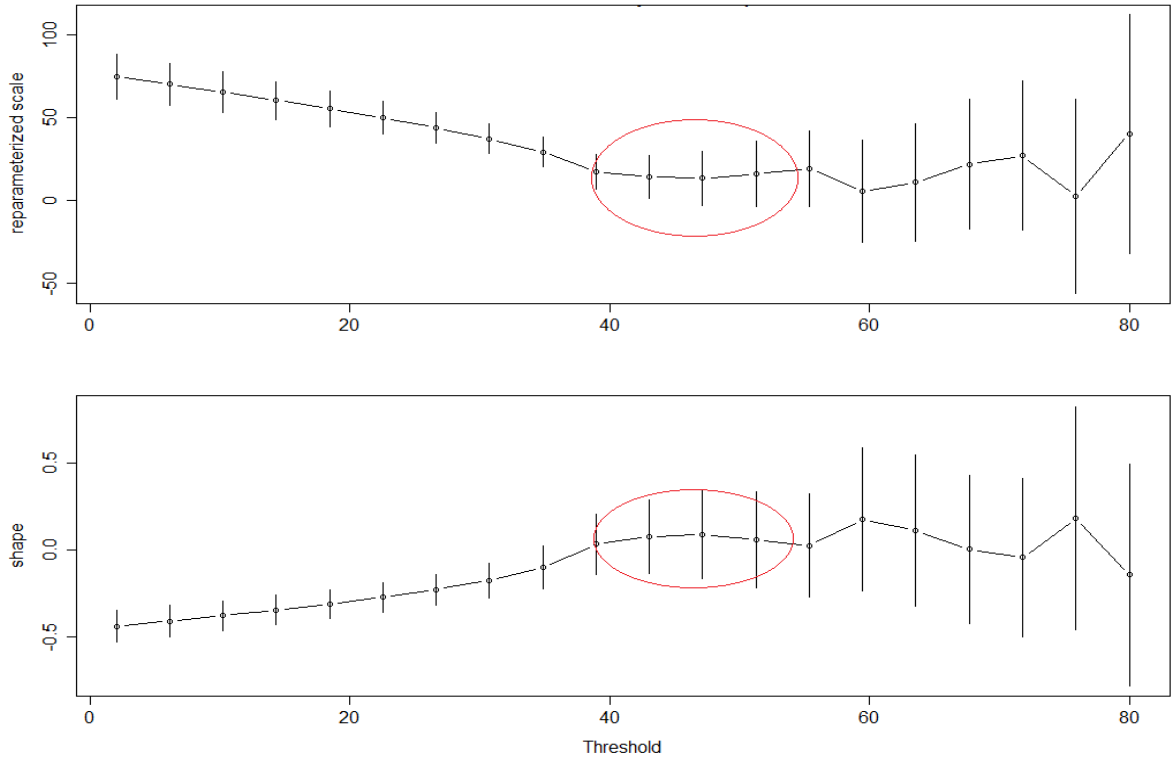

Figure B8. Parameter estimates against threshold for daily rainfall data at Patargo station.

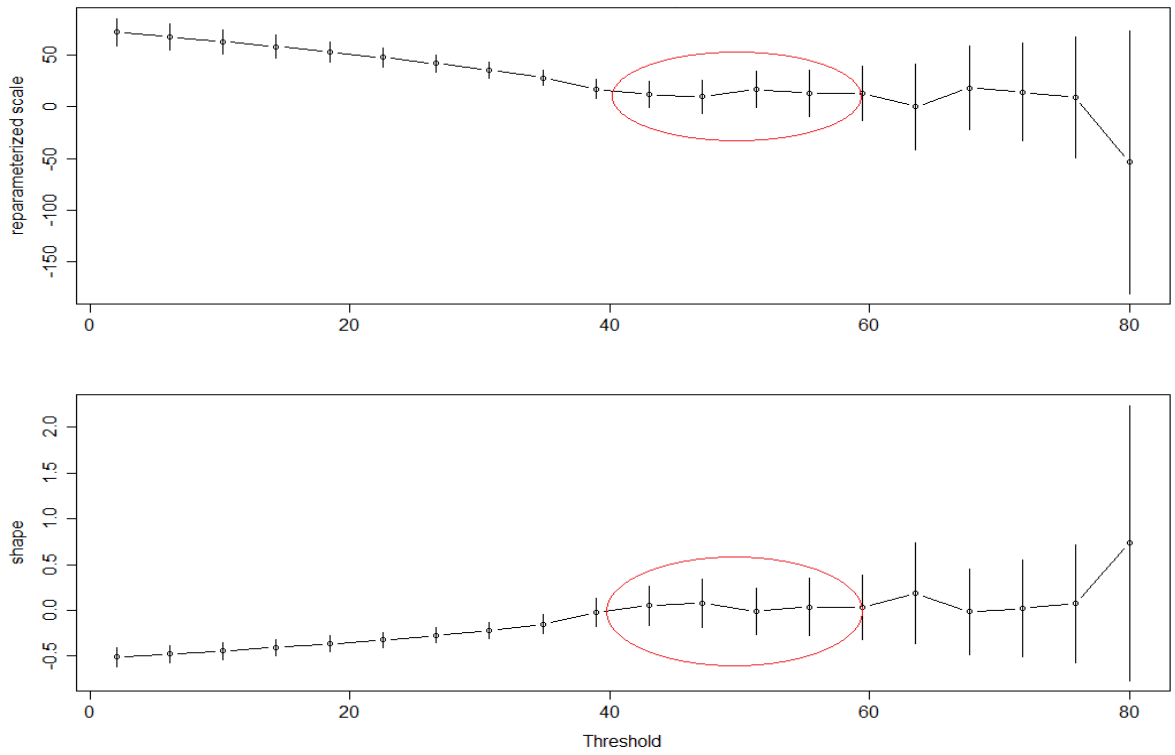

Figure B9. Parameter estimates against threshold for daily rainfall data at Pénéssoulou station.

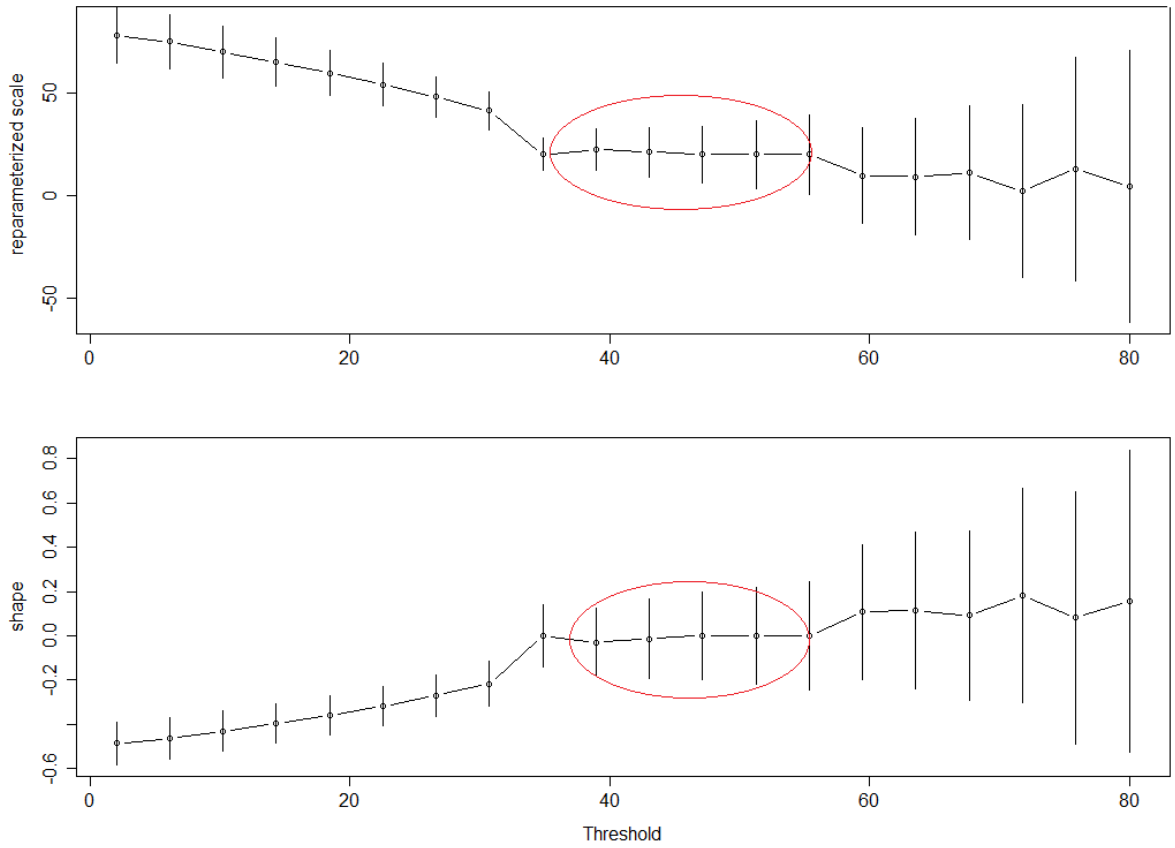

Figure B10. Parameter estimates against threshold for daily rainfall data at Pira station.

Table 0-1: Parameters of WaSiM model used in this study and their ranges

WaSiM Model					
Parameters	Meaning of the Parameters	Initial Ranges		Final Ranges	
DD	Drainage density	1	500	139.33	249.32
KI	Interflow coefficient	1	500	35.46	89.20
Dr	Direct runoff storage coefficient	1	500	29.28	68.99
KK	Baseflow coefficient in the equation qb = Q_{01} * exp(-KK/z) (m)	0.05	2	0.60	1.18
Q_{01}	Baseflow coefficient in the equation qb = Q_{01} * exp(-KK/z) (mm d^{-1})	0.05	2	0.57	1.49
Ksat	Saturated hydraulic conductivity[1] (m s^{-1})	10E-09	10E-2	10E-07	8.96E-02
Krec	Recession constant with soil depth[2] (m s^{-1})	0	2	6.44E-04	1.99
RSC	Soil surface resistance[2] (s m^{-1})	1	200	40.80	99.84
RSE	Leaf surface resistance[2] (s m^{-1})	1	200	80.48	99.78

(1): for each soil type and soil layer; (2): for each land use type

Table 0-2: Parameters of SWAT model used during this study and their ranges

SWAT model						
Parameters	Type[1]	Meaning of the Parameters	Initial Ranges		Final Ranges	
SOL_AWC().sol	R	Available water capacity of the soil layer	-1	+1	0.375	0.441
SURLAG.bsn	V	Surface Runoff Lag time	0.05	24	0.166	0.191
CH_K2.rte	V	Effective hydraulic conductivity in main channel alluvium	0	1.5	0.830	0.960
ESCO.bsn	V	Soil evaporation compensation factor	0	1	0.023	0.027
ESCO.hru	V	Soil evaporation compensation factor	0	1	0.012	0.014
CN2.mgt	A	SCS runoff curve number for moisture condition II	-10	+10	-7.762	-6.545
RCHRG_DP.gw	V	Deep aquifer percolation fraction	0	1	0.057	0.069
ALPHA_BF.gw	V	Baseflow alpha factor (days)	0	1	0.265	0.296
GWQMN.gw	V	Treshold depth of water in the shallow aquifer required for return flow to occur (mm)	0	200	86.084	106.762
GW_SPYLD.gw	V	Specific yield of the shallow aquifer (m^3/m^3)	0	4	0.004	0.005
OV_N.hru	V	Manning's "n" value for overland flow	0.01	30	0.236	0.281
EPCO.hru	V	Plant uptake compensation factor	0	1	0.912	0.987
GW_DELAY.gw	V	Groundwater delay (days)	0	100	31.330	35.499
REVAPMN.gw	V	Threshold depth of water in the shallow aquifer for "revap" to occur (mm)	0	50	0.017	0.020
GW_REVAP.gw	V	Groundwater "revap" coefficient	0	0.2	0.195	0.198
SOL_K().sol	R	Saturated hydraulic conductivity	-1	+1	-0.869	-0.806
SOL_BD().sol	R	Moist bulk density	-1	+1	0.175	0.209

(1)-**V** means the existing parameter value is to be replaced by the given value, **A** means the given value is added to the existing parameter value, and **R** means the existing parameter value is multiplied by (1+ a given value).

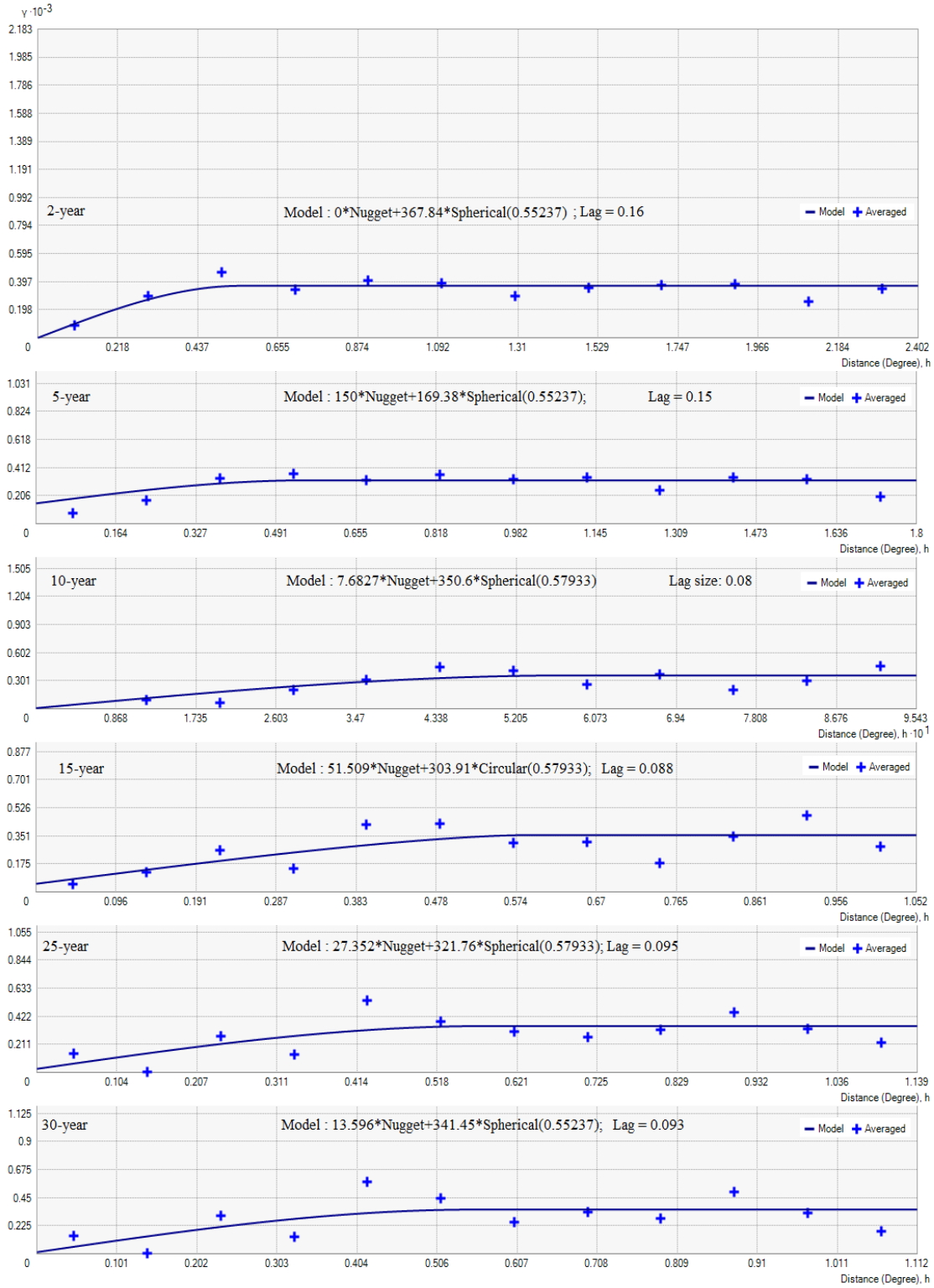

Figure B11. Modelled variograms corresponding to the percentage changes in heavy rainfall of different return periods.

- **Brief explanation of the hydrology between Atchérigbé and Domè in one and Savè and Bonou in other hand**

Analyzing these data, we strangely realize that Bonou has lower maxima than Save since Bonou is at downstream and Save at upstream. Same observations are made for Dome at downstream and Atchérigbé at upstream. This fact was already observed by Le Barbé et al. (1993) who explained it in the following words. It seems that between the confluence of Ouémé and Okpara in one hand, Ouémé and Zou in the other hand, we have some losses of water along of the river. Losses recorded along the reach are accompanied by significant flood reduction. This could be due to the rapid decrease of the riverbed slope which varies just after the confluence from 1.7 to 0.2%; accordingly the maximum recorded at the upstream is greater than the one of the downstream.

A part of this lost water is likely used to supply the swampy zones and lakes (like Aziri Lake and Sele Lake) located in the region. But, areas which are likely to be inundated along of the Ouémé and Zou Rivers at the upstream of the confluence do not exceed 80 km2. It is not consequently possible to explain the losses only by the overflowing of water in those areas, even when counting for the evaporation. It seems realistic to impute a large amount of the deficit to infiltrations which likely occur when crossing the major geologic accident called the post-Eocene fault with direction SW-NE', partitioning the Zou near Domè and Ouémé close to Bonou.

The same phenomenon is observed for the Zou between Domè and Atchérigbé. In fact Domè and Atchérigbé are situated in the previously described geomorphological context with rapid decrease of the riverbed slope and geological contact between the basement formations and those of continental terminal.